DESIGN AND DEVELOPMENT OF SYMMETRIC REFLECTIVE COMPOUND PARABOLIC CONCENTRATOR (SRCPC) FOR POWER GENERATION

Garry Zamani Naman

Submitted for the degree of Doctor of Philosophy

Heriot-Watt University

Institute of Mechanical, Process and Energy Engineering

School of Engineering and Physical Sciences

December 2016

ABSTRACT

This thesis presents a detailed design, simulation, optical performance, construction and experimental validation carried out on a novel non-imaging static symmetric reflective compound parabolic concentrator (SRCPC). By considering the seasonal variation of the sun's position, a concentrating Photovoltaic (CPV) system with precise acceptance angle and low concentrating ratio will be an ideal alternative to conventional flat plate photovoltaic (PV) modules in harvesting the power from the sun. The SRCPC is a suitable choice well designed to achieve optimum precise acceptance angles and concentration ratio for this purpose. The optical performance theory study shows that a truncated symmetric reflective CPC with acceptance half-angles of 0° and 10° (termed as SRCPC-10) is the optimum design when compared with the symmetric reflective CPC designs with acceptance half-angles of 0° and 15° and 0° and 20° in Penryn and higher latitudes. An increase in the range of acceptance angles decreases the concentration ratio but an increase in the range of acceptance angles is achieved by truncating the concentrator profile which will reduce its cost as well. Ray tracing simulations indicates that the SRCPC-10 exhibited the maximum optical efficiency and steady slope compared with others. The simulated maximum optical efficiency of the SRCPC was found to be 94%. In addition, the SRCPC-10 was found to have a more uniform intensity distribution at the receiver and a total daily-monthly energy collection compared to the other designs. Thermal modelling of the CPV system with the SRCPC-10 concentrator shows that the solar cell operating temperature can reach up to 70°C for irradiance of 1000W/m^2 at an ambient temperature of 25° at a wind velocity of 2.5m/s. The integration of the thermal management system is able to control and maintain the temperature to 29°C. The modelled thermal and electrical efficiencies were 47% and 15% respectively with a heat transfer coefficient of 54.29W/m^2K thereby bringing the system efficiency to 62%. The maximum power of the SRCPC-10 when characterised in an indoor controlled environment using solar simulator was 5.96W at 1000W/m^2 at a cooling flow rate of 0.0079L/s with average conversion efficiency of 8.97%. The maximum power at 1200W/m^2 and 0.031L/s was 7.14W with conversion efficiency of 10.57%. The maximum increase in efficiency from non-cooling to cooling is 2.54%. The efficiency increased because of cooling is relatively 40%. The outdoor characterisation (validation) of the SRCPC-10 shows that the maximum power was 7.4W at 1206W/m^2 on a sunny day. The maximum electrical conversion efficiency of the SRCPC-10 in outdoor conditions was found to be 10.96%. These results revealed that this designed SRCPC-10

is capable of collecting both direct and diffuse radiation to generate power. Therefore, the SRCPC-10 could be used to provide a solution to the increasing demand on electricity to the energy mix, leaving a clean environment for future developments.

DEDICATION

Dedicated to my beloved Heavenly Father, faithful wife (Nsa'alianung) and children (Deborah, Abigail and Paul)

ACKNOWLEDGEMENTS

I wish to take this golden opportunity to express my profound gratitude to those who supported, encouraged, motivated and assisted me throughout my research and writing, without their help this thesis would have been a mirage.

My deepest thanks to my supervisors, Prof Hari Upadhyaya, Prof Tapas K. Mallick and Dr Baixin Chen whose exceptional mentoring capabilities, openness to discussions, suggestions, encouragement, motivation, criticisms, flow of thoughts, vision and love motivated me to desiring always to explore new concepts, methods, and technology if not because of them this thesis work would have been impossible.

My special thanks to Assistant Prof Nazmi Sellami who sacrificially assisted in no small measure in the lab work, site setting, made useful suggestions and contributions including simulation and proof reading the thesis.

Special thanks to our Solar Energy groups colleagues in the Institute of Mechanical, Process and Energy Engineering, most specific, Dr A. Ivaturi, Dr P R Bobbili, Dr Fruh Wolf, Dr Bennett, Dr Gudrun Kocher, Dr O'Donovan Tadhg, Ghanizadeh Tabriz Atabak, Acosta Edwin P, AL Mustapha Muhammad Nurudeen, Marius Dewar, Sorush Khajepor, Maka Ali, Tariq Chaudhary, Onne Okpu, Amber Ityona, Elsaye Elsaye A, Salem Salem M, for their technical advice and support during this thesis project.

Also, my special thanks to my amiable collaborative Solar Energy group at Energy and Sustainability Institute of The University of Exeter especially Dr S. Senthilarasu, Dr N Sarmah, Dr Baig Hassan, Dr Micheli Leonardo, Shivangi Sarmah, Prabhu Selvaraj, Meng Xian long, Katie Shanks, Al Badwawi Rashid, Alrashidi Hameed, Alsiyabi Idris Alfaifi Bandar, Issa Walid, Ullah Habib technical advice and support during this research. The contributions of Nosa and Nouf Allehiani (Princess) are too significant to be ignored.

I am endeared to thank the management and staff of School of Engineering and Physical Sciences (EPS) and IMPEE support staff particularly Mylene-Honore'L'Hortalle, Harlim Jongky S, Anna Mazur, Mc Gill Sarah E, McCulloch Grace, Genna Nothard to mention but a few for processing multiple paper work.

I do appreciate most importantly The Federal Government of Nigeria through Petroleum Technology Development Fund (PTDF) for funding and supporting my research

ACADEMIC REGISTRY

Research Thesis Submission

Name:	Garry Zamani Naman		
School/PGI:	School of Engineering and Physical Sciences		
Version: *(i.e. First, Resubmission, Final)*	Re-submission	Degree Sought (Award and Subject area)	PhD Mechanical Engineering

Declaration

In accordance with the appropriate regulations I hereby submit my thesis and I declare that:

1) the thesis embodies the results of my own work and has been composed by myself
2) where appropriate, I have made acknowledgement of the work of others and have made reference to work carried out in collaboration with other persons
3) the thesis is the correct version of the thesis for submission and is the same version as any electronic versions submitted*.
4) my thesis for the award referred to, deposited in the Heriot-Watt University Library, should be made available for loan or photocopying and be available via the Institutional Repository, subject to such conditions as the Librarian may require.
5) I understand that as a student of the University I am required to abide by the Regulations of the University and to conform to its discipline.

* *Please note that it is the responsibility of the candidate to ensure that the correct version of the thesis is submitted.*

Signature of Candidate*:*		Date:	

Submission

Submitted By *(name in capitals):*	GARRY ZAMANI NAMAN
Signature of Individual Submitting:	
Date Submitted:	

For Completion in the Student Service Centre (SSC)

Received in the SSC by *(name in capitals):*			
Method of Submission *(Handed in to SSC; posted through internal/external mail):*			
E-thesis Submitted (***mandatory for final theses***)			
Signature:		Date:	

TABLE OF CONTENTS

LIST OF TABLES

LIST OF FIGURES

NOMENCLATURE

Symbol	Definition	Unit
a’	Half Side of the Exit Aperture	m
A_p	Surface Area	m^2
A_1	Acceptance Aperture Area	m^2
A_2	Exit Aperture Area	m^2
C_{geo}	Geometric Concentration Ratio	
C_{max}	Maximum Geometric Concentration Ratio	
C_p	Specific Heat Capacity of Water	J/kg°C
D	Diameter	m
DC	Direct Current	A
Di	Inner diameter of a receiver tube	m
Do	Outer diameter of a receiver tube	m
2-D	Two-Dimension	
η_{elect}	Electrical Efficiency	%
$\eta_{optical}$	Optical Efficiency	%
η_{th}	Thermal Efficiency	%
G_a	Effective incident solar radiation on aperture plane	W/m^2
G_D	Direct solar radiations	W/m^2
G_{diff}	Diffuse solar radiation	Wm^2
G_G	Global Solar Radiation	W/m^2
H	Full Height	m
H_T	Truncated Height	m
I	Electric current	A
I_i	Intensity of a single ray	W/m^2
I_o	Total intensity on the aperture	W/m^2
I_{rec}	Intensity on the receiver	W/m^2
I_{sc}	Short circuit Current	A
I_m	Maximum Current	A
L	Length	m
$\dot{m}$	Mass Flow Rate	kg/s
N	Vector along the Normal	
n	Refractive Index of Dielectric material	
N_{re}	Number of reflection	
P	Power	W
P_m	Maximum Power	W
PNR	Reflectivity	
$\dot{q}$	Heat transfer rate	$W/(m^2K)$
Q_a	Acceptance Half Angle	rad
Q_i	Incident ray	
Q_r	Reflected Ray	
Q_T	Truncated Half Acceptance Angle	rad
$2Q_a$	Acceptance Angle	rad
R_r	Reflected Ray or Reflected vector	

R	Distance of earth from the sun	m
R_s	Series resistance	Ω
R_{sh}	Shunt resistance	Ω
S	Absorber Width	m
T_{cold}	Initial Temperature or Ambient Temperature	
T_{hot}	Hot Temperature	°C
T_{in}	Inlet (Initial) Temperature	°C
T_{out}	Outlet (Final) Temperature	°C
T_{sc}	Solar Cell Temperature	°C
T_{tank}	Water Tank Temperature	°C
ΔT_{in}	Change in Temperature	°C
U	Overall Heat Transfer Coefficient	W/m^2K^{-1}
V	Velocity	m/s
$\dot{V}$	Volume flow rate	m^3/s
V_m	Maximum Voltage	V
V_{oc}	Open Circuit Voltage	V
W_iCPV	Windows with integrated concentrating photovoltaic	
α	The Width of the Half Entry for Truncation	m
k	Boltzmann constant	m^2kgs^{-2}
λ	Wavelength	nm
ρ	Density of water	Kg/m^3

Abbreviations

a-Si	Amorphous silicon
ACPC	Asymmetric Compound Parabolic Concentrator
ACPPVC	Asymmetric Compound parabolic Photovoltaic Concentrator
AM	Air Mass
AMO	Air Mass Zero
AM1	Air Mass One
AM1.5	Air Mass one point five
BACPV	Building Application of Concentrating Photovoltaic
BAPV	Building application Photovoltaic
BIPV	Building Integration Photovoltaic
BiPVT	Building integrating Photovoltaic Thermal
BOS	Balance of system
CAD	Computer Aided Design
Cdte	Cadmium telluride
CHPS	Combine Heat and Power Solar
CIS	Copper Indium deselenide
CPC	Compound Parabolic Concentrator
CPV	Concentrating photovoltaic
CPV/T	Concentrating Photovoltaic and Thermal
CR	Concentration Ratio
c-Si	Crystalline silicon
CSP	Concentrating Solar Power

CuInSe	Copper Indium dissellenide
DiACPC	Dielectric Asymmetric Compound Parabolic Concentrator
DSSC	Dye sensitised solar cells
E-W	East-West Plane Directions
ERC	Energy Research Centre
EMA	Ethylene Methyl Acetate
EVA	Ethylene Vinyl acetate
FPSC	Flat Plate Static Concentrator
FF	Fill Factor
GaAs	Gallium Arsenide
HTC	Heat Transfer Coefficient
I-V	Current – Voltage
LGBC	Laser Groove Buried Contact
LSC	Luminescent Solar Concentrator
LST	Local Solar Time
LT	Local Time
MCPV	Miniature concentrating photovoltaic
MJ	Multi Junction
M_{PPT}	Maximum Power Point
N_aREC	National Renewable Energy Centre
NOCT	Normal Operating Cell Temperature
PMMA	Polymethyle Methacrylate
OPV	Organic Photovoltaic
PV	Photovoltaic
PV/T	Photovoltaic/Thermal
PU	Polyurethane
SEH	Solar Eliptical Hyperbolic
S-N	South North Plane Direction
SRCPC	Symmetric Reflective Compound Parabolic Concentrator
TIR	Total Internal Reflection
UV	Ultra-Violet

LIST OF PUBLICATIONS

1. G.Z. Naman, S.Nazmi, N.Sarmah , A.Ivaturi, S.Senthilarasu, P.R.Bobbili, H.M.Upadhyaya , T.K. Mallick (2014) Compound Parabolic Concentrators' Design for Equatorial Africa. *A proceeding of 1st African Photovoltaic Solar Energy Conference and Exhibition (1st Africa PVSEC)* at Durban ICC, Durban, South Africa March 27th -29th 2014, pp 91-97
2. G.Z Naman, S.Nazmi, N.Sarmah, A.Ivaturi, S.Senthilarasu, P.R.Bobbili, H.M.Upadhyaya and T.K.Mallick (2014). Development of a Concentrated Photovoltaic hybrid system for Heat and Power Generation in Nigeria. *A proceedings of 10th Photovoltaic Science Application and Technology (PVSAT-10) Conference and Exhibition* at Loughborough University, April 23-25, 2014

Publications under preparations at the time of submission.

3. G.Z. Naman, H.M.Upadhyaya, S.Nazmi and B.Chen, T.K.Mallick. Performance analysis for active cooling for concentrators' best performance. (Solar Energy in preparation).

4. G.Z.Naman, S.Nazmi, B.Chen, H.M.Upadhyaya and T.K.Mallick. Optimum tilt angle modelling for concentrators' performance in building applications. (Renewable Energy in preparation).

5. G.Z.Naman, H.M.Upadhyaya, S.Nazmi, T.K.Mallick and B.Chen. Perfomance evaluation and validation of designed SRCPC concentrator in Equatorial Africa. (Applied Energy in preparation).

Chapter 1 **INTRODUCTION**

1.1 Introduction

The positive influence of energy cannot be understated. It is considered as a prime agent in the generation of wealth and a significant factor in the economic development of any country and the living standard of the people. Universally, the importance of energy in economic development is recognised. Also, historical data verify that there is a strong relationship between the availability of energy and economic activity. The demand for energy today has led to research in various technologies so that the gap between the demand and supply of the commodity can be satisfied.

The sun is the source of much energy depending on the method and technology use for its extraction. The sun's irradiance is about 63MW/m^2 at a distance of one astronomical unit of 1.495 x 10^{11}m, being the mean earth-sun distance where the sun is subtended by an angle of 32° [1]. The geometry of the sun to earth dramatically reduces the solar energy flow down to about 1000W/m^2 on the earth's surface. The energy supplied by conventional energy viz, fossil-fuel has caused global warming and environmental pollution. The remedy to this pollution is to harness renewable energy sources. To harness the solar energy, the solar cell is the most important component used to convert solar radiation from the sun directly into electricity. The conversion of solar energy to electrical energy is not yet cost effective to take over conventional energy generation because of the expensive nature of the solar cell system which includes PV modules and balance of system (BOS) costs. However, this is surmountable by the use of solar concentrators' and hybrid systems. The expensive solar cells can be replaced with inexpensive concentrator materials where power generation per square meter is higher. Therefore, to enhance the performance of the Concentrating Photovoltaic system, the design plays a significance role. Concentrators are designed to fall into the categories of low or high concentrators. The imaging concentrators fall into the categories of high concentrators while non-imaging concentrators follow the low type concentrators. Therefore, concentrating photovoltaic research is motivated by the fact that there is potential cost reduction of solar electricity because only a small solar cell is required to generate a huge amount of power. By using optics materials, smaller amounts of expensive photovoltaic materials can collect radiation from the sun light from a large area using less expensive concentrating lenses where it becomes more economical and cost effective.

The annual energy consumption in 2013 worldwide was reported to be $5.527x10^{20}$ J which is slightly higher than $4.1x10^{20}$ J solar energy incident on the earth's surface in an hour [2]. From the vast and essentially infinite fuel source, solar energy is playing a significant role among the sources of renewable energy. Apart from using solar energy for domestic applications, it has become more important to use solar energy for industrial purposes and power applications in the present energy scenario [3]. Solar energy collection systems as we consider the operational conditions and designs for thermal and photovoltaic applications, they are studied separately as solar thermal collector and photovoltaic collector.

Solar concentrators come in the forms of Compound Parabolic concentrator (CPC) [4], concentrating solar power (CSP) [5], and concentrating Photovoltaic (CPV) [5], Linear Fresnel reflectors, Central receiver reflectors, parabolic dish and parabolic troughs [5]. Parabolic troughs can use direct solar radiation called beam radiation. This is also known as direct normal irradiation. The irradiation is not deviated by cloud, fumes and dust in the atmosphere but reaches the earth surface as a parallel beam. The solar hybrid systems of renewable energy utilization have attracted considerable attention from Engineers and Scientists during the last decade. This is because of their higher efficiency and stability of performance compared to individual solar devices. Naturally, solar energy devices intended for use fall into two main categories depending on the method of its conversion for example, heat or electrical or thermal collectors and photovoltaic modules accordingly. The solar thermal energy collectors are special kinds of heat exchangers which converts solar radiation into thermal energy using a transferable moving fluid medium. The solar collector is the major component of any solar energy system. Ideally, the device absorbs the incoming solar radiation, and then converts it into heat energy. Usually, the transferable fluid could be air, water or oil for useful purposes and application. These applications could be drying agricultural products, heating, cooling applications in conjunction with the auxiliary heaters for air conditioning in buildings.

The most useful way of utilizing solar energy is the Photovoltaic (PV) which directly converts solar radiation into electricity. The 'Photoelectric effect' exhibited by solar cells is the energy conversion process which is used to convert sunlight energy into electricity. The PV system consists of solar cells and also auxiliary components. The first practical conversion of solar radiation into electric energy was done by researchers in 1954 at the Bell Telephone Laboratories using a p-n junction type solar cell that achieved

6% efficiency [1]. The space program became the advent through which the photovoltaic cells were made from semi-conductor grade-silicon which quickly became the power source of choice for use in satellites. Between 15-20% are the common solar power conversion efficiencies [2]. Subsequently today, a new area has emerged combining both methods of energy conversion in the name of Photo-thermo conversion. [3]. In other words, the solar energy conversion into electricity and heat with a single device called hybrid Photovoltaic-thermal collector (PVT). Heat and power in this way are produced simultaneously. This is an important area of developing efficient devices that can satisfy both demands.

For long term technical life-span of a concentrating system, the reflectivity of the compound parabolic concentrator reflector was evaluated to be very high for long term stability. Different types of reflectors materials were analysed in this work. Also, there was assessment of the optical properties and degradation of the reflecting surfaces. There was a shift in focus which stems from performance of concentrating solar hybrid systems evaluation to analyse optical properties of reflecting materials. This shift was informed by the fact that the overall aim was to contribute to the solar energy technology improvement.

Solar cells when exposed to solar irradiations, there is increase in temperature due to the fact that not all the solar radiations are absorbed by the solar cell but some are deposited as heat on the solar cell. This high temperature effect reduces the conversion efficiency of the solar cell thereby decreasing the power generation. These temperature effects reduce the benefits and introduce losses in the system. The best and simple solution is to cool the solar cells. The cooling in this application is active by using a fluid transferable medium through a heat exchanger. In some other cases, the means of cooling is passive using fin cooling systems; natural cooling using air and forced cooling by the use of pump or fan mechanism. As water is being used as transferable medium, the extracted heat can be used for heating, drying, swimming pools and desalination. An attempt has been made in this thesis to quantify the heat loss arising from concentrating systems, which is entirely a non-imaging solar concentrator designed, constructed and experimented.

1.2 Spectrum of the sun

The sun has an effective blackbody surface temperature of 5777K [1]. The continue nuclear reaction enables the sun to emit electromagnetic radiation having a continued spectrum that matches that of a blackbody radiation at that temperature. The measurement of the solar radiation that reaches the outside of the earth atmosphere in terms of power is measured per unit area perpendicular to the sun's diction. The solar constant G_{sc} being the extra-terrestrial radiation of the sun is 1.353kW/m^2 which is internationally accepted [1]. The sun's spectrum outside the Earth's atmosphere is considered as air mass zero (AM0) referred to in Figure 1.1. The air mass zero spectrum is different from the blackbody radiation at 5777K due to the different transmissivity on the surface of the sun at different wavelengths. Further to this, the spectrum changes due to absorption and scattering by gas, water, clouds and dust particles after entering the Earth atmosphere at AM0. The solar radiation is attenuated by 30% while entering the Earth atmosphere [6]. The solar radiation attenuation inside the Earth atmosphere depends on the path length of light travelled. At the time the sun is directly overhead, the spectrum is AM1. Due to changes in the sun's position from the overhead depending on the angle of the overhead, the air mass varies and is given in Equation 1.1 [7].

$$\mathrm{AM} = \cos^{-1} \mathrm{Qz} \qquad 1.1$$

where Q_z is the angle subtended by the sun to the earth

The Sun's AM0 and AM1.5 light spectral distribution is shown in Figure 1.1. Furthermore, to this, a standard spectrum and radiation intensity has been adapted for comparison of the different solar PV technologies. The Internationally and universally accepted standard terrestrial solar spectrum is AM1.5 and 1000W/m^2 for radiation intensity [7, 8].

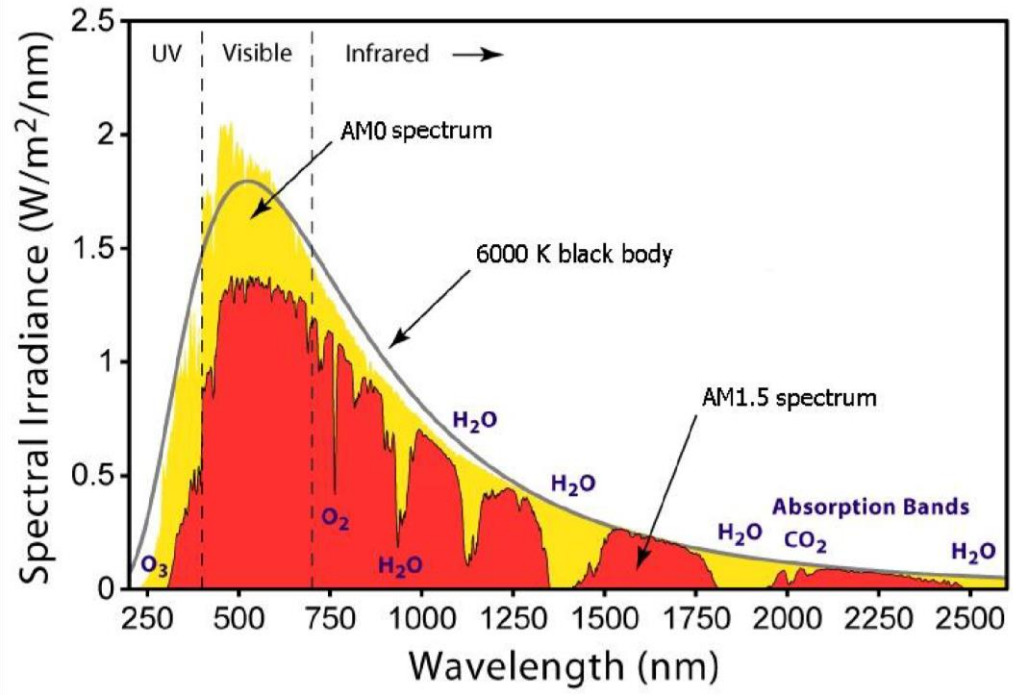

Figure 1.1: Sunlight spectral distribution of AM0 and AM1.5 and blackbody spectrum[7-9].

1.2.1 ***Direct, diffuse and global radiation***

The solar radiation is incident directly from the sun above the Earth's atmosphere. At the point of solar radiation entering the earth's atmosphere, some of the radiation is scattered by dust, gases and vapour. At the surface of the earth, the solar radiation is scattered and reflected by the surrounding and it is call diffuse solar radiation. At some locations on the surface of the earth, the total radiation is a combination of both direct and diffuse radiation. Depending on the location, the contribution of diffuse radiation on a horizontal plane is 10-20% even on a clear sunny day [7, 9]. The direct radiation differs in spectrum from the diffuse radiation spectrum but the diffuse radiation is rich in short wavelengths. The combination of direct and diffuse radiation on the earth surface at a particular location is defined as Global radiation. In practical terms, the global radiation on a horizontal plane refers to both the direct and diffuse radiation [8]. Therefore, it is necessary when reporting the global radiation surface different from the horizontal; it becomes necessary to mention the plane as well. From the foregoing on a horizontal surface, the global radiation is given in Equation 1.2 [10-13].

$$Gr = D_r + D_{iff} \qquad 1.2$$

where Gr is global radiation, Dr is direct radiation and Diff is the diffuse radiation. In the context of this thesis, we shall refer to the internationally accepted definition of the terms direct, diffuse and global radiations.

1.3 Solar cells materials used in concentrating photovoltaic and thermal technology

1.3.1 Suitable requirement for solar cell materials

There are many different semiconductor materials, which have been used to make the layers in different types of solar cells. Each of these materials has its own qualities and drawbacks. The suitable requirements are; (1) the first fundamental requirement for a material to be suitable for solar cell application is the band gap matching to solar spectrum. It is between 1.1eV-1.7eV. (2) Each of the material must have high life time of charge carriers. (3) Readily available and consistent. (4) There should be toxicity control. (5) Easy techniques of reproducible deposition. (6) Large area production suitability. (7) It must have good photovoltaic conversion efficiency. (8) Durability and stability.

Solar cells can be categorised into three main groups depending on the historical development as it followed [14] referred to generations of solar cells. These categories are:

- Crystalline Silicon (c-si) solar cells (1^{st} Generation): Initial developments on wafer based Si technology.
- Thin film solar cells (2^{nd} Generation): These are based on best materials utilisation as thin films of a-Si (amorphous silicon), CIGS (Copper Indium Gallium diSelenide), CdTe (Cadmium Telluride) which are a few micro meter thick can absorb over 98% photons as opposed to c-Si which has to be over 200 micro meters to absorb similar amount of photons illuminating the solar cell.
- Multi-layer Tandem cells (3^{rd} Generation): aim at achieving high efficiency devices but still use thin-film second-generation deposition method. Their focus will be compatibility with large scale implementation [15].

1.3.2 ***Photovoltaic (PV) solar technology***

Photovoltaic (PV) is a semiconductor device that generates electricity when light falls on it. The photons of the absorbed sunlight displace the electrons from the semi-conductor absorber materials when sunlight strikes the PV cells. The excited electrons thus produced are separated across the semiconductor junction (generally explained in c-Si) by the built-in electric field developed at the space-charge region to produce a Photo voltage across the two terminals. This method of generating electrical power through the conversion of solar radiation into direct electricity current is called the ‘’photovoltaic effect’’. The section below describes in brief some of the prominent PV technologies, which have made their mark in demonstrating commercial production successfully in terrestrial and space application

1.3.3 ***Silicon solar cells***

1.3.3.1 ***Single crystalline silicon***

Photovoltaic cells made from semiconductor grade silicon quickly become the main power source for use on satellite with the advent of space program [16, 17]. The conversion efficiency of solar modules now ranges between 10.5-25.6% [18]. What has hindered the wide spread use of silicon cells is the relatively high cost of manufacturing involving high capital cost of equipment for materials and devices processing, although significant cost reduction has been achieved as low as $0.50/Watt-peak due to high volume of production [19]. Silicon cells have another disadvantage of the use of toxic chemicals in manufacturing. This is why the search for environmentally friendly and low cost solar cell alternatives. Silicon has demonstrated high efficiency and robustness of the product over 25 years of lifetime guarantee by manufacturers and leads the PV market with over 85% share. The best single crystal solar silicon today has reached an efficiency of 25.6%. Silicon solar cell modules commercially are available with conversion efficiency as high as 18% [20] as illustrated in Figure 1.2

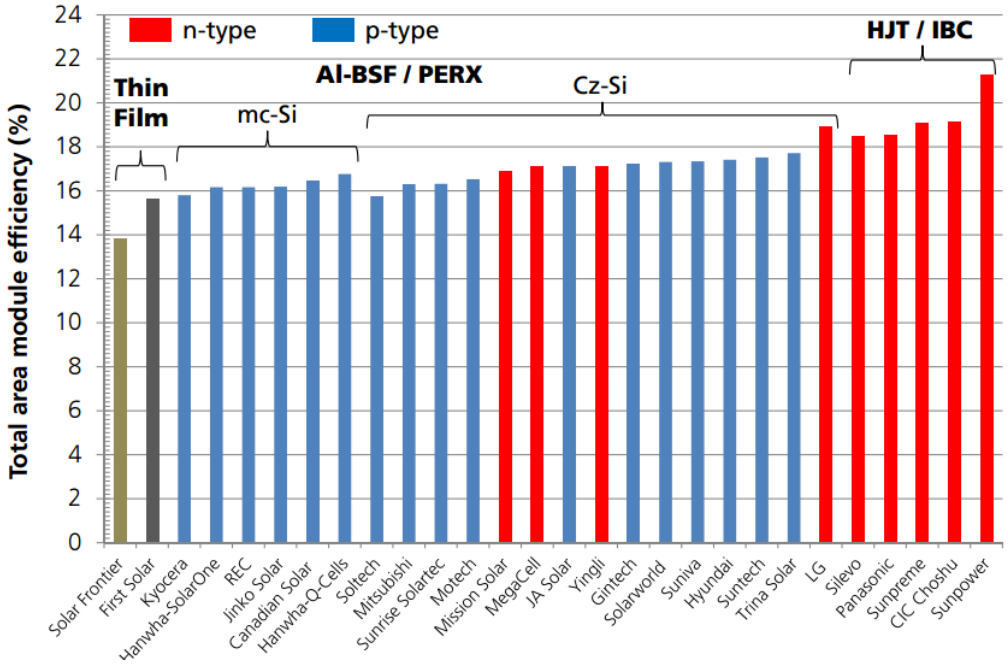

Figure 1.2: Graph showing current efficiencies of selected commercial PV module [21]

1.3.3.2 *Polycrystalline Silicon*

This is consisting of small grain of single crystal silicon. Polycrystalline cells are less energy efficient than those of the single crystalline silicon cells. They hinder the flow of electrons thereby reducing the power output of the cell. A commercial module of polycrystalline silicon energy conversion efficiency ranges between 15-18% [22].

1.3.3.3 *Amorphous Silicon*

The first thin film PV modules commercially produced of amorphous silicon (a-si) which are only the thin film technology that has had an impact on the overall PV market. This discovery is dated back to 1974. Amorphous silicon in particular has received much attention as a material for thin film solar cells because of its significant advantage of high sunlight absorptivity that is about 40 times higher than that of single crystal silicon. Only a thin layer of amorphous silicon is sufficient of making PV cells of about 1µm thick when compared to 200 or more micro-meters thick of crystalline cells Also, amorphous silicon provides cost effective fabrication because of its low raw material requirement. Amorphous silicon has low production energy requirement. For instance, the deposition temperature is less than 300°C. With obvious advantage of being a thin film technology, a-Si can be deposited on very low cost substrates such as steel, glass and plastics. When compared with the c-Si cells, the total material cost and

manufacturing cost of a-Si is lower per unit area. The efficiency reported so far is 10.2% [23].

1.3.3.4 *Compound Semiconductor (III – V Group Solar Cell)*

The high cost of production is the disadvantage of III–V compounds in photovoltaic devices. More to this, crystal imperfections, including unwanted impurities, many times reduces the device efficiencies where alternatives low cost deposition methods cannot be used [24, 25]. Mechanically, these materials are significantly weaker than silicon. In terms of weight, unless very thin cells can be produced to take advantage of their high absorption coefficient, the high density of the materials is also a disadvantage. The above mentioned drawbacks led to them being considered as uncompromising materials for single junction for terrestrial solar cells.

The development of III – V based devices were initially taken primarily because of their potential for space application. The prospects and high conversion efficiencies together with radiation resistance in the demanding environment of space power generation reduction against the high material cost.

1.3.5 Compound Thin Film Solar Cells

A thin film semiconductor layer of PV materials in a thin PV cell can be deposited on low cost supporting layer such as glass, metal or plastic foil. Materials of thin film have higher light absorptivity than crystalline Si materials. The deposited layer of PV materials is extremely thin from a few micro-meters to even less than a micro-meter. A single amorphous cell can be as thin as 0.3μm. Materials that have thinner layers yield significant cost saving. Deposition of thin film materials can be carried out by a number of vacuum or non-vacuum deposition techniques directly onto glass or metal substrates. As a result, the manufacturing process is faster using less energy. More suitable search for thin film materials shows a-Si (already discussed above), copper Indium di-sulphide (CIS), Cadmium Telluride (CdTe) together with copper Indium di-Sellenide ($CuInSe_2$) with all other related alloys for the production of low cost thin film solar cells which are established as the most promising candidates for the forth coming generation of solar cells [21]. For example, First Solar (US company) has demonstrated the lowest payback time and module costs and is producing over 10 GW of solar power annually [26]. The single cell efficiencies of CIGS and CdTe technologies are 21% respectively [18].

1.3.4 ***Dye Sensitized Solar Cells (DSSC)***

The widely investigated Dye sensitized solar cells (DSSC) as next generation solar cell because of their simple structure and low manufacturing cost. They provide an economically and technically credible alternative concept to today's p-n junction photovoltaic devices. In the now, photovoltaic technologies that are commercially available are based on inorganic materials. These materials requires high costs and high energy preparation methods [27]. Figure 1.3 shows best research solar cells conversion efficiencies improvement over the years.

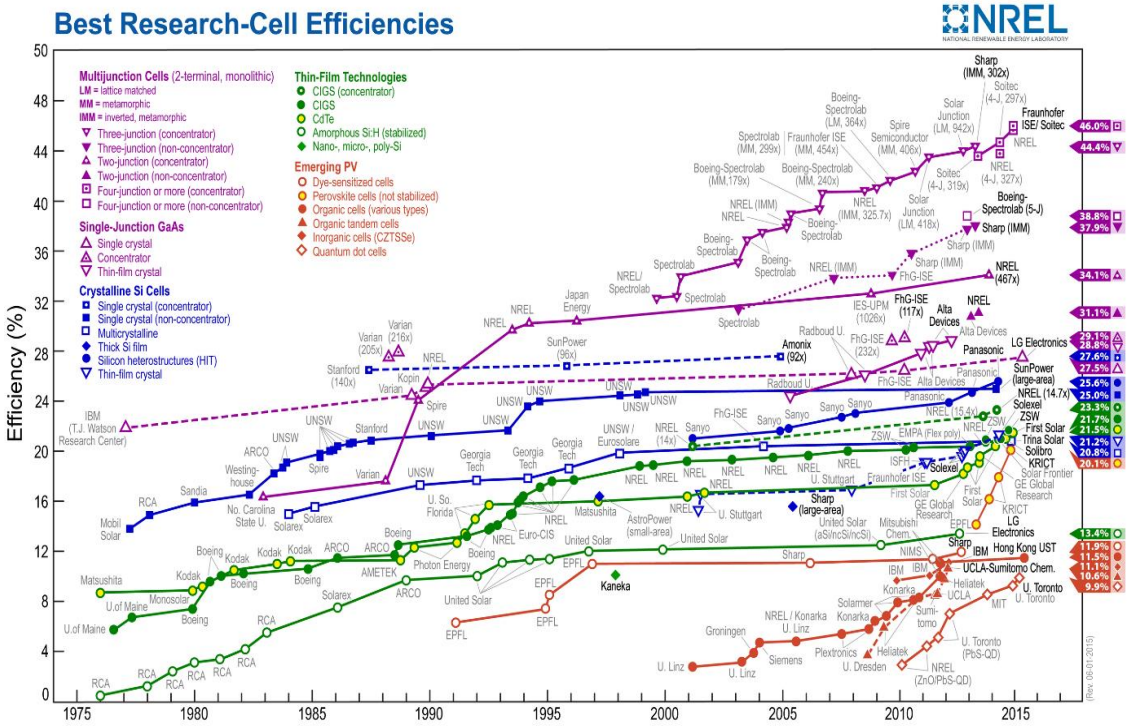

Figure 1.3 Best research Solar cell conversion efficiency improvement over years [28]

1.4 Solar energy collector

A solar energy collector in a general term can be defined as a device that collects the sun's energy and converts it into a more usable form. By the term device, it refers to a system that includes concentrator, receiver, tracking and cover elements. A receiver involves absorber, insolation and cooling but this is depending on the application. The role of the concentrator is to direct the solar radiation from the acceptance aperture to the exit (absorber) aperture as shown in Figure 1.4. The concentrator cover protects the entire system from dirt, moisture, water, degradation, oxidation and corrosion. The sun-tracking element is needed to change the orientation of the collector depending on the position of

the sun. For high concentrating solar collectors, the sun tracking is very essential because it is capable of maintaining the peak power output position of the concentrating Photovoltaic. It also adjust the load on the concentrator for maximum efficiency and changing the position of the concentrator relative to the sun's position. At industrial level, the average terrestrial solar radiation of 1000W/m^2 is not enough for thermal application and it is not economically attractive for photovoltaic operation due to the low conversion efficiency of solar cells. High concentrating of solar radiation causes increase in flux density on a small area of a receiver. The flux density when it is high provides higher temperature for thermal application and in photovoltaic application higher electrical output [8].

1.4.1 ***Solar concentrator***

A solar concentrator is an optical device that collects the solar radiation incident on the acceptance aperture area A and delivers it to a usually smaller absorber area B. The constituents of a solar concentrating system include an entrance aperture area, Exit or receiver area and reflector/refractor surface as shown in Figure 1.4. The side of the concentrator by which solar irradiation enters the concentrating system is called the entrance aperture. The section that absorbs the solar radiation is called the receiver.

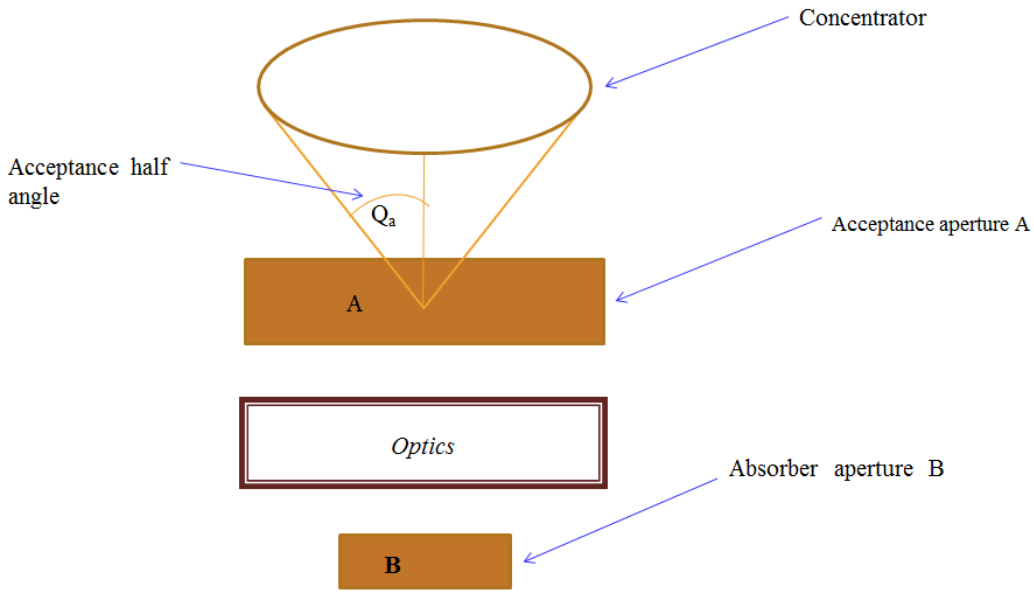

Figure 1.4: Showing the constituents of a solar concentrating system.

There are many different concentrator profiles and designs used to achieve high optical efficiency for different applications over the years [29-31]. Looking into the optics of the reflector or refractor, concentrators are mainly divided into two categories for

instance the imaging (high) concentrators and non-imaging (low concentrators) [32, 33]. It implies from the definition that concentrators with imaging optics forms an image of the sun on the receiver like convex lens, parabolic mirrors etc. On the other hand, concentrators with non-imaging optics do not form any image of the sun but only concentrates the solar irradiation over a specified area [29, 34].

1.4.2 ***Concentration Ratio***

The ratio of the energy flux at the receiver to the energy flux at the acceptance aperture of the concentrating system is termed as the concentration ratio and it is related primarily to the aperture and receiver areas of the system [8]. We have two major concentration ratio definitions which basically are 1) Optical concentration ratio and 2) Geometrical concentration ratio [35, 36] as defined below. The latter is commonly used.

1.4.3 ***Optical concentration ratio***

Optical concentration ratio is also called 'intensity concentration ratio' or 'flux concentration ratio' and it is defined as average energy flux on the absorber to the aperture of the system [37]. The average flux on the receiver is considered because the energy flux on the receiver surface is not homogeneous. Also, in another way, local concentration ratio on the absorber can be defined as the ratio of the flux at any point of the receiver to the aperture. Another term used for optical concentration ratio is 'suns'. For example if the flux on the absorber is 3 times the flux on the aperture, the concentration ration is termed to be 3 suns [38, 39].

1.4.4 ***Geometrical Concentration Ratio***

The most commonly used definition for concentration ratio is the 'geometrical concentration ratio' which is defined as the ratio of the aperture area to the absorber area. It is described as:

$$C_g = \frac{A}{B} \qquad 1.3$$

Where $C_g$is the geometrical concentration, *A* is the acceptance aperture area and *B* is the absorber area. The theory of the concentration limit is established by using the radiative heat transfer between the two sources, the sun and the absorber.

1.5 Research problems facing compound parabolic concentrators' technology

The research to resolve related energy challenges or problems is very important because life is directly affected by energy and its consumption. There are parameters that affect the total electrical and thermal energy output in compound parabolic systems. These are;

1 The drop of electrical efficiency is because of the solar radiations increasing the temperature of the PV modules because not all are absorbed.
2 In non- imaging concentrators, mis -match effects in solar cells are caused by non-uniform irradiance as well as tracking errors, which usually occurs at the peripheral of the array. This challenge is a crucial draw back that affects the electrical performance of CPV systems because maximum output power of the array is majorly reduced. The factors that cause mismatch include temperature variations, non-uniform irradiance, solar cell quality, shading, soiling as well as solar cell ageing.
3 For effectiveness and further reduction of the cost of electricity generation, optimal system design is necessary so that maximum solar energy can be harnessed from CPV solar cells. In most cases, it is also discovered that the delivered electrical power in field conditions is usually less than the array ratings.
4 Another significant problem in non- imaging concentrator systems is the non-uniform distribution of solar irradiance that is mostly located around the receiver edges. This defect is mainly caused by optical designs limitation and structure mis- alignment.

Scholarly, the principles of solar concentration is well understood but further research work has to be conducted in the areas of

System losses, Practical designs to bring the cost low, Operation and maintenance issues, Non-uniformity of incident flux distribution on the cell, System cost reduction, System stability, System efficiency, Stochastic nature of the sun and Solar Energy storage issues [40].

The negative effects of the above mentioned further research areas has great impact or general influence on the technology which causes hot spots, current mismatch,

system overall efficiency reduction, long payback periods, high cost of technology and temperature dependency.

1.6 Identified CPC technological possible solutions

1.6.1 Non-Uniform of solar flux distribution

In the present decade, many research work and discussions on the improvement of solar concentrators' optical design to produce more uniform solar illuminations are available [41] at high concentration. Usually the overall current of CPV solar cells that are mostly connected in a densely array arrangement is mostly dependent on the solar flux distribution of a solar concentrator. Other factors, which may include imperfection of mirror geometry, sun shape, aberration, and circumsolar effect, are issues that make it impossible to produce perfect uniform illumination on a CPV receiver. This is causing some significant losses in the overall output power as well as the average conversion efficiency [42]. Meanwhile, there exist some considerable efforts in the study of partially shaded PV rays for maximizing mismatch losses [43].

The barriers to higher Photovoltaic efficiency lie within the science. The key element of any concentrated photovoltaic system is the solar cell. The design of solar cells plays a significant role towards improving the performance of CPV systems. There is a significant difference from these concentrator solar cells to one sun cells in many ways. These ways include the method of manufacture, the overall cell design and the performance. Generally the concentrated solar cells involves bus bars surrounding the perimeter of the cell which can be permitted without blocking any of the incoming light [44].

1.6.2 Temperature dependent of CPV solar cells

When designing concentrating photovoltaic systems, cooling of photovoltaic solar cells is one of the major concerns. The solar cells may experience both long – term [irreversible] damage and short term [efficiency loss] degradation due to excess temperature. Therefore the design consideration for cooling solar systems include the following – 1] minimal power consumption by the system, 2] low and medium temperature, 3] system reliability and 4] sufficient capacity for dealing with worse case scenarios. There are many methods that can be employed for cooling of concentrating

solar photovoltaic cells. It will be interesting to know that the optimum cooling solutions differs between single cell arrangement, linear concentrators and densely packed photovoltaic cells. Typically, single cells only needs passive cooling even under very high concentrations greater than 150 suns [45].

1.6.3 Concentrator cells cooling requirement

The subsequent replacement of expensive photovoltaic area with less expensive concentrating mirrors or lenses by concentration of sunlight onto photovoltaic cells is seen as one method to lower the cost of solar electricity. It is noted however that only a fraction of the incoming radiations striking the cell is converted into electrical energy. The remainder of the absorbed will be transformed or converted into thermal energy in the cell [46]. The imperative major design considerations for cooling of photovoltaic cells are;

Material quantity; Materials used in photovoltaic solar cells should be kept low for the sake of cost, weight and embodied energy considerations [47]

Cell temperature; Concentrating photovoltaic cells efficiency decreases with temperature increases [48]. Long term degradation is being exhibited by the cells will generally specify a given temperature exceeds some limits [49]. Manufacturers of solar cells will generally specify a given temperature degradation co-efficient and a maximum operating temperature for the cell [49].

Reliability and function ability: for operational cost to be keep minimum, simple and low maintenance solutions are further necessary. Toxic materials use maximization due to health and environmental concern should be critically looked into. An important aspect is the system reliability. The failure of the cooling system could lead to the destruction of PV cells. The solution to system reliability is that the cooling system should be designed to deal with worst case scenarios which may include tracking anomalies, power out stages, power restoration, and electrical faults within the modules [50].

Non-temperature uniformity; Due to non-uniform temperatures across the cells [51], the cell efficiency is known to decrease. In most of the photovoltaic modules, cells in their members are electrically connected in series as well as parallel connected too. A

given power output series connection increases the output voltage and decreases the current, thereby reducing the ohmic losses.

Current matching problem; It is important to note that when cells are connected in series, the cell that gives the smallest output will limit the current. The situation is known as "current matching problem". Due to the decrease in cell efficiency as a result of temperature increase, the cell of the highest temperature will limit the efficiency of the whole string. The solution to "current matching problem" is the use of bypass diodes can be incorporated in the design [44]. This will bypass the cells when we reach a certain temperature. In this arrangement, you lose the output from this cell while the output from the other cell is not limited or you keep a uniform temperature across each series connection [52].

Reverse bias break down protection by bypass diode; CPV cells can be protected from reverse-bias break down that could cause permanent damage to the cells. If every solar cell is connected in parallel with bypass diodes in opposite polarity. The bypass diode is forward biased so that the current array can safely pass through the combination of cell-bypass-diode when the cell is shaded or receives lower solar irradiation. The role of bypass diodes is very vital to avoid those CPV cells receiving low irradiance become the load of other CPV cells receiving high irradiance for an array exposed to non-uniform solar irradiance. An alternative path for the current is created by the by-pass diode so that the underperforming CPV is protected. The diode will turn on and hold the corresponding cell or groups of cell to only a small negative voltage which can help to limit any further drop in the total voltage of the whole array when the array current passes through the bypass diode [53].

Pumping power; The pumping power should be kept to minimum as the power required of any active component of the cooling circuit is a parasitic loss [53].

Thermal usability energy; The extracted thermal energy from cooling if used, can lead to a significant increase in the overall conversion efficiency of the receiver [44]. It is necessary for the above constraint to desire to have a cooling system that delivers water at high temperature as possible. To further avoid losses and additional heat exchanger, an open loop cooling system may be of advantage.

Geometry of concentrators; To differentiate between concentrators according to their method for concentrating mirrors or lenses is sensible. As a result that the requirements for cell cooling differ considerably between the various types of concentrators geometries, it is necessary to group concentrators accordingly.

Shading; Shading issues are different from lens and mirror concentrators. The cells are normally placed underneath the light source if lenses are used thereby indicating that shading by the cooling system does not occur. In the case of mirror systems, the cells are generally illuminated from below. This makes shading an important issue for consideration when designing the cooling system. Categories of concentrators can be grouped as follows.

Densely packed modules; Systems that are point forward like parabolic dishes, or heliostat fields, the solar cells receiver generally consist of a multitude of densely packed cells. The solar cells receiver is usually placed slightly away from the focal plane so that the uniformity of illumination can be increased. To further improve image flux homogeneity, secondary concentrators called kaleidoscopes may be used. Densely packed modules present greater problems for cooling than linear geometry and single cells. This is because except for the edge cells, each of the cells only has its rear side available for heat sinking. In principle, it means that the entire heat load must be dissipated in a direction normal to the module surface. By implications generally, passive cooling cannot be used in densely packed module array at their typical concentration levels.

Single cells; sunlight radiations is usually focused onto each cell and individually focused onto each cell individually in small point focused concentrators. It implies that each cell has an area roughly equal to that of the concentrator available for heat sinking. Solar cells with 50x concentration should have 50 times its area available for spreading of heat. At quite high concentrations levels it means that passive cooling can be used. Various types of lenses for concentration are commonly used for single cell systems. Also, where reflective concentrators transmit the concentrated light through optical fibres onto single cell is another variant [54].

Linear geometry; Parabolic troughs and linear freshener lenses uses linear focus system typically. In the linear geometry, the cells has less area available for heat sinking due to the fact that two of the cells sides are in close contact with the adjacent cells. By

implication, it means that the area available for the heat sinking extend from two of the sides and the back of the cells.

1.7 Aims and objectives of this thesis

The goal of this thesis is to design and develop a novel prototype CPV system of non-imaging symmetric reflective compound parabolic concentrator that is focus at reducing the cost of the existing conventional PV modules by reducing the area of silicon solar materials used and replacing them with lower optical cost concentrator materials for the purpose of generating heat and power.

Therefore, my objectives in achieving this goal is:

- To identify and assess CPV technologies that have high electrical yield.
- To identify PV materials that have high efficiencies suitable for electricity generation.
- To identify CPV systems and technologies that are reliable, stable and cost effective and their efficient design through modelling elements.
- To identify major challenges/limitations of CPV technologies in order to proffer better remedies and reduce operating temperature.
- To compare and contrast CPV systems in order to match the appropriate PV materials for satisfactory power generation.

The designed of non-imaging symmetric reflective compound parabolic concentrator is also aimed at reducing the cost of the existing conventional PV modules by reducing the area of silicon solar materials used and replacing them with lower optical cost concentrator materials. Also, high land cost will be minimized, system cost reduction will be possible, achieving high efficiency and system reliability. This thesis investigated the possibilities of increasing the conversion efficiency of the solar energy system which in turn will reduce the cost of electricity generation and the heat that is produced. Emphasis is placed on the materials used to be durable, efficient and reliability of the entire system. The use of low-cost but efficient reflectors, heat exchanger and flow rates, and durable frame work for electricity output increase from solar cells can make solar electricity to be very near to cost-competitiveness in building integrated photovoltaic as combine heat and power generation (CHP) systems. To facilitate and commercialise the widespread use of solar energy technologies, it was thought through to have systems that

can be easily installed, operated and maintained. Increase in demand of solar energy technologies, cost competitiveness will increase large-scale production. This mass production will further force down the cost of materials, technologies and the energy eventually. The improvement of the performance of solar concentrators for increasing power and thermal energy production, at a low-cost, different low concentrating photovoltaic and thermal hybrid system with different geometries and reflectors were considered with respect to their optical and energy conversion efficiency.

1.8 Novelty of the designed and developed symmetric reflective CPC

The following novelties are identified in this thesis,

- Design and development of a non-imaging concentrator that requires no tracking and it is focused at achieving high efficiency, reliability and reducing the system cost.
- Design and integration of a heat exchanger to monitor and control the temperature effect in order to increase the efficiency, and use of waste heat.
- To ensure the design principle collects maximum solar radiation within the boundary acceptance angles to match the 3x concentration ratio by using high reflective materials.
- Due to the trade-offs of concentration with practical constraints which include size, cost and weight, the system to be designed will be truncated to reduce cost without losing much concentration.

1.9 Outline of this Thesis

Chapter 1 is the introductory part which presents the aims and objectives of the research work carried out. A brief summary of the thesis outline is also presented.

Chapter 2 is the literature review of concentrating photovoltaic systems, technology development and advancement, technology challenges and barriers, cooling methods and classifications, concentrator application, designs contribution in concentrators technology as well as design challenges facing the technology is also discussed in detail. Identified possible solutions to the technology challenges and the challenges tackled in this thesis.

Chapter 3 is the methodology approach to offer solution to the identified gap in the technology. Symmetric Reflective Compound Parabolic Concentrator technology is

considered in this thesis. A detailed design geometry is presented. Also, detailed optical modelling is presented with ray tracing using Optis Works Software for different acceptance angles, optical flux distribution and optical efficiencies is also presented. Design specifications, CAD drawing, cost analysis are also included here.

Chapter 4 presents the heat exchanger design and its construction for integration in the concentration system for heart extraction. Types of heat exchangers, application of heat exchangers, the choice of flat plate heat exchanger design and the dimension of a parallel flow heat exchanger is presented. The volume flow rate, the rate of heat transfer, thermal and electrical efficiencies estimation are detailed as well as the construction of this designed heat exchanger.

Chapter 5 presents a detailed construction of the twin SRCPC Concentrator and its indoor characterisation. The materials used, solar cells soldering, encapsulation materials and procedures, and heat sink compounds are discussed. The heat exchanger integration, experimental set up and instrument used are presented. Results and discussions of the indoor characterisation are also presented here. The volume flow rates, power generation by the SRCPC and effects of radiation changes are also shown. Agreement between optical efficiencies and experimental efficiencies are confirmed.

Chapter 6 is the SRCPC outdoor experimental characterisation. The SRCPC model outdoor composition is detailed. Optimum angle tilt modelling, location of the experiment site and the outdoor experimental set up with the apparatus are described. Solar cell temperature measurement before concentrating, without cooling and with cooling, during concentrating without cooling and with cooling. SRCPC power output modelling and electrical modelling of I-V simulation results used to study the effects of concentration ratio is also detailed. The effect of incident angles as well as the result of the experiment are also presented and discussed.

Chapter 7 gave some concluding remarks on the main findings. Also a few recommendations on future work that could be further undertaken in this thesis and related fields for performance improvement and facilitate a broader market penetration of low-concentrating photovoltaic systems.

Appendix is where data, figures, tables, and results are kept which can be referred to from the chapters.

Chapter 2 **LITERATURE REVIEW**

2.1 Summary

This Chapter presents the history and basic concept of concentrating Photovoltaic systems. Different types of concentrating designs are introduced and summarised. The Chapter reviews the different nonimaging concentrators starting with the fundamental concepts and optics reflective surface being the focus of this research. The technology development and various concentrators' designs are considered with focus on the challenges and possible remedies. In addition, different methods of cooling and overall system efficiency are considered. The symmetric hollow reflective compound parabolic concentrator is the focus in this piece of work. Its principle of operation, truncation, optical modelling, angle of incidence, acceptance and exit apertures, edge principle and ray tracing, and I-V characterisation is reviewed in detail.

2.2 The history and early research on photovoltaic/thermal (PV/T)

2.2.1 ***Basic concept***

The photon energy of solar cells corresponds to the energy band gap under which generation of electricity does not occur. Electron-hole-pairs are not generated by photons of longer wavelength but heat is dissipated as their energy in the cell. The most common photovoltaic modules can convert 15-18% of the incident solar radiation into electricity. This is dependent on the type of solar cells that are being used and their working conditions. Also, much solar irradiance is converted as heat which may lead to extreme cell working temperature at about 50°C ambient temperature. This is illustrated in Figure 2.1.

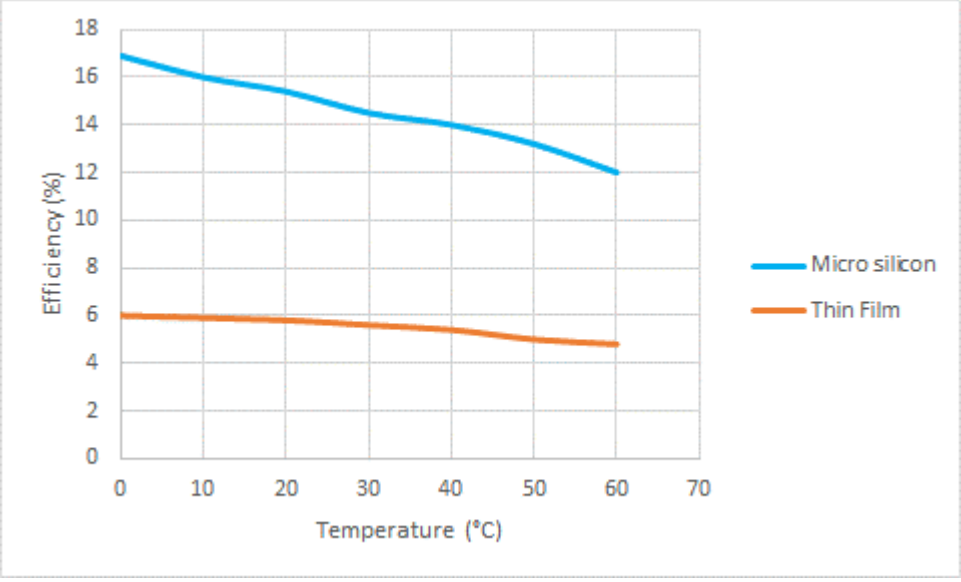

Figure 2.1: Cell efficiency against temperature increase as adopted in reference [55].

Two undesirable consequences may arise; (i) There may occur a drop in cell efficiency, for instance 0.4% per ^{o}C rise for c-Si cells, and (ii) if the thermal stress remain for a long period, a permanent structural damage of the module could occur [56, 57].

2.3 The physics behind silicon changing with rise in temperature

The increasing temperature decreases solar cell performance. This is fundamentally because of increased internal carrier combination rates. In a general note, the performance ratio decreases with latitude because of the temperature. In addition, it is known that regions with high altitudes have high performance ratios due to low temperatures. Also, PV module with less sensitivity to temperature are preferable for high temperature regions. Those that are more responsive to temperature will be more effective in the low temperature regions. Therefore, the geographical distribution of solar concentrating Photovoltaic energy potential considering the effect of irradiations and ambient temperature on solar concentrating systems performance is necessary [58].

There are other critical cell parameters that affects cell performance against temperature which includes temperature coefficient, fabrication process routing, solar cell electrical parameters, wafer type, wafer sensitivity and impurities. The all have impact on solar cell performance in terms of temperature coefficients [59]. Also, quantitative study analysis reveals different cell performance sensitivity to specific parameters which includes the critical growth, the use of electronics grade or upgraded metallurgical grade silicon wafers with the fabrication process used [59]. The temperature coefficient of the

short circuit current is shown to be an important factor in the tendency of the temperature coefficient of the maximum power. Therefore, this phenomenon is the impacting factor for the superior temperature observed in solar cells fabricated from upgraded metallurgical grade silicon wafer.

The solar cell characterisation under standard test conditions is performed at 25°C. It is observed, however that the operating temperature may change significantly from this value in concentrating Photovoltaic installations. The main operational conditions depends on outdoor temperature, available solar illumination level, local wind speed, location of the CPV system and its capacity to dissipate the heat generated [59, 60].

2.3.1 ***Temperature coefficient***

It becomes necessary to consider the temperature coefficient (CT) of solar cells for the prediction of the real power that can be produced in an installation under operating conditions [60]. Take for example, the normal operating temperature is 45°C, the temperature dependence of maximum power output (P_{mpp}) in terms of its temperature coefficient can be linearly parameterised and the power output standard test will be

$$P_{mpp}(T) = P_{mpp}(25°C)(1 + CT.P_{mpp}(T\text{-}25°C)) \quad 2.1$$

It is important to note that this maximum power of a standard silicon photovoltaic module increases by 0.66% if the CT.Pmpp changes from 0.45% / °C to -0.42% / °C ***[59].***

2.3.2 ***Current industrial fabrication processes of silicon solar cells***

Considering the consequential current industrial fabrication processes of silicon solar cells, the solar cells fabricated from upgrade metallurgical grade silicon (UMG-Si) substrates are becoming more common. This is because of their comparable efficiencies with respect to the electronic grade silicon (EG-Si) solar cells together with their low cost.

Another most important issue with the solar cells processed with the UMG-Si substrate is that they behave as a function of temperature. Publications available presenting a study of the temperature coefficients of solar cells with respect to substrate type (UMG-Si against EG-Si) [61] or the resistivity [62]. It is made known by these publications that the $CT.P_{mpp}$ of solar cells made from UMG-Si is lower than the standard cells made from EG-Si. This is notable because of the strong improvement photocurrent

with increasing temperature. Furthermore, to this, the temperature coefficients are well anticorrelated to the solar cell resistivity.

It is important to know that the fabrication process has a notable influence on both the electrical and parameters and the CT of the solar cells [63]. Produced solar cells from high efficiency fabrication processes has high open circuit voltage and power. Additionally, there is almost linear relationship that has been demonstrated between the $CT.P_{mpp}$ and V_{oc} [64].

2.3.3 Temperature effects on electrical parameters of silicon solar cells

According to Varshni equation (2.2), the band gap energy changes due to the consequence of the temperature variation.

$$E_g(T) = E_g(0) - (\alpha T^2 / (T + \beta)) \qquad 2.2$$

Where E_g (T) is the band gap of the semiconductor at a temperature of T, E_g (0) is the value at (0) K while α and β are constants depending on the semiconductor materials. From Equation 2.2, as the temperature increases the band gap decreases. Due to this fact, the short circuit current of a solar cell increases with temperature due to the possibility of absorbing photons with lower energies to create e-h pairs [59, 65]. Also, there is a built-in junction potential in Voc and in efficiency as the silicon band gap moves further away from the optimum of 1.35eV for one sun AM1.5G spectrum.

Electron mobility rate depends on temperature as well as decreasing with temperature. As temperature increases, atoms vibrate more and hinder electrons passing through the lattice. This is called phonon or thermal scattering. It is responsible for the limitation on the carrier mobility in EG cells at temperatures and above standard test conditions.

2.3.4 Material impurity

The content of impurities affects the mobility of electrons thereby decreasing lightly with them as shown in Equation 2.3.

$$\frac{\mathbf{1}}{\boldsymbol{\mu T}} = \frac{\mathbf{1}}{\boldsymbol{\mu phonon}(\boldsymbol{T})} + \frac{\mathbf{1}}{\boldsymbol{\mu impurity}\,(\boldsymbol{T})} \qquad 2.3$$

Where μphonon is a phonon-mediated attraction and μimpurity is the developed u-finite atomic approach for the single impurity Anderson model.

It is worth noting on the other hand that the UMG-Si wafer compare to EG-Si wafer produces a weaker mobility reduction with increasing temperature [66]. The temperature coefficient of the short circuit density (CT Jsc) becomes higher in UMG-Si solar cells. Additional factor to be considered in the variation of the short circuit current density is the dependence of the Shockley Read Hall (SRH) recombination and lifetime with temperature.

Industrial silicon wafer is dominant with this type of recombination, which has a significance influence on the effective lifetime. UMG-Si wafers compensation is known to produce an increase in their effective lifetime [67].This parameter is correlated with the Jsc. Furthermore, this increment on the lifetime is stronger with temperature and has a larger influence on the Jsc than the weak reduction mobilities.

2.3.5 ***The Fill Factor coefficient***

The Fill Factor coefficient (CTFF) is defined as

$$\frac{1}{FF}\frac{dFF}{dT} = (1\text{-}1.02FFo)\left(\frac{1}{Voc}\frac{dVoc}{dT} - \frac{1}{T}\right) - \frac{Rs}{\left(\frac{Voc}{Isc}\right)}\left(\frac{1}{Rs}\frac{dRs}{dT}\right) \qquad 2.4$$

Where FF is the idealised fill factor without series resistance and Rs is the cell series resistance. It means that higher variation of the CT Voc implies higher changes on the FF without temperature. In addition to this, silicon solar cells with lower FF because of higher Rs are expected to have a worse dependence of FF with temperature.

Figure 2.2 illustrates the impact of how open-circuit voltage is affected by temperature rise [68]. Also, many of the parameters have some temperature dependence but the most significance effect is due to the intrinsic carrier concentration that depends on the band gap energy for example, lower band gaps giving a higher intrinsic carrier concentration, Higher temperatures giving higher intrinsic carrier concentrations [68, 69].

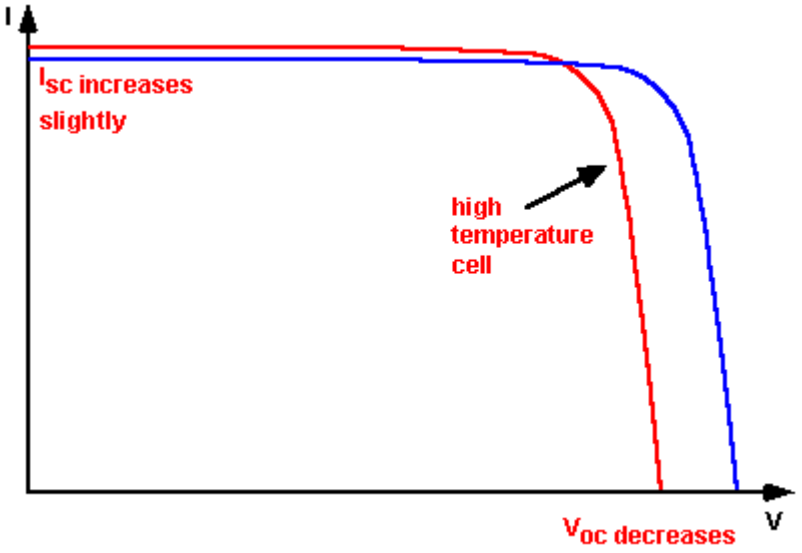

Figure 2.2: Temperature effect on I-V characteristic of a solar cell

Through the means of heat extraction using fluid streams like air, water, the PV cells are cooled thereby improving and increasing the electricity yield. It is conceptually better to design how to re-use the extracted heat energy by the coolant. This will improve the energy yield per unit area of the panel or in the building integration installation the facade. This is where the PV/T hybrid solar technology system is involved. Therefore, PV/T hybrid technology is combination of photovoltaic and solar thermal components into a module that will increase the solar conversion efficiency of the module thereby making the best economic use of the area. Simultaneously, the PV/T module can both generate electricity and heat. The PV/T technology is developed for the most purpose of removing the accumulated heat from the PV surface and the heat is used appropriately. The technology also allows the PV cooling for the purpose of increasing electrical yield or efficiency. The PV/T hybrid system represents a new direction for renewable generation of heat and power [55].

2.4 The physics of photovoltaic cells

Fundamentally, the photovoltaic cells produce electricity by the use of sunlight. Photoelectric effect is the means by which this made possible. At the interaction between a photon of energy with a matter, the photon gives up its energy in order to promote an electron to a higher energy level. The increased high electrical energy cannot be harnessed if the excited electron is not prevented immediately from going back to its ground state. This electrical energy may be needed to supply current to a load as in photovoltaic cells.

This could also supply an electro-chemical by charging the electro chemical potential energy.

2.4.1 ***Effective photovoltaic energy conversion requirements***

Three fundamental photovoltaic energy conversion requirements are significant. They are;

1. A high probability of photon absorption
2. A charge separation mechanism for removing excited electrons before they naturally recombines with the valence they left behind. Such is achieved using some kinds of interface or junction where different electronics or electrochemical properties attracts the electrons irreversibly away from the point of excitation.
3. There is the requirement of electronics transport to move the separated charge to an external circuit where its electrical potential energy will be exploited.

Semi-conductor p-n junction, which is the classical model of a solar cell, provides these three mechanisms described above. Figure 2.3 represents the photons that are charged, the band gap and the means of charged separation.

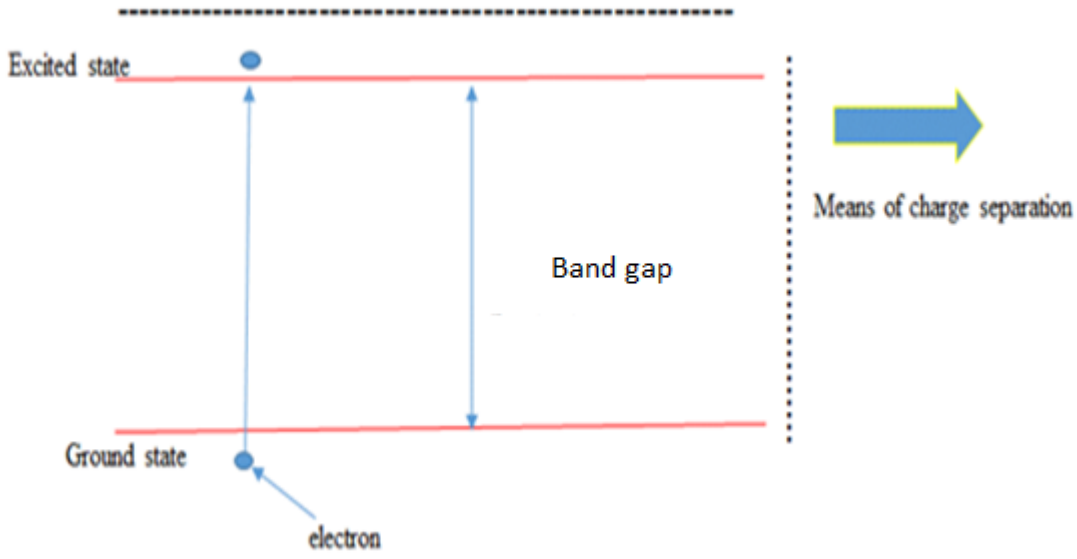

Figure 2.3: Shows three mechanisms requirements of electron charged, electron transport and means of separation

From the system layout above, electrons are excited across the band gap of a semi-conductor and charge separation is achieved by a charged p-n junction between layers of semi-conductors of different electronics properties. The application of this is only in solid state p-n junctions. Also, the application of this principle is equally to other types of photo-converters based on other types of junctions. The understanding of semi-conductors' interaction with light gives a better idea of how semi-conductor solar cell works.

2.4.2 ***PV/T technology development over decades***

Much research work on the concept of PV/T has been carried out in the last three decades both experimentally and numerically by many researchers [70]. This technology consists of collectors and concentrators. The hybrid photovoltaic/thermal technology collectors' are very useful systems or devices which combine the productivity of electricity and heat simultaneously. Research in this technology in the 1990s has been a global response to the environmental deterioration of the construction industry in the building integrated-photovoltaic (BIPV) options [71]. Depending on the PV/T design, they are classified either as collectors or concentrators type base on the heat removal fluid [70]. In the last decade, different research people have examined the technology which include; Luque A [72, 73], Akbartzadeh A, Wadowski [74] and Hollick. Also, Moshfegh B [75] and Brinkworth [76] all reported that when solar cells were added to the solar thermal metallic cladding panels, the overall efficiency was improved. [77] Akbartzadeh and Wadowski reported concerning concentrators type (C-PV/T) systems where he suggested on a heat-pipe base coolant design that is a linear trough-like system. The cells were vertically mounted toward the end of copper flat pipe having a condenser area and the designed system was for 20x concentration. In a general note, research and development efforts on the PV/T collector systems in the last decades majored on how to improve the cost performance ratio when you put together the PV and solar thermal systems working side by side. Structurally and functionally [55], PVT modules can be very different. The distinguishing factor in the classification of the module is the type of coolant used. It could be water, air, refrigerant and heat-pipe fluid based types. The applied physical structure could determine the classified as Building Integrated, flate-plate and concentrated types. In actual building application project, PV/T air systems were generally adopted in North America and European markets even though the efficiency of PV/T water system was confirmed higher. In Japan, the advantage of PV/T

water over PV/T air was explored so that houses carrying PV/T water were sold commercially in late 1990s but the construction work came to a standstill due to lack of profit making [78].

Presently, the photovoltaic is a commercially and technically matured technology. It is capable of generating and supplying electricity energy in a short and mid-term basis. The total energy so far supplied by photovoltaic installations is 0.1% globally [55] while as at 2011, renewable energy resource contribution globally stands at 13.3% with a notable future high potential [79]. The hybrid solar photovoltaic/thermal system in a general understanding is a combination of both photovoltaic and solar thermal system or components that simultaneously produce electricity and heat using the same integrated system or components [71].

2.5 Photovoltaic/thermal module cooling classification

As earlier mentioned, PV/T modules could be structurally and functionally different depending on the coolant used. These could be refrigerant based PV/T, heat-pipe based PV/T, water based PV/T and air based PV/T.

2.5.1 Heat –pipe based PV/T

Effective heat transfer mechanisms is considered in heat –pipe based PV/T which combines the principle of both thermal conductivity and phase transition. Figure 2.4 shows a typical heat pipe consisting majorly of three components or sections as (1) Evaporated section (Evaporator), (2) Adiabatic section and (3) Condensed section (Condenser) [55].

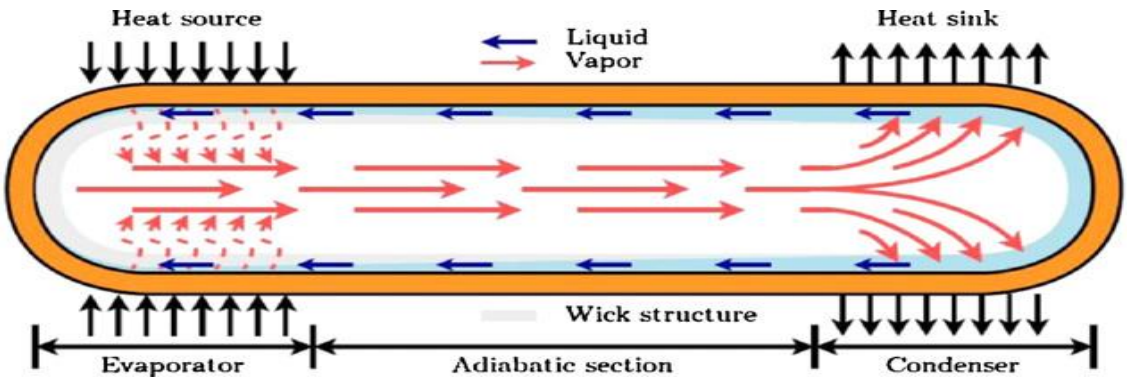

Figure 2.4: Conventional heat-pipe schematic [55] .

This ideally, provides a solution for heat transmission and removal. Recently, studies have been carried out on PV/heat-pipe combination by Zhao Y et al [80-82] where a PV/ flat-plate heat-pipe array was proposed for co-generation of electricity and hot air / water. The photovoltaic layer and flat-plate heat-pipe prototype module was containing numerous micro-channel array acting on the evaporation section of the heat pipes. The condensation section which releases heat to the passing fluid and the heat within the section is condensed due to the heat discharged at the other end. It is clear from his claim that the flat-plate geometry ratio is more efficient because of the excellent thermal contact between the PV cells and the heat extraction devices. This culminated into smaller thermal resistance and higher overall solar conversion efficiency. The PV efficiency in this way could increase from 15-30% on the condition that the surface temperature is controlled to around 40-50°C. The module overall conversion efficiency was around 40%. In a similar way, Qian Jian Feng, Zhang Ji-Li and Zhang J in their separate articles introduced a new concept for building integrated PV/T system using oscillating heat pipe [83]. The façade assembled components or system was designed to transport heat from the concealed PV cell (OHP-BIPV/T) as indicated in Figure 2.5.

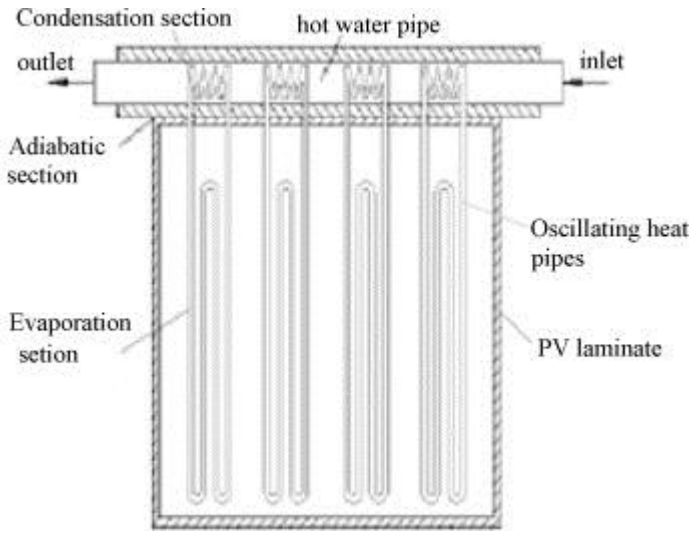

Figure 2.5 OHP-BIPV/T model schematic diagram.[55]

The oscillating heat pipes, headers, finned tube, graphite conductive layer, metal frame, PV laminate module and insulations were what consisted in the system. The working fluid within the metal heat-pipe when in operation will absorb heat from PV cells and be evaporated into vapour fluid. In this way, the vapour will flow up into the finned tube where it is condensed when heat is release to the passing fluid where it then returns back to the absorber by gravitational and capillary forces [55].

2.5.2 *Air Based PV/T*

The air PV/T shown in Figure 2.6 is a solution to PV cooling in which the designed product provides a simple and economical solution where the extracted heat from the module can be used to heat the air by natural or forced flow. The forced air circulation is more efficient than the natural circulation because of the convective and conductive heat transfer, though the net electrical gain is reduced by the additional fan power. The extensive investigation of thermal, electrical, hydraulic and overall performance as performed by Hegazy [84] of four types of flat plate PV/T air collectors and Xing Xing Zhang also. PV/T air type module is usually designed for application of end-users who have demand for hot air, space heating, agricultural/ drying or increase ventilation as well as the electricity generation. Usually with this type of module, air can pass through from top or bottom and sideways. In comparison, PV/T air collectors are not efficient enough with the liquid fluids despite the manufacturing cost of air PV/T collectors being quite low.

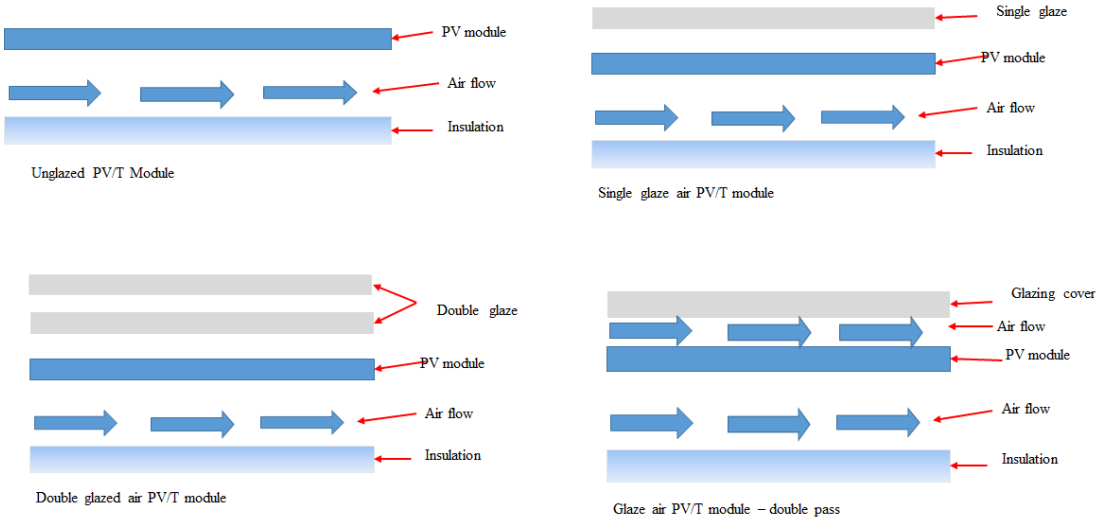

Figure 2.6 PV/T air based modules as adopted [55].

2.5.3 *Water based PV/T.*

The structures of conventional flat plate solar collectors and water-based PV/T are similar. A fixed serpentine or a series of parallel tubes are underneath the absorber which is attained with numerous PV cells that are series or parallel connected. The cooling fluid being water is forced to flow across the tubes and if the water temperature remains lower, the PV cells will be cooled thereby increasing the electrical efficiency. The flowing water will be heated by absorbing the PV heat which will be delivered to certain heat

devices to heating. This flowing water as coolant may be consumed. Alternatively, it may be cooled in the heating services and may equally flow back to the module to regain heat. In comparison to the air-based system, the water-based PV/T systems may achieve the enhanced cooling effectiveness because of the higher thermal mass of water against the air thereby achieving both higher electrical and thermal efficiencies of the systems. In addressing several water flow patterns of PV/T, Zondag [85] included namely; channel, tube, sheet free flow and dual absorber types which are shown schematically in Figure 2.7 [86].

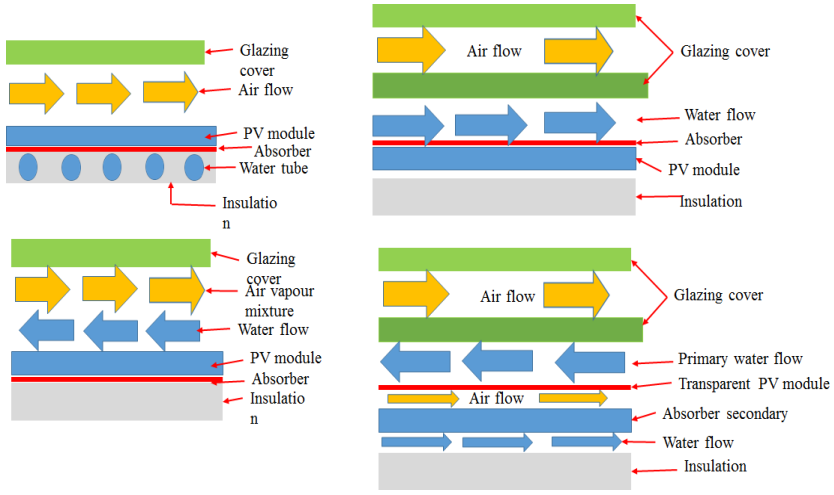

Figure 2.7 Water-based PV/T [85]

2.5.4 ***Advantages and disadvantages of flat plate PV/T collectors***

There are numerous advantages and disadvantages of the photovoltaic and solar thermal technology. The main advantages include: 1) PV/T collectors enables the generation of power and heat using the same system. 2) The flat plate PV/T systems have low maintenance culture. 3) It is a clean technology that is environmentally friendly thereby free from toxic waste and radioactive materials. 4) It has high performance and reliable when radiation is available. 5) Flat plate PV/T systems have highly credible system with life span expectation between 20-30 years. 6) It is a noiseless technology which does not pollute or emits CO_2. 7) In the long run, it is a cheap technology. 8) It saves space compared to PV and 9) It has high efficiency.

The demerits of flat plate PV/T are: 1) This has initial high production and installation cost and expensive. 2) It is non-uniform cooling for instance it need innovative designs. 3) The technology is not suitable for integration with many present

roof systems. 4) It requires larger space for separate systems (heat and electricity). 5) Payback – the system has long payback periods. 6) The system is stochastic in nature.

The PV/T technology is a promising system for low energy housing residential market according to Bakker [87]. Bazilian pointed out [88] that PV/T technology systems are designed especially for low temperature application due to the fact that the combination of both systems must be compromised. The classification of flat plate PV/T collectors are categorised according to the working fluid used. They are mostly applicable as either grid-connected or as standalone systems as it is a more profitable investments when certain conditions are met according to Talavera [89].

2.5.5 *Classification of flat plate PV/T collectors*

Figure 2.8 summarises how PV/T flat plate collectors are classified according to the type of working fluid used. This can be air PV/T collector, water PV/T collector or a combination of air and water flat plate PV/T collectors. Another distinguishing factor is the present of the absorber collector underneath the flat plate. What comprise a complete design of flat plate PV/T collectors include; glazed or unglazed glass cover, encapsulated materials, solar cells, absorber collector and thermal management system.

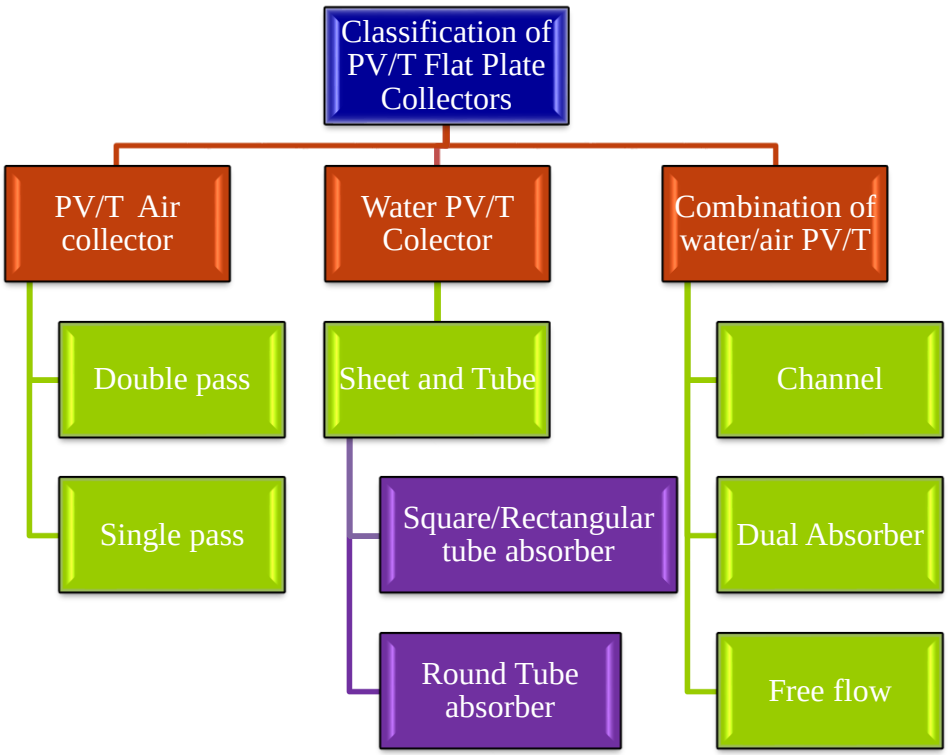

Figure 2.8: Classification of Flat Plate PV/T Collectors

Similarity between the principal classification of PV/T systems and PV system exists as commercially standalone or grid-connected. In the case of grid-connection or utility interactive, parallelism is the system operation and interconnection with the electricity utility grid. The grid connected PV/T systems component is the converter or inverter or the power conditioning unit and thermal storage. The stand-alone are designed to operate independently of the grid utility which sometimes is sized to supply DC or AC electrical load [89].

2.5.6 ***Single pass air collector***

Alfegi et al [90] performed a Mathematical model PVT air collector including PVT with compound parabolic concentrators having fins. Top and bottom sides of the model were concentrated on both sides of the absorber collector to predict the thermal and combined PV/T performance as shown in Figure 2.9.

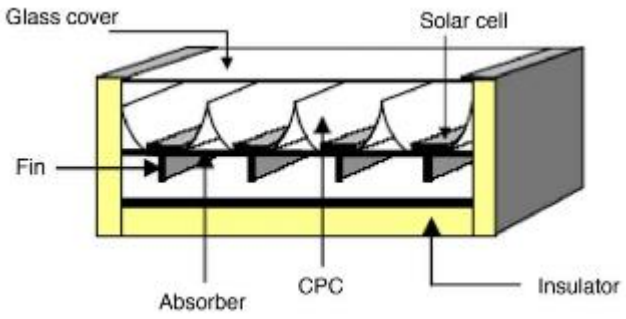

Figure 2.9: Single pass PV/T air collector (PVT) with compound parabolic concentrator having fins cross section [90].

Air is the working fluid that flows between top glasses of the absorber collector to the bottom plate of the absorber. The result using solar irradiance of 400W/m^2 indicates that the combined PV/T efficiency increases 26.6% to 39.13% and the mass flow rate changes to 0.09 from 0.0316kg/s. The comparative study performed to investigate the effect of mass flow rates on efficiencies of electrical and thermal of hybrid collector has been performed as shown in Figure 2.10 having a single pass rectangular tunnel absorber collector design to generate hot air and electricity while the spiral flow has been designed to generate hot water and electricity.

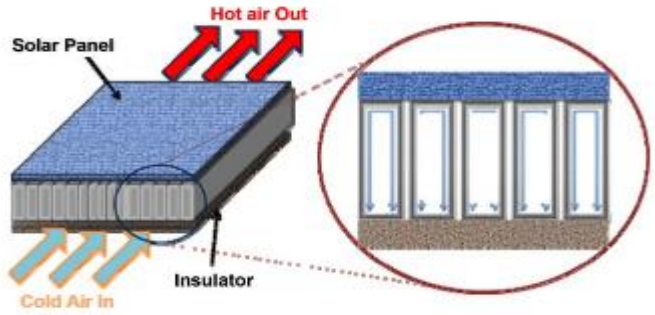

Figure 2.10: PV/T air collector having a rectangular shape absorber collector[91].

The result of the experiment shows that the single flow absorber collector produced a combined 64% PV/T efficiency with electrical efficiency of 11% having a maximum output power of 25.35W while the single pass rectangular tunnel absorber collector has a combined PV/T efficiency of 55% with the electrical efficiency of 10% along with maximum output power of 22.45W.

2.6 Concentrator (PV/T) development and designs

It is desirable for many applications to deliver energy at temperatures higher than those possible with flat-plate collectors. By decreasing the areas from which losses occur, energy delivery can be increased. This happens by interposing an optical device between the source of radiation and the energy absorbing surface. Compared to a flat plate collector at the same absorber temperature, the absorber will have smaller heat losses. Two related approaches are possible. The first one is the use of non-imaging concentrators and the second one is the use of imaging concentrators. There are many designs of concentrating collectors. Concentrators can be reflectors or refractors. Some can be cylindrical or surface of revolution while others can be continuous or segmented. Also, receivers are convex or concave; some are flat, covered or uncovered. Where the geometrical concentration ratio is greater than 2.5, many tracking modes are possible. These forms the approximate factors by which radiation flux on the energy absorbing surface are increased [92].

2.6.1 Overview of concentrated photovoltaic/thermal (CPV/T) development in the last decade

The concentrated photovoltaic and thermal (C-PV/T) use instead of flat plate type is able to increase the radiation intensity on the solar cells. Due to the significantly lower cost of the reflectors relative to the solar cell, this approach is promising. There is much

higher efficiency solar cells though they are more expensive than the flat plate module cell which has higher current that can be used. The complex sun tracking mechanism can attract additional cost [93].When there exist non-uniform temperature across the cell, there will be cell efficiency decrease. The output voltage is increased using series connection but decreases the current with a given power output thereby reducing the ohmic losses. Also, it should be noted that the cell at the highest temperature will limit the efficiency of the entire string. This situation is called the 'current matching problem'[94]. The design of the coolant circuit should keep the temperature low and uniform. The design should be simple, reliable and keep parasitic power consumption to a minimum. There are basically three grouped categories of concentrators with the use of lenses or reflectors. These are; (1) Linear geometry. (2) Single cells and (3) densely packed modules. More concentrator materials per unit cell and absorber area are needed for highly concentrating systems. The advantage of using lenses is more appropriate than reflectors because of their lower weight and material costs. It should however be known that concentrator systems which uses lenses are unable to focus scattered light thereby limiting their usage a different places largely with clear weather. To obtain better electrical output using 'liquid' as the coolant is more effective that using 'air'. For medium to high temperature hot water, for cooling, desalination or other industrial processes, reflector -type C-PVT systems are best. A flat plate collector may give a high efficiency than the concentrator type collector when both are directly facing the sun at lower operating temperatures. When the working temperature gradually increases, then, the performance gap will diminish. The large exposed surface of a flat plate collector incurs more thermal losses at higher temperature differential.

Resell et al in Lleida (at 41.7^{o}C North) of Spain constructed a low concentrating PV/T experiment using a combination of flat plate channel-below PV (opaque) collector together with Linear Fresnel concentrator collector which worked on two –axis system[95]. The combined efficiency result was 60% at a concentration ratio of about 6×. The analysis re-instituted the importance of the cell absorber thermal conduction. In Australia, a combined heat and power solar (CHAPS) collector system was designed and developed for single tracking. The system was linear trough but cooled by water for the row of cells having anti-freeze and anti-corrosive additives flowing in internally finned aluminium pipe. The system was glass-on-metal parabolic reflectors at 92% reflectance. The concentrating ratio was 37x. The light was focused on c-si solar cells (at about 20% conversion efficiency under standard condition) using an aluminium receiver [96]. The

system gave a thermal efficiency of 58%, the electrical efficiency was 11% while the combined system efficiency was 69% under typical operating condition of measurement.

Kribus et al [97] developed a miniature concentrator PV system that can be installed on any rooftop considering the fact that heat cannot be transported over long distances. The solar cell is greatly reduced when he concentrated sunlight about 500 times. The design was similar to a satellite dish but on a small parabolic dish and relatively easy to handle without the use of special tools. The concentrator can be benefited by the good mechanical properties of steel and the high solar reflectance of aluminium because cost reduction can be realised by using laminating thin aluminium foil on steel substrate. Stainless steel parabolic reflectors can have less mechanical support than aluminium reflectors. Here, there is assurance of more even light distribution over the cells which will give better cell efficiency. The solar radiation is asymmetric in high latitude countries like Sweden over the year because of the high cloud coverage during the winter months, hence, concentrated to a small angular of high irradiation. This can attract the use of high economical stationary reflectors or concentrators. Nilson et al [126] carried out a test at Lund University on an asymmetric compound parabolic reflector having two truncated parabolic reflectors that were made of anodized aluminium and aluminium laminated steel accordingly. The changing of the back reflector from anodized aluminium to aluminium laminated steel did not change the energy output in their measurement results. It was also found that the optical cell position should face the front reflector. The achievable result is that there is lowest cost for electricity generation if there is no space restriction. In residential buildings where there is limited roof space, they recommended that the solar cells should be placed on both sides of the absorber as the cost of adding cells to the other side of the absorber is relatively low if a trough with cells on one side of the absorber is constructed. A theoretical study on a two stage hybrid device that involves solar cells working with an energy flux concentrator having a heat –top-electrical/mechanical energy converter was presented by Vorobiev et al [98, 99]. In this study, two possibilities were explored as follows;

1. System with separation of "thermal solar radiation" and

2. System without solar spectrum division and solar cell operating at high temperature.

The result shows that the total conversion efficiency is around 35-40% with a concentration of 1500× as in the first case. With the use of GaAs base single junction cell

having room temperature efficiency of 24% as in the second case was subjected to concentrated sunlight using a concentration ratio of 50x. The energy conversion in total was between 25-30% and can be improved further by using a higher concentration ratio.

2.6.1.1 *Cooling application in building integration*

Recently, cooling has been applied to building installation and to PV concentrators earlier [100]. The parameters that affect the total electrical and thermal energy output in PV/T hybrid systems includes; the heat extraction mode, the solar energy input, the operating temperature of the system parts, the wind speed and the ambient temperature. The drop of electrical efficiency is as a result of the solar radiations increasing the temperature of the PV modules because not all are absorbed. There are various technologies of solar thermal energy collectors [101] which are special kinds of heat exchangers that convert solar radiation into thermal energy using a transport medium or fluid movement with different technologies. We cannot understate the huge demand of electricity and heat in industries, countries and institutions for different application of air-conditioning systems, building integration photovoltaic/thermal (BIPVT), water desalination, solar cooling, solar heat pumps and solar greenhouse. Since industries needs indicate high demand for electricity and heating, this requirement could be met using hybrid PV/T for this energy increasing demand as demonstrated by USA 503MW and Saudi Arabia intending 41GW [102]. The PV/T systems have a life span between 20-30 years and a negligible maintenance cost [103, 104]. Much detailed work in theoretical modelling of PV/T collectors have been developed showing how electrical and thermal outputs are related. In performance comparison of a combined PV/T collector with conventional PV/T systems, there is increase solar energy conversion and potential cost benefits [105]. Not much work has been done in the field of medium to high concentration PV/T collectors. This may be due to the demand of tracking the sun and achieving effective cooling of the cells and also non-uniformity in flux distribution. The spectral beam splitting is the only one concept that reduces the heat flux on cells and permits or allows high temperature application.

2.6.2 ***Review of photovoltaic/thermal hybrid technology***

Hybrid photovoltaic/thermal is a system by which two technologies are matched together to produce both electricity by the PV and heat by the thermal in the same system. It seems to be a logical idea to develop a device that can comply with both demands since

the demand for solar electricity and solar heat are always supplementary. The solar photovoltaic cells use a fraction of the incident solar radiation to produce electricity and the balance is turned into waste heat majorly in the cells which increases the cell temperature of the PV. As a result, the efficiency of the module diminishes. Part of this heat is recovered by the photovoltaic/thermal technology and uses it for practical applications. The electrical efficiency is maintained at satisfactory level by the simultaneous cooling of the PV modules; hence the PV offers a better way of putting to use solar energy with higher overall efficiency. PV/T integration has many alternative approaches. These include; water or evaporator collector, there can be selection among air types, polycrystalline/ mono crystalline/amorphous silicon (pc-si/c-si/a-si) or thin film solar cells, concentrators or flat plate types, natural or force fluid flow, glazed or unglazed panels, building- integrated or stand-a-lone features and so on. In the past decade, research and development work has been done in PV/T technology which has a gradual increase in the level of activities [106].

2.6.3 ***Designs contributions in concentrators technology***

A higher degree of temperature is required of concentrating photovoltaic systems to operate than flat plate collectors. The rejected heat collecting by CPV system brings us to CPV/thermal systems. The system is providing both electricity and heat. CPV/T use in conjunction with concentrating reflectors that has significant potential to increase the power production from a specific solar cell area. Research is going on presently in the development of CPV/T reflectors for more electricity and heat generation. Many researchers in the past and now are working to bring the multipurpose hybrid system to fulfil the ever-increasing demand of both thermal and electrical energy and protect the environment for future generation.

In 2005 [108], Hjothman et al designed and experimented a double pass photovoltaic thermal solar air collector with CPC and studied the performance over a range of operating conditions. The studied CPC absorber of the hybrid photovoltaic/thermal (PV/T) collector consists of an array of solar cells for generating electricity using compound parabolic concentrator (CPC) to increase the radiation intensity falling on the solar cells and fins attached to the back side of the absorber plate to improve heat transfer rate to the flowing air. There are seven basic components of the set up experiment as follows; (1) Double pass photovoltaic/thermal solar collector. (2) The temperature measurement system. (2) The wind speed measurement system. (4) The

air flow measurement system. (5) The current measurement system. (6). The data acquisition system and (7) the solar radiation measurement system. The experimented results showed that electricity production in a PV/T hybrid module decreases with increase temperature of the airflow. This by implication means that the air temperature should be kept as low as possible. Alternatively, the system should deliver hot air for other purposes. It is necessary that there should be a trade-off between maximum electricity and production of hot air at reasonable high temperatures. Therefore, the PVT, CPC and fins' simulation of the hybrid system used have a potential significance increase to the power production and reduction of the cost of photovoltaic electricity.

The author of ACPPVC [109, 110] designed, constructed and experimented a prototype of an ACPPVC for building facade integration in the UK as shown in Figure 2.11.

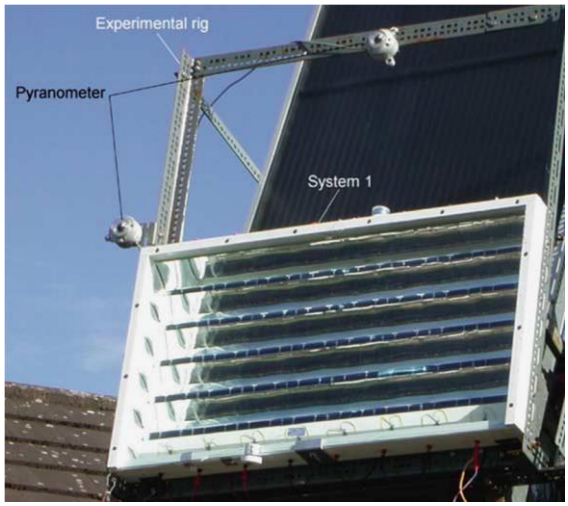

Figure 2.11 Design ACPPVC for building façade integration in the UK [111]

The electrical and thermal characterisation analysis of the ACPPVC based on measurements recorded for a period of 10hrs for 20 days duration. He removed the reflector system from the PV panel in order to provide a non-concentrating PV panel for the purpose of comparing against the concentrator panel. The active solar cell was the same in the two cases. The experimented results indicated that the power produced by the ACPPVC was 1.62 times that of the power generated by the flat PV panel. The power increase is 2.0 theoretically which is 18% higher than the experimental measured value. This implies that this reduction is due to the series resistance between the tabbing wires of the individual solar cells. Even though the power increased by a factor of 1.62, it was discovered that the aluminium back plate temperature of the concentrator panel was

higher than that of the flat panel by 12^0C. The designed, constructed and experimented work achieved approximately 8.5% electrical efficiency by the flat system compared to 6.8% achieved by the ACPPVC having 65% fill factor [112]. A novel miniature concentrating Photovoltaic (MCPV) was designed and analysed [113] as shown in Figure 2.12

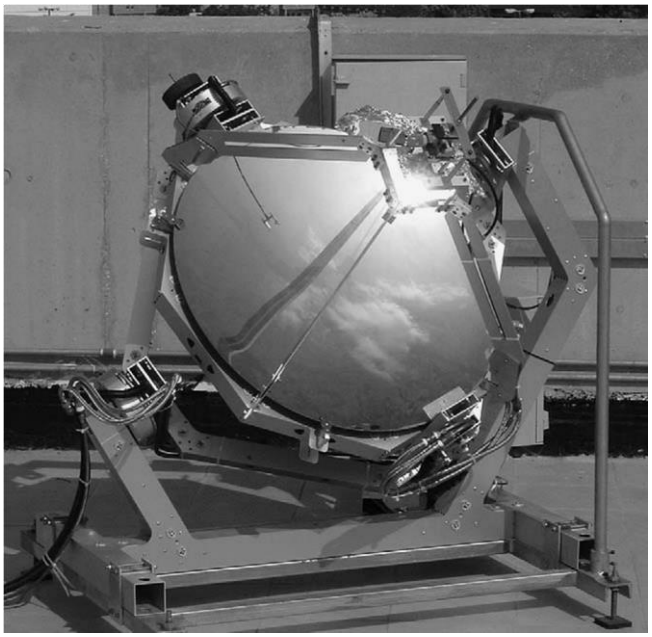

Figure 2.12: The novel designed miniature concentrating photovoltaic/thermal systems [114].

The MCPV/thermal system produced about 140-180W of electricity and 400-500W of heat. Not like the Photovoltaic/thermal (PV/T) collector, the MCPV derived heat is not limited to the low temperature applications. It can operate over a wide range of temperatures to provide thermal energy which is applicable for water heating and also for desalination, cooling and industrial heat process. The result of the MCPV was analysed and the system performance indicates that at elevated temperatures, the electrical efficiency is lower while most of the lost electricity is recovered as heat. The MCPV system is best installed very close to the consumer where both the electrical and thermal multiple energies are needed. In the increasing demand of energy with clean environment, the result shows that the new approach has great promising prospects.

The author of PRIDE [115] designed and fabricated a low concentrating second generation PRIDE concentrator shown in Figure 2.13. The second generation PRIDE concentrator was made using low cost dielectric materials with 6mm wide solar cells having a geometrical concentration ratio of 2.45. The novel design had an injection

moulding technique to manufacture large volume low photovoltaic concentrator most suitable for building façade integration. From the electrical investigation performance, a single PRIDE concentrator module produced power output of 78W using 1000Wm^{-2} incident solar radiation intensity. There was a fabricated similar non-concentrating panel for output power comparison. It was discovered that the 2nd –G PRIDE system achieved a maximum power ratio of 2.01 for a range of incident solar radiation intensities having electrical conversion efficiency of 10.5%. He concluded that the new design being the 2nd–G PRIDE concentrator possesses increased durability compared to the first generation PRIDE concentrator which predicts 40% reduction in cost over similar non-concentrating systems.

Figure 2.13:Designed and fabricated second generation dielectric PRIDE concentrator photovoltaic module [116].

The author of 3-D SEH concentrator [117] designed a new 3-D concentrating photovoltaic for a stationary solar concentrator that will be compact enough to incorporate into BIPV and more precisely into transparent facades and roof or window shown in Figure 2.14. He proposes an innovative idea for solar powered doubled glazed windows with integrated photovoltaic (WICPV). The designed novel was non-imaging stationary 3-D solar concentrator (SEH) filled with dielectric materials. It was working on Total Internal Reflection. The model was designed, and optically studied. The results from the experimental studies provided clear validation of the optical model developed using ray tracing techniques. The overall result promoted the use of the stationary SHE and also

made it attractive for the used in transparent facades and roofs in buildings. It requires no tracker. It maintained the natural lighting of the building space and thereby reducing the general cost and allowing access to solar energy.

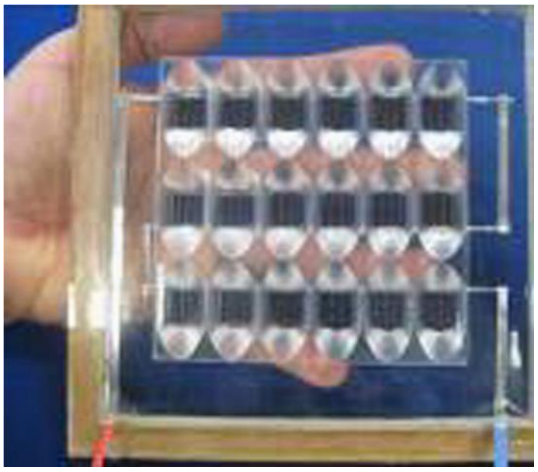

Figure 2.14: Transparent window CPV module [118]

The experimental and numerical study by the author [119] on non-concentrating and symmetric unglazed compound parabolic photovoltaic concentration systems shown in Figure 2.15 presented the evaluation performance of the flat PV-string and PC-CPC systems. In his comparative analysis of the two systems without and with cooling of the PV cells, the results indicate that cooling the PV cells significantly enhanced the power output of the system.

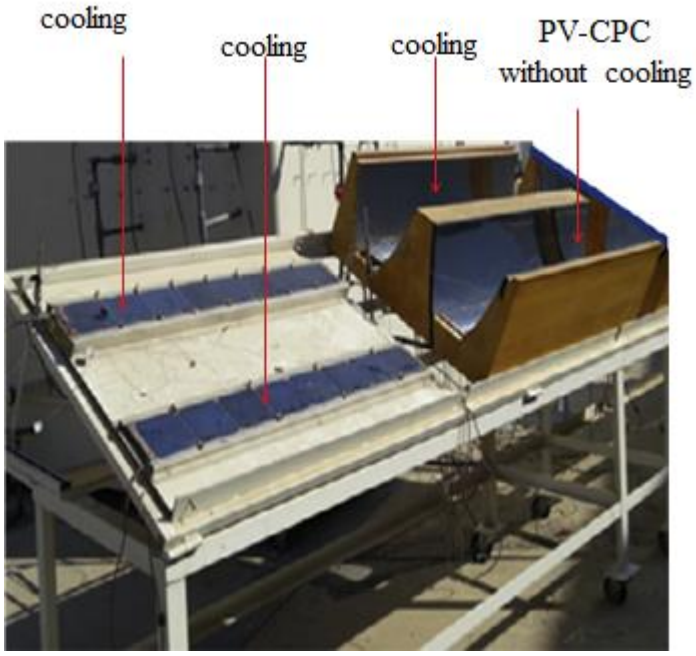

Figure 2.15: Designed PV-CPV [1]

The maximum power output of the PV-CPC system with cooling is approximately 34W which is about twice the power output in the absence of cooling. It was found out that the power output of the PV-CPC system is much higher than that of the PV string without and with cooling by 23% and 39% respectively. There is good agreement when numerical and experimental data are compared. It was also found out that the maximum percentage differences between numerical and experimental power output for the PV with and without cooling, are 5% and 7% respectively.

An optimal orientation of PV/T collector with reflectors was designed by Kostic at el [120]. For more electrical and thermal energy, flat reflectors for solar radiation have been mounted on PV/T collectors. They designed the reflectors with the movable PV/T collector system. The electrical and thermal efficiency of PV/T collectors with and without reflectors in optimal position have been calculated in this work. The total saving efficiency and energy efficiency of PV/T collectors have been determined using the experimental results. The without reflectors energy-saving efficiency PV/T collector was found to be 60.1%. This is significantly higher than for the conventional solar thermal collectors. Adversely, the energy-saving efficiency for PV/T collector with reflectors in optimal position is 46.7%. This is almost equal to the thermal efficiency of a conventional solar thermal collector. From the foregoing, the energy-saving efficiency of the PV/T collector decreases slowly with the solar radiation intensity concentration factor.

At Australia in 2005, a parabolic trough photovoltaic/thermal collector with a concentration ratio of 37× was designed by Coventry at ANU. The ANU CHAPS collectors for the thermal and electrical efficiencies are shown during ideal conditions. When compared with a flat plate thermal collector, it indicates that the CHAPS collector has a lower efficiency at temperatures near ambient due to optical losses. Due to the much reduced surface area, it does not suffer the rapid increase in thermal losses as the operating temperature increases. The experiment result when measured under typical operating conditions revealed the thermal and electrical efficiencies are found to be 58% and 11% accordingly, hence a combined efficiency of 69%. It is significantly high enough [121].

2.7 Recent appreciable progress in concentrating photovoltaic technology

Despite the required further research in CPV systems, there is yet a noticeable increasing solar efficiency. CPV technology is highly promising not only to increase the amount of power generation but to also reduce the cost of the overall system. Its reduction

raw materials intake required for manufacturing and recycling improvement allows it to be economically feasible to be used for various applications. Kurtz S. and Geisz J [122] in their recent paper underscored the benefits of using CPV. The basic components of a CPV system is made up of 1) Concentrator solar cell, 2) thermal dissipating heat system, 3) an optical system which could be refractive or reflective, 4) tracking mechanism and 5) a supporting system or casing frame. The effective output performance of the CPV system hinges on how individually or corporately these components perform [123]. Through the huge investment in solar concentration, CPV is viewed to be one of the most effective ways of trimming down the overall energy generation cost by the use of 1) Parabolic trough [124], 2) Parabolic dish [125, 126], 3) Fresnel lenses [127, 128], 4) Compound parabolic concentrators [129, 130], 5) V-Groove mirrors [131, 132], 6) Refractive Prism [133, 134], 7) Luminescent glass [135-137].

The key driver in CPV research and technology is to make CPV more cost effective on Levelise cost of electricity level and to achieve high efficiency. Therefore, most of the effort made in research aims at increasing the efficiency of the solar cell and module at all levels. Figure 2.16 shows the increase in efficiencies since 2000. It also shows the progress made by research and development for CPV modules with expectations. The expectation of European Photovoltaic technology platform in 2011 is indicated as the trend line [138]. There are potential and significant higher efficiencies being expected and foreseen. Due to the facts mentioned, the European Commission in 2014 presented the plan integration roadmap while in September 2015, presented a new integration strategic energy technology plan for the acceleration of the transformation of the European energy system. Furthermore, to this, the European Photovoltaic Technology Platform and the Solar European Industry initiative are merged to become operational in January 2016. The new body, European Technology and Innovation Platform Photovoltaic (ETIP) is charged with the scope to focus and cover areas of

- Market development and competitiveness
- Research and Innovations
- Industry policy and
- Education

The ETIP PV will also focus on activities on the opportunities and challenges facing the European PV industry with a view to improving the competitiveness of the European PV industry in the feedstock supply, equipment manufacturing, cell and module production

and providing technical solutions for grid integration, market solutions and installation [139].

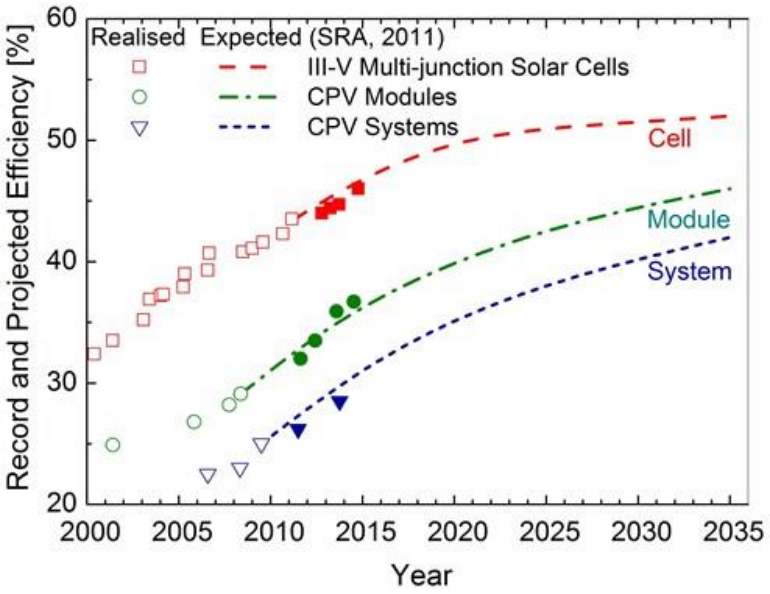

Figure 2.16 III-V multi-junction solar cells and CPV modules development record efficiencies [138]

2.8 Compound parabolic concentrators (CPC) applications

Compound parabolic concentrator is specially designed in a shape of two parabolas for solar collecting. It falls within the family of non-imaging concentrators. It is considered among the collectors having the highest possible concentration ratio. It is designed to be a stationery solar collector. CPCs have a relatively high temperature operation with high cost effectiveness. The most potentially favoured option for solar power to pursue conventional sources is the CPC. The temperature rise which affects the conversion efficiency is threatening the technology. An increase in operational temperature will correspondingly decrease the solar efficiency. For the electrical efficiency to be improved, proper cooling of the solar cell is mandatory. Heat extraction is then very necessary. This thesis seeks to address researches on compound parabolic concentrators in solar power generation application. The basic concept, principle and design of CPC are covered. Thermal and optical models of CPCs are also considered. The thermal application of CPCs and challenges are also included**.**

2.9 Requirement to increase solar cells efficiencies by heat extraction method

Through the means of heat extraction using fluid streams like air, water, the PV cells are cooled thereby improving and increasing the electricity yield. It is conceptually better to design how to re-use the extracted heat energy by the coolant. This will improve the energy yield per unit area of the panel or in the building integration installation the facade. This is where the PV/T hybrid solar technology system is involved. Therefore, PV/T hybrid technology is a combination of photovoltaic and solar thermal components into a module that will increase the solar conversion efficiency of the module thereby making the best economic use of the area. Simultaneously, the PV/T module can both generate electricity and heat. The PV/T technology is developed for the most purpose of removing the accumulated heat from the PV for the purpose of electricity generation. The technology also allows the PV cooling for the purpose of increasing electrical yield or efficiency. The PV/T hybrid system represents a new direction for renewable generation of power [140].

2.10 Compound parabolic concentrators' geometric optics

2.10.1 ***Principle***

Compound parabolic concentrators optical performance is dependent on geometric design and properties of material used in the manufacture of collectors, reflectors, and in some designs, covers. In general, the geometric characteristics are represented by geometric parameters which include, 1) acceptance aperture area, 2) receiver area, 3) concentration ratio and 4) acceptance angle [141]. Figure 2.17 shows a typical CPC for all the parameters as proposed by R. Winston [142-144].

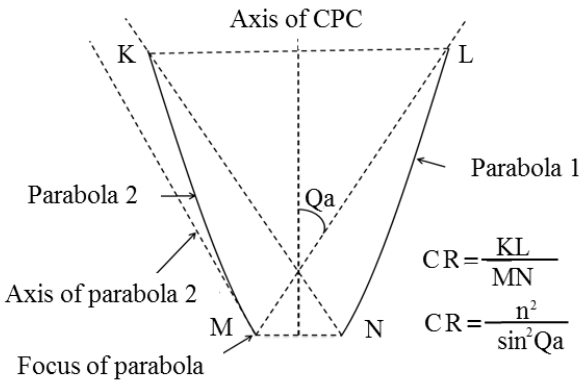

Figure 2.17: An early type of CPC configuration

There are two parabolic reflectors involved here. We have parabola 1 and parabola 2. These formed an aperture area at the top and exit area at the bottom where the solar incident flux is received. This also is called a receiver area where the incident solar radiation is absorbed. The two symmetric reflective parabolas can be truncated and rotated about the CPC axis. Reflective parabola 1 has tangential line at the edge to the perpendicular to the aperture surface and same situation to reflective parabola 2. Figure 2.17 above is called full CPC. The bottom edge of reflector parabola 1 is the focal length of reflective parabola 2. All the rays parallel to the axis of parabola 2 will be reflected to its focal point. This is the same with parabola 2 as well. The acceptance half angle of the CPC is denoted by Q_a. By the principle of light reflection, any rays within the acceptance angle will reach the receiver at the end. The concentration ratio CR is the ratio of the aperture area to the receiver area. The authors proved this concept [144]. The ideal concentration ratio for two-dimensional CPCs can be calculated using equation 2.5, as the inverse of the sine of the acceptance half angle.

$$CR = \frac{1}{\sin Qa} \qquad 2.5$$

In the case of three-dimensional CPCs, the ideal maximum concentration ratio is the inverse of the square of the sine of the acceptance half angle as denoted in equation 2.6 .

$$CR = \frac{1}{\sin^2 Qa} \qquad 2.6$$

In general the acceptance half angle varies from 3° to 90°, also the concentration ratio of most CPCs falls between 1- 10 which is lower than the concentration ratio of tracking concentrators [145].

2.10.2 ***CPC design***

In CPC design, we have the hollow CPC and the dielectric CPC. The design principle of collecting sunlight in both is the same. In this thesis, we are considering the hollow compound parabolic concentrator.

2.10.3 ***Hollow CPCs***

The hollow CPC is a well-known design in non-imaging optics by now. It is a 2D concentrator. If no limit is placed on the direction of the output rays of a hollow CPC

having acceptance angle of Q_a, then the concentration ratio (CR) = $\frac{1}{Sin\ Q_a}$ is the maximum achievable in theory. To use the hollow CPC as a stationery concentrator, the acceptance aperture region must be sufficiently large to accommodate the area corresponding to the sun's direction during the desired collecting time. By using hollow CPCs as stationery concentrators, it is practically impossible to get twelve hours per day [146].

2.10.4 ***Dielectric optics***

Dielectric CPCs are well known. The best method to increase the concentration of a hollow stationery CPC is to fill it with dielectric medium that has a refractive index of n>1. The expectation is that, the concentration of the CPC has increased by a fraction of n being that the CPC has a 2D structure. It is noted that the effective concentration has increased more than just n times. The theoretical maximum concentration of dielectric CPC can be n^2 times higher instead of just n times. The extra enhancement is related to the increased acceptance of the skew rays as the direct reason its property was first derived by the author [147].

2.10.5 ***Edge ray principle***

The geometry of CPC design can be approached using different methods. The most popular is the edge ray principle [148] CPC in solar thermal. From the edge ray principle, any rays from the rays that are enclosed by the edge rays of the source will reflect to the solar receiver. This implies that also reflecting rays entering at the maximum angle shall be tangential to the surface of the absorber. The principle holds for any convex shape or receivers. CPCs of 2D developed using the edge ray principle do achieve maximum concentration ratio as pointed out in equation 2.1 [145, 149]. The figure 2.17 above is a two dimensional CPC showing profiles that corresponds to flat absorbers. By the edge ray principle, all the rays incident on parabola 1 with incident angle $Q_a$are reflected to focus M, the edge of the absorber surface and vice visa for parabola 2.

2.10.6 ***CPC modification***

Some modifications are made for particular purposes in addition to the basic designs. The very common modification is truncation.

2.10.7 *CPC truncation*

The compound parabolic concentrators in their original nature are that the parabolic surface is very tall when it is compared to the scale of the collecting aperture. This requires a lot of materials to build it. The challenge is even worse with dielectric CPCs. The reason is that the inside must be filled with solid dielectric medium. This becomes heavy and bulky and it is not only hard for installation but high cost in manufacturing and materials. By truncation it means to cut off the upper part of the CPC. By the truncation principle, the CPC gives up very little concentration in exchange for a considerable reduction of the height of the parabolic surface. As materials are reduced by removing the part of the entrance aperture end, the cost of the CPC is lowered. This trade-off is economically preferred [145, 148, 150].

2.10.8 *Total internal reflection*

Another trade-off issue with the dielectric CPC is the issue of cost and consideration. The dielectric CPC may require reflective coating on the parabolic surface close to the bottom. This requires an extra manufacturing process with material cost. The extra cost can be removed by using the CPC having total internal reflections (TIR). Here, we can also see that the price paid is a very slight reduction in concentration [142].

Some authors in 1975 and 1976 quantified and presented the influence of truncation on concentration ratio [110]. An author in 2004 also made a mark in truncation to get a remarkable geometric concentration ratio [151]. Therefore, loss in concentration ratio is insignificantly small for useful truncation.

2.10.9 *CPC height tolerance analysis*

In August 2010, Optisworks in their white paper concerning Solar CPC modelling released a tolerance analysis which provides a tool that will help the designers to make a balance decision. Figure 2.18from the left side below indicates that the truncated CPC height is defined as the tolerance variable and the total flux on the detector which is also defined as the tolerance analysis target.

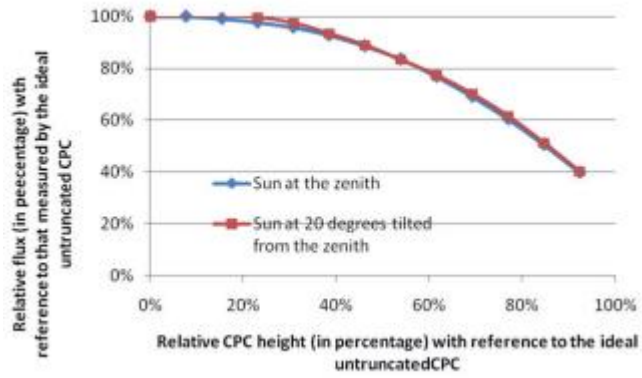

Figure 2.18: Impact of CPC height on the flux collection efficiency [151].

At each sample point, the analysis process will automatically sample a user-defined variable range and simulate the total flux. Also from the right of Figure 2.18, we could see the impact of relative CPC height on the flux measured by the detector with the sun position at 0° (meaning the blue curve in Figure 2.18 above) and 20° (meaning the red curve) at the Zenith .The truncation percentage and the flux attenuation percentage are both referred to the original un-truncated CPC. Between the two curves, a similarity indicates that the impact of CPC height on flux is consistent at different sun positions within the designed incident angle. Using the information provided in Figure 2.18 will help designers make trade-off decisions in conjunction with their own specifications. From the above as an example, if 15% flux loss reduction is acceptable, then the CPC can be truncated as much as 50% from its original height [54, 152, 153].

2.11 Compound parabolic concentrator modelling

Modelling of compound parabolic concentrators in solar thermal application is majorly targeted at collecting heat from solar radiation. To do this, three aspects are involved. 1) Optical modelling, 2) Thermal modelling and 3) Integrated modelling. From the foregoing, there are many constructed optical, thermal and integrated models carried out by many researchers to investigate compound parabolic concentrators performance [154].

2.11.1 ***Optical modelling***

To design the geometry of non-imaging concentrators, many methods can be used. The most widely used are three. These are Integral design methods, edge ray principle method and flow-line method. Analytically, the optical performance for a complex 3-D

geometry cannot be determined. Therefore, a detail ray tracing simulation is required so that the optical performance can be determined [110, 115, 155]. There are majorly two things achieved when using optical modelling. These include; Energy between absorbers, reflectors, covers and envelopes is simulated and the desired parameters such as optical efficiency and intercept factor that gives the solar flux distribution in the absorber direction. Ray tracing is the most efficient and widely used technique to investigate optical performance of any optical device.

2.11.2 ***Optical efficiency simulation***

In order to predict the power output of the SRCPC module during the outdoor conditions, it is necessary to simulate the optical efficiency for different incident angles in different locations for different solar azimuth angles because of the fact that the sun moves in different planes throughout the day. For the different radiations, the optical efficiency needs to be calculated as the SRCPC during the outdoor conditions is expected to collect both direct and diffuse radiations.

2.12 Incidence and azimuth angle calculations

The angles of incidence of the Sun rays calculations on the SRCPC require understanding of solar geometry. The geometry describes the relationship between the earth and the sun. Furthermore, it is the relationship between the product of the sun, solar radiation and any location on earth. This refers to relationship with incoming beams of solar radiation and a plane of any particular orientation. It is represented by the position of the sun relative to the plane. The sun's position in relation to the orientation and position of the entry aperture of the SRCPC are described below. Their conventional angle symbols [156] are represented in the calculations below.

Hour angle: It is denoted by ω as the angular displacement of the sun east or west of the local meridian due to rotation of the earth on its axis at 15^{o} per hour being negative (-) in the morning and positive (+) in the afternoon**.**

Latitude: It is the angular location north or south of the equator and it is positive northward lying $-90^{o} \leq \phi \leq 90^{o}$**.**

Declination angle: It is the angular position of the sun at solar noon when the sun is on the local meridian with respect to the plane of the equator. It is positive northward and lies -23.45º ≤ δ ≤ 23.45º.

Surface azimuth angle: This angle is the deviation of the projection on a horizontal plane of the normal to the surface from the local meridian with zero due south. It is negative eastward and positive westward and in range -180º ≤ γ ≤ 180º.

Slope angle: It is the angle between the plane of surface in question and the horizontal; 0º ≤ β ≤180º.

Solar azimuth angle: This is the displacement angle from south of the projection of beam radiation on the horizontal plane. The displacement west of south is positive and east of south is negative.

Zenith angle: This is the angle between to the vertical and the line to the sun, for instance the angle of incidence to the beam radiation on a horizontal surface denoted by θ_z.

Solar altitude angle: It is the complement of the zenith angle, for instance the angle between the horizontal and the line to the sun.

Angle of incidence: The angle of incidence is represented by θ and it is the angle between the beam radiation on a surface and the normal to that surface. To calculate the angle of incidence θ using the approximation equation by Cooper [157] as shown;

$$\cos\theta = \sin\delta \times \sin\phi \times \cos\beta - \sin\delta \times \cos\phi \times \sin\beta + \cos\delta \times \cos\phi \times \cos\beta \times \cos\omega + \cos\delta \times \sin\phi \times \sin\beta \times \cos\omega. \quad 2.7$$

From the optimum angle calculation, the slope angle β being the angle of inclination of the SRCPC to the horizontal is 28.6º while the latitude of Penryn ϕ = 50.17º, The angle between the sun passing the highest level and the equatorial plane (north positive) is the declination angle. This angle is calculated using another Cooper equation [157] and [158].

$$\delta = \sin^{-1}(\sin 23.45°)\ \mathrm{Sin}\ (0.986(n_{day} - 81))) \quad 2.8$$

(Where n_{day}= number of day in the year). Therefore, δ = 22.9°.

In order to calculate the the hour angle, it is best calculated from the solar time, ω = 0 when the sun is at the highest level for instance at 12pm solar time where each hour corresponds to a length of 15º. The hour angle is counted negatively in the morning ant positive in the afternoon. To illustrate further, ω = -45º occurs at 9am while ω = 30º occurs at 2pm.

There is a slight difference between the Local Time (LT) and the Local solar time (LST). The angles on incidence are calculated at Local solar time but and interestingly the generated power by the SRCPC is measured and recorded using the local time. Duffie and Beckman [156] gave the equation of LT as a function of the LST as

$$LT = LST - 4\boldsymbol{L_{ST}} - \boldsymbol{L_{LOG}} + E \qquad 2.9$$

Where; L_{ST} is the standard meridian for local time zone where Penryn the site of this experiment is $L_{ST} = 0º$. L_{LOG} is the longitude of Penryn, $L_{Log} = -5.10ºE$ is the equation of time in minutes which is written as :

$$E = 229.2(0.000075 + 0.001868CosB - 0.032077SinB - 0.014615Cos2B - 0.04089sin2B). \qquad 2.10$$

$$\text{Where } B = (\boldsymbol{n_{day}} - 1)0.986 \qquad 2.11$$

The angles of incidence on the SRCPC model is calculated using the detailed equations above as installed on the 2nd floor of ESI building in University of Exeter, Penryn Campus. The lower the incidence angles, the better for the SRCPC model in terms of higher optical efficiency.There is the requirement to calculate the solar azimuth angle γ because it determines the horizontal section plane of the modeled SRCPC where the angle of incidence is located. It can be calculated using this equation [156] ;

$$\gamma = \sin\omega \times \cos^{-1}\frac{\text{Cos}\,\theta \times \text{Sin}\,\phi - \sin\delta}{\text{Sin}\theta \times \text{Cos}\,\phi} \qquad 2.12$$

Where $\text{Sin}\,\theta = \text{Sin}\delta\text{sin}\phi + \text{Cos}\omega\text{Sin}\delta\text{Cos}\phi$

The final calculations for the modelling of the power generated by the outdoor SRCPC model is largely contributed by these imperative equations. The optical efficiencies of the SRCPC for the incidence angles in all the vertical section planes as earlier mentioned must be calculated.

2.13 Optical efficiency simulation for different solar azimuth angles

The solar azimuth angles and incidence angles are both calculated from equations (2.12) and (2.7) accordingly. It is worth to note that when the solar azimuth angle $\gamma = 0^{o}$, the angles of incidence are located in the plane perpendicular to the SRCPC entry aperture. Therefore it suffice to say that the indoor study was primarily meant to validate the optical model, hence using -90^{o} or 90^{o} was sure enough for the process of optimisation. In this application a light source with different angles of incidence at different azimuth angles is used between $-90^{o} \leq s \leq 90^{o}$. For the fact that the SRCPC is to be tested in outdoor conditions, the light spectrum emitted by the light source is changed to air mass (AM 1.5) in the simulation [159].

2.13.1 ***Ray tracing***

Ray tracing in compound parabolic concentrators allows rays through a system of reflecting surfaces. Light follows the reflection law in all optical systems. Ray tracing is developed and widely used as a tool to analyse geometric optical properties in CPC by applying the law of reflection. Ray tracing has been the best way to trace the path of light

2.14 The theory of photovoltaic cell and its characterisation

For characterizing the electrical behaviour of a solar cell or a photovoltaic PV module, the single diode model or one exponential diode model is mostly used. The reason is that the theoretical curve generated by this model fits the real

Current and voltage (I-V) characteristics of most of the PV modules with very good accuracy[160]. The electrical behaviour of the PV module can be precisely predicted for any conditions of irradiance and temperature when the five parameters of the model can be extracted conditions of irradiance and temperature.

2.14.1 ***I-V characterization theory***

Photovoltaic cells are usually modelled as a current source in parallel with a diode. In the absence of light present to generate any current, the photovoltaic cell acts like a diode. At the instance of focused solar intensity incident increase, the photovoltaic cell generates current. This is shown in Figure 2.19.

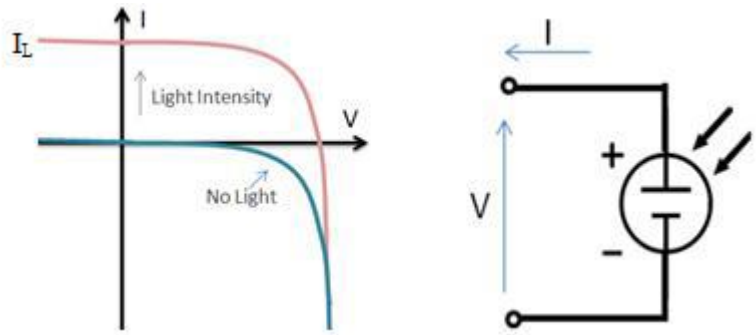

Figure 2.19: Associated electrical diagram of I-V curve of photovoltaic cell[161]

2.14.1.1 *Ideal PV cell*

Usually, in an ideal photovoltaic cell, the total current (I) is equal to the current I_t generated by the photoelectric effect minus the diode current (I_D) using the equation

$$I = I_t - I_D\left[e^{\frac{qV}{kT}}-1\right] \qquad 2.13$$

Where q is the elementary charge = 1.6 $\times 10^{-19}$coulombs, k is the Boltzmann constant, T is the cell temperature in Kelvin and the measured cell voltage that is either produced in the power quadrant is V. A two diode model is more accurate but for simplicity, our concentration will focus on single diode model [161].

2.14.1.2 *Simplified circuit model*

Figure 2.20 illustrates the simplified equivalent circuit model for a photovoltaic cell using a single diode model. The simplified equivalent circuit model is known as the associated equation as shown below where R_s is series resistance, R_{sh} is shunt resistance and n is ideality factor.

$$I = I_t - I_D\left(\exp^{\frac{q(V+IR_S}{n.k.T}} -1\right) - \frac{V+IR_S}{R_{SH}} \qquad 2.14$$

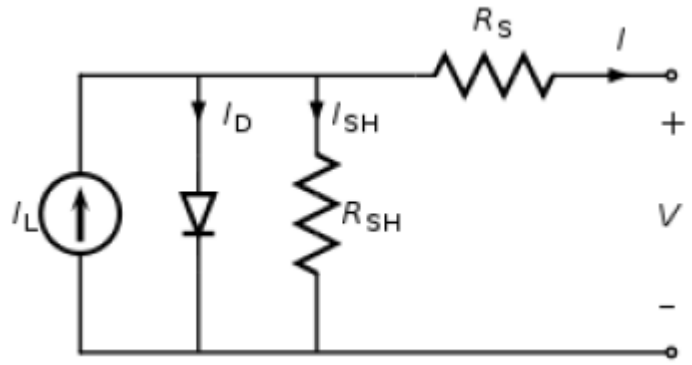

Figure 2.20: Simplified equivalent electrical circuit of a photovoltaic cell (Single diode model)as adopted [160, 162]

2.14.1.3 *Short circuit current (I_{sc})*

When a photovoltaic cell is illuminated, the I-V curve has a shape shown in Figure 2.21.

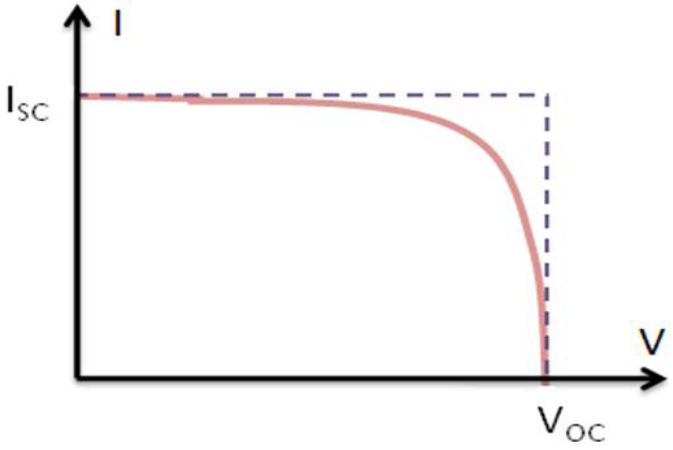

Figure 2.21: I-V Sweep curve illuminated

The voltage across the measuring load is swept zero to V_{oc}. At this point many parameters can be determined from this data as illustrated in the section. Furthermore, the short circuit current corresponds to the short circuit conditions when the voltage is equal to zero and the impedance is low. It is calculated using Equation 2.15.

$$V\ (at\ I=0) = \boldsymbol{I_{sc}} \qquad 2.15$$

The short circuit current I_{sc} occurs at the beginning of the forward-bias sweep. This the maximum current value in the power quadrant. However, in a perfect case, the maximum current value is the total current produced in the solar cell by photon excitation where $I_{SC} = I_{MAX} = I_t$ for the forward-bias quadrant.

2.14.1.4 *Open circuit voltage (V_{oc})*

The instance at which open circuit voltage occurs is at the point when current is not passing through the cell.

$$V \text{ (at } I = 0) = V_{oc} \qquad 2.16$$

The open circuit voltage is also at maximum voltage difference across the cell for a forward-bias sweep. This occurs in the power quadrant where

$V_{OC} = V_{MAX}$ (in the forward-bias quadrant).

2.14.1.5 *Maximum power point*

The generated power by the cell in watts along the I-V sweep can be easily calculated using the equation

$$P = IV \qquad 2.17$$

The power will be zero and the maximum value for power will occur at I_{sc} points. At the maximum power point, the maximum voltage and current are known to be V_{MP} and I_{SC} accordingly as shown in Figure 2.22 [163, 164].

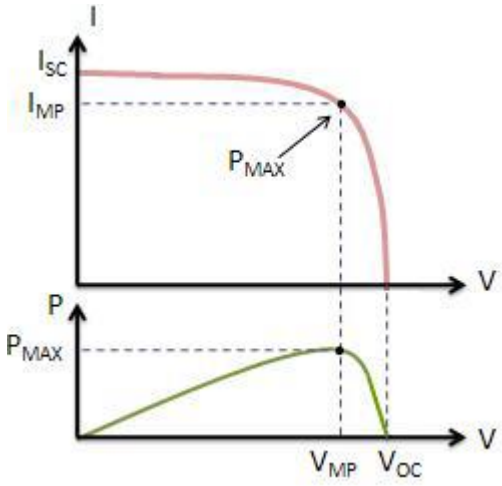

Figure 2.22: I-V sweep showing maximum power point, maximum current and maximum voltage[163]

2.14.1.6 *Fill Factor (FF)*

The Fill factor is defined as essentially a measure of quality of the solar cell [165]. This is calculated as

$$FF = \frac{I_{MP} \times V_{MP}}{I_{SC} \times V_{OC}} = \frac{P_{MAX}}{P_T} \quad 2.18$$

Where P_T is the theoretical power of the cell. Figure 2.23 shows I-V sweep from where the FF is calculated.

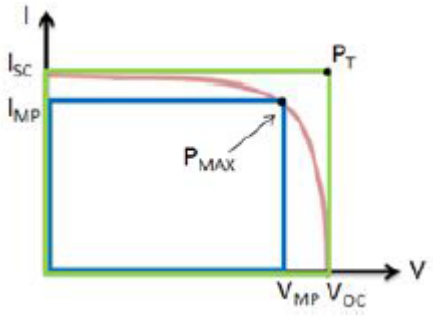

Figure 2.23: I-V sweep showing the maximum points used in calculating Fill Factor

By comparing the theoretical power P_T that will be output at both the short circuit current and open circuit voltage, the FF is calculated. Furthermore, the Fill Factor graphically can also be interpreted as a ratio of the rectangular areas illustrated in Figure 2.23. In an ideal situation, a large fill factor is desirable. This corresponds to square-like I-V sweep. Fill factors typically ranges from 0.5 to 0.82.

2.14.1.7 *Efficiency*

The ratio of the electrical power output (P_{out}) to the solar power input(P_{in}) into the Photovoltaic cell is called the efficiency (η).

$$\text{Maximum efficiency } (\eta_{max}) = \frac{\text{Maximum power out } (P_{MAX})}{\text{Power input}} = \frac{P_{out}}{P_{in}} \quad 2.19$$

Where P_{in} is considered as the irradiance of the incident light. It is measured in $\frac{W}{m^2}$ which is generally taken to be 1000 W/m^2. The I-V parameters are also affected by ambient conditions such as intensity, temperature and the spectrum of incident light. Due

to this purpose, it becomes necessary to test and compare PV using similar light and temperature conditions.

2.14.1.8 *Series resistance (R_s) and Shunt resistance (R_{sh})*

The efficiency the solar cell is decreased by the dissipation of power across internal resistances. In almost all modelling, the parasitic resistances can be modelled as series resistance R_s and parallel shunt resistances R_{sh} as illustrated in Figure 2.24.

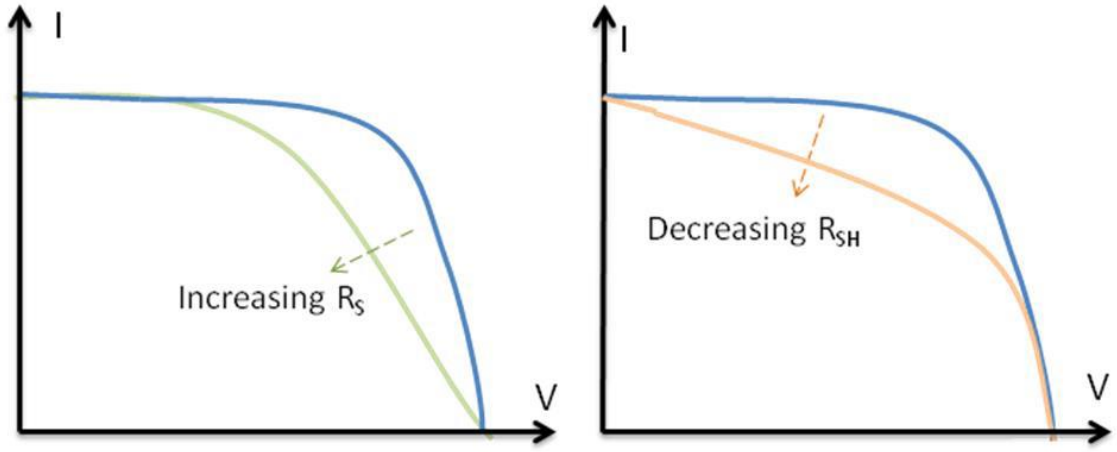

Figure 2.24: Effects of series and shunt resistances diverging from ideality [163]

Shunt resistances would be infinite in most cases and would not provide an alternative path for current to flow in an ideal solar cell. However, the series resistances would be zero thereby resulting to no further voltage drop at the load. The fill factor and maximum power will decreased by increasing series resistances and decreasing shunt resistances. There will be a drop in open circuit voltage if the shunt resistances are decreased largely. Also, the short circuit current will drop if the series resistances are increased significantly.

2.14.1.9 *Obtaining resistances from I-V curve*

The shunt resistances and series resistances can be measured using the inverse slope as depicted in Figure 2.25.

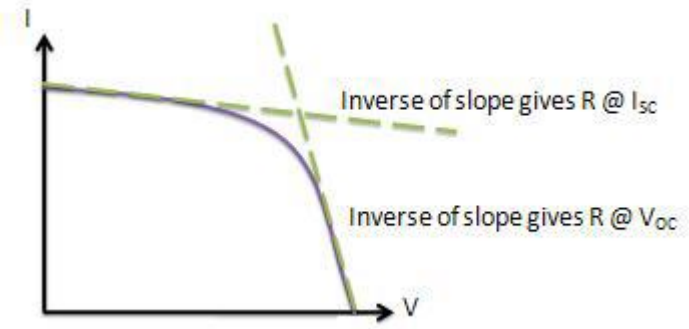

Figure 2.25: Obtaining series and shunt resistances using inverse slope method

2.14.1.10 *Considerations of temperature measurement*

In all semiconductors, the crystal used to make photovoltaic cells are sensitive to temperature. It is a known phenomenon that when the photovoltaic cell is exposed to higher temperatures, the short circuit current increases slightly while the open circuit voltage drops significantly. Figure 2.26 depicts the effect of temperature on I-V curve.

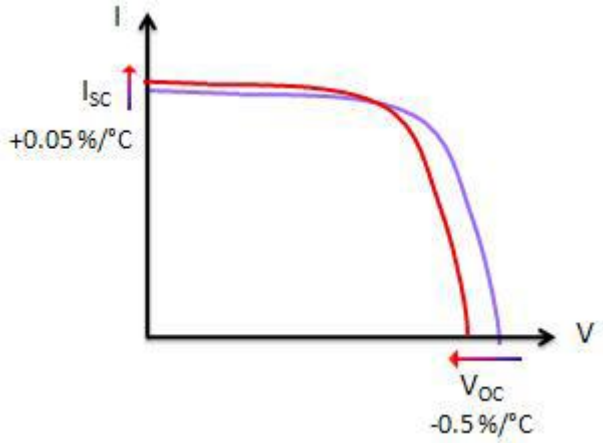

Figure 2.26: Showing temperature effect on I-V curve[163]

Higher temperatures results in a decrease in the maximum power output for a specific set of ambient conditions. The current and voltage curve differs according to temperatures. It becomes very important to record the condition under which the I-V curves was conducted. The temperature can be measured using thermocouples, sensors such as RTDs and thermistors.

2.14.1.11 *Module I-V curves*

The shape of the I-V curves does not change for a module of array of photovoltaic cells but it is scaled up based on the number connected in series and in parallel. Figure 2.27 shows the I-V curves for module and arrays when n is the number of cells connected in

series and m is the number of cells connected in parallel while short circuit current and open circuit voltage are for individual cells.

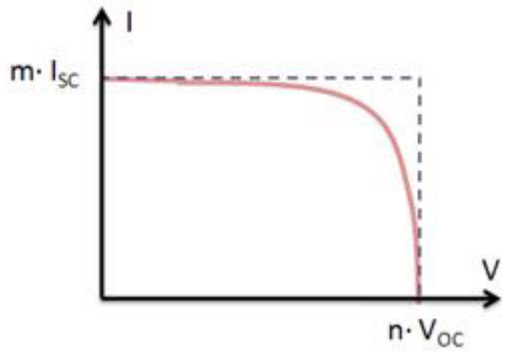

Figure 2.27: Modules and array I-V curves

2.15 Conclusion

The literature review is an overview study of the basic introduction in concentrating photovoltaic and thermal with special interest in the history, basic concept, technological challenges, solar cell materials, methods, design, comparative analysis, recent appreciable progress, cooling and absence of cooling, system cost, capacity installation and companies involved in advancing the technology. Deep literature study into research scenarios of concentrating photovoltaic has been made. Introduction to imaging and non-imaging are mentioned. Issues including symmetric and asymmetric designs are also reported. Manufacturing and temperature effects are detailed. There are strong indications that the system cost, installation cost and operational cost will gradually be coming down and the payback period will be significantly reduced. The literature review reveals significant progress in CPV installation across regions in the world. Also there is a need to consider the designs of concentrating PV for building facades, roofing tiles and stand-alone systems since they require no tracking devices for this applications. From the foregoing, the present research work is undertaken for proper detail investigation on design and performance analysis of a reflective symmetric compound parabolic concentrator. Therefore, the theoretical and experimental investigations has been underlined for both concentrator design, development and performance characterisation of the system. This piece of work is in no small measure expected to achieve meaningful progress in research of reflective symmetric compound parabolic concentrators and thereby advancing progress in concentrating photovoltaics.

Chapter 3 SYMMETRIC REFLECTIVE COMPOUND PARABOLIC CONCENTRATOR DESIGN AND OPTICAL MODELLING

3.1 Summary

A comprehensive design and optical characterisation analysis is presented for symmetric reflective compound parabolic concentrator (SRCPC). The optical study employs the use of ray tracing techniques using commercial software to characterise the optical efficiency which is a function of the incident angle of all incoming radiation. The optical flux distribution at the exit aperture of the SRCPC is investigated. After the design and simulation study, the SRCPC is constructed with indoor characterisation studies carried out for the purpose of validating the optical model. Presented in this chapter are the various different techniques and tools employed in the design and development of the SRCPC which comprises the manufacturing process and framework of the thesis.

3.2 Design construction constraints

Certain practical problems arise which requires further care in actual designs of SRCPC. The practical design constraints of the SRCPC system includes system cost, size, weight and land cost. I would have wish to construct the 8 (1m x1m) concentrators in one for standard size solar measurement of m^2. This was constrained by not having a sizeable solar simulator to test it after design and the cost to construct it was out of budgetary limit.

3.3 Design constrains for consideration

Many practical design considerations and problems needs to be considered while designing and constructing solar collectors of symmetric reflective compound parabolic concentrators (SRCPC). These include acceptance aperture, exit aperture, innovative design, geometry design methods, design principle, absorber size reduction, design concentration and collector height, absorber misalignment [166].

3.3.1 Acceptance aperture

The acceptance aperture is the number one parameter to be considered. This allows the control of incidence irradiations into the concentrator. It also maximises the acceptance angle of the geometry that permits the collection of solar irradiations at different angles. It ensures that the design principle collects maximum solar radiation within the boundary acceptance angles to match the concentration ratio.

3.3.2 *Exit aperture*

Another important parameter is the rectangular receiver aperture known as the exit aperture. This is the focal point of the parabola where the solar cell is located to collect reflected rays from the parabolic reflectors which fall from the sun. These rays are converted into 1) electrical power and 2) heat energy by the solar cells.

3.3.3 *Reason for choosing LGBC 50mm x 50mm silicon solar cells*

The major reasons for choosing this type of solar cell are because i) they form a rectangular exit aperture that matches the available shape of the solar cell thereby reducing wastage of solar cell materials. ii) It is design for concentration ratio of less than 10× that fits into the concentrator chosen in this thesis and iii) it is commercially available at reasonable cost and well-defined performance.

3.3.4 *Innovative design*

The 3x parabolic reflective concentrator has the innovation of a series and parallel heat exchanger designed to evaluate comparatively the heat extraction methods using fluids. The effect of mass flow rate of the working fluid was investigated in both series and parallel flow of the rate of heat transfer.

3.3.5 *Geometry design method*

There are several methods used in the design of non-imaging concentrators [154, 167]. The most widely employed methods are, 1) Edge ray principle method, 2) Integral design method, 3) The flow-line method. In this research, edge ray principle is adapted. Through the edge ray principle, a detailed ray tracing simulation was carried out. This was to enable us predict the optical performance of a 2D symmetric reflective compound parabolic carried out in this research.

3.3.6 *Design principle*

In ideal concentrators, the design principle requires that the receiver touch the reflector. Any gap between receiver and reflector causes some optical losses. Three

approaches can be considered if the basic concentrator geometry must remain unchanged. These three approaches are; a) Absorber size reduction: Initially, 100mm absorber width was chosen. After much analysis, 50mm absorber width was considered for this design model construction, b) the parabolic reflector height has to be truncated to a reasonable height and the CR was altered to achieve a desired goal and 3) the absorber was modified to sit on the heat exchanger.

3.3.7 Desired concentration and collector height

The height of a collector for a given concentration ratio and absorber perimeter is another practical consideration. There are so-called shadow lines that exist for any un-truncated CPC forming an angle with the optic axis of the collector. There exist a constant distance from the point where they cross irrespective of the concentrator design to the top of the collector. This distance to the level of the bottom of the collector depends on the receiver of the collector shape. Here, the absorber is constrained to lie entirely between the shadow lines having a perimeter. There must be a reflecting involute if the absorber does not extend from one shadow line to the other. The effect of compound parabolic concentrator truncation on the height and concentration ratio varies slightly according to collector type.

3.3.8 Absorber misalignment

There are flux losses and additional errors from incorrect alignment of absorber and reflectors. In fact, the magnitude of the temperature drop across an absorber can be estimated. It is known that the solar flux distribution at the absorber varies with time. It becomes very instructive to consider the worst possible case that could happen when the sun is incident on the collector at the acceptance angle. Then for a wedged flat absorber, most of the flux is concentrated on the edge of the absorber from where it must be conducted into the solar cell for electricity generation. The associated heat was conduct away by a transferable fluid medium and if a hot spot is formed. The above considerations were taken care of in this piece of work.

3.3.9 Solar cell used in the SRCPC model

To build up the CPV module in the thesis, the Laser Groove Buried Contacts (LGBC) solar cell presented in Figure 3.1: Silicon solar cells designed to operate at <10

suns used in the SRCPC model was used. National Renewable Energy Centre (NaREC) provides this solar cell used. The LGBC silicon solar cells are designed to generate electricity for concentration ratio of ≤ 10x suns [46] . Their thickness, number of fingers and distribution on the solar cells are illustrates in Figure 3.1. The 50mm x 50mm silicon solar cell is made from an original silicon wafer.

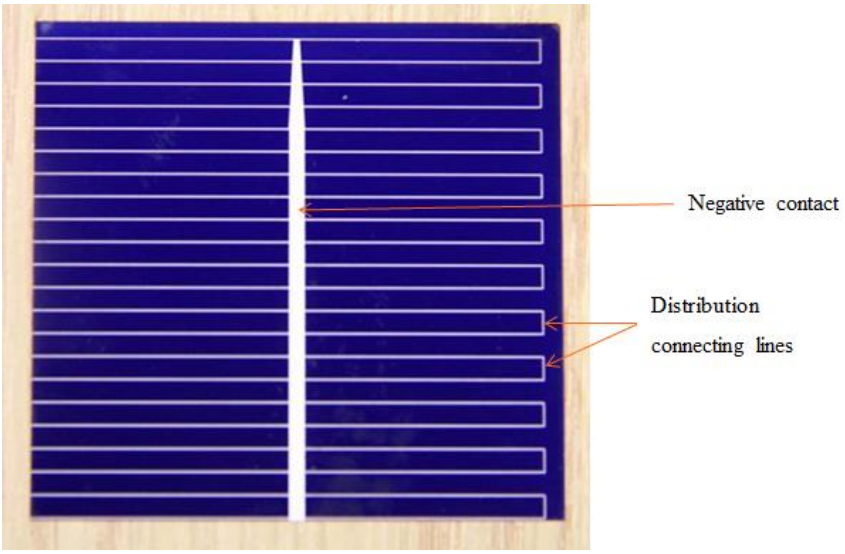

Figure 3.1: Silicon solar cells designed to operate at <10 suns used in the SRCPC model

3.3.10 ***Design of the SRCPC***

The parabolic shape of the SRCPC coordinates need to be calculated and drawn. For this to be done, the coordinates are defined in a system in which the y axis represents the axis of the right parabolic curve where the origin lies on the axis of the symmetry. The coordinate ($\times_{0,}$ Y_0) represents the origin of the intended coordinates system. While x, y defines the centre of the exit aperture. Also, the Y- axis represents the axis of the SRCPC. Equations 3.1 to 3.14 below were used for the calculations [168] and to plot the graphic CPC. Figure 3.2 is the designed 3suns hollow concentrator expected to achieve totally internally reflection.

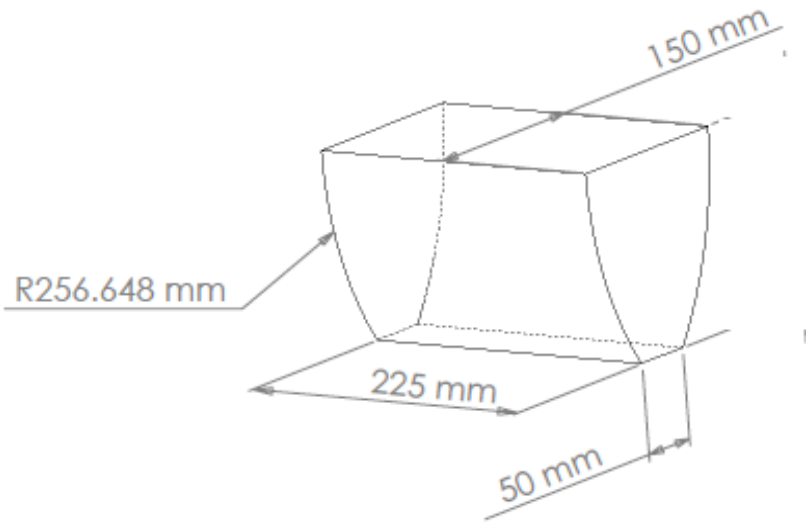

Figure 3.2: Diagram of 3× hollow SRCPC showing the expected dimensions and to achieve totally internally reflection

3.3.11 ***Geometric concentration ratio***

The role of concentration in solar conversion of solar concentrator is considered from the view of the definition as an optical device that collects the solar radiation that is incident on an aperture area KL and delivers it to a usually smaller absorber area MN. As shown in Figure 3.3.

Mathematically, it is expressed as $C_{geo=\frac{KL}{MN}}$.

Where C_{geo} is the geometric concentration ratio, KL is acceptance aperture area, and MN is absorber or solar cell area as illustrated in Figure 3.3: Geometry of SRCPC.

Two most important parameters are specified to complete the geometry of a fully designed and developed un-truncated hollow compound parabolic concentrator. These are the acceptance half angle Q_a and the width of the flat absorber S. The acceptance half angle used for the geometric construction of the reflective concentrator is 10º after a careful mathematical energy modelling with two others angles 15° and 20° as in Figure 3.3. Its optical efficiency and energy generated inform its choice. The absorber width S = (MN) as shown in Figure 3.3 which was decided to be 50mm base on solar cells market availability and review studies. Table 3.1 shows un-truncated and truncated parameters used for energy modelling and CPC development

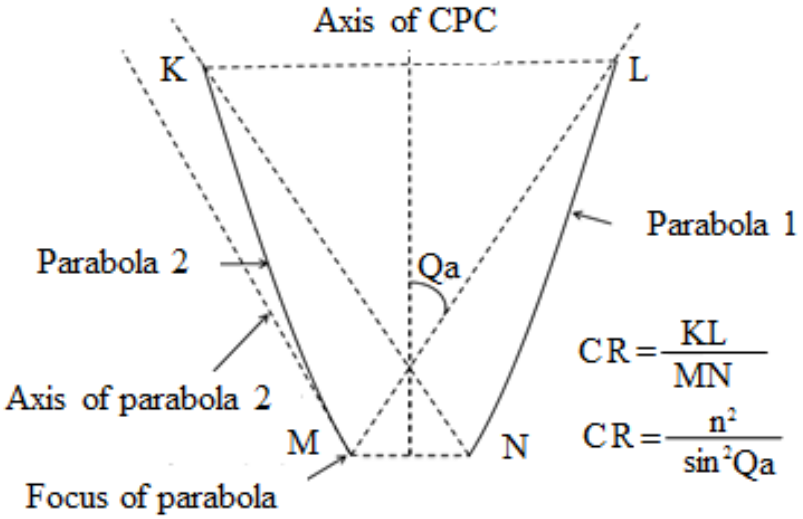

Figure 3.3: Geometry of SRCPC

Table 3.1: Showing un-truncated and truncated parameters used for energy modelling and CPC development

S/N	Half acceptance angle (°)	Solar cell width (mm)	Initial CPC height (mm)	Truncated height (mm)	Acceptance aperture (mm)	Initial CR	Reduced CR
1	10°	50	958.27	105.73	150	5.76	3
2	15°	50	453.79	138.14	150	3.86	3
3	20°	50	269.52	269.52	146.19	2.92	2.92

The width of the acceptance aperture is denoted in Figure 3.3: Geometry of SRCPC as KL using equation 3.1. The parameters were calculated using the excel spreadsheet but by using Equations 3.2 to 3.13. Smaller acceptance angles give higher optical efficiencies than wider acceptance angles was the reasons for the choice of acceptance angle.

$$W = \frac{S}{\sin Qa} \qquad 3.1$$

Un-truncated Height H of the symmetric reflective compound parabolic concentrator (CPC) is given as in Equation 3.10.

$$H = S(1 + S(\frac{1}{SinQa}) (2 \tan Q_a) \quad 3.2$$

The focal length (F) of the parabola is given by equation 3.11 shown in Figure 3.13, which is the same as solar cell width denoted as MN in Figure 3.13.

$$F = (\frac{S}{2}) (1 + \sin Q_a) \quad 3.3$$

Apex parabola $X_{0 = -(} \frac{S}{2}) (1 + F \sin Q_a)$ or 3.4

$$= - (\frac{S}{2}) (1\text{-}SinQa) – (Sin\ Qa)^2 \quad 3.5$$

$$Y_{o =(\frac{S}{2})(1+ \sin Q_a)} (\cos Q_a) \quad 3.6$$

At the base of the focal length of the parabola

$$X_1^1 = S(\cos Q_a) \quad 3.7$$

$$Y_1^1 = \left(\frac{S}{2}\right) (1 - \sin Q_a) \quad 3.8$$

An incremental variable X^1 was used as an independent parameter such that

$$X^1{}_{n+1} = X^1{}_n + \boldsymbol{\delta} X_1 \quad 3.9$$

$$Y^1_{n+1=(\ X^1_{n+1}\ )^2} /4F \quad 3.10$$

Where δX_1 is some suitable small increment such that

$\frac{W}{N} > 100$

This is where the right side of the CPC side wall profile in the desired coordinates systems was then determined using the above equations and with

$$X_n = X^1{}_n (cos\ Q_a) – Y^1{}_n (sin\ Q_a) + X_0 \quad 3.11$$

$$Y_n (X_n) = X^1{}_n (sin\ Q_a) + Y^1{}_n (cos\ Q_a) + Y_0 \quad 3.12$$

For the left parabola

We have

$$Y_n\,(-X_n) = Y_n + X_n \qquad 3.13$$

(Where these incremental are both in the Y-axis and X-axis).

By using the concentration and the thermodynamics limit, the maximum geometric concentration allowed by physical observation laws is related to the angular field of view, which is given by

$$\boldsymbol{C_{max}} = \frac{\boldsymbol{n}}{\boldsymbol{Sin\ Qa}} \qquad 3.14$$

Where n is the refractive index at absorber surface if dielectric materials are used, also C_{max} >1 for instance, MN <KL. The optics must limit the field of view which is defined simply here by a cone of half angle Q, Where Q = $2Q_a$ being the acceptance angle.

It is worth note that the best designs for achieving high concentration is the design having circular surround field with a tall tower. The next best to these designs are those with small values of half acceptance angle (Q_a) with high corresponding tower heights that are acceptable. The ratio of the length of the entrance aperture to absorber is given as $\frac{\mathbf{1}}{\boldsymbol{Sin\ Qa}}$ .This is where the design achieves maximum concentration in an ideal case. The Concentration Ratio has a maximum limit of $\mathrm{CR} = \frac{1}{\mathrm{Sin2Qa}}$.

The technology in this design is non-imaging. The traditional imaging optics involves the formation of source on the target. There are two main design problems that non-imaging optics tries to solve better than imaging optics. These are, i) Solar energy concentrators- It maximises the amount of energy applied to a receiver. This is typically to a solar cell or thermal receiver and ii) Illumination- It controls the distribution of light so that it is evenly spread over the solar cell area and it completely blocked other areas.

3.4 Design specifications

The specifications for the designed symmetric reflective compound parabolic concentrator are as shown in Table 3.2. It shows the dimensions used to construct the 2D SRCPC. The fixed exit aperture of 50mm was used to calculate the dimensions.

Table 3.2: Design specification used for the construction of 2-D truncated SRCPC

Parameters	Dimension
Half acceptance angle (θa)	10°
Focal length	29.34mm
Un-truncated SRCPC height (H)	958.27mm
Truncated concentrator height (H)	105.73mm
Acceptance aperture area	225mm x 150mm
Exit aperture area	50mm x 225mm
Entry aperture width	150mm
Entry aperture length	225mm
Solar cell width	50mm
Concentration ratio	3×
Exit aperture width	50mm
Parabola area	105.73mm x 225mm

3.5 Choice of materials and engineering properties

There are many possible methods of achieving the construction of the twin SRCPC. The best possible method to produce the SRCPC that will ensure delivery of highest precision levels of professionalism is the use of Stratasys or Fortus 3D printers. The problem with this method is that it is extremely costly. It is a paramount need for the optimised SRCPC concentrator prototype to be constructed in the most economical way possible. Two possible close materials would have been used for the construction of the SRCPC concentrator. These are aluminium and stainless steel.

*3.5.1 **Aluminium***

It has the engineering property of not rusting easily but its disadvantages for this application far outnumbered the advantage. This includes; its limitation to certain geometric features using economical process. It is far more expensive than steel. It is

difficult to weld, abrasive to tooling and prone to severe spring back. It has construction limitations.

3.5.2 ***Stainless steel***

The choice of stainless steel was necessary for the manufacturing of the SRCPC prototype due to the fact that it has great corrosive resistance to forms of deterioration. It possesses mechanical properties for specific temperature range (it is a low –cost-heat treatable grade for non-severe corrosion application). No limitation to geometric features. This material is available, has fabrication characteristics and is least expensive. The use of laser machine was employed to cut the right and left parabola. The SRCPC support stand was slotted to accommodate the geometric parabola which form the upper aperture (acceptance aperture) and lower (exit aperture).

3.5.3 ***Excel Program***

Equations 3.1 to 3.17 were used for programming in Excel to generate x, and y coordinates. These coordinates were used to produce the graphic right and left parabola at a focal point where the solar cell is placed. We first produced graphic parabola using acceptance angles of 0° and 10°, [111]. Parabolas of 15º, 20º, 30º, 40º, 50º, 60º, 70º, 80º were also produced for the purpose of seeing the shape.

3.5.3.1 ***Results***

The coordinates shown in Table A3 in Appendix produced a graphic design of un-truncated hollow SRCPC as depicted in Figure 3.4 while Figure 3.5 is the schematic side view with detailed dimensions of the concentrator.

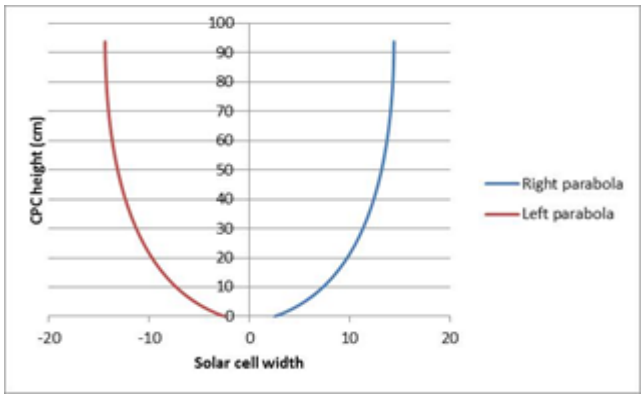

Figure 3.4: Graphic designed un-truncated CPC of 10° acceptance half angle and 50mm absorber from the coordinates generated

3.5.4 ***Design cost of SRCPC system***

The designed SRCPC was tall to about 1m in height, weighty, bulky and subjected to force majeure and may be difficult to install without weighty brackets. The cost of materials and quantities used to produce the designed un-truncated SRCPC is as shown in table 3.3. It was truncated after a careful study for economic reasons. The detail truncated SRPCP is shown in Figure 3.5 while Table 3.4 shows the cost to construct the designed truncated SRCPC.

Table 3.3: Cost to construct designed un-truncated SRCPC

Material	Dimension	Quantity	Unit Price	Total Cost
Stainless steel sheet 304 grade	3mm thickness (958.27mm)	1m x4m	£576.89	£576.89
LGBC silicon Solar cells	50mmx50mm	1 Packet	£600	£600.00
Low Iron glass	4mm thickness (484mm x 486mm)	1	£44.10	£44.10
Construction of Parabolic Frame work 1	225mm x R256.65mm x 958.27mm	4	£388.98	£1,555.56
Construction of Parabolic Frame work 2	R256.65mm 50mm x 150mm	4	279.99	£1,119.96
Thin film reflective	Single side	40m x 1.2m	1	£84.99
Internal Glazing rubber gasket	6.4mm x 1.2mm x 5mm	5m	£12.99	£12.99
External glazing rubber gasket	6.4mm x 5mm	5m	£16.89	£16.89
Kapton tape	(High temperature heat resistance)	1 Roll	12.4	12.4
Aluminium tape	50mm x 45m	1 Roll	7.99	£7.99
KAVAN DC water pump	12v, 1.5A, Capacity= 1.81 L/S, (0.0302L/s)	1	24.99	£24.99
Thermal cavity insulation foam	2.88m^2/sheet	1	41.29	£41.29
Thermal expanding form	750mL	1	7.99	£7.99
Thermal conductivity paste (Heat sink compound)	4.0W/Mk(-40 to 400°C)	2 Bottles	£36.92	£73.84
Thermal insulating pipe	polyethylene 13mm	4 x 2m	£1.04	£4.16
Clear lacquer (Advance acrylic) formula	300mL	2 bottles	£7.49	£14.98
Sylgard 184 Elastomer	A set	1	£49.99	£49.99

Water insulation tank	2 Gallons capacity	1	£26.99	£26.99
Water pipes	10mm diameter	10m	£0.99	£9.90
Araldite rapid	2 x 15mL tubes	2 set	£7.36	£14.72
24 hours mechanical timer		1	£13	£13.00
Weather proof electrical extension cable	20m, 13A	1 Coil	£34.99	£34.99
Wieldable aluminium bar	50mmx 952mm x 8m	1 bar	£11.06	£11.06
M6 grub screws	1 packet	1	£7.80	£7.80
Stainless steel pipe	6mm x 1mm thickness		£14.88	£14.88
Alkaline finger battery	50 in a packet	1	£14.98	£14.98
SRCPC enclosure	1m x 0.49m, x 0.49m	1	£1,200	£1,200.00
Ground mounted parabolic support brackets		4	£165	£648.00
Fluxide	Pro 12mL Pen solder	1	£4.59	£4.59
Soldering lead	Berzomatic lead free rosin		£8.99	£8.99
Soldering wire connector	500g	1	£12.90	£12.90
				£6,271.81

Table 3.4: Cost to construct designed truncated SRCPC

Material	Dimension	Quantity	Unit Price	Total Cost
Stainless steel sheet 304 grade	3mm thickness (958.27mm)	1m x4m	£576.89	£63.46
LGBC silicon Solar cells	50mmx50mm	1 Packet	£600	£600.00
Low Iron glass	4mm thickness (484mm x 486mm)	1	£44.10	£44.10
Construction of Parabolic Frame work 1	225mm x R256.65mm x 958.27mm	4	£388.98	£171.11
Construction of Parabolic Frame work 2	R256.65mm 50mm x 150mm	4	279.99	£123.20
Thin film reflective	Single side	40m x 1.2m	1	£9.35
Internal Glazing rubber gasket	6.4mm x 1.2mm x 5mm	5m	£12.99	£12.99
External glazing rubber gasket	6.4mm x 5mm	5m	£16.89	£16.89
Kapton tape	(High temperature heat resistance)	1 Roll	12.4	£12.40

Aluminium tape	50mm x 45m	1 Roll	7.99	£7.99
KAVAN DC water pump	12v, 1.5A, Capacity= 1.81 L/S, (0.0302L/s)	1	24.99	£24.99
Thermal cavity insulation foam	2.88m^2/sheet	1	41.29	£41.29
Thermal expanding form	750mL	1	7.99	£7.99
Thermal conductivity paste (Heat sink compound)	4.0W/Mk(-40 to 400°C)	2 Bottles	£36.92	£73.84
Thermal insulating pipe	polyethylene 13mm	4 x 2m	£1.04	£4.16
Clear lacquer (Advance acrylic) formula	300mL	2 bottles	£7.49	£14.98
Sylgard 184 Elastomer	A set	1	£49.99	£49.99
Water insulation tank	2 Gallons capacity	1	£26.99	£26.99
Water pipes	10mm diameter	10m	£0.99	£9.90
Araldite rapid	2 x 15mL tubes	2 set	£7.36	£14.72
24 hours mechanical timer		1	£13	£13.00
Weather proof electrical extension cable	20m, 13A	1 Coil	£34.99	£34.99
Wieldable aluminium bar	50mmx 952mm x 8m	1 bar	£11.06	£11.06
M6 grub screws	1 packet	1	£7.80	£7.80
Stainless steel pipe	6mm x 1mm thickness		£14.88	£14.88
Alkaline finger battery	50 in a packet	1	£14.98	£14.98
SRCPC enclosure	1m x 0.49m, x 0.49m	1	£1,200	£132.00
Ground mounted parabolic support brackets		4	£165	£71.28
Fluxide	Pro 12mL Pen solder	1	£4.59	£4.59
Soldering lead	Berzomatic lead free rosin		£8.99	£8.99
Soldering wire connector	500g	1	£12.90	£12.90
				£1,656.80

The material cost for the un-truncated SRCPC is £6,271.81 and the truncated SRCPC cost £1,656.80. By truncation, £4,615.01 is saved with slight trade-off with concentration ratio. At proof of concept, the technology is not cost effective but at scale-up level, it is the best technology with lots of benefits.

3.5.5 ***Dimension of the SRCPC***

After the design of the SRCPC, It was seen to be too tall in height (H) as shown in Figure 3.5 when compared to the width of the diameter of the collecting aperture. It was truncated for economic purposes as revealed in Table 3.3 and Table 3.4.

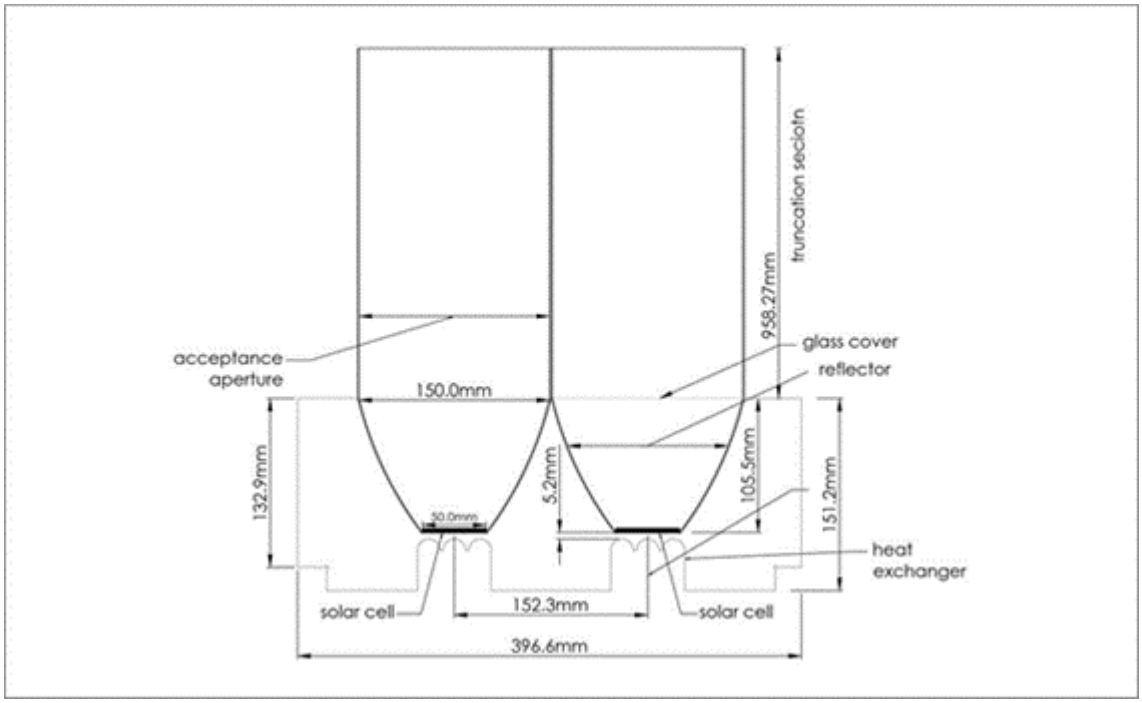

Figure 3.5: Schematic side view of the un-truncated SPCPC

3.6 SRCPC truncation

By truncation as illustrated in Figure 3.6, it means cutting away part of the entry aperture without losing much concentration of the system. This is to say that truncation brings about a considerable reduction in the height of the SRCPC with negligible decrease in concentration. Full height (H) equation for SRCPC is given by

$$H = \frac{2\,a' + (1/\sin Qa)}{2\,\tan Qa} \qquad 3.15$$

Where

Q_a= half acceptance angle

a'= half side of the exit aperture

The truncation height equation of the SRCPC is

$$HT = \frac{F\,Cos(\Phi_T - Qa)}{\sin^2\frac{\Phi_T}{2}} \qquad 3.16$$

Where Φ_T is the truncated half acceptance angle.

The width of the half entry aperture for a truncated SRCPC is given by

$$aT = \frac{FSin(\Phi_T - Qa)}{\sin^2\frac{\Phi_T}{2}} - a' \qquad 3.17$$

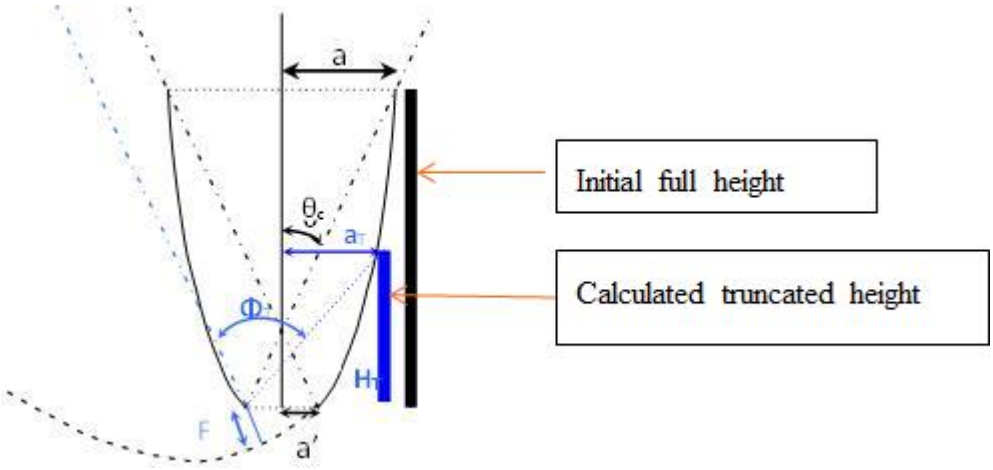

Figure 3.6: Initial full height and calculated truncated height[171]

Different plots have been drawn by Rabl [142] in which he explores the effect of truncation on the concentration ratio of 2D CPC [172]. Equations 3.16 and 3.17 are used for the calculation of the truncated height values and the corresponding ratios. Therefore, Φ_T will be equal to $2Qa$ and the truncated SRCPC will be given as $\frac{2Qa}{2} < \Phi_T < \frac{\pi}{2} + Qa$.

It was then necessary to vary the truncated angleΦ_T using $2Qa + 1)$ to $(\frac{\pi}{2} + Qa)$. This was incremented each time by a degree. These were the equations used to calculate the corresponding truncated height H_T and width of the truncated aperture area (a_T). The concentration ratio of the SRCPC was calculated by dividing the a$\frac{\pi}{2}$. Initially, the geometrical concentration ratio of the SRCPC was equal to 5.76 but reduced to 3 after truncation. The acceptance half angle is given by $Qa = 10°$. The truncated dimensions were calculated for the case of half acceptance angle $Qa = 10°$ while a'=25mm.

Truncation therefore is a practical concentrator design approach to reduce cost by cutting off part of the entrance SRCPC aperture height and reduce the SRCPC material

to be used. The fact remains that a truncated SRCPC collects less solar power and less concentration ratio because of the reduced aperture magnitude. This is a trade-off between energy collection efficiency and manufacturing cost. The Optiswork tolerance analysis tool provided help for the designer to make a balanced decision.

The truncated SRCPC has the height H=105.73mm, acceptance aperture area (150mm x 225mm), acceptance half angle =10° and the concentration ratio is 3x. The percentage height truncation was 89% off. The concentration ratio reduction of 47.9% corresponds with loss of 89% of the SRCPC height. The retaining of 11% height for the concentrator corresponded with the concentration ratio of 3x. The concentration ratio dropped from 5.76 to 3.0. This reduction in concentration when compared to the advantage gained by truncating the SRCPC gave a reasonable reduction in prices of steel sheet and reflective film [172]. It also gave a practical flexibility of its used in building application. Figure 3.7 shows the graphic design of truncated SRCPC whose coordinates were fed into SolidWorks software to produce a solid structure of the truncated SRCPC.

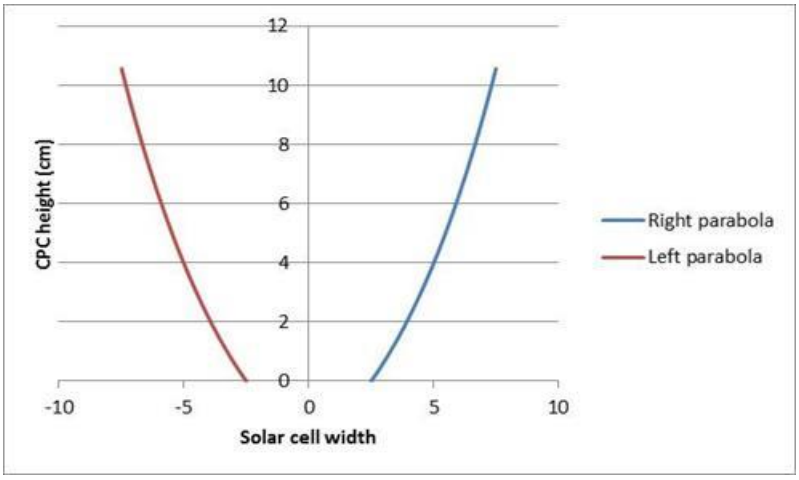

Figure 3.7: Graphic designed truncated CPC of 10^{o} acceptance half angle and 50mm absorber from the coordinates generated

From the Solid Works software, the graphic design was extruded to give the developed 2-D solid 3x hollow reflective concentrator as shown in Figure 3.8.

It is worth to note that all parabolas are symmetrical. They look as if they are a reflection on a mirror that were right down the middle of the graph. If one is mirrored as a reflection of the other, the graph of the parabola can change direction, width and direction. The coefficients of x^2 and x^0 as well as the constant are very important because they help to control and determine the desired direction (angles), position, widths

(acceptance aperture and exit aperture). This is why the use of simulation method will give a perfect and smooth determinant curve than the mirror reflection.

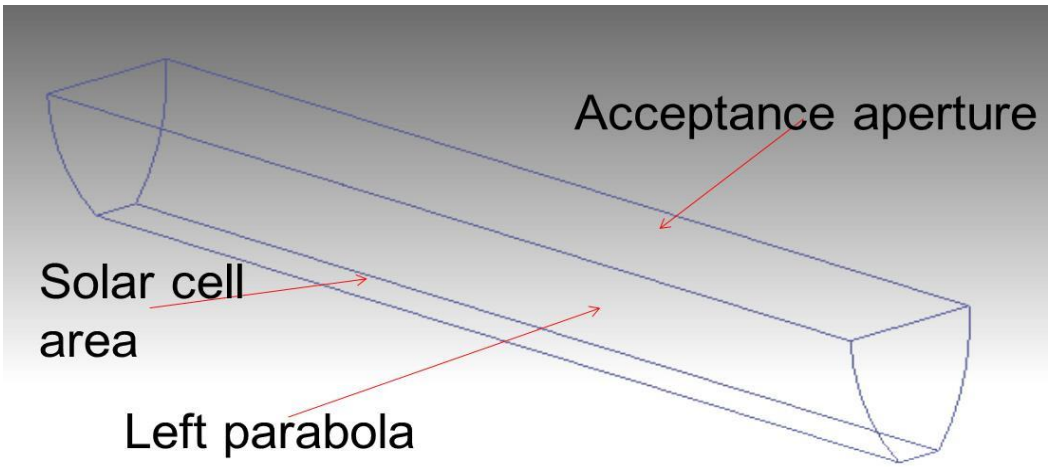

Figure 3.8: Designed and developed 2-Dimension solid 3x hollow reflective Concentrator from Solid Works

It is therefore necessary to understand the description of a 2D CPC taking into consideration the geometry and construction. A 2D typical modelling study constructed with reflective material is hereby presented. The optical model developed is validated using indoor experimental study and a solar simulator to check optical efficiencies for the symmetric reflective concentrator. The constructed concentrator with reflective material is investigated theoretically and experimentally. Comparative study on reflectors and refractors has already been carried out but the result is used to improve the reflective concentrator system [173-175].

3.7 SRCPC Optical Modelling

3.7.1 Simulation measured flux

Automatically, the analysis process will sample a user-defined variable range and the total flux at each sample point is simulated. It became necessary to illustrate the impact of relative SRCPC height on the distribution flux measured with the sun position at 0°. The percentages of the flux attenuation and percentages of truncation are all referenced to the original un-truncated SRCPC. From the graph, it indicates that the impact of SRCPC height on distribution flux is consistent over different sun positions with the SRCPC designed acceptance angle. This graphical information helped to make a trade-off decision coupled with the designer specification.

3.7.2 Ray tracing

The edge-ray principle is employed to study the trajectory of a ray of sunlight when it is passing through an optical system. It is important to use the ray tracing technique to analyse the optical performance. Solar rays are reflected or refracted when they heat the surface of the solar concentrator. The side walls of the SRCPC are assumed to be entirely spectacular with reflectivity equals to 0.94 because most solar concentrator reflectivity surfaces are nearly 0.94. The percentage losses of the light rays are only 6% of its power after reflection. The direction of the reflected ray and the refracted ray from this assumption make the same angle with respect to the normal concentrator surface.

3.7.3 Law of reflection

The law of reflection states that the incident ray, the reflected ray, and the normal to the surface of the mirror all lie in the same plane. More to this, the angle of incidence (Qi) is equal to the angle of reflection (Qr) [176]. It is possible to generalise the ray trace for all cases of reflection by transforming the reflection ray into vector form. The law of reflection can be transformed to a vector equation as

$$R = I - 2\,\overrightarrow{NI}.\overrightarrow{N} \qquad 3.18$$

Where unit, **I** is incident vector, **R is** reflected vector, **N is** vector along the normal pointing into the reflecting surface. It is easier and enough to have a 2D ray tracing analysis for the solar concentrators without tracking systems because the incident angle do not vary during the day at all or the variation is in one plane only. In solar concentrators that are static, the incident angles will be the angle of incident of the solar rays but this varies in different planes during the day. At the exit aperture, the 2D ray tracing does not give enough information for the illumination distribution. This study carried out a 2D ray tracing on the SRCPC. The solar incident rays are considered as a beam radiation. All the rays entering the SRCPC are parallel with the same energy and evenly spaced. The solar rays will either hit the exit aperture without reflecting or hit one of the side walls to be reflected. Three scenarios are observed here after the first reflection; 1) The incident rays will exit the SRCPC from the entry aperture and disappear, 2) Hit another ray, 3) The same side wall to be reflected yet again or reach the exit aperture where the solar cells are placed or they exit the SRCPC from the entry aperture and disappear into space.

3.7.4 ***Optical model***

It was necessary to build an optical model in order to investigate the optical characteristics of the symmetric reflective compound parabolic concentrator. Figure 3.9 shows the optical model flow chart process [174]. The light source to be defined in the flow chart refers to the light source in the Optis software. The visual checks are carried out in the Optis software for the determination of solar rays coming in and solar rays exiting for the calculation of the optical efficiencies.

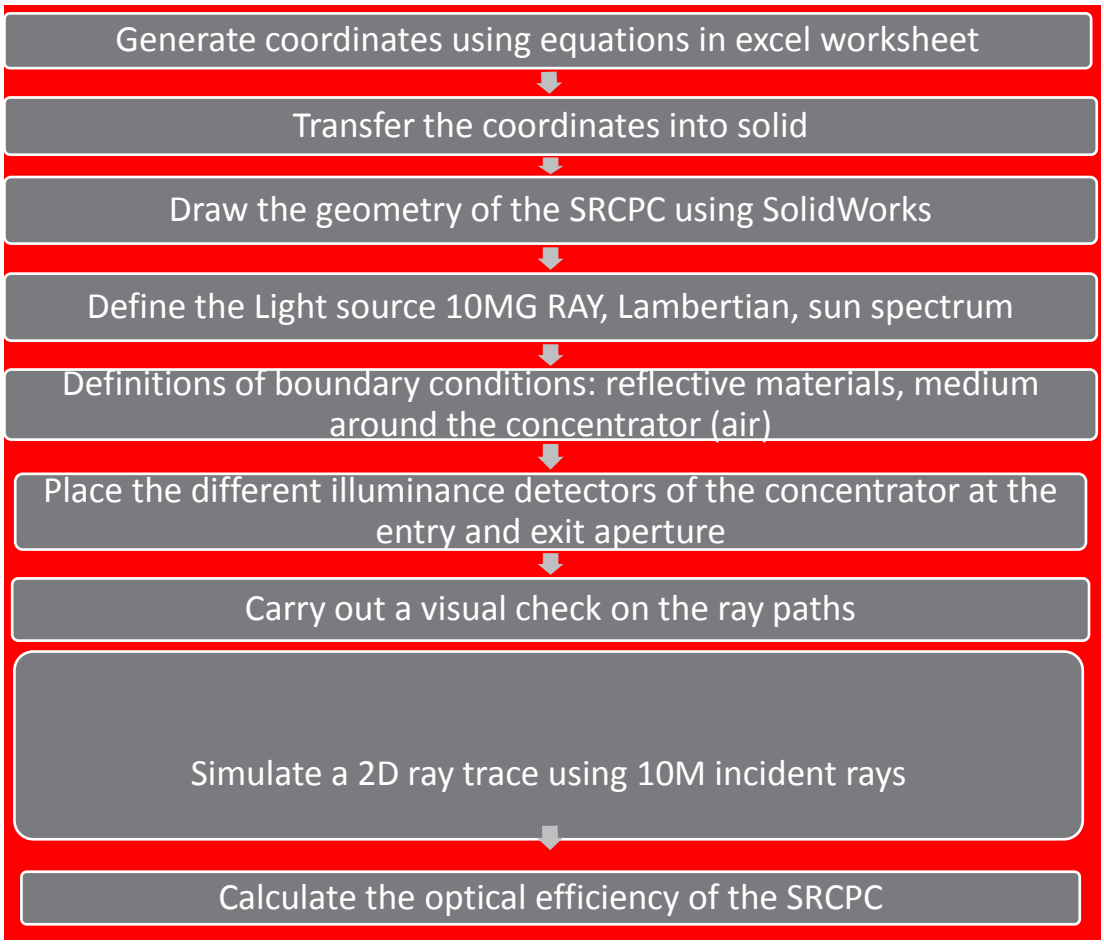

Figure 3.9: Optical model flow chat process

3.7.5 ***Ray tracing simulation process***

The Optis tolerance analysis tool was used to carry out the ray tracing. At the different incident angles, the rays that enter the SRCPC are those starting from the perpendicular (vertical rays) to the surface of the entry aperture. They are considered as incident angles of 90 degrees at noon time to the entry aperture. They are considered as

incident angles to the 90 degrees. The highest simulated efficiencies are 94% as shown in Figure 3.14 and Figure 3.15. It is important and beneficial to master the ray tracing technique and also understand the behaviour of the incident rays concentrated by the optical device. The advantages of using the Optis software includes; i) the flexibility of drawing any complex geometry is possible as optis works is an add-in with solid works software CAD. They both represents integrated software that could draw the optical device and for the optical simulation. 2) The time of simulation in Optis works is about ten minutes thus saving time. The results can be obtained rapidly in various and different formats for the optical flux. During each simulation at the beginning, the numbers of incident rays entering the entry aperture are determined. Also, the direction of the incident rays is equally specified by two directions. The first one is the S-N (south north) plane called $QS-N$. the second angle is the E-W (east-west) plane called $QE-W$. It is by these two directions that the projection of the incident angles Q on the S-N and E-W planes are represented.

Considering all possible directions of the incident ray, the ray will move through the planes between the S-N or E-W plane and diagonal. This is later referred to all directions. It is important to note that the incident ray regardless of which plane it happens to be in, it is always measured to the normal. To differentiate between the incident rays that are at a consistent angle but different projection, for example incident rays of 15° but in the diagonal plane or lies between the diagonal and E-W plane, it is referred to by the two angles representing its projection on the S-N and E-W plane as the incident angle in the simulation. It is ensured that the incident ray be tracked in all planes giving a detailed analysis of all the incident rays in all the possible planes. It is observed that the incident angle is either within the acceptance angle (-10° $<$ Q $<$+10°) or outside (Q $>$-10°). The simulation result shows; 1) the number of rays exiting the SRCPC from the exit aperture, 2) Concentrated rays, for instance n (their x, y, coordinates). 3) The number of reflected rays for each ray concentrated and 4) a drawing of the path of all incident and reflected rays.

From the simulation carried out using Optis Works in Solid Works, the incident angles used were from 0° to 35°. The acceptance aperture half angles were 10°, 15° and 20° [151, 177]. Each of these acceptance half angles was simulated in the S-N and E-W directions to obtain results. The incident angles were choosing at intervals of 5° and optimised in various directions up to 35°. The input radiation is 1000W/m^2. The input

and output were recorded. The optical efficiency was calculated. The flux distribution across the concentrator was equally measured. The ray tracing results are shown in the Figure 3.10 (a) to (f).

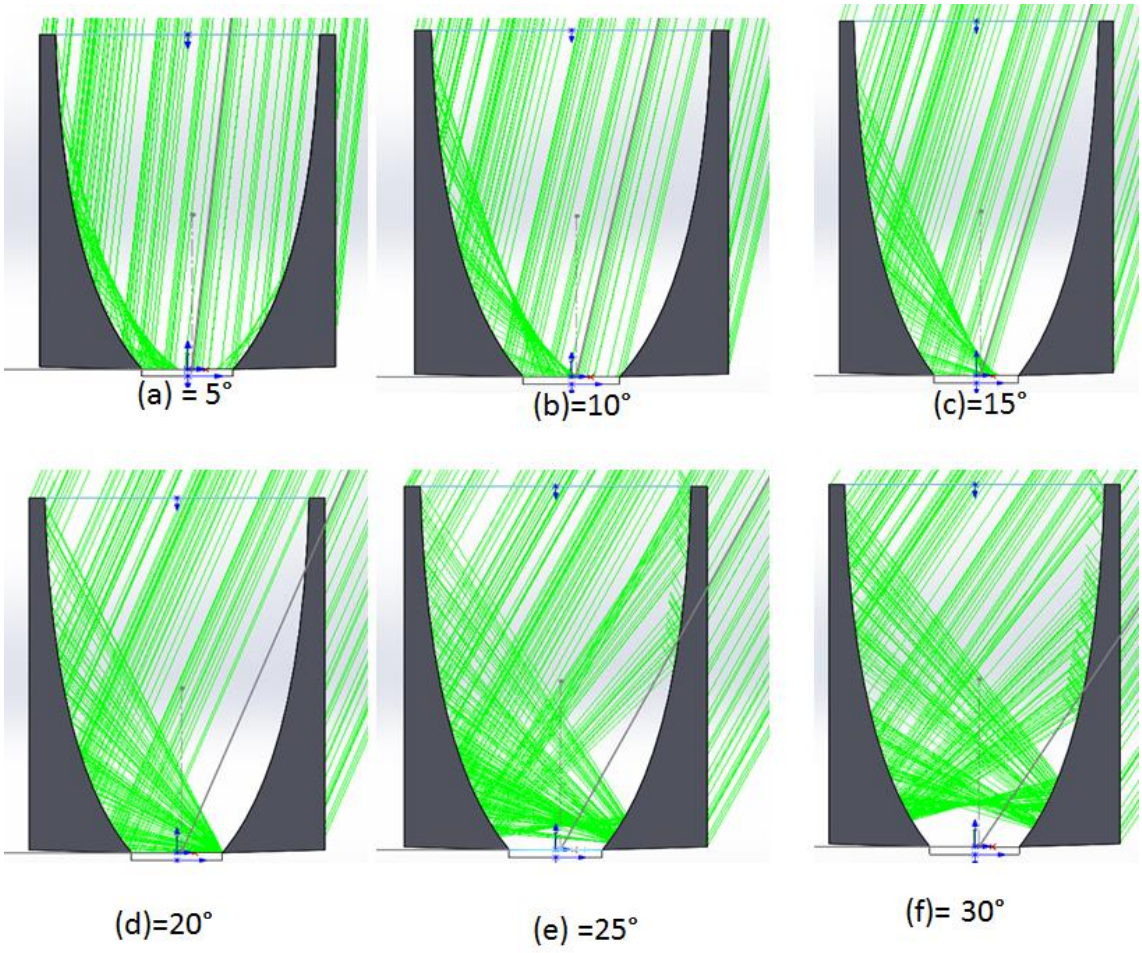

Figure 3.10: Ray trace diagrams for un-truncated SRCPCs at (a) to (f).

All the concentrators have the same 0° acceptance angle. PV absorber width is common but differ in acceptance aperture widths and concentration ratio. The ray tracing for un-truncated SRCPC shows much energy coming into the concentrators. It is observed and seen in Figure 3.11 that when the incident rays are at angles 0°, 5°,10°,15°,20° and 25° to the glass aperture cover that they rays are either incident directly on the PV absorber or reflected away from the absorber after a number of reflections at the reflector. The flux distribution also differs in many that are incidence at the PV absorbers. The flux distribution spread across the PV cells in some and uniformly distributed while others created a likely hot spot. As the angle increases, the rays are completely reflected away from the absorber. Smaller acceptance angles give high and better flux distribution at the absorber and energy [177]. It is clearly seen in Figure 3.11 that some of the incident rays are not incidence at the absorber in the S-N direction but few. The amount of incident

rays has equally dropped because of the truncation and the concentration ratio has changed. The incident rays at half acceptance angle 10° seems uniformly distributed than all others. Under each concentrator is the flux distribution displayed during the simulation. Figure 3.12 illustrates ray trace diagrams and flux distribution in the East – West directions as well as shows the ray trace diagrams and the flux distribution under each of the truncated SRCPC for a range of solar incidence angles. The solar rays carries equal amount energy each. This is determined by dividing the number of incidence rays on the aperture with the total incidence radiations.

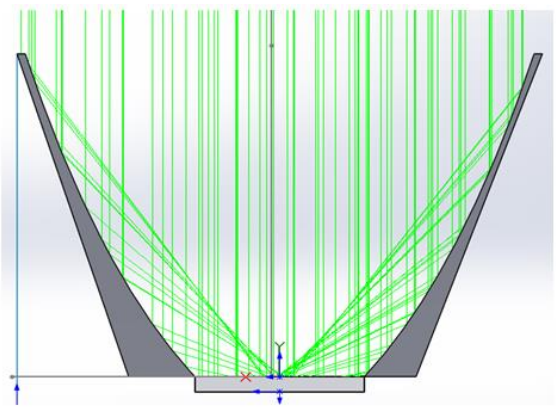

(a) = 0°

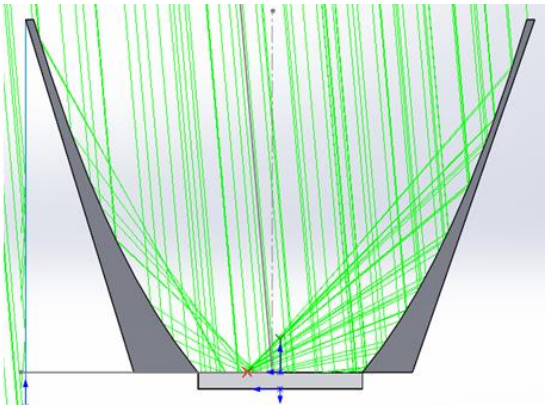

(b) = 5°

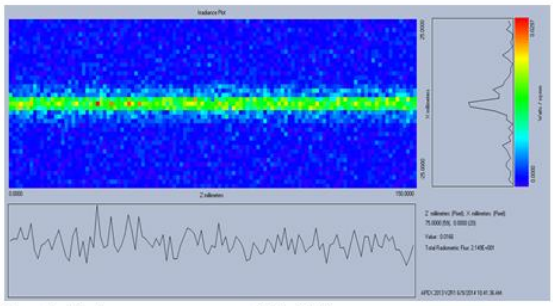

Flux distribution at concentrator (a) in S-N direction

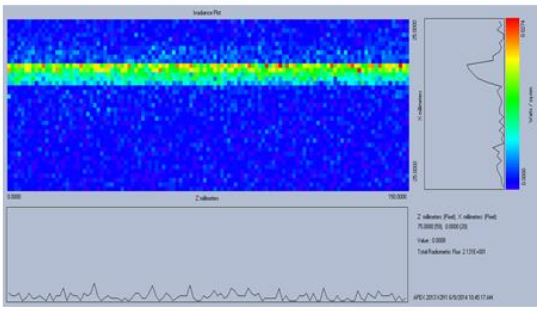

Flux distribution at concentrator (b) in S-N direction

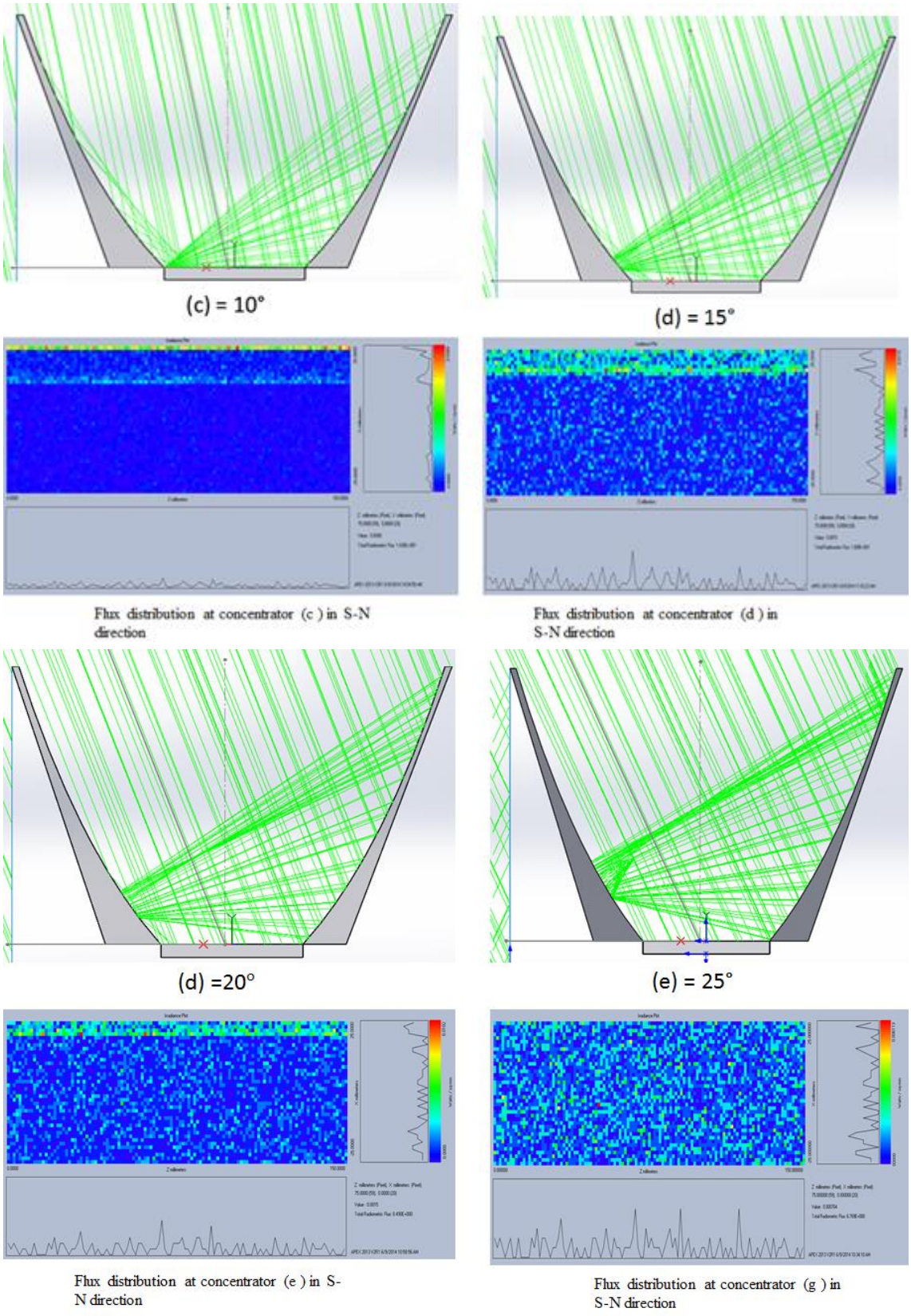

Figure 3.11: Ray trace diagrams and flux distribution under each concentrator for truncated SRCPCs in the S-N direction at (a) to (f).

Figure 3.12: (c) has a uniformly flux distribution better than others which does not constitute a hot spot in the solar cell. It is also observed that the wider the acceptance angle the less rays concentration. Each reflector is truncated at the vertical aperture by different amounts to facilitate integration in a plane building facades. The purpose of truncation is for economic reasons or reducing the quantity of reflectors materials, bulky nature, cost and weight. The percentage height truncation was 89% off. The concentration ratio reduction of 47.9% corresponds with loss of 89% of the SRCPC height. The retaining of 11% height for the concentrator corresponded with the concentration ratio of 3x.

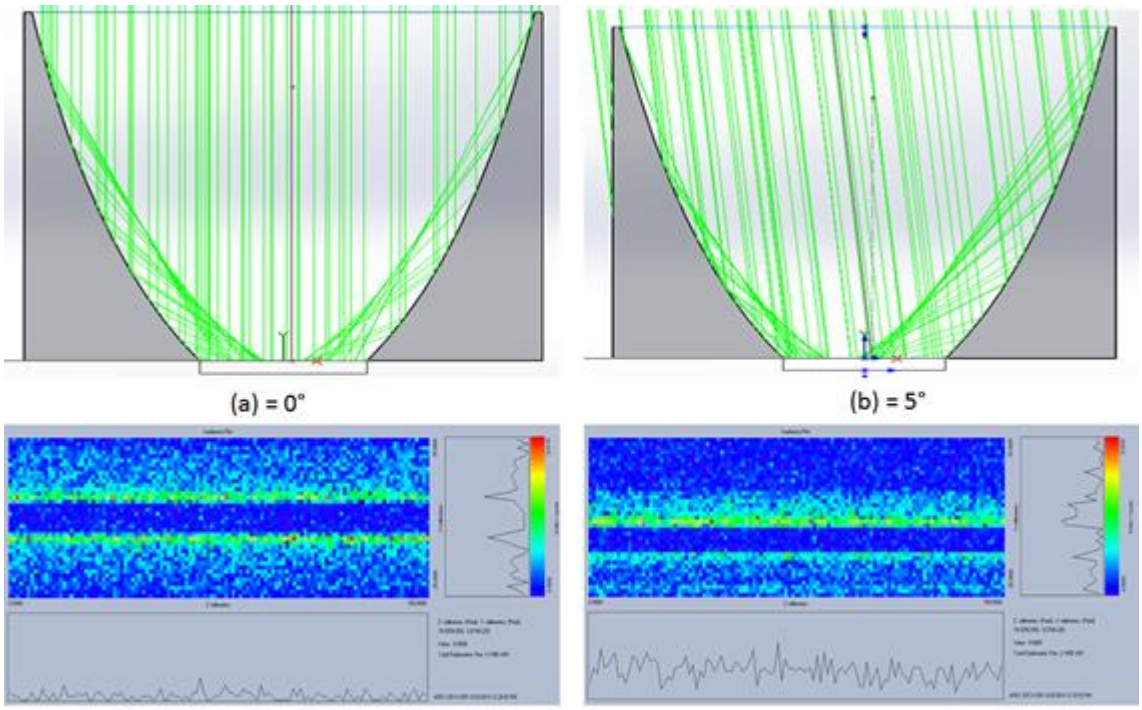

Flux distribution at concentrator (a) in E-W direction

Flux distribution at concentrator (b) in E-W direction

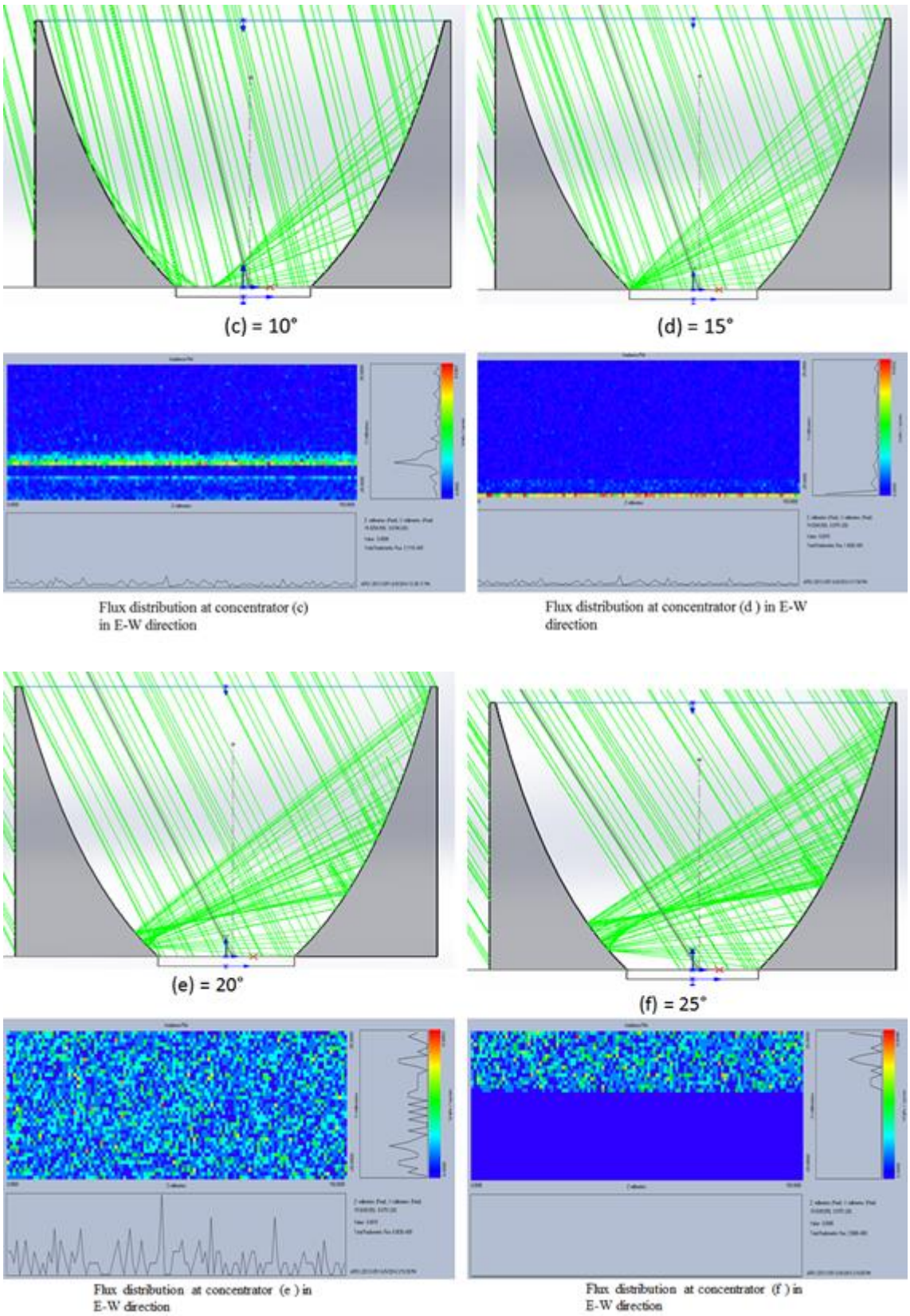

Figure 3.12: Ray trace diagrams and flux distribution under each concentrator for truncated SRCPCs in the E-W direction at (a) to (f)

3.7.6 Optical properties measurement of reflective thin film material used

Solar energy system efficiency is determined to a large extend by the optical properties (meaning absorbtance, transmittance and reflectance) of the system components. It is clear that the optical performance play an upper limit on the entire performance of the system. It is therefore vital in solar energy research to perform optical characterisation of the system components. The absorbtance of the solar cells, the reflectance of the concentrator reflectors and the glazing cover are the significant properties for concentrating photovoltaic system. The optical properties of system components of CPV/T systems are studied using different techniques but in this work, Perkin-Elmer 1050 was used. Effort was concentrated on Perkin-Elmer 1050 to measure solar cells absorbance (k), transmittance percentage and reflectance solar cells, thin film and glass materials. By learning the use of different spectrophotometers of Perkin-Elmer 1050, the spectral reflectance, transmittance and absorbance of planar reflectors, solar cells and glazing materials were measured. It basically consists of two large sampling compartments, a variety of snap-in modules and accessories, including a general purpose optical bench, integrating spheres, a universal reflectance accessory, a light source, detectors and filters. It was used to achieve high level of sensitivity, speed and resolution in the NIR range. Also, it was able to simplify the analysis of difficult samples of high absorbing and low iron glass, thin film filters and optical coating. The achieved reflectivity result for thin film reflector used was in the range of 68% – 83% for UV spectrum of 250-500nm, 84% - 82% for visible light (AMO) of 500-750nm, for the blackbody spectrum (750-1000nm) it was 82% - 86% and the AM1.5 spectrum (1500-1750nm) had 83% - 81% as shown in

Figure 3.13. The simulated optical reflection was 94% while the measured reflectivity of the thin film used was between 84% to 82% of the visible light. The reflectivity percentage of the material used was below expectation compared to the reflectivity percentage used in the optical modelling. This difference might be because of high reflection, non-specular reflection of the incident light beam, tracking errors, slope errors and receiver alignment errors. However, the two results were similar and close to expectations.

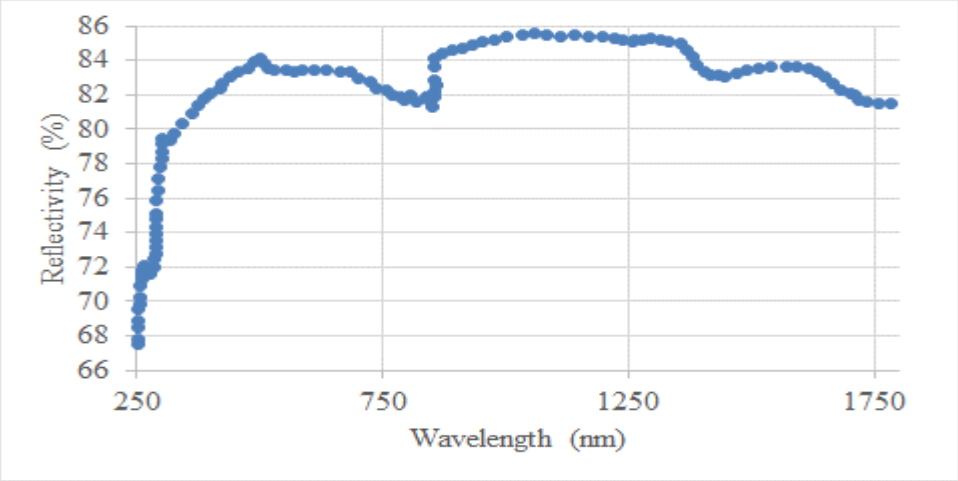

Figure 3.13: Results of the reflectivity thin film reflector used in the developed SRCPC carried out.

3.7.7 ***Optical flux distribution***

For optical flux distribution, the exit aperture concentrated rays differs in the flux distribution to those at the acceptance and the entry aperture of the SRCPC. At the same time, each case of the different incident angles, there will be a different illumination distribution. During the simulation process by using the OptisWorks software, a few assumptions are made as follows ; 1) The parabolic sidewalls simulation are 94% reflective, 2)The rays are considered to be the beam radiation that has an area which is dependent on the distribution of the incident ray at the entry aperture.

As it can be seen in Figure 3.8 that the entry aperture is considered as a rectangular area for calculations to be made easy while at the point which the ray reaches the exit aperture, it is considered as rectangular of smaller size. The principle of superposition of rectangular area at the exit aperture is then used to get the data for the optical flux distribution.

The SRCPC optical flux denotes the number of rays concentrated in same area of the exit aperture. This is obtained as follows, each solar ray is considered as an area of a rectangle but the size of the rectangle is dependent on the number of rays that enters the entry aperture area. The optical flux distribution of non- dimensional numbers represents the number of rays hitting the same areas. Also, this is equivalent to the local concentration ratio. All incident rays have a non-dimensional value that is equal to 1. It is the optical flux distribution that illustrates how the concentration is distributed on the exit aperture.

The energy value of concentrated rays falling on the same area after reflection sum up to give the optical flux value. It is important to note that if the energy of the incident rays at the entry aperture is equal to 1000 W/m^2, then the energy at a specific area of the exit aperture of the SRCPC should be equal to 1000W/m^2 multiplied by the optical flux of that specific area.

In order words, it is a general method to determine the energy of the radiation of the exit aperture of the SRCPC for any energy of the radiation of the incident rays. It is obvious to see that the results of the optical flux distribution indicate that the energy on some areas of the exit aperture are 50 times the energy of the exit rays. They could be defined as the hotspot areas that are located in different positions at the exit aperture depending on the incident angle. They are located in different positions at the exit aperture depending on the incident angle. They are located in the corner at normal incident rays to the entry aperture as shown in Figure 3.14 (d), (e) and (f) respectively. At an incident angle of 20 degrees in the diagonal plane, many of the rays concentrated constitute a hot spot at the middle of a concentration.

3.7.8 ***Optical efficiency of the SRCPC***

The SRCPC acceptance angle is determined from the results of the variation of the optical efficiency. It is a function of the incident angle of the input light rays. For concentrators that are ideal, 100% of the rays within the acceptance angles are collected, the ray trace from the results gives the number of rays collected for different incident angles θ and the number of reflection (Nre) of each ray before reaching the exit aperture. Therefore, the optical efficiency is defined as

$$EFF_{optical} = \frac{\boldsymbol{PNre}}{\boldsymbol{number\ of\ incident\ rays\ at\ the\ entry\ aperture}} \qquad 3.19$$

Where P= 0.94 (reflectivity of the thin film side reflector of the SRCPC). The three concentrators were optimised and simulated in the S-N and E-W directions for each of them. The energy input and output were measured in order to get the optical efficiencies of each.

From Figure 3.14, it is seen that the smaller the acceptance half angle of the concentrator, the higher the optical efficiency. On the other hand, as the acceptance half angle increases, the lower the optical efficiency. Type 10°concentrator along direction gives much higher optical efficiency and a steady slope than other types. Also, Figure 3.14 and Figure 3.15

shows the combined optical efficiencies of the SRCPC concentrators under 0.94 reflectivity using 50mm solar cell in the W-E direction and diagonally.

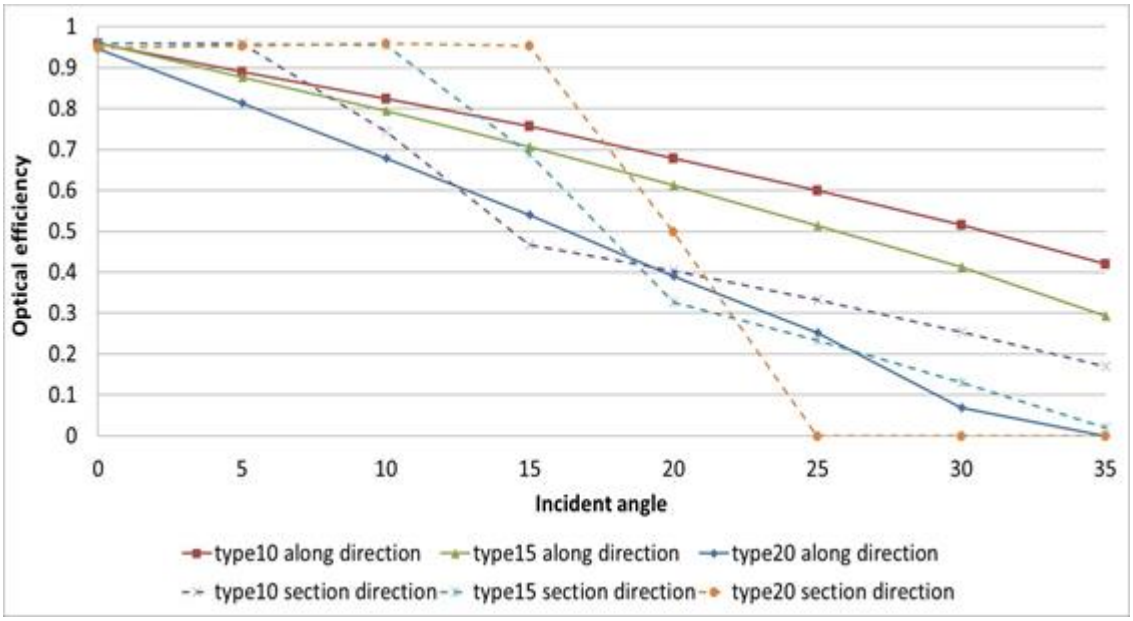

Figure 3.14: Different directions of incident angles of the three concentrators indicating their optical angles displaying the decaying nature of efficiencies along the incident angles

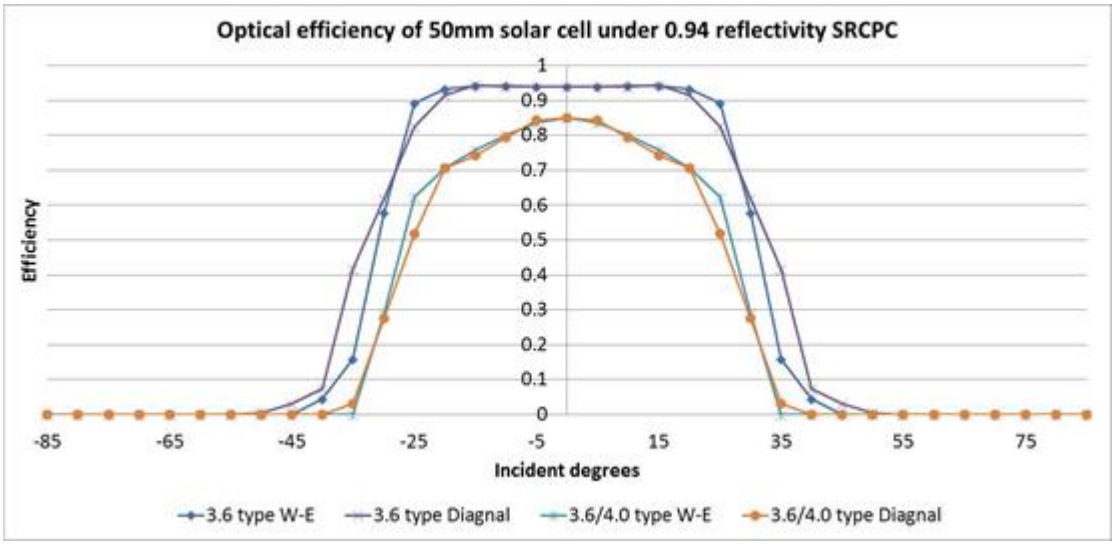

Figure 3.15: Combined Optical efficiencies of the SRCPC concentrator under 0.94 reflectivity using 50mm solar cell at the W-E and diagonally

Figure 3.15 shows that both directions have large optical efficiencies towards noon and after noon. When designing a solar concentrator and to simulate its performance, generally, an important assumption is very essential. That is to say that it is necessary having uniform optical flux distribution and uniform temperature on the surface of the solar cell. As observed in the graphs above, that the flux distribution is uneven in some cases and this will have an effect on the solar cell efficiency [178]. As a designer,

it was ensured that the focused illumination has to be uniform to a level that the total efficiency of the SRCPC system does not reduce. Luque and Andreev [179, 180] as well as the Franklin and Coventry [181] discussed the efficiency drop in the CPV systems which are as a result of the non-uniform optical flux. As the solar irradiance increases, there is also increase in solar cell efficiency.

Also, at the same time, at the peak of intensity and the increase of temperature generates resistive losses in the cell because of the internal resistant in the cell material. It will reach a stage where the increase in resistive losses is equal to or surpasses the efficiency increase because of the radiation concentration. The preferred solution could be cooling of the system and decreasing the distance between the conducting fingers in the solar cells. It happens in concentrator cells through decreasing the spacing between the conducting fingers by the use of low resistant substrate for the cell and also introducing a back surface field [highly doped back substrate]. It permits lowering the bulk and contacting resistances. Active cooling medium is an effective means of heat transfer too. All the techniques used allows or makes it possible to manufacture cells and optimised for several hundred suns [30]. However, from the result so far, it can be concluded that a SRCPC formed for 2D compound parabolic concentrator is an ideal concentrator for the half acceptance angle $(Q_a) = 10°$.

3.7.9 ***Validation of the optical model***

An experimental study is carried out in order to validate the optical model that is developed. The next sections describe the computer manufacturing of the SRCPC model and the results obtained.

3.8 Computer aided drawing (CAD) of the symmetric reflective compound parabolic concentrator (SRCPC)

The prototype (proof of concept) CAD twin SRCPC was assembled to form a standard 1m x 1m size which constituted 8 numbers of concentrators. This was to form a $1m^2$ area standard measurement of solar radiation. The reason for this was to check what power can be generated using the standard measurement. Unfortunately, no solar simulator with this capacity was available to be used to simulate for the achievement of this desire. The Plan assembled original un-truncated CAD drawing with dimensions is shown in Figure 3.16 ready to be constructed. They further translated the design into

CAD. The CAD design was translated by the computer into a list of instructions the manufacturing computer can interpret. The experimental SRCPC model has a rectangular acceptance aperture of 150mm x 225mm and exit aperture area of 50mm x 225mm with a truncated height of 105.73mm. The SRCPC inside surfaces are covered with commercial reflective films having reflectivity of 85.9%, which is closer to the 94% reflectivity value entered in the simulation.

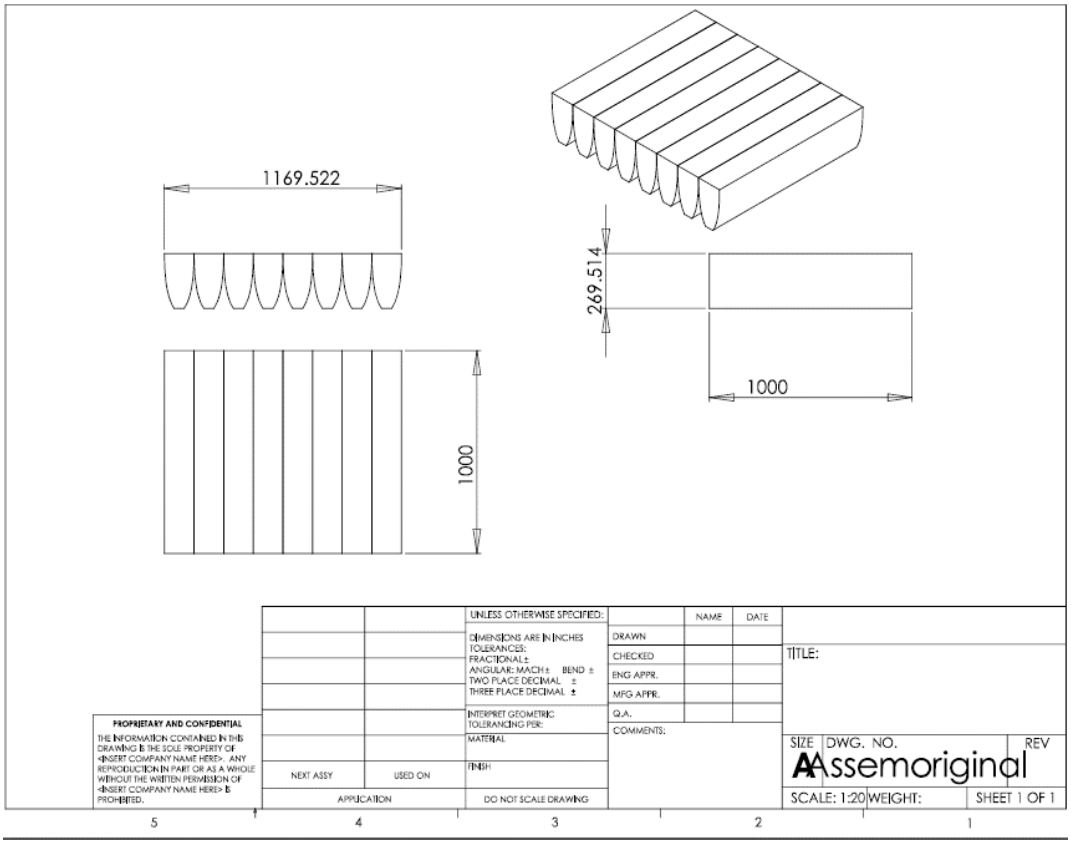

Figure 3.16: Plan assembled original un-truncated SRCPC CAD drawing showing 8 concentrators in 1m x 1m dimension

It also shows Plan assembled original un-truncated SRCPC CAD drawing indicating 8 concentrators in 1.0m x 1.0m dimension while Figure 3.17 shows the truncated of same SRCPC CAD drawing. Figure 3.18 shows the structural support stands and brackets during installation after commercialisation.

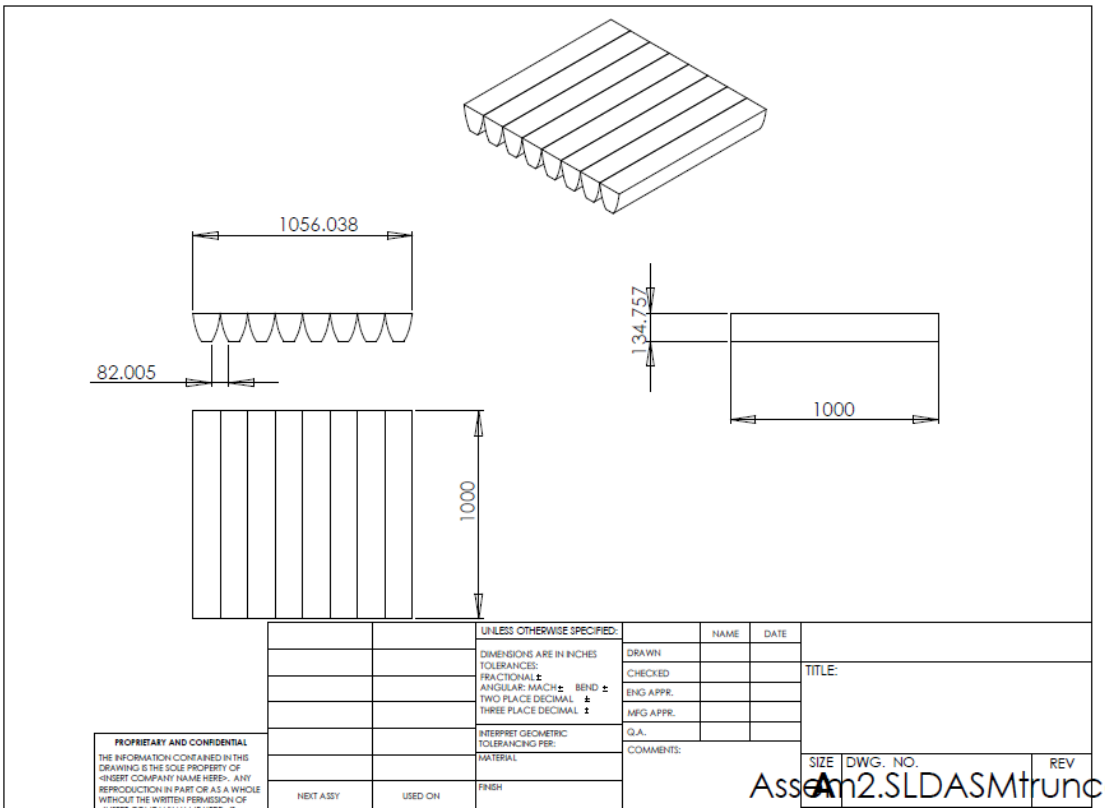

Figure 3.17: Plan assembled original truncated SRCPC CAD drawing showing 8 concentrators in 1m x 1m dimension.

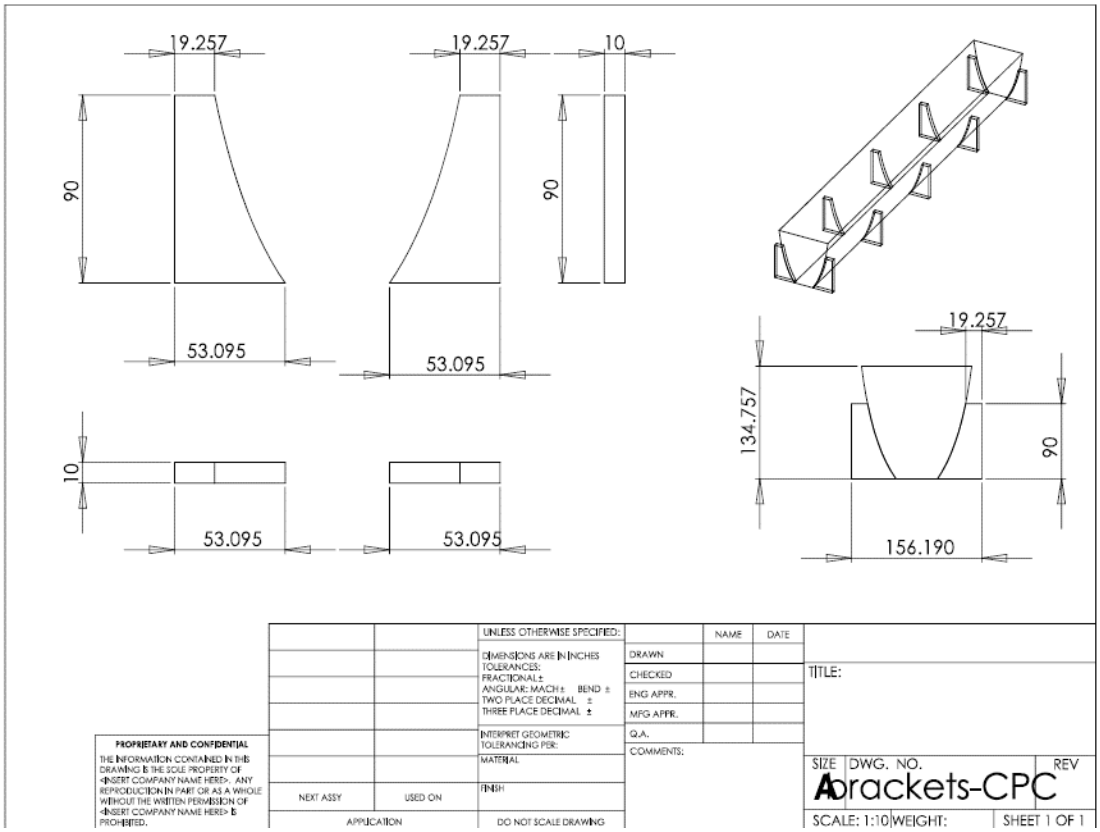

Figure 3.18: Plan assembled original truncated SRCPC CAD drawing showing a concentrator with supported brackets stands having dimensions at installation

Figure 3.19 shows complete designed schematic diagram of the designed model of SRCPC covered with tough low iron glass, the reflective film and all accessories. The largest available solar simulator in the University of Exeter Penryn Campus can only carry two concentrators because its effective area is 21cm x 21cm. The proof of concept was reduced to match this area.

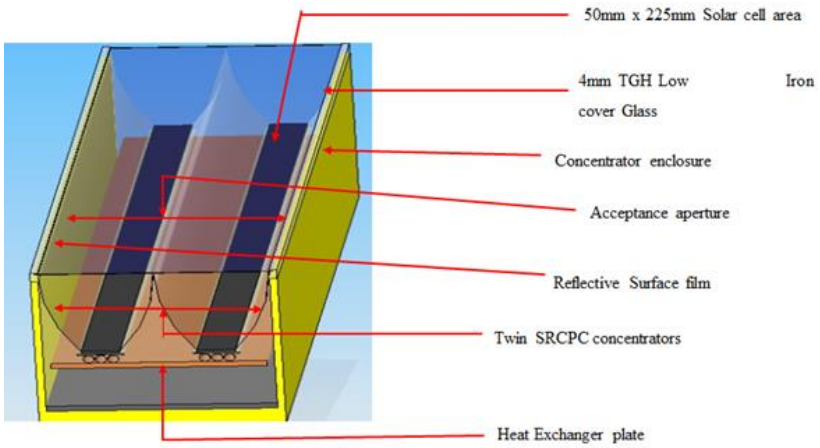

Figure 3.19: Shows schematic experimental model of SRCPC covered with the reflective film

3.8.1 ***Solar cells soldering***

Eight LGBC solar cells designed for a concentration of $\leq$ 10x are connected in a string of four in series and then 2 rows in parallel. The solar cells are cemented underneath with thermal heat sink and placed on top of a heat exchanger. The solar cells are encapsulated with Sylgard materials on top of the solar cells. The soldering of the solar cells using lead free PV ribbons having a thickness and width of 0.1mm respectively. The thickness of the bus bars of the solar cells have 1.0mm width. The PV modules are connected by a lead free PV ribbon with 3mm width with and without the SRCPC and a measuring instrument. The following procedures for the electrical connections are ; a) The required length of the lead free PV ribbon is cut and cleaned [i.e. the length between the positive of one solar cell to the negative of the next solar cell], b) Soldering flux is applied to ensure that the surfaces of all the components to be soldered are cleaned, free from grease, moisture and dirt, c) The soldering iron maintained at a controlled temperature of 350°C is used to heat the surfaces and lead free ribbon at the same time for the connection. At the tip of both ends of the connection pieces, an amount of liquid flux is applied for a more controlled and effective use of the soldering material.

The importance of flux cannot be underscored as it is a key component in soldering because it removes oxidation that hinders solder from bonding to metals. A small amount of solder using a soldering rod is applied to both ends of the connector piece of the PV ribbon. The use of too much solder can cause overflow during tabbing with cells thereby causing short circuit. Too much use of the solder can cause increase of series resistance of the module. The procedures for soldering includes: 1) The positive (backside of the solar cell) is connected with one end of the connector piece first. The same is carried out to all the solar cells to be used. Low temperature soldering is used as high temperature soldering can cause serious damage to the solar cells. 2) The solar cells are aligned using the soldering board for the next stage of soldering to the front side [negative of the solar cells] but the gap between cells must be maintained. 3) During the connection process, force must not be exerted on the solar cells in order not to cause cracks or damage thereby causing open circuits. 4) Four solar cells are connected from positive to negative to make a string for one side of the rectangular concentrator which is 225mm long. The same process is followed for the second string for the second concentrator. 5) These two strings that were connected serially, were then connected in parallel. 6) The positive terminal and negative terminal are insulated using polarised coding tubes. 7) The last step which is very important is to check if there are any short circuit connections in each string and after the final connection.

3.8.2 Materials for encapsulation

After applying the thermal conductivity paste at the back of the solar cells, the solar cells are placed on top of the heat exchanger that had been insulated. The strings of solar cells are aligned on top of the heat exchange to avoid the concentrator touching or causing damage to the cells. The alignment was done to ensure that the concentrator reflector was very touching the solar cell without any gap between them. The encapsulation material Sylgard – 184 silicon elastomer mixed to proportion is casted on top of the solar cells. In solar applications, Sylgard – 184 elastomer is a two part silicon that cures to a flexible elastomer for the protection of electrical and electronics device. In solar cells it is used to encapsulate or adhesive. Sylgard – 184 silicone is supplied as a base and curing agent in two separate containers that are mixed in the proportion of 10:1 by weight. Volatile compounds are released during the mixing process when mixing the base and the curing agent. Therefore all weighing, mixing, and stiring must be carried out wearing nitrile gloves and in a fume cupboard. The mixture is normally stirred for 10

minutes thoroughly. This is meant to be done gently in order to minimise the amount of bubbles formed. When the mixture is further allowed to settle for ten minutes, the majority of the air bubble evaporates. It is called the pre-treatment stage. After this, the mixture is placed in a vacuum chamber. The purpose is to ensure that all remaining air bubbles that are trapped inside the mixture and all visible bubbles are removed when the process is repeated 3-4 times. The duration for preparing the encapsulation is 30-35 minutes approximately but it is depending on the amount of bubbles introduced during stirring.

In applications, hard adhesive is required for priming prior to pouring the encapsulation materials onto the solar cell assembly. To both the solar cell and glass, a liquid primer (Dowcoming primer – 92 – 023) is applied to the current work. The use of primer enhances the adhesion between Sylgard and a wide range variety of surfaces .i.e. metal and glass. Therefore, the surfaces must be thoroughly air- dried close to application of the primer and the material to be encapsulated. For best results, the primer is applied using brush. It should be applied with thin but uniformly coated and wiped off after application. This is allowed to dry for ten minutes. If left for a longer duration, the primer begins to form a white pigment. Therefore it is necessary that as soon as the primer dries, the encapsulating materials prepared be poured onto the solar cell. The Sylgard – 184 silicone elastomer is either cured at room temperature of 25 degrees or heat can be applied to speed up the curing process [182]. Also room temperature curing is allowed to avoid any misalignment of the cells from the heat exchanger and the concentrator position.

*3.8.3 **Experimental setup***

The first test was the measurement of the electrical power outputs under different conditions. The electrical power of each string was measured separately and also measured together both in series and parallel. Various conditions were used in the testing with and without the SRCPC using the WACOM simulator. MP 160 IV tracer and a computer were uses to record the results. At the standard reporting conditions, the spectral light distribution resembles the global distribution. Mammo et al in his experimental measurements used this same conditions [183]**.** Different measurements and conditions were used to carry out the experiment. Measurements of the strings connected in parallel individually with and without SRCPC, with and without heat exchanger were carried out at different solar intensities. The volume flow rates were also varied to achieve high efficiency. The WACOM simulator used has no need of varying angles. Also, a stable

wooding area for the sample [SRCPC] was already provided. The indoor characterization chapter explain better. However, it is a fact to know that Optis works can generate a larger amount of incident rays thereby resulting in better resolutions of the optical flux distribution. It is also sure that this does not impact on the accuracy of the output of the results but for the aesthetical presentation where the resolution is notably clearer. Throughout this thesis work, Optis works was used to carry out all the optical study.

3.8.4 ***Conclusion***

The studies of the SRCPC hollow concentrator include the use of different optical simulation and commercial Optis software. Three concentrators with acceptance half angles of 10°, 15°, and 20° were designed, modelled, simulated and the optical performance predicted for symmetric reflective compound parabolic (SRCPC). Extensive optical analysis was carried out for these concentrators. The maximum optical efficiencies achieved by these concentrators (10°, 15°, and 20°) acceptance half angles were 94%, 94% and 91% respectively. They maintained high optical efficiencies over the collection range for each of them. This implies a perfect parabolic geometry. The truncation affected slightly the energy input at the acceptance and exit aperture. The energy distribution for the different concentrators vertically seem to be the same at direct solar radiation and distributed uniformly. However, there are variations and hot spots at some few instances. The remaining work in this thesis depends largely on this chapter. It introduces nearly all the theoretical and experimental techniques that are used to characterise the novel symmetric reflective compound parabolic concentrator presented in the next chapters.

Chapter 4 **HEAT EXCHANGER DESIGN AND ITS CONSTRUCTION**

4.1 Summary

Reflective and refractive optical materials are used by concentrating photovoltaic to concentrate a large amount of solar energy onto a small area of PV material. Electricity production cost can substantially be reduced by the use of CPV systems. Nevertheless, the associated increase in temperature with CPV systems post a significant hindrance to the realization of this potentials that may in turn lead to rapid degradation of the system. Moreover, during this high temperature conditions the open circuit voltage of the PV receiver is also reduced thereby leading to a corresponding loss in power output. Therefore, it becomes unavoidable to gain an understanding of the thermal energy transfer mechanism of the low concentrating photovoltaic systems. The thermal model developed for low concentrators illustrates various thermal transfer and dissipation mechanisms which occurs within the SRCPC systems. The purpose of this chapter is to measure the temperature rise and its control. The purpose of incorporating and using the heat exchanger in the system was to check and estimate the amount of heat that can be extracted from the system which can be used for other applications and also to bring down the temperature of the system to standard temperature so as to ensure the overall system operate at best efficiency. This thesis will further discuss the thermal and optical systems designed with a focus on the system parameters as a thermal management system is employed.

4.2 Introduction

In non-imaging or low concentration photovoltaic systems, efficient thermal management will increase maximum power output and at the same time increase operational lifespan of the system significantly. Further to this, it becomes fundamentally important to develop a thorough understanding of the thermal transfer along with the dissipation mechanisms that are associated with concentrating photovoltaic systems [184]. The symmetric reflective compound parabolic concentrator (SRCPC) system is a low concentrator under consideration here, which has four standing parabolic reflectors optically designed. The geometric concentration ratio is 3x. Two strings of four solar cells each are electrically connected to a set of reflective parabolic concentrators.

The temperatures of the SRCPC are to be recorded without a thermal management system and later with thermal management system. The developed thermal model will be assessed under various environmental conditions. Results in this chapter will further allow incorporation of thermal management systems in design and operation of this low concentrating photovoltaic systems.

or heat to be transferred from solar cells of compound parabolic concentrators there is need to estimate the efficiency, size and cost of equipment that is necessary to transfer a specified quantity of heat energy at a given time. This will follow a heat transfer analysis [185].

The parameters of heat exchangers and solar cells does not depend so much on the quantity of heat to be transmitted but depends on the rate at which heat is to be transferred within some boundary given conditions. The determination of the rate of heat transfer at a temperature difference is the major problem required to size a solar collector to provide energy to a particular building or home.

4.3 The design parameters of a parallel flow heat exchanger

The size of the heat exchanger can be considered by energy balance of the system, which is the power received by the concentrator Absorber, Qc, balances by the power converted to the electricity, Pm, the power transferred to air, Qair, and the power transferred to the heat exchanger, Qe,

$$Q_c = P_m + Qair + Qe \qquad 4.1$$

In this study, water is used for both the hot fluid carrying the heat from concentrator and the coolant. Table 4.1 shows the parametric calculations used for designing the heat exchanger.

Table 4.1: Showing parametric calculations used for designing the heat exchanger

Density of Collant (kg/m^3)	Tcolant in (°C)	T collant out (°C)	T air (°C)	Temp of absorber surface (°C)	Diamater of in/out let pipe (m)	Volum rate (m^3/s)	C (water, J/kg K)	Qe (W)	Qc (W)	Pm (W)	L(m)	Area of collector (m^2) Ap	U(w/m^2 K)	Thermal efficiency of exchanger	Total thermal Effeciency	Heat transferred to Air (W)
1000	25	50	25	70	0.006	7.065E-08	4192	7.404	11.25	3	0.225	0.01125	1.671	0.658	0.733	0.846
1000	25	48	25	70	0.006	7.065E-08	4192	6.812	11.25	3	0.225	0.01125	2.841	0.605	0.733	1.438
1000	25	45	25	70	0.006	7.065E-08	4192	5.923	11.25	3	0.225	0.01125	4.596	0.527	0.733	2.327
1000	25	40	25	70	0.006	7.065E-08	4192	4.442	11.25	3	0.225	0.01125	7.521	0.395	0.733	3.808

The heat transfer rate from concentrator to the air can be estimated by,

$$Q_{air} = U_h A_p (T_s - T_a) \qquad 4.2$$

where U_h is the effective heat transfer coefficient ($W/m^2 K$) of air flowing crossing the absorber surface, which is difficult to choose as it varies with design and flow parameters, while, can be estimated from the experiments; Ap is the area of absorber surface. This area is to be decided by the heat transfer rate balance (Eq. 4.1). Ts and Ta are the temperatures of absorber surface and air, respectively.

The heat transfer rate by coolant of the heat exchanger can be calculated by using the coolant volume flow rate $\dot{V}$ (m^3/s) by,

$$\dot{q_e} = \rho \dot{V}\, C\, \Delta T_c \qquad 4.3$$

where ρ is the density of coolant (kg/m^3); ΔT_c the temperature difference between the temperatures at the coolant flow out and flow in, C is the specific heat capacity of coolant (kJ/(kg K)),respectively. The coolant in this study uses water.

By Eq 4.1 to 4.3, we have,

$$A_p = [Q_c - P_m - Q_e]/[U\,(T_s - T_a)] \qquad 4.4$$

Meanwhile, once the size of the exchanger is decided, the effective heat transfer coefficient, U_h, can be estimated. From experiments, the coolant volume flow rate is measured as **7**.065E-8 m^3/s (7.065E-5 L/s) with coolant mean flow velocity of 2.5mm/s and the diameter of the pipe of 0.006m. With the heat capacity of water being 4.192 kJ/(kg K) and density of 1000 kg/m^3, the heat transfer rate by the coolant can be estimated using Eq 4.3 as 7.4W when inlet and outlet temperature of coolant is assumed to 25°C and 50°C, respectively. The inlet temperature is estimated by the temperature of the absorber surface.

In this study, the area of the exchanger marches the area of absorber, L=0.225 m and the width b=0.05m (A_p=0.01125 m^2), as shown in Table 4.1 . Then the effective heat transfer coefficient is estimated for our heat exchanger as, U_h=1.67W/(m^2 K) when the absorber temperature is chosen as 70 °C (at the maximum temperature) and air temperature of 25 °C and the with estimated power absorbed flux by the collector of 1000 (W/m^2).

4.4 Thermal efficiency of the solar collector

With the estimated heat transfer coefficient, the thermal efficiency of the solar collector can be estimated by the heat transfer rate by the heat exchanger and that to the air with estimated power absorbed by the collector, Q_c, as

$$\eta_{th,s} = (Q_e + Q_a)/(A_p G_T) \quad 4.5$$

Where Ap =0.01275m is the area of the solar abstractor. The thermal efficiency is about 76% if the power absorbed flux by the collector of G_T =1000 W/m^2 under the conditions discussed in 4.3. And the thermal efficiency of heat exchanger, defined by, = $(Q_e)/(A_p G_T)$ is about 67%, while 39% if the coolant inlet temperature is 40 °C.

4.4 Design of flat plate parallel flow heat exchanger

The common types of flat plate heat exchanger design offers improved efficiencies for their size. They are known to provide a relatively large heat transfer surface in a small space. They can also operate a higher fluid pressure. Therefore, designed parameters are shown in Table 4.2.

Table 4.2: Heat exchangers design parameters of covered SRCPC system

G_T	1000W/m^2
$\dot{m}$	0.0562L/s
D	6mm/8mm
ρ	1000L/s
T_{in}	25°C
T_{sc}	70ºC
C_P	4.184J/kgºC
I_m	0.883A
V_m	2.479V
Thickness of aluminium sheet	0.00952m
B	0.05m
L	0.225m
A_{ac}	0.03375m^2
A_{rc}	0.2347m^2
A_p	0.01125m^2
R’	0.84
α_P	0.9, 0.8
τ_g	0.95
$\dot{q}$	10.36W/m^{2}K
U	54.29W/m^{2}K
V_w	2.5 mm/s
η_{th}	47.07%
η_{elect}	15%

Figure 4.1 shows the designed flat plate heat exchanger. This design was meant to allow a small amount of space between each plate to allow the heat transfer fluid (water) to circulate and extract heat from the plate as it flows. Due to the fact that the surface area of the plate exchanger is large, it permits maximum contact between the transfer fluid that allow for effective and efficient heat transfer. For multiple parallel flow of water in and out of the heat exchanger, the channel tubes were calculated to be 6mm in diameter occupying the surface area. The channel tubes were 6 in number while the inlet and outlet ports were calculated to be 8mm in diameter but the connecting pipes were 10mm clipped at each end. The inlet and outlet pipes has an inner diameter to be the same with the inner channel tube but the outer diameter serves as a stopper and connector as illustrated in Figure 4.2. This flat plate heat exchanger design is a parallel flow type because the heat extracting fluid flow in the same direction through the six tubes of 6mm diameter in the heat exchanger being the transverse of the top view as shown in Figure 4.3. This application is in small heat water – to – water transfer application. The finished designed product of the heat exchanger is shown in Figure 4.4 where the 6 numbers of

6mm diameter channel tubes were sealed with M8 grub screws. Figure A1 in appendix shows the design inlet and outlet pipes of the heat exchanger with the inner and outer dimensions in mm.

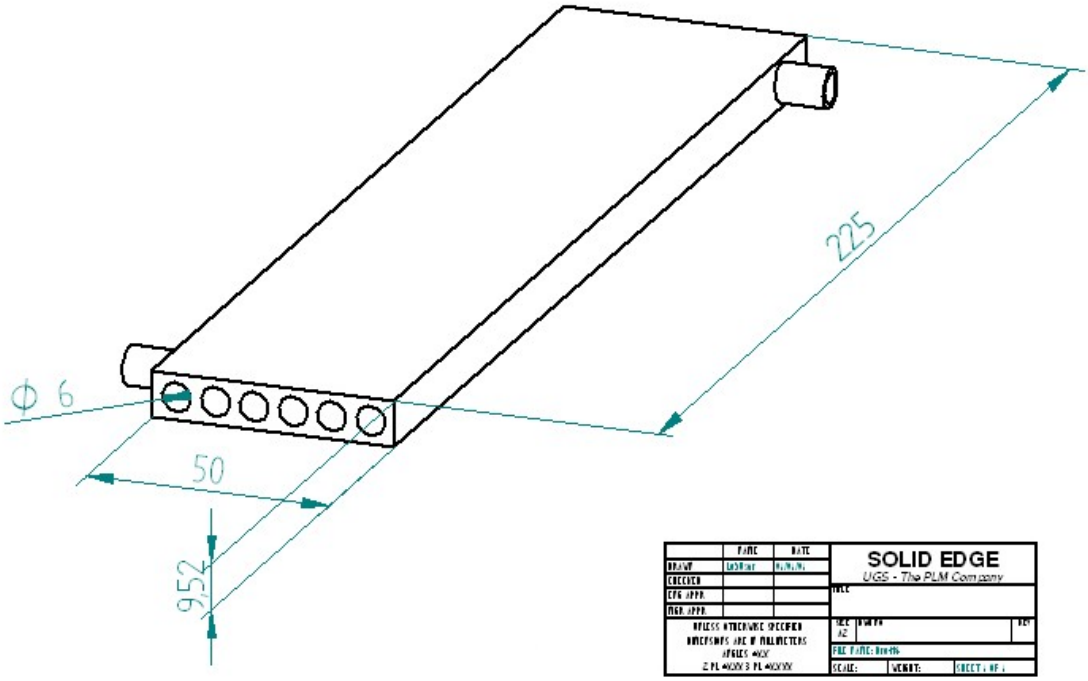

Figure 4.1: Designed flat plate heat exchangers showing dimensions

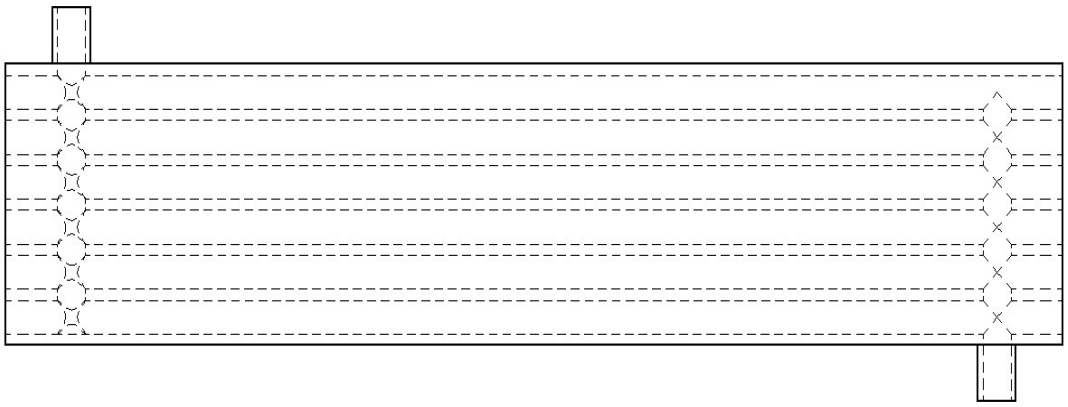

Figure 4.2: Showing a schematic diagram of the channel tubes layout in the designed flat plate heat exchanger.

Figure 4.3 Shows transverse top view of the designed heat exchanger indicating parallel flow direction from the inlet to the outlet.

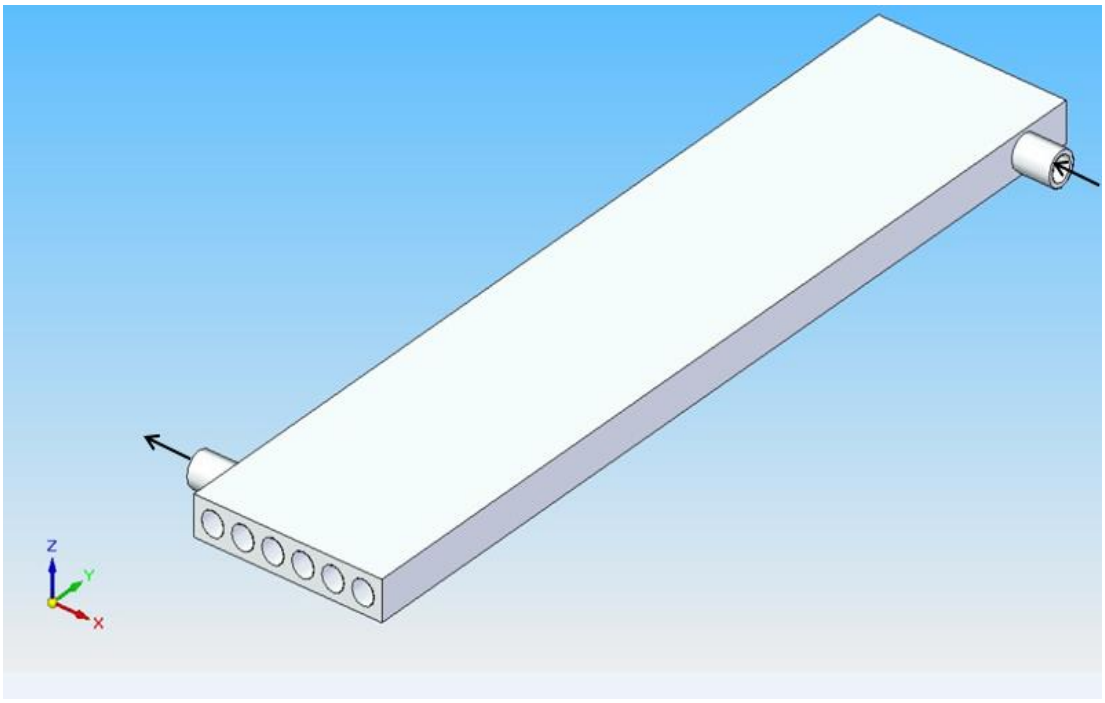

Figure 4.4: Finished designed parallel flow flat plate heat exchanger product.

4.5 Heat Exchanger construction

The flat plate heat exchanger used in this study is constructed using weld able aluminium flat sheet with a thickness of 9.525mm x 50mm x 225mm. Six apertures serving inlet and outlet ports were drilled each having a dimension of 6mm through the length of 225mm. Computer Aid program was used to set the parameters while a lathe

machine with sized drilling bits was use to bore the holes. Due to lack of a drilling bit long enough to accommodate the length of the heat exchanger; it was divided into two equal parts and welded back using 6mm diameter connectors inside the heat exchanger. The surface was smoothened using a smooth filing machine. The finished constructed heat exchanger is shown in Figure 4.5. Due to the inlet pipe connecting the two heat exchangers, there were little modifications in the position of the outlet pipe. A 10mm diameter pipe was used as the connecting pipe. Clear Acrylic laquer gloss was applied to the surface to act as an insulator and to avoid leakage of current. Thermal conductivity paste was applied between the surface of the heat exchanger and the solar cells. A thermal insulating material was placed under and around the heat exchanger to avoil heat losses excaping under neath.

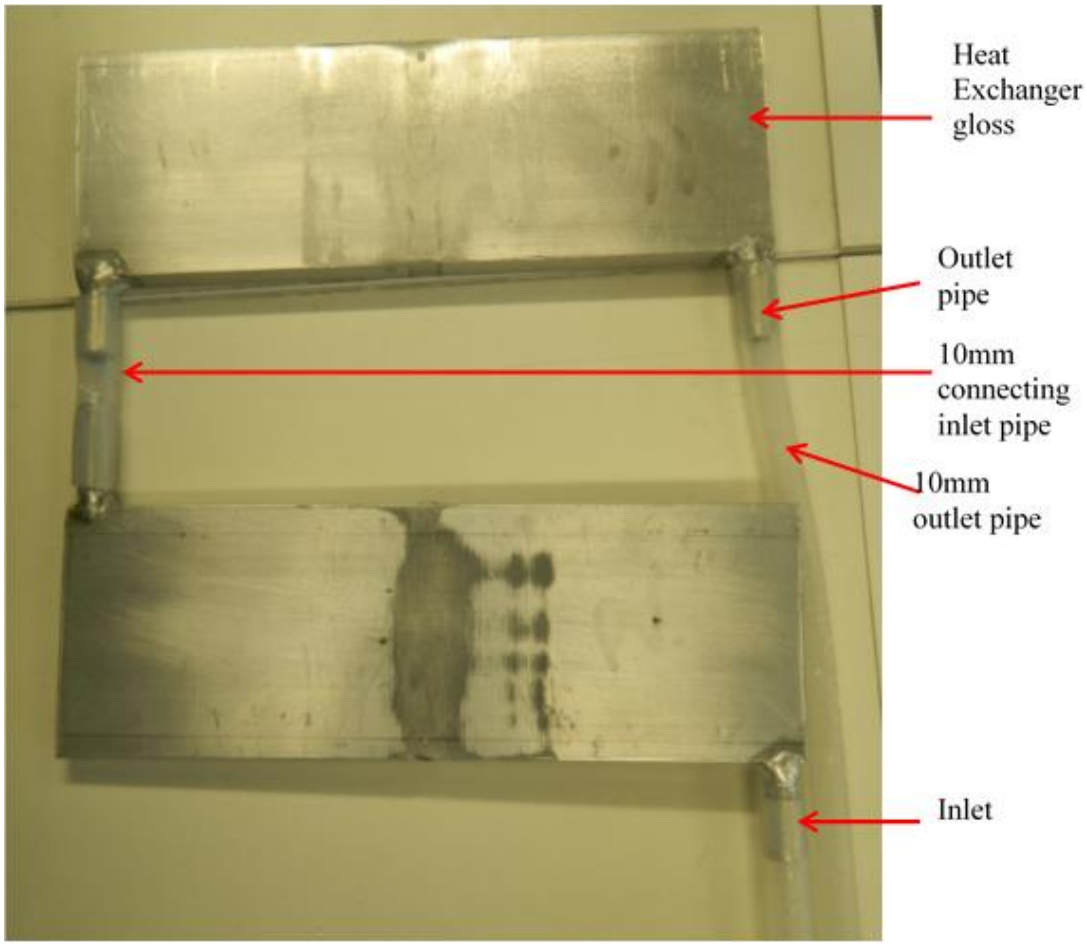

Figure 4.5: Designed and constructed heat exchanger

4.6 Low concentration photovoltaic thermal modelling

It has become very necessary to develop and have experimental evaluation to fully understand the energy transfer mechanisms that are connected with non-imaging

concentrating systems. Therefore, a thermal model is used to predict the operating temperature of concentrating photovoltaic systems and also assess their thermal management requirements [189].

4.6.1 ***Various ways of dissipating energy.***

Thermal management system or thermal modelling is hinged on the principle of energy conservation. It states that energy cannot be created or destroyed but it is changed from one form to the other. Irradiance is the only one form of energy unto the concentrating Photovoltaic system but various ways exist through which energy is dissipated. These include electrical, radiation and convection. This is indicated in Figure 4.6 as energy dissipated and energy absorbed. Energy is also loss through optical materials and reflection. The anti-reflective properties of solar cells make energy lost through reflective negligible.

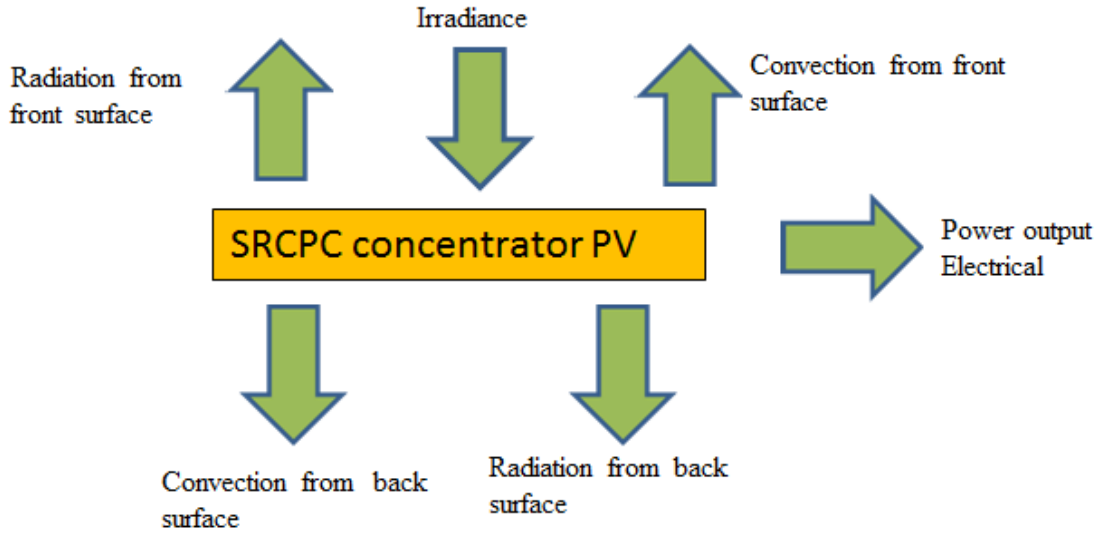

Figure 4.6: Various ways of dissipating and absorption of energy in low concentrating Photovoltaics.

4.7 Thermal model and initial performance of the heat exchanger

4.7.1 ***The purpose of thermal modelling***

It is necessary to have an energy balance model for concentrating photovoltaic and thermal systems. The concentrating photovoltaic and thermal system including its environment are characterised using a set of input parameters in the model. The system's electrical and thermal efficiencies are the main outputs of the model. Optical losses are

accounted for in the energy balance model. Furthermore, thermal losses are a derivative from a thermal network model of the hybrid absorber. The performance of the solar cell is modelled as a function of the temperature together with the solar radiation. The model strength is confirmed by a sensitivity analysis of all input parameters. The operating temperature influence on the electrical and thermal performances and the total efficiency of the system is checked. Also in the model, the limitations of maximum electrical and thermal power output are verified. The concentration ratio influence on the electrical and thermal performance of these two power outputs are analysed in detail [190].

4.7.2 ***Developed thermal model***

The developed thermal model was based on the principle of conservation of energy with many assumptions thus; 1) A parallel heat flow systems [one dimension] is considered. 2) The heat capacity of insulation, absorber, glass cover and solar cell is insignificant. 3) There is no temperature slope across the thickness of glass, insulation and solar cell materials. 4) There are negligible ohmic losses in the solar cells. 5) The covered SRCPC heat exchanger water medium system is in quasi state. 6) Irradiance is the only source of incident energy. 7) The thermal energy is dissipated through convection and radiation for the conversion of irradiation into electrical energy. Figure 4.7 shows a cross-sectional side-view of the covered SRCPC described.

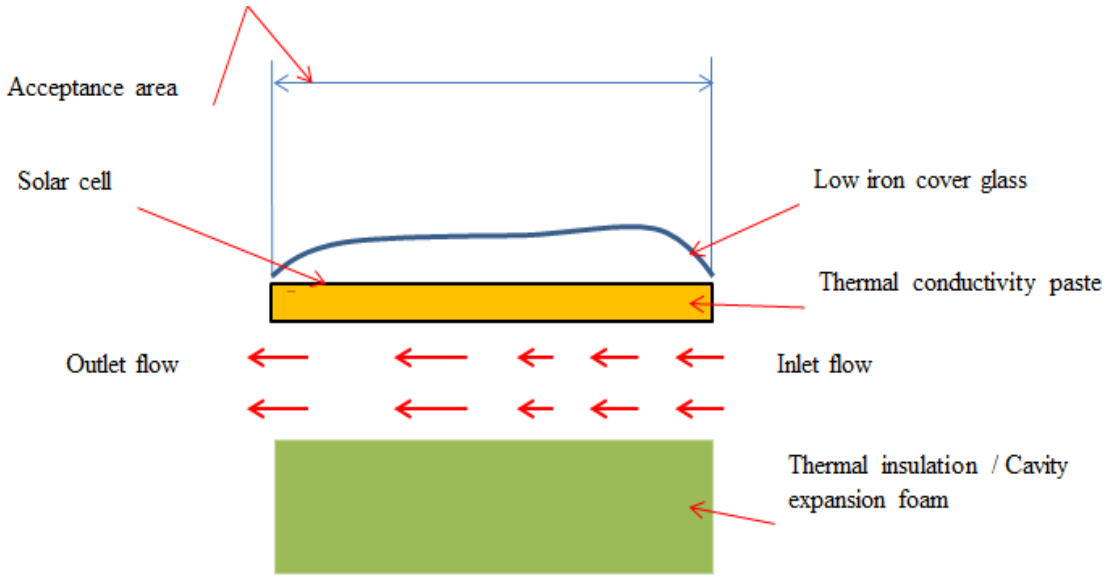

Figure 4.7: Cross-sectional side view of proposed covered SRCPC

4.8 The working principle of the thermal model

In order to increase the overall performance of the SRCPC system, a thermal management system [heat exchanger] is integrated in the SRCPC system design. Figure 4.8 is a cut section schematic diagram of the SRCPC thermal management system showing the channel tubes where the acceptance aperture is greater than the receiver aperture.

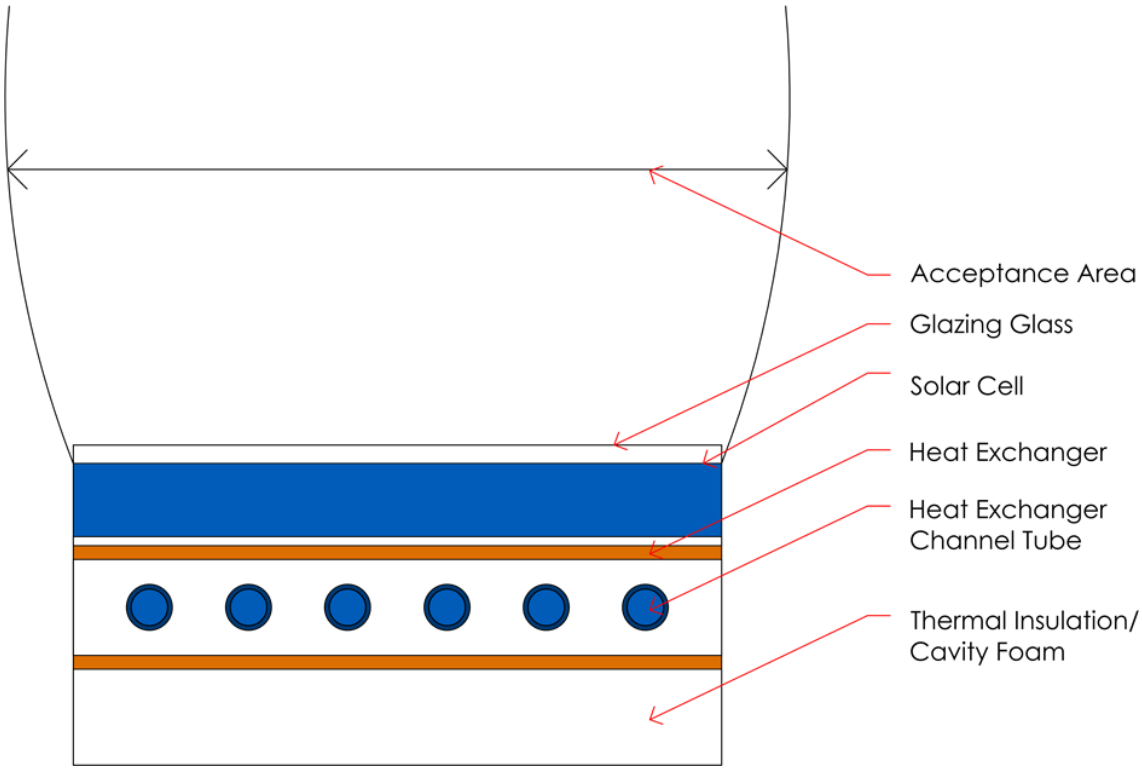

Figure 4.8 A cut section front view schematic diagram of SRCPC water tubes of the thermal management system (heat exchanger).

In this case, the receiver lies on a heat sink paste on top of the heat exchanger that has 6 tubes parallel flow channels to each other as one dimensional water flow system. At the bottom of the heat exchanger is a thermal insulation material and around the SRCPC to prevent thermal losses but heat is radiated through the heat transferable fluid being water. At the opposite ends of the heat exchanger, there are the inlet and outlet pipes that are covered with thermal insulation to prevent heat losses and weather interference.

The aperture area of the symmetric reflective compound parabolic concentrator is considered as A_a. The solar energy incident on aperture area after reflection from the parabolic reflector is allowed to fall on the receiver PV. The PV absorbs part of the

radiation while some are transmitted and others deposited as heat. At this point, there is a transfer of thermal energy from the solar cell PV through the thermal conductivity paste to the heat exchanger plate where the tubes carrying the heat transferable fluid medium radiates the heat away to the tank. By this means, the temperature of the heat exchanger plate increases thereby increasing the water temperature which flows in the tubes. The continuous repeat of the cycle extract the heat from the solar cell and the temperature is kept constant and stable.

The water inlet temperature from the tank is considered as T_{in}while the water outlet temperature at the other end of the exchanger plate is T_{out}. T_{sc} is the solar cell temperature and $T_{tank}$is the temperature from the tank. Thermocouple (K-type) are used to measure each of the temperatures.

For the energy balance of compound parabolic concentrator collector with the fluid flowing can be written in terms of the absorber components and fluid flowing components.

4.8.1 ***Absorber***

The rate of solar radiation absorbed by the absorber PV is equal to the rate of thermal energy transferred from plate to fluid plus the rate of thermal energy loss from plate to the ambient [189, 191].

$$\rho\alpha_p\tau_g G_T A_{ac} = F'U_{pf}(T_{sc} - T_{out})A_{rc} + U\,(T_{sc} - T_{tank})A_{rc} \qquad 4.6$$

Solar radiation rate absorbed by the absorber	Thermal energy transfer rate from plate to the fluid	Thermal energy loss rate from plate to the ambient

Where G_T is the solar radiation at irradiation level at 1000W/m²

A_p Is the area covered by the absorber

A_{rc} Is the receiver area covered by the glass

A_{ac} Is the aperture area over the glazed portion

R’ is the reflectivity of the reflector

α_p Absorptivity of the absorber

τ_g Is the transmissivity of glass

F' Is the flat plate efficiency of the collector

U is the overall heat transfer coefficient

T_{sc} Is the temperature of the solar cell

T_{out} Is outlet temperature

T_{in} Is the inlet temperature

T_{tank} Is the tank temperature

4.8.2 ***Fluid flowing***

The rate of heat carried by flowing fluid below the absorber is equal to the rate of thermal energy transferred from the plate to the fluid

For instance

$$\dot{m}C_p\Delta T = F'U\,(T_{out} - T_{in}) \qquad 4.7$$

where C_p is specific heat capacity of transferable fluid.

4.9 Measured results and discussions

During the indoor characterisation, the volume flow rate that stabilised the measured parameters is $0.007929\frac{L}{s}$ and Table 4.3 shows the stabilised parameters under 1 sun. The average of each parameter is recorded below each column.

Table 4.2: Shows stabilised measured parameters during the indoor characterisation

	Tin (°)	Tout (°)	Tsc (°)	Time (mins)	Current (A)	Voltage (V)	Power (W)
	33.4	33.7	30.7	00:02	1.4050	4.8706	5.9802
	33.3	33.3	31.8	00:05	1.7278	4.8590	5.9623
	32.9	33.2	32.1	00:08	1.7220	4.8552	5.9608
	32.8	33.1	32.4	00:10	1.7203	4.8520	5.9564
	32.6	32.9	32.6	00:13	1.7200	4.8469	5.9468
	32.5	32.8	32.8	00:17	1.7235	4.8424	5.9337
	32.5	32.8	33.1	00:19	1.7262	4.8422	5.9384
	32.4	32.7	33.2	00:22	1.7273	4.8376	5.9309
	32.4	32.6	33.4	00:25	1.7290	4.8314	5.9154
	32.4	32.6	33.5	00:28	1.7182	4.8344	5.9190
	32.3	32.5	33.8	00:31	1.7226	4.8262	5.9075
	32.3	32.5	34	00:34	1.7198	4.8229	5.9023
	32.3	32.5	34.1	00:37	1.7247	4.8185	5.8968
	32.3	32.6	34.3	00:40	1.7174	4.8139	5.8821
	32.3	32.5	34.3	00:43	1.7214	4.8137	5.8867
	32.3	32.5	34.5	00:46	1.7280	4.8121	5.8808
	32.2	32.5	34.6	00:49	1.7199	4.8059	5.8785
	32.4	32.6	34.8	00:52	1.7181	4.8084	5.8791
	32.3	32.6	34.9	00:55	1.7206	4.8032	5.8748
	32.3	32.5	35.1	01:01	1.7296	4.7978	5.8628
	32.2	32.5	35.3	01:04	1.7268	4.7990	5.8645
	32.2	32.4	35.4	01:07	1.7214	4.7949	5.8591
	32.1	32.4	35.5	01:11	1.7226	4.7949	5.8534
	32	32.3	35.7	01:13	1.7279	4.7876	5.8467
	32	32.3	35.8	01:13	1.7306	4.7852	5.8491
Average	32.428	32.676	33.908		1.7108	4.8222	5.9027

The electrical efficiency of the water-cooled symmetric reflective compound parabolic concentrator is the ratio of the electrical output to the incident solar radiation as in Equation 4.10. Also, in like manner, the thermal efficiency of the water-cooled SRCPC is the ratio of the output heat to the incident solar radiation as in Equation 4.9. The electrical efficiency when cooling is applied is

$$\eta_{elect} = \frac{P_m}{A_p G_T}$$

$$= \frac{5.9027151W}{\left(\frac{0.02m^2 X 1000W}{m^2}\right) x\ 3}$$

$$= 9.8\%$$

The thermal efficiency during the cooling process is

$\eta_{thermal} = \dot{V} C_p \Delta T / A_p G_T$

$= (0.007929(1.225)\frac{kg}{s} \times 4184\frac{J}{kg^{\circ}C} \times (32.676\text{-}32.428\ ^{\circ}C)) / (0.0225m^2 \times 1000W/m^2)$

$= 36.5\%$

The electrical and thermal efficiencies calculated here is a strong indication that a large amount of heat was extracted from the SRCPC system. This is showing a high performance increase in the electrical efficiency and sharp decrease in the thermal efficiency. This is a proof that the designed integrated heat exchange performed to bring down the temperature of the system to a standard temperature and ensured overall system operated at best efficiency. The parameters used in achieving the thermal modelling system are shown in Table 4.2.

4.10 Conclusion

The design and construction of a rectangular heat exchanger for parallel flow has been presented. It has dimensions and parameters used to calculate the thermal and electrical efficiencies of the system in order to estimate its performance. This heat exchanger was integrated and tested. This was meant to check and also control the temperature effect of solar cell which was coupled to the SRCPC system for the purpose of increasing the conversion efficiency of the solar cell. The effect of the mass flow rate was monitored and ensure saturation level is reach for parametric stability for enhancing performance. The estimated heat was extracted from the SRCPC system by bringing down the temperature thereby allowing the system to operate at overall best efficiency.

Chapter 5 CONSTRUCTION AND INDOOR CHARACTERISATION OF THE TWIN SRCPC MODULES

5.1 Summary

In this chapter, an overview of the construction of the SRCPC modules is provided and the indoor characterisation of the twin SRCPC modules results is also presented. This is based on the simulation results obtained from chapter 3. The materials used for the construction of the SRCPC concentrators are presented. The performance of the electrical I-V and power curves with and without the heat exchanger under different and varying conditions of the fabricated twin SRCPC are measured and compared. The results obtained are used to calculate the experimental optical efficiencies that are compared with the simulated optical efficiencies achieved in the previous chapters to validate the optical model. The indoor characterisation is to test the SRCPC in an ideal conditions to confirm the optical predictions.

5.2 Introduction

By using ray tracing techniques on three different half acceptance angles, three concentrators' profiles were emerged but only one was selected after optimisation for the SRCPC module. These three concentrators were selected out of numerous acceptance half angles. They had different heights and concentration ratio but had to undergo a detailed step-by-step optimisation process using SolidWorks and OPTIS software. The SRCPC concentrator optical performance has been calculated using ray tracing simulations. However, a validation of the optical model is needed before the data can be used to predict the electrical performance of the SRCPC module. With the experimental results obtained, it will validate the results obtained from the optical simulation. Therefore, this chapter describes and presents the construction of the SRCPC prototypes and the test results of their performance under indoor conditions.

5.3 Fabrication of the symmetric reflective compound parabolic concentrator (SRCPC)

Advanced computer controlled manufacturing equipment technology was employed by Pentland Precision Engineering Limited for the construction of the parabola shape of the concentrator. Its use was very important because the shape of the parabola constructed has a very complicated and precise geometry profile.

5.4 Assembling the twin Symmetric Reflective Compound Parabolic Concentrator

The SRCPC concentrator was manufactured in parts. The major parts of the SRCPC are 1) the front view and support, 2) back view and support and four parabolas. To assemble the CPC, light pressure was applied during the assembling to the joints until set. Clamps, wood, metals and tapes were used to reframe the structure around as shown in the appendix. This is to enable us get the geometric designed dimensions of the SRCPC accurately. In preparation for the professional adhesive application, the surfaces were sand papered and cleaned to be free from iron chips, corrosion, dust, dirt and grease. Acetone solvent cleaner was used for this purpose. The parabolic components were set perfectly before applying the professional adhesive araldite rapid.

5.4.1 ***Araldite Rapid***

Araldite rapid is a strong two-component with fast setting and long lasting solvent, free professional adhesive having water resistant which bond metals together was used to hold together in position the parabolas with the front and back views in accurate designed geometric positions and dimensions [192]. The professional adhesive allows five minutes working time, twenty minutes handling time and three hours full strength time. To prepare the adhesive for use, the cap between the syringe plungers was snapped broken off. The plunger was pressed to dispense equal quantity of both components into a clean disposable surface container and the cap was re-fit to close the nozzles. It was thoroughly mixed for at least 30 seconds until satisfactorily mixed and was ready for used in the next five minutes. The professional adhesive was first applied to the front view of the CPC and allowed for 4.5 hours before applying the same adhesive to the back view. Sharp blades were used to remove any excesses. This adhesive has a high resistant temperature between -45 and 65 °C, to oil, chemicals mechanical impact resistance. The formulation is environmentally friendly and eco-friendly packaging for easy recycling. Figure A2, Figure A2, Figure A3, Figure A4, Figure A4, Figure A5 and Figure A6 in the Appendix shows the assembling of the twin SRCPC using clamps and vice machine, front view, side view , top view and bottom view respectively [192].

5.5 Measurement of optical parameters for the thin film reflector materials

Perkin Elmer 950/1050 instrument was used for the accurate measurement of solar cells absorbance by using the 150mm integrating sphere accessory. This is installed in a Lambda 950 as indicated below. The lambda 950 or integrating sphere accessory occupies the second sample compartment. Also, standard calibration procedures is required for a calibrated mirror or calibrated spectral on white reference plate. Extra care was taken when measuring the absorptance using the integrated sphere. It was ensured that the samples were clear while the coating needs to be applied to fairly thin substrates. Glass slides were ideal. The applied coatings to thick substrates run the risk of some of the reflected light being clipped on the port of return of the reflected light into the sphere.

5.5.1 Transmission measurement of solar cells and reflectors using the integrated sphere

The percentage transmittance measurement had little considerations as long as the measuring sample is large enough to cover the transmittance port of the sphere but the sample and reference beam was aligned properly. The sphere was set for total percentage reflection. This means that specular exclusion plug port was in place. The correction setting in the method was ensured that the 0% transmittance baseline was checked.

5.5.2 Reflectance measurement using the integrated sphere

There were a number of considerations put in place for reflectance measurements. 1) The reflectance was measured in Absolute %R. This means that the spectrum was corrected for the reference material. A light spectrum was the reference material as well as the dark level (0%R) of the sphere. 2) UVWin-lab V6 has the capability to define the calibration file in the method because the reflectance spectra correction is performed automatically due to the fact that data is being required in real- time. 3) It is vital to note that no calibration data is required for transmission data collection. The use of this instrument helped to achieve reflectivity result.

5.6 Thermally toughened soda lime silicate safety glass

5.6.1 ***Low iron glass***

A 4mm toughen (TGH) low iron glass that is polished all round corners 4-36mm radius with the surface area of 483mm x 486mm was used as the exterior glazing cover for the SRCPC enclosure. The choice of this low iron glass was informed by the many essential characteristics and radiation properties it possesses. These essential characteristics are; a) the resistance against sudden temperature changes and temperature differentials is 200°C. b) The snow, wind, permanent and imposed load resistance is 4Ω. c) The low iron glass has direct airborne sound insulation of 30(-2;-2). d) The thermal transmittance of the U-value is 5.8 W/m^{2}K. These essential characteristics performance data are shown in Table A1 in the Appendix including the following radiation properties;

- The light transmission of the glass is 0.92
- The light reflection of the glass is 0.08
- The solar energy transmission is 0.91 while [194].

5.7 Thermal and electrical insulation of the solar cell

5.7.1 ***Aluminium plate insulation preparation***

The top surface of the heat exchanger was used as the aluminium plate. In order to insulate the aluminium plate from contact with the electrical components of the solar cell, 300ml clear lacquer spray was used because it has advanced acrylic based formula to provide a tough and durable high gloss protective finish on the solar cell aluminium plate surface. It achieved the best finish required for the solar cell insulation. The clear lacquer spray was sprayed several times to provide a thin insulating layer and was allowed to cure for some minutes before another applications. A satisfactory insulation layer was attained before the heat sink compound plus was applied.

5.7.2 ***Soldering paste***

A soldering paste or flux-oxide was applied to the ends of the connector, positive and negative before melting the soldering lead with 350°C props for strong soldering. The purpose of the flux is to remove dirty, moisture and any rust that may hinder bonding. Figure 5.1 is the finished soldered solar cells ready to be tested for used.

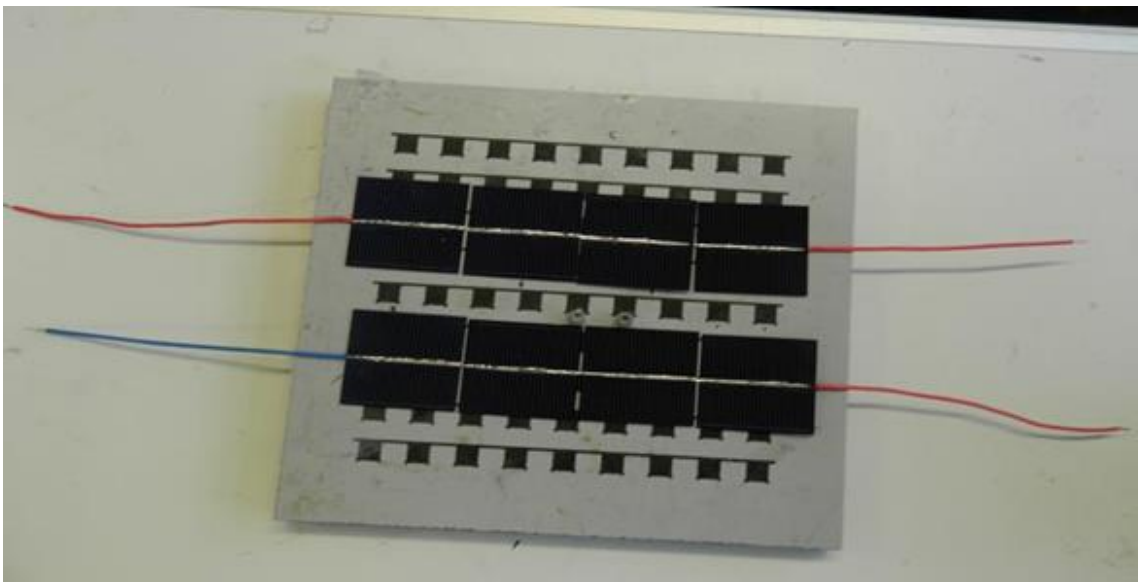

Figure 5.1: Showing solar cell soldered for testing

Figure 5.2 represents the solar cells that were soldered for use in the constructed SRCPC which was tested for continuity before use. The test confirmed that there was no open circuit in the connection. It also confirmed the desired output current and voltage of the strings.

Figure 5.2: Showing measurement of the string of solar cells to ensure proper connections, voltage and current values after the soldering process.

5.7.3 ***Solar cell encapsulation***

Photovoltaic modules uses encapsulation material to increase the lifetime of the solar cell by protecting them from i) slightly mechanical pressure, ii) moisture ingress, iii) insects, rodents and birds desecrations, iv) dirt and dust penetration and v) weathering effect [195]. The encapsulation material needs to have very good transmission properties in the UV-visible wavelength range, to minimise the optical losses, [196].

5.7.4 ***Encapsulation materials***

The encapsulation material is expected to have low modulus and stress relieving properties especially for commercial PV modules. For CPV application, the encapsulation material should also have good adhesion properties. The most popular encapsulation material is Ethylene vinyl acetate (EVA) for commercial PV. In this project, Silicone encapsulating materials that are found to be more suitable alternatives to EVA is the sylgard elastomer. This is due to the following properties it possesses [197].

It has high temperature stability because it operates between -45°C to 200°C. Also, at high peak temperature, there will be no degradation. They are known to be very good electrical insulators and flame resistance polymers. The silicon elastomer modulus is low and consistent for a wider temperature range and the modulus provides mechanical stress relief for the solar cell in the CPV module than the EVA. They have high durability and low degradation in outdoor conditions. For over 25 years, PV modules having silicon encapsulating elastomer from Dow-corning have been reported to have very good satisfactory performance. Silicon elastomer adheres strongly to substrates including aluminium and glass. It assists for the protection of the solar cell from corrosion and moisture. The silicon elastomer is hydrophobic and permeable to gas and vapour. This allows transmission of water trapped in the interface and moisture pickup becomes low. Silicon elastomer encapsulation material from Dow-corning is used in this project. It is commercially known as Sylgard-184. The company ‘’Dow-corning’’ has a range of different clear and transparent materials in Sylgard series. From the numerous materials, Sylgard-184 is found a suitable option having features such as, good flame resistance, viscous liquid, high tensile strength, room temperature curing, [198].

5.7.4.1 *Sylgard processing and curing*

The Sylgard 184 silicone elastomer components 'A' and 'B' were mixed in the ratio of 65g to 6.5g in a conical flask. It was thoroughly mixed and stirred for more than 30 minutes manually before it was transferred to the vacuum drying oven to test the effect of heat fluctuations and allow the mixture to settle. There was cure to minimise air entrapment before it was used. The mixed substance was poured on top of the solar cell for the purpose of encapsulation. It was cured at room temperature at 25°C for 48 hours before used. It was observed that the encapsulation was not dried enough. It was returned to the vacuum drying oven for 45 minutes at 100°C. Under the typical data cured time, the curing time is specified to be:- 1) 48 hours at room temperature of 25°C, 2) 45 minutes at 100°C, 20 minutes at 125°C and 10 minutes at 150°C.

There was no exothermic, curing by-products or solvent during the curing process. It maintained constant cure rate regardless of sectional thickness of degree of confinement. The service curing range temperature was between -45°C to 200°C. The Sylgard 184 silicone elastomer was used to encapsulate the solar cells device from mechanical damage. The solar cells were sealed with a thin layer of the mixed Sylgard. The engineering properties of transparency of substance and constant cure rates were maintained. Sylgard is suitable for the protection of electrical and electronics devices in solar application [199].

It was important to measure experimentally two optical properties of the encapsulated material in the laboratory due to the fact that the manufacturer did not supply such information. Absorption coefficient and refractive index variation are the properties. The experimental set up described below is used to measure these two properties.

5.7.4.2 *Measurement of encapsulation refractive index*

To measure the refractive index of different materials especially the encapsulated Sylgard material used for the mechanical protection of the solar cell, the most precise equipment used is the Ellipsometry equipment. The sensitive optical technique Ellipsometry equipment determines optical properties of a sample material that is less than 50 microns thickness [195-198, 200]. To implement this, a simple idea was to initiate a thin of polyurethane. 1) Measure the two parts of the polyurethane materials by ratio, 2) Guard the solar cells from all the edges using a clean glass plates, 3) Allow it to cure before

you remove the side protected edged glasses, 4) The thickness of the thin film of the polyurethane protecting the solar cells was measured or tested to be about 10 microns.

The VASE Ellipsometer (J.A.Woollam Inc) was used to test the polyurethane. To conduct measurement using the Ellipsometer, light must be incident at various different angles relative to the normal for different wavelengths on the thin polyurethane materials covering the solar cells. The Ellipsometer has a software already incorporated to calculate the refractive index variation of the encapsulated materials as a function of the wavelength. The polyurethane material refractive index that was used to protect the solar cell used in the symmetric reflective compound parabolic concentrator is illustrated in Figure 5.3 being a function of the wavelength. From the graph, it is a clear indication that polyurethane manifest normal dispersion in the visible and near UV spectral regions until the wavelengths of 400nm. Similarities are observed that the refractive index of the polyurethane material is similar to that of PMMA material refractive index [6].

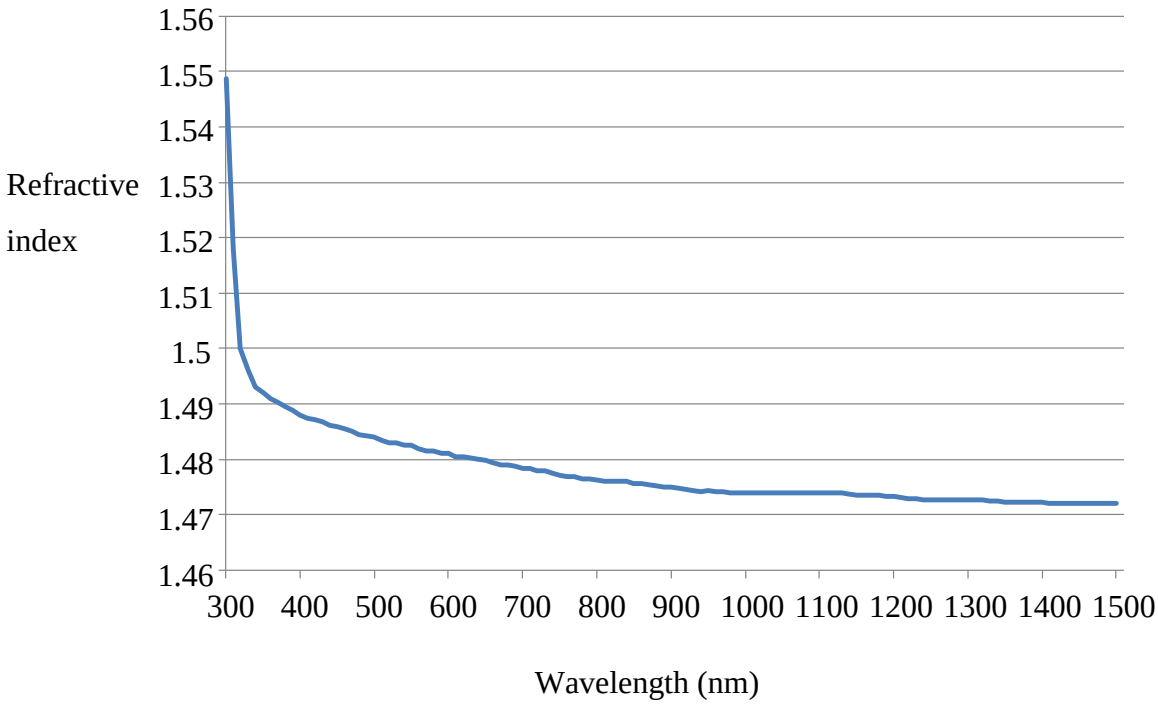

Figure 5.3: Refractive index of polyurethane used to encapsulate solar cells used in SRCPC

5.7.4.3 *Insulating electrical part of solar cells from heat exchanger plate*

It was necessary to provide a thick tough durable high gloss protective finish on the heat exchanger surface where the solar cell will be located. The most suitable product used for this was the Clear Lacquer spray 300ml advanced acrylic formula. Its outstanding

properties includes. It must be used on metals and pearlescent paints. It always ensure best finish achievable and correct colour match. It is used on cellulose finish. It was sprayed several times until we ensured that it formed a thick layer of tough durable high gloss protection on the heat exchanger surface to insulate electrical part on the solar cell when it is in contact with the heat exchanger.

5.7.4.4 *Heat sink compound plus*

Before the solar cell encapsulation, a heat sink compound was used to spread the heat dissipated by the solar cell to the aluminium plate to transfer away heat using the transferable fluid. A heat sink metal oxide filled with silicon oil paste was used to give superior thermal conductivity for thermal coupling of electrical and electronic components. The superior thermal conductivity was achieved at high temperature with excellent non-creep characteristics. The compound is electrically insulated to ensure no current leakage can be formed should the paste come into contact with other parts of the assembly. This product was used because it dissipates a large amount of heat quickly and effectively. It is a superior thermal conductivity at very high temperatures and it is easy to handle. The specific resistance is 1x1015Ωcm. It has a maximum operating temperature of 200°C and a minimum operating temperature of -50°C with a thermal conductivity of 3W/mk. The paste collects the heat from the solar cell and dissipates it on the heat exchanger plate which transfers the heat by a transferable medium (in this case water) [201].

5.7.4.5 *Heat exchanger integration*

The designed heat exchanger was integrated in the SRCPC system by placing it under the solar cell. The heat exchanger was first coated with a thick gloss liqueur to insulate it from any electrical contact or leakage. The heat exchanger was seated on a thermal insulation foam while a thermal conductivity paste was spread on top of it before the solar cells were arranged on top of the heat exchanger. Two inlet and outlet pipes were connected for the flow in and flow out of the heat extracted fluid.

5.8 Experimental methods and set-up

This section describes the experimental methods and the instruments employed in this work to measure and analyse the performance of the SRCPC hybrid system. In this

section also, the tools used for the evaluating, optimising and simulating the system performance are described.

5.8.1 *General description*

The experimental set-up includes; a WACOM super solar simulator having super high pressure short arc UV lamps and Xenon short arc lamps, EKO I - V measuring system, Power supplies for super high pressure short arc UV lamps and xenon short arc lamps, data logger, thermocouple system, LCD display unit, strings of four solar cells, two unit model designed concentrators, water pump, reservoir and solar cell reference sample.

5.8.2 *The solar simulator*

A solar simulator by description is a system that emits light equal to the natural sunlight so that it can test various features of PV cells, modules and concentrator. A WACOM super solar simulator model WXS-220S-20, AM1.5G IEC60904-9 Class AAA was used for analysis of various concentrating systems. It employs special mirrors to produce composite of light from xenon and halogen lamps in order to produce results that rectifies the previous unsatisfactory qualities. It produces rays in the unit to have a spectrum distribution which is very similar to the natural solar spectrum. It was used to effectively analyse and evaluate the properties high efficient solar cells and the designed model concentrator. The effective irradiating area of this super solar simulator is 210mm x 210mm. The direction of irradiance is down shining. The solar cell sample has to be examined to ensure conformity with the I-V curves using the WACOM super solar simulator as shown in Figure 5.4 as well as the simulator accessories.

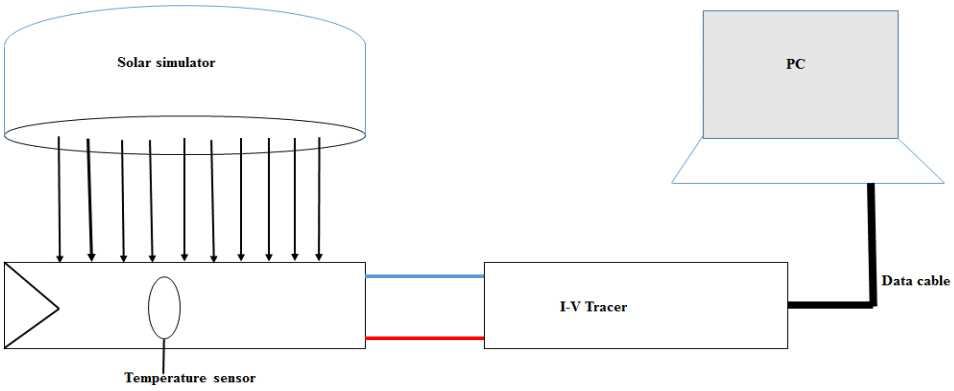

Figure 5.4: Block diagram of experimental set up of the twin reflective symmetric compound parabolic concentrator for indoor characterisations using WACOM simulator

The method of measurement is that at a position of 500mm below the collimator lens where a sample is placed at the effective radiated area. The simulator has seventeen xenon lamps positions and each of the lamps is rated 5kW. This xenon light has super high pressure short Arc UV lamps. The irradiated light is opened on the sample and the parameter measurement is recorded by the data measuring system. The solar simulator in conjunction with the I-V measuring system was used for measurement of current (I), voltage (V), power, fill factor (FF), irradiance distribution, concentrator performance and cell conversion efficiency. In this case the I-V curve was measured and compared with the reference solar cell sample.

5.8.3 ***Advantages of solar simulator over the sun***

The solar simulator has advantage over the sun in that the intensity of the solar simulator light can be varied with time and results are achieved in a shorter period. It will take much longer time if the same characterisation was to be performed in outdoor conditions. The simulator allows thorough characterisation of the optical parameters of concentrating systems during a short period. Solar intensity and other ambient conditions are non-controllable because they vary continuously under outdoor conditions. Under outdoor conditions, it is difficult to determine the cause and effect of PV system when tested. The WACOM super solar simulator being an indoor simulator allows the applied conditions to be controllable thereby making the cause and effect to be clearly identifiable. The super solar simulator used in this project gave a uniform distribution of illumination over a relative area that was analysed. The effective radiated area of the simulator could not cover the twin unit model designed concentrators.

5.8.4 ***Solution preferred by WACOM super solar simulators***

In WACOM super solar simulator, the collimating angle is within ±3°. The spectral match is approximating AM1.5G. This is between 400nm – 900nm within ±25%. At every 100nm, the spectral width is 900≈1100nm. The positional uniformity of irradiance is within ±2% at 1sun by the use of xenon lamps. The effective irradiance area is 210mm x 210mm and the irradiance direction is down shining.

5.8.5 ***Measurement of volume flow rate***

The flow rates were measured in litre per second. A DC high quality geared electric pump with self-priming which pumps in forward or reverse directions was used. The pump has a pumping capacity of 1.81L/min, Voltage =12V and current =1.5A. The pump was connected to a dc source where varying voltages were used to pump water into a capacity flask of 900ml per time (seconds). The time was recorded for the same pumping of 900ml using 2V, 4V, 6V, 8V, 10V and 12V. This process was repeated and average value for each voltage was found. The flow rate was calculated as shown in Table 5.1.

Table 5.1: Measured volume flow rate using Kavan GmbH dc pump and conversion to L/s

Voltage	Time (s)	Volume (ml)	Ave volume flow rate(L/m)	Volume flow rate (L/s)
12	29.13	900	1.852	0.031
11	31.13	900	1.735	0.029
10	33.38	900	1.618	0.027
9	36.63	900	1.474	0.025
8	40.87	900	1.331	0.022
7	47.32	900	1.141	0.019
6	56.71	900	0.952	0.016
5	69.61	900	0.776	0.013
4	90	900	0.600	0.010
3	112.79	900	0.476	0.008
2	153.63	900	0.352	0.006

Figure 5.5 shows the graph to illustrate the volume flow rate against the pump motor voltage below.

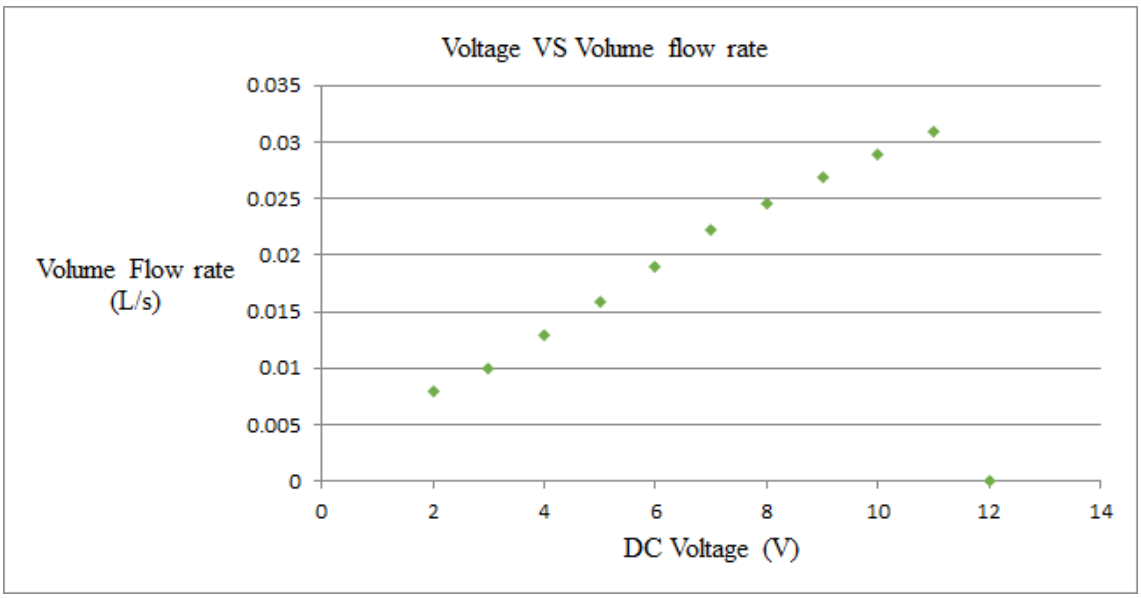

Figure 5.5: Shows the voltage vs flow rate of the pump used during the experiment.

5.8.6 Two strings of silicon monocrystalline solar cells used for the measurement

The solar cells used to test the designed model twin concentrator are a string of four monocrystalline solar cells. The dimension of a solar cell used is 50mm x 50mm. Each string was connected in series as shown in Figure 5.6 as well as the detail schematic connections of the two strings.

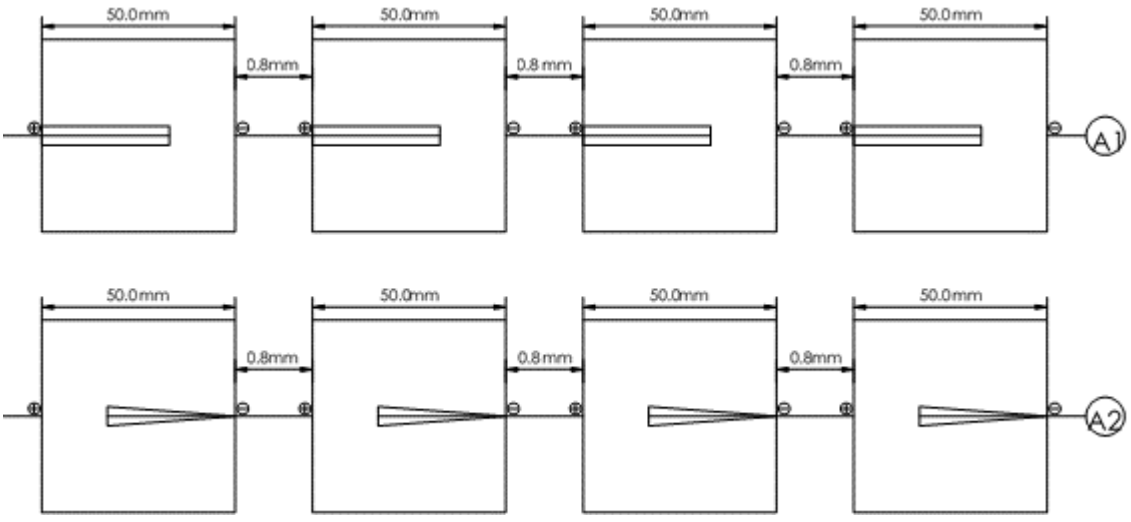

Figure 5.6: Strings (A1) and (A2) of monocrystalline silicone solar cells connected serially for the characterisation

The indoor experimental was conducted under various conditions of time, temperatures, volume flow rates, with and without cooling, with and without concentration for proper performance investigation. The symmetric reflective compound parabolic

concentrator (SRCPC) was exposed to the solar simulator radiation rays of 1 sun and later 1.2 suns.

There were series of measurements carried out to investigate the performance of the SRCPC as follows;

A. Two strings of LGBC silicon monocrystalline silicon solar cells without CPC and without heat exchanger in series at 1000W/m^2.

B. Two strings of LGBC silicon monocrystalline solar cells with CPC and without heat exchanger in series at 1000W/m^2.

C. Two strings of LGBC silicon monocrystalline solar cells without CPC and without heat exchanger in parallel at 1000W/m^2.

D. Two strings of LGBC silicon monocrystalline solar cells without CPC and without heat exchanger but varying time at 1000W/m^2.

E. Two strings of LGBC silicon monocrystalline solar cells without CPC but with heat exchanger, volume flow rate 0.007929167L/s but varying time at 1000W/m2.

F. Two strings of LGBC silicon monocrystalline solar cells without CPC but with heat exchanger, volume flow rate 0.01L/s but varying time at 1000W/m2.

G. Two strings of LGBC silicon monocrystalline solar cells with CPC, without heat exchanger and no volume flow rate but varying time at 1000W/m^2 and

H. Two strings of LGBC silicon monocrystalline solar cells with CPC, heat exchanger and volume flow rate voltage of 0.007929167L/s but varying time at 1000W/m^2.

5.9 Results and discussions

The results presented is a comparative experimental analysis of two flat photovoltaic strings and compound parabolic concentrator systems with and without heat exchanger, with and without concentrator at different flow rates. The flat PV strings solar cells are located at the bottom of the concentrator and subjected to cooling to reduce the temperature effect. The cooling configuration performance was evaluated experimentally.

The measurements were taken using the I-V tracer at a maintained constant room temperature. The incident angle of the simulator could not be changed as it stands perpendicular to the concentrator; it could not be possible to vary the tilt angle of the concentrator from 0º to 90° at 5º intervals to achieved different incident angles results. This is because the simulator is positioned at 90º downward radiation.

5.10 Current and Voltage (I-V) characteristics of the SRCPC

The results from the IV tracer could show the electrical performance of the SRCPC current-voltage characteristics. The IV curves of the designed and constructed SRCPC parameters are presented and comparisons are made.

5.10.1 SRCPC concentrators coupled with solar cells

The SRCPC is a twin concentrator which was assembled using a total of eight (8) solar cells. Each concentrator was coupled with four (4) solar cells connected to it in series and later connected in parallel to give a desired output. The solar cells dimensions were 50mm x 50mm connected at intervals of 0.8mm gap to each other.

5.10.2 Established conventional I-V curves

Figure 5.7 is the standard conventional I V curve measurement that is established in the experiment without the concentrator and without the heat exchanger or flow rate at 1000W/m^2 from the solar simulator. The measured parameters are without cooling and without the SRCPC. The I-V curve of the 2x4 strings of solar cells connected in series are measured. The Isc = 995mA, Voc 2476 mV and the maximum power Pm = 1876 mW while Imp = 926mA, Vmp = 2026mV and the Fill factor = 0.76. The experiment was carried out under a room temperature of 26.7°C at 1sun.

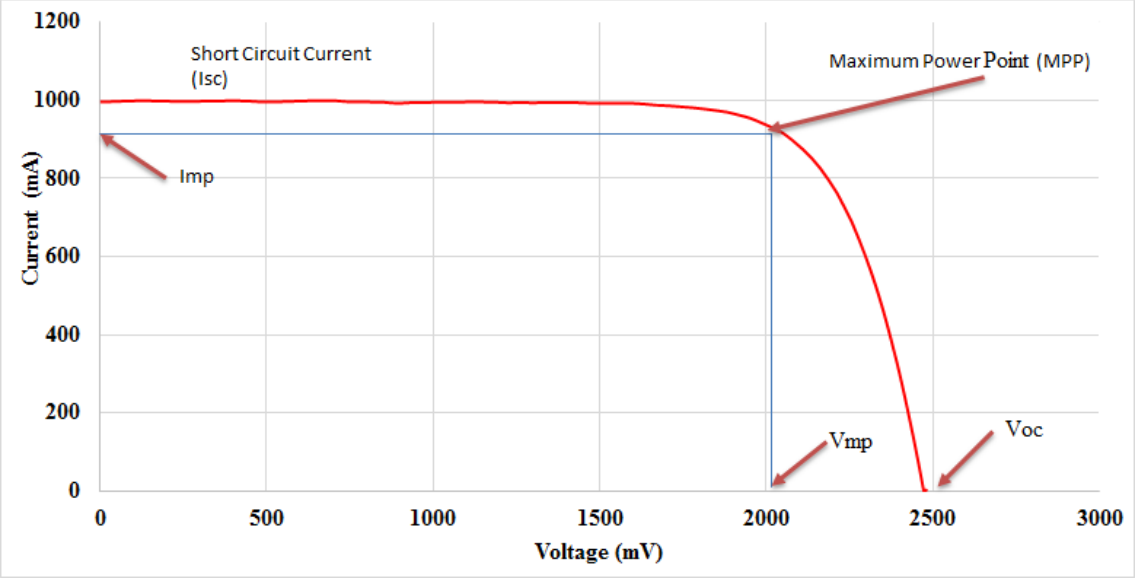

Figure 5.7: Expected normal I-V curve of 2 x 4 solar cells connected in series at 1 sun without concentrator

Figure 5.8 shows the expected I-V curve of the 2x4 strings of solar cells connected with the SRCPC at room temperature of 27.1°C without cooling. The measured parameters with the SRCPC. are; Isc= 2403.12mA, Voc = 5090.86mV, Pm = 8223.97mW, Imp = 2167mA, Vmp = 3795mV, while the Fill Factor = 0.672.

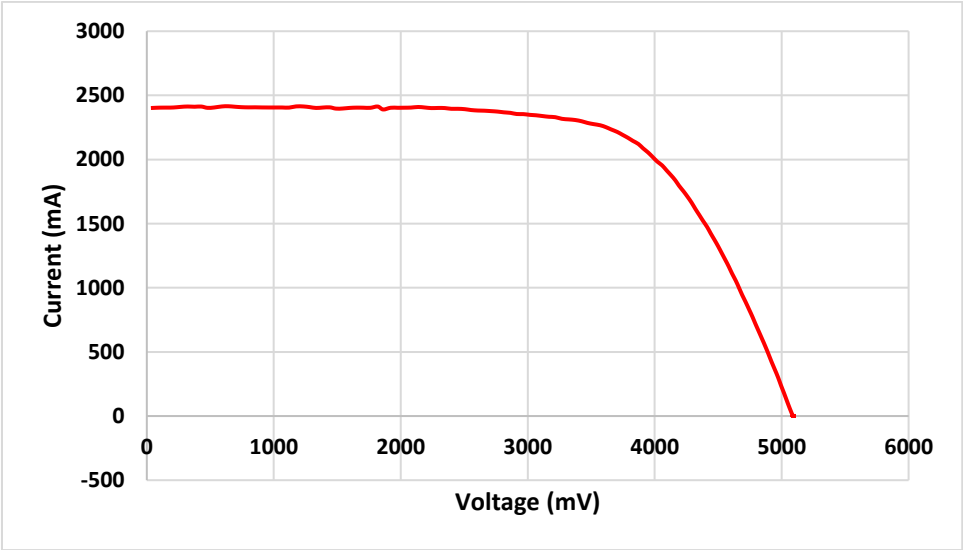

Figure 5.8: Expected normal IV curve of 2 x 4 strings connected with concentrator at 1 sun

The string of crystalline silicon PV was tested in air without CPC and without cooling for a period of 1hr 9mins. Figure 5.9 shows the results of the temperature effect on I-V curve during concentration. The most affected parameter is the open circuit voltage. The is a considerable drop from the starting at 26°C to 70°C.

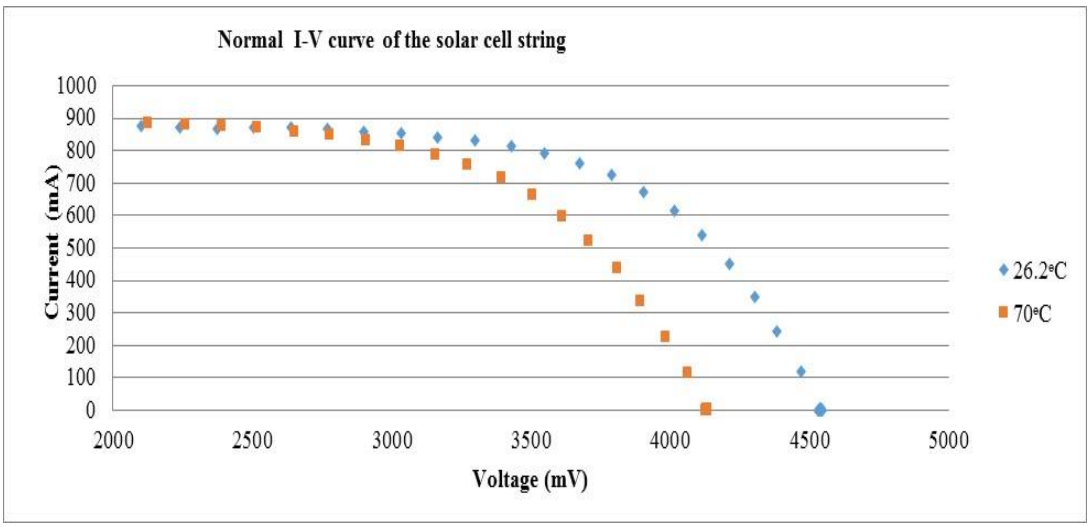

Figure 5.9: Temperature effect on I-V curve

Figure 5.10 shows the temperature rise against time and the power curve without cooling in Figure 5.11. Figure 5.12 illustrates the drop in power and efficiency of the solar cell while Figure 5.13 further shows the combined effect of temperature rise on LBGC crystalline silicon solar cell parameters with slight increase in I_{sc}.

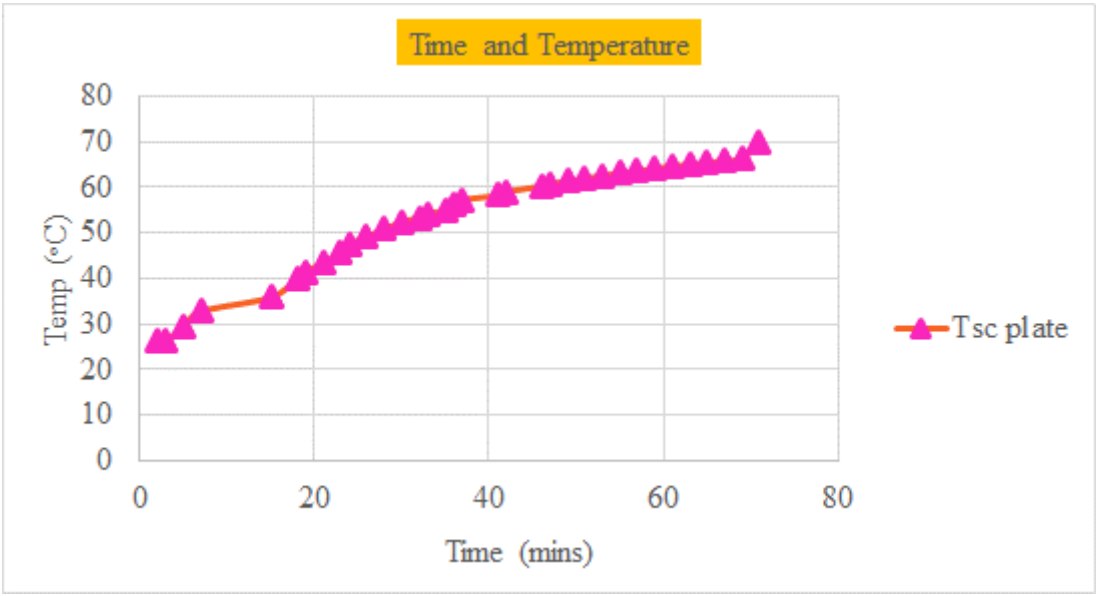

Figure 5.10: Temperature effect on solar cell and time variation without CPC and cooling

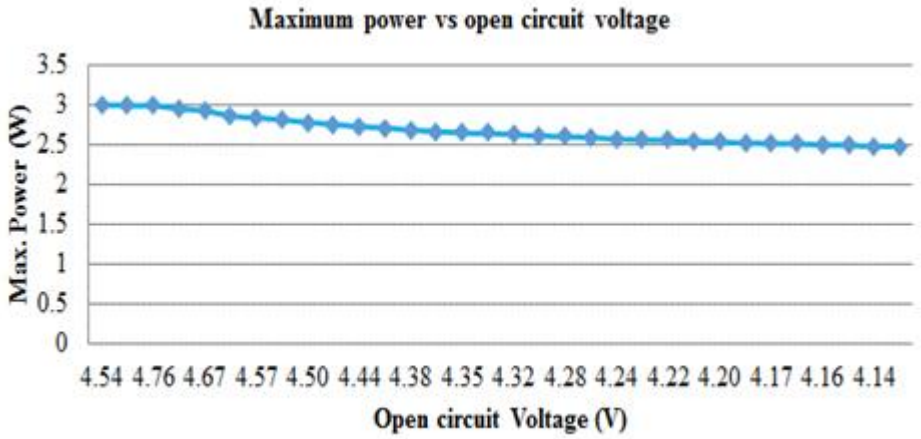

Figure 5.11: Variation of maximum power with open circuit voltage during the experiment at 1 sun without cooling

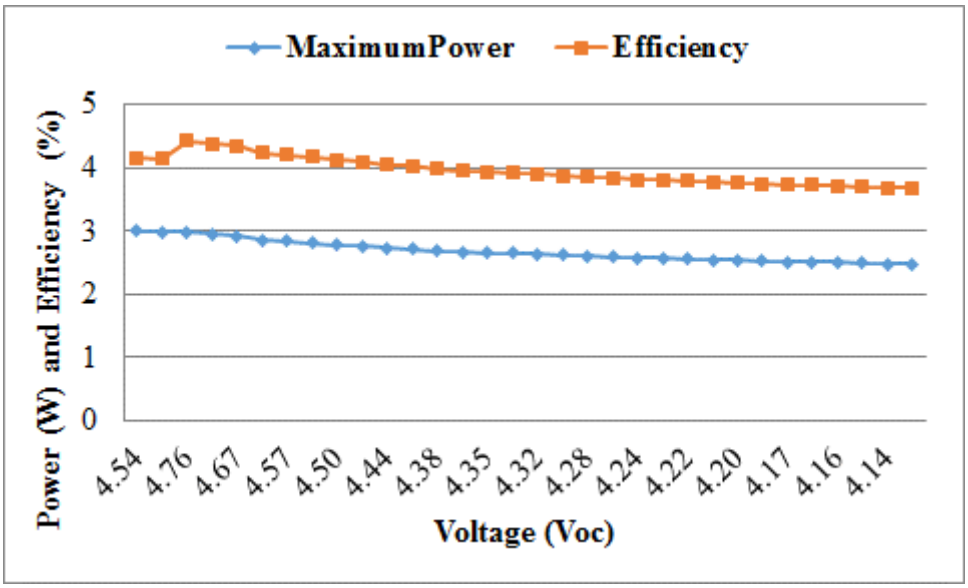

Figure 5.12: Variation of maximum power with open circuit voltage of the 2x4 silicon solar cells without cooling at 1 sun

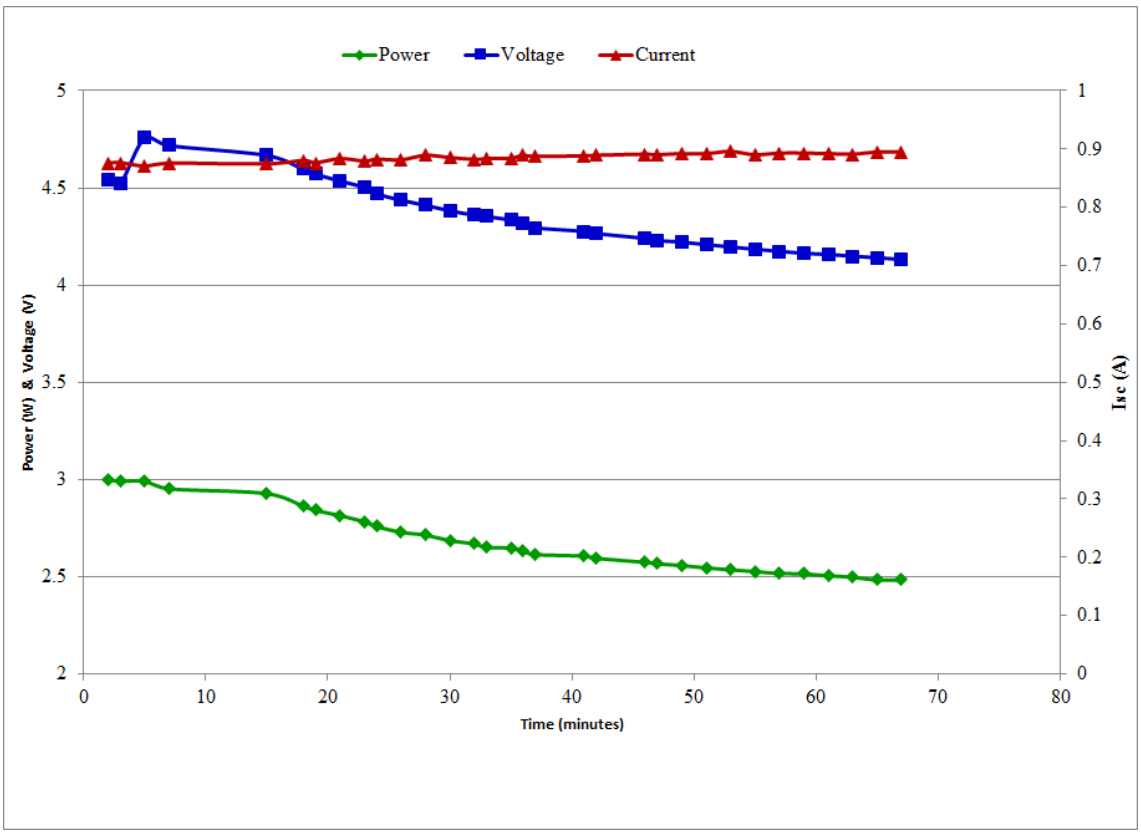

Figure 5.13: Variation of maximum power, opened circuit valtage and short circuit current with time at 1 sun

5.10.3 ***Discussion***

The experiment tested the 2x4 strings of silicon monocrystalline solar cells without CPC and without heat exchanger but varying time at 1000W/m^2. The experiment was carried out to check the effect of temperature rise on PV parameters. It was also to proof of predictions in Chapter 4. The test period was 1hr 9mins. The solar radiation from the simulator is 1000W/m^2. The solar cell temperature was expected to rise and a decline was expected from the parameters except the I_{sc} that increases slightly. The maximum parameters were recorded at a temperature of 26.2^{o}C at first measurement to be I_{sc} = 0.876A, V_{oc} = 4.52V, P_{max}=2.99W and Fill factor = 0.707. It was observed that as the solar cell temperature was rising, the parameters were gradually declining in magnitude. The experiment lasted for 1hr 9mins to attain the 70°C predicted in Chapter 4 to ensure significance changes in the recorded parameters. The PV maximum parameters at the temperature of 70°C are: I_{sc} = 0.895, V_{oc}=4.132v, P_{max}= 2.483W. Figure A7 in Appendix shows the full I-V curve and the expected solar cell temperature effect. This experiment confirmed the prediction of solar cell temperature rise, which necessitates the imperative

for solar cells cooling to maintain standard temperature in order to improve and increase efficiency.

The general observation in the indoor characterisation is that at normal controlled room temperature, as radiation is focused on the solar cell strings, not all the radiation is absorbed by the solar cells. Part of the radiation is deposited as heat. The heat causes the temperature to rise. The rise in temperature leads to a drop in other parameters except the current that increases slightly as shown above which is expected.

5.10.4 ***SRCPC concentration and cooling***

The concentration of solar radiations on the SRCPC and cooling of the PV used to observe the temperature effect at 1 sun started here. A flow rate of 0.00689L/s was used in order to observe the trend of changes in parameters and to check if we can achieve volume flow rate before the calculated value. It was observed that the volume flow rate applied varied periodically. The applied volume flow rate was observed to be insufficient to cool the solar cell as revealed in Figure 5.14. At the starting of concentrating solar radiation on the SRCPC, the parameters seem to be stable but after a progression of 20 minutes, the parameters began to decrease indicating that the flow rate used was not sufficient to extract the heat from the system. The Figure 5.15 shows I-V curves for different parameters curves at a restricted flow rate in order to observe parametric behaviours. It was observed that the used flow rate of 0.00689 L/s was not sufficient to cool the solar cells. We resulted to this method because of unavailability of calculated flow rate pump at Heriot Watt University.

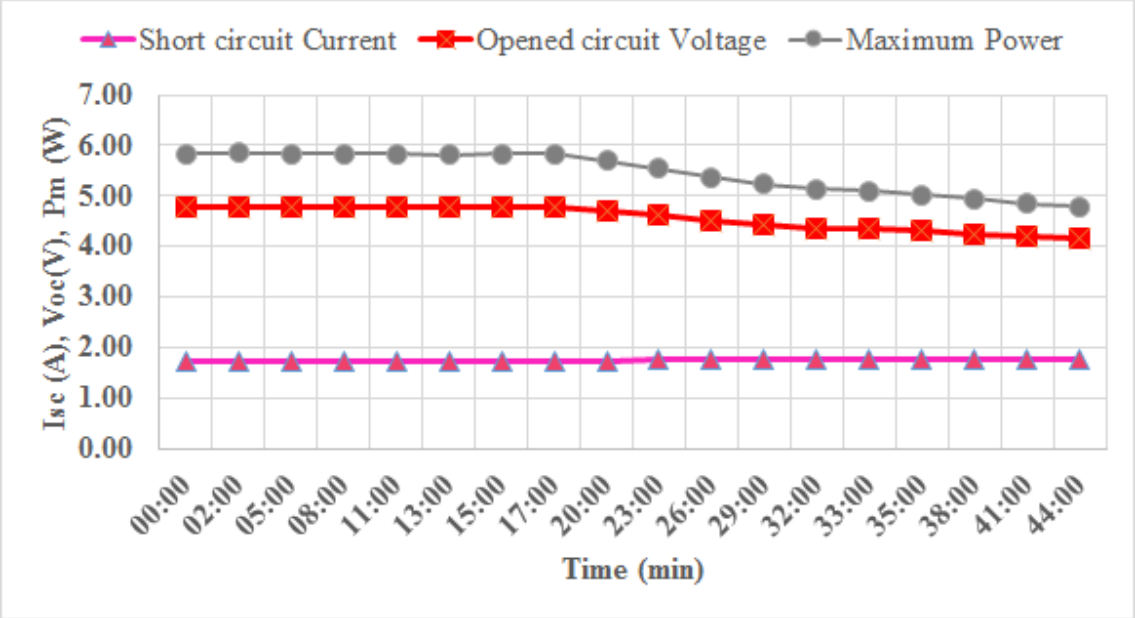

Figure 5.14: Shows volume flow rate of 0.00689L/s and observed effect on parameters

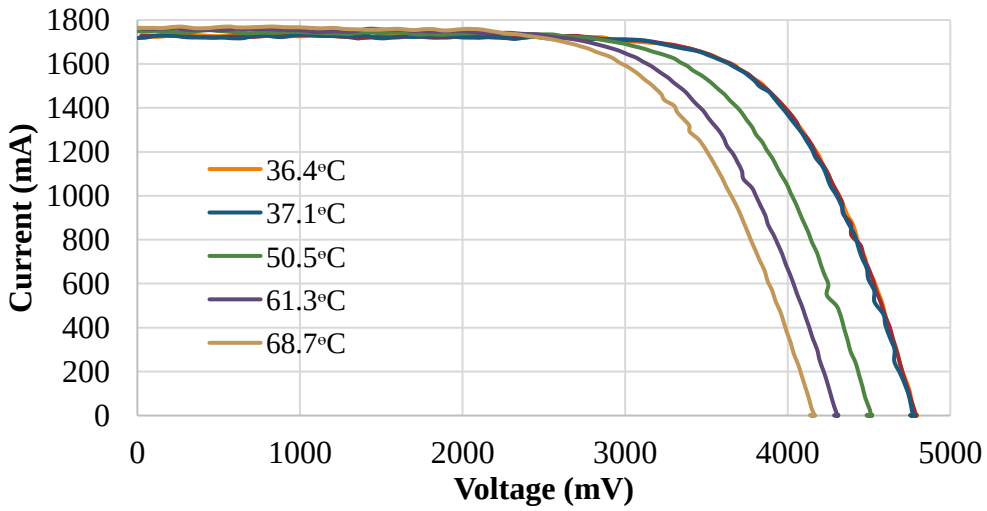

Figure 5.15: Shows I-V curves for different temperatures at a flow rate of 0.00689L/s

The combined parameters against time for the insufficient flow rate is further buttressed in Figure 5.16. The volume flow rate used, which was insufficient, is 0.00689L/s.

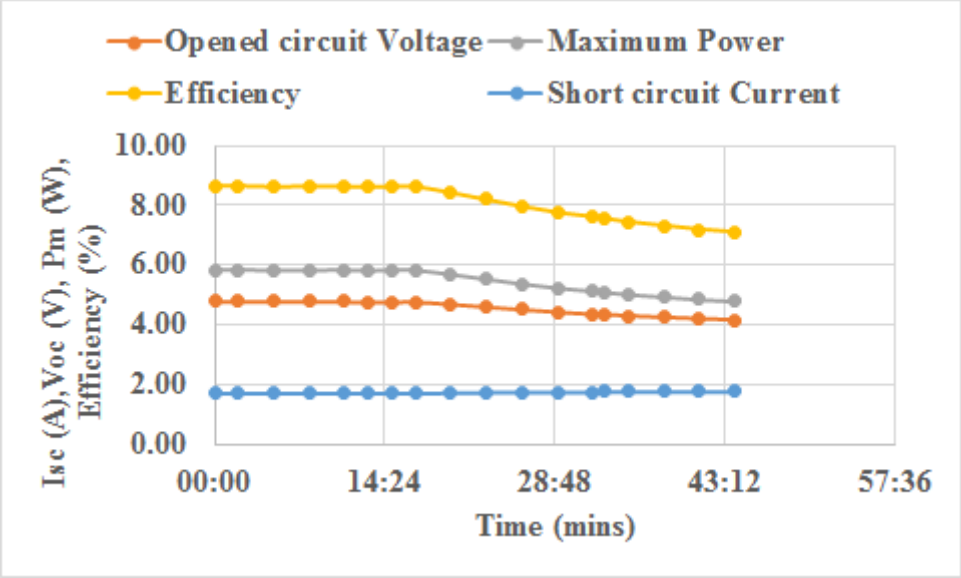

Figure 5.16: Performance indicators of volume flow rate of 0.00689L/s to stabilise SRCPC parameters using 1 sun.

5.10.5 ***Delivery pump head***

As an alternative, a DC KAVAN pump was found and could deliver 1.81L/mins or 0.03017L/s. This suggested the different use of flow rates until a satisfactory flow rate that extract the heat was reached. The DC pump has a current of 1.5A and voltage of 12V. This could deliver a power of 18W. An external source was used to power the pump because the SRCPC model did not have enough capacity to power it.

5.10.6 ***Effect of increased mass volume flow rate***

The volume flow rate was increased to 0.007929L/s for duration of 1.2hrs. The SRCPC parameters were stable and the efficiencies increased. This is illustrated in Figure 5.17, Figure 5.18 and Figure 5.19 respectively. The efficiency without concentration and without flow rate at highest was 4.8% and lowest at 4.6% while the efficiency of concentrating and cooling at highest was 9% and lowest 8.7%. The percentage efficiency increase between highest and low is 47% at one sun. The temperature difference during the test period 1.6°C

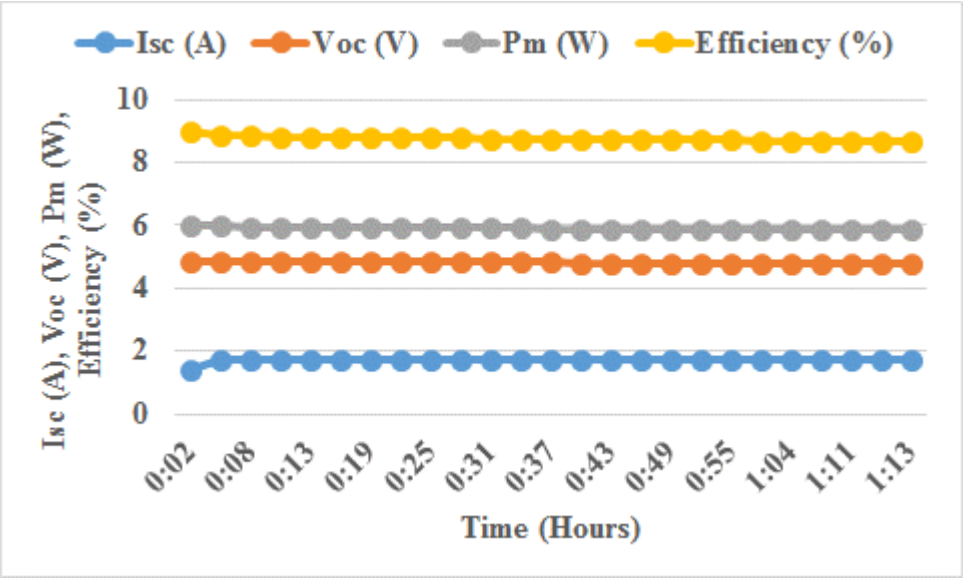

Figure 5.17: Stability of parameters due to increased volume flow rate (0.007929L/s) and efficiency stability were attained.

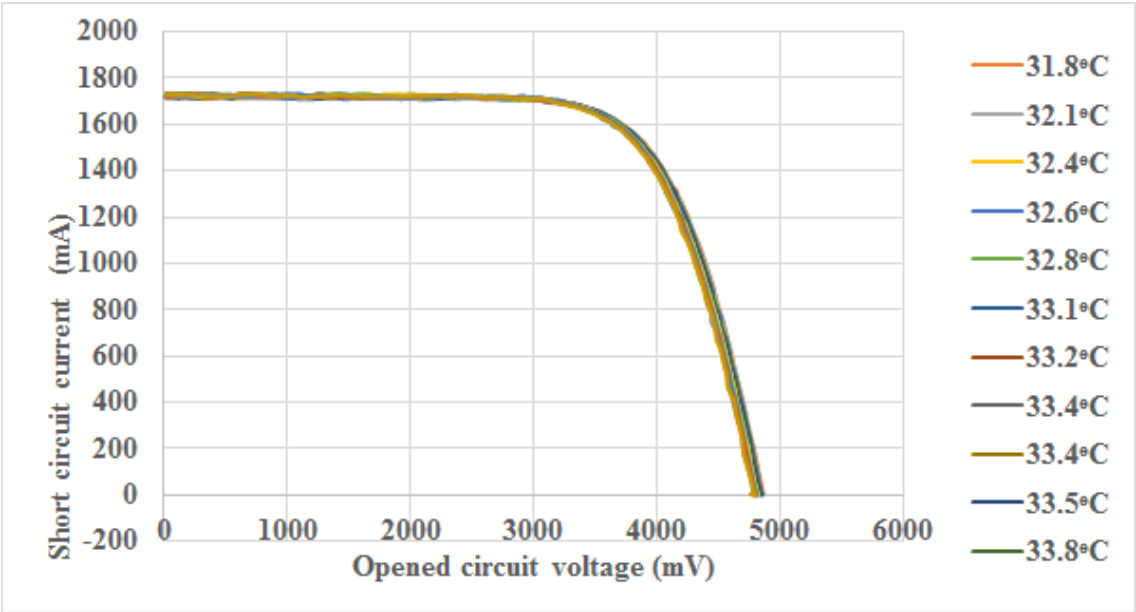

Figure 5.18: Stability of IV curves and SRCPC performance parameters using the volume flow rate of 0.007929L/s at 1 sun.

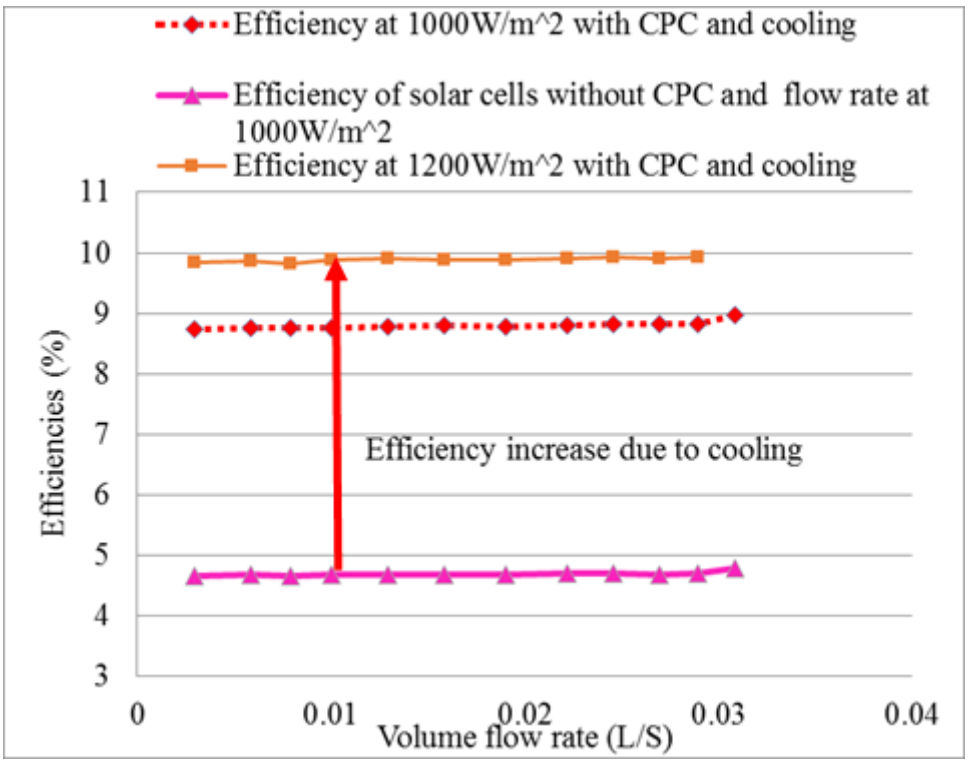

Figure 5.19: Efficiency stability as a result of cooling the solar cells at 1 sun

5.10.7 ***Effect of further increase of mass volume flow rate***

The volume flow rate was increased to 0.0222 $\frac{L}{s}$ to check the effect this will have on parameters. The solar cell temperature T_{sc} was fluctuating between 28.5°C and 29.9°C while the inlet temperature T_{in} dwindled between 31.3°C and 32.3°C for 1.55hrs test period. The outlet temperature T_{out} was also observed to be between 31.5°C and 32.6°C. The short circuit current $I_{sc}$was observed to be 1.628A at starting and 1.637A when the experiment stopped. The open circuit voltage fluctuated between 4.868V and 4.772V. The generated power by the system was 5.818W and 5.662W. In general terms, the parameters differences during the starting and stop of the experiment were negligible At saturation volume flow rate, the parameters became stable. Table 5.2 illustrates the stability in operating temperature and parameters with negligible differences.

Table 5.2: Shows stability in operating temperature and parameters at a volume flow rate of 0.0222L/s

Time (mins)	Time	Tin	Tout	Tsc	Current	Voltage	Power
	(mins)	ºC	ºc	ºc	(A)	(V)	(W)
0	12:15	31.3	31.5	29	1.628	4.868	5.818
3	12:18	31.3	31.6	29	1.627	4.871	5.811
6	12:21	31.4	31.6	28.6	1.63	4.866	5.805
9	12:24	31.4	31.6	28.8	1.627	4.861	5.801
12	12:27	31.4	31.6	29	1.637	4.858	5.792
15	12:30	31.4	31.7	28.8	1.635	4.855	5.792
18	12:33	31.6	31.8	29.2	1.632	4.851	5.782
21	12:36	31.6	31.8	29.6	1.632	4.847	5.773
24	12:39	31.7	31.9	29.4	1.629	4.845	5.756
27	12:42	31.6	31.9	29.5	1.626	4.839	5.762
30	12:45	31.7	31.9	29.5	1.638	4.834	5.759
33	12:48	31.8	32	29.9	1.639	4.832	5.748
36	12:51	31.8	32	28.6	1.631	4.838	5.738
39	12:54	31.8	32	28.5	1.635	4.822	5.743
42	12:57	31.8	32	29	1.633	4.82	5.732
45	13:00	31.8	32.1	28.5	1.636	4.818	5.74
48	13:03	31.9	32.1	28.6	1.637	4.815	5.725
51	13:06	31.9	32.1	29.2	1.639	4.811	5.725
54	13:09	32	32.2	28.8	1.63	4.807	5.722
57	13:12	32	32.2	28.9	1.636	4.807	5.721
60	13:15	31.9	32.2	29	1.633	4.802	5.689
63	13:18	31.9	32.2	29.1	1.634	4.801	5.703
66	13:21	32	32.2	29.2	1.644	4.798	5.689
69	13:24	32	32.3	29.3	1.638	4.796	5.697
72	13:27	32	32.3	29.4	1.637	4.791	5.683
75	13:30	32.1	32.4	29.5	1.635	4.787	5.675
78	13:33	32.1	32.4	29.6	1.632	4.78	5.666
81	13:36	32.2	32.4	29.7	1.637	4.783	5.664
84	13:39	32.2	32.4	29.8	1.639	4.779	5.682
88	13:43	32.2	32.5	29.9	1.64	4.771	5.649
90	13:45	32.3	32.5	29.5	1.639	4.791	5.694
93	13:48	32.3	32.6	29.2	1.637	4.772	5.662

The operating temperature of the solar cell when compared with the inlet and outlet temperatures during the testing time was almost the same. This is illustrated in Figure 5.20 showing time against temperature. Figure 5.21 is the I-V cure under the testing conditions while Figure 5.22 illustrates the stability of all parameters despite further increased flow rate. The common and efficient method of cooling implored in this project is active water

cooling for the polycrystalline silicon solar cells during the concentration of the solar radiation.

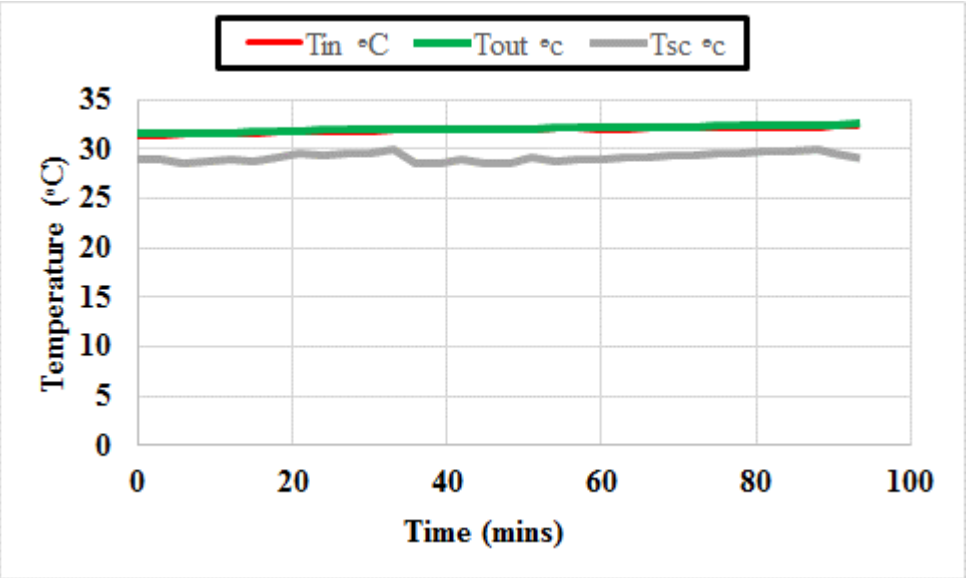

Figure 5.20: Temperature and parameters stability remain the same with further increase of volume flow rate to 0.222L/s

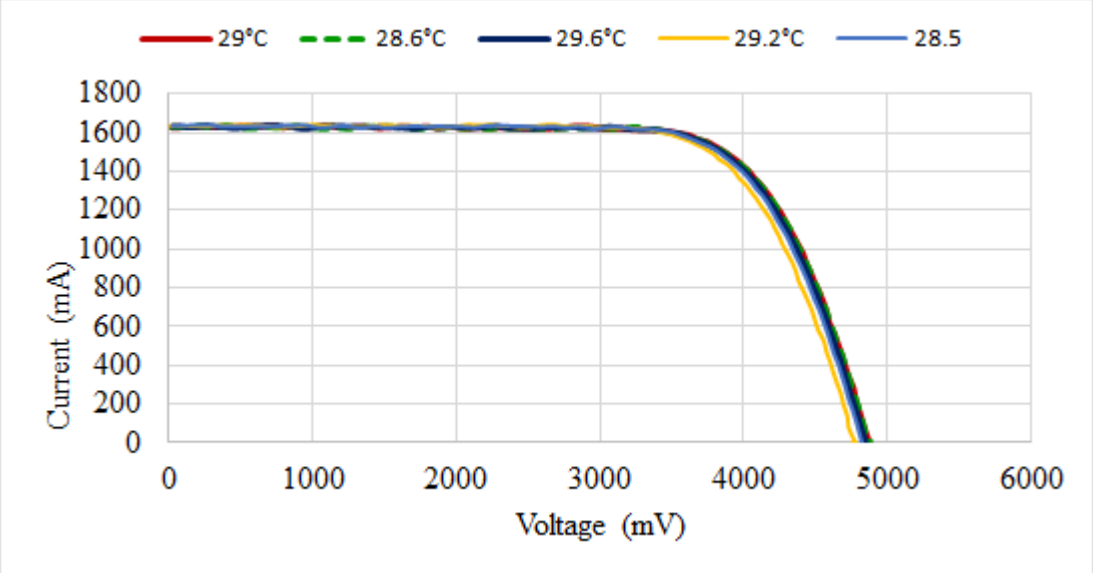

Figure 5.21: I-V curve stability with further flow rate increase to 0.0222L/s

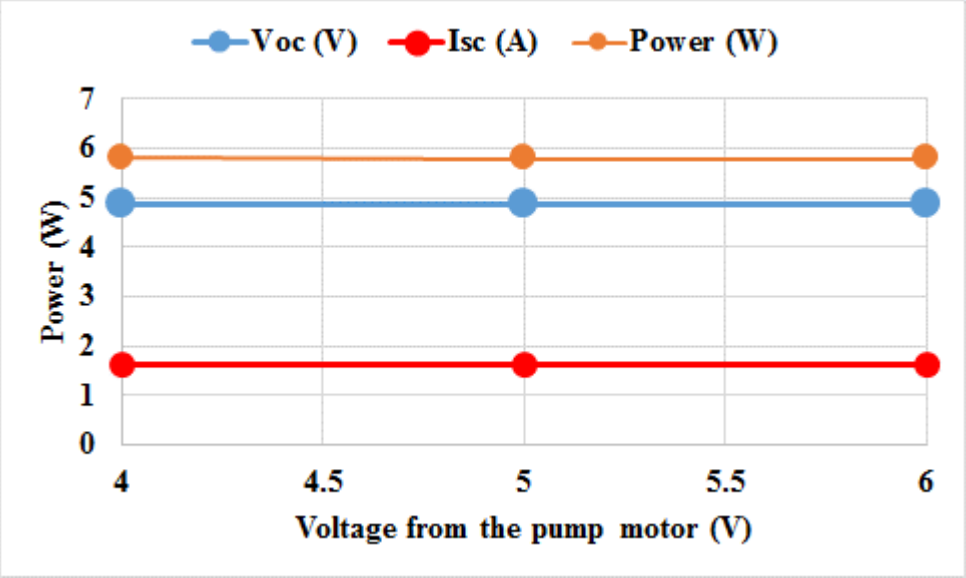

Figure 5.22: Showing stability of parameters despite change in volume flow rate and longer period of testing using increased volume flow rate of 0.022 (L/s).

5.10.8 ***The effect of volume flow rate on efficiency***

Recall that electrical efficiency is given by $\eta_{elect} = \frac{Power\ output}{G_T A_P}$. The different efficiencies from the power output recorded from the SRCPC were calculated using the excel sheet. Some excel sheet calculated efficiencies are shown in Table 5.3 for illustration.

Table 5.3 Some calculated efficiencies from various flow rates at 1sun and 1.2suns showing how fast parameters decline without cooling and their stability with cooling.

EfficiencyNo CPC, No flow rate at 1000W/m^2	Efficiency at 1000W/m^2 with SRCPC without cooling	Efficiency at 1000W/m^2 at 0.012929L/s	Efficiency at 1000W/m^2 at 0.015858L/s	Efficiency at 1000W/m^2 at 0.0222L/s	Efficiency at 1200W/m^2 with SRCPC and without cooling (eff. droping fast	Efficiency at 1200W/m^2 at 0.0222L/s	Efficiency at 1200W/m^2 at 0.01L/s	Efficiency at 1200W/m^2 at 0.005858L/s
4.1620	8.8692	8.9706	8.6494	8.6193	10.5659	10.1985	10.3852	10.5319
4.1424	8.8625	8.8332	8.6622	8.6089	9.9037	9.8148	9.9185	9.9778
4.4311	8.8537	8.8308	8.6442	8.6000	9.6193	9.8222	9.8978	9.9556
4.3748	8.8617	8.8242	8.6376	8.5941	9.3096	9.8163	9.9185	9.9437
4.3378	8.8342	8.8100	8.6404	8.5817	9.0578	9.7704	9.9096	9.9304
4.2415	8.8514	8.7907	8.6441	8.5807	8.8089	9.7615	9.8889	9.9230
4.2104	8.8570	8.7977	8.6306	8.5659	8.6222	9.7585	9.8770	9.8815
4.1704	8.8434	8.7865	8.6378	8.5526	8.4222	9.7659	9.9141	9.8681
4.1230	8.8672	8.7636	8.6408	8.5474	8.2519	9.7556	9.8756	9.8667
4.0874	8.8589	8.7689	8.6246	8.5363	8.1156	9.7763	9.8311	9.8815
4.0444	8.5657	8.7519	8.6268	8.5319	8.0281	9.7615	9.8533	9.8815
4.0222	8.3356	8.7441	8.6115	8.5156	7.8993	9.7600	9.8415	9.8667
3.9807	8.1383	8.7360	8.6143	8.5007	7.7704	9.7585	9.8652	9.8667
3.9556	7.9301	8.7142	8.6295	8.5081	7.6933	9.7467	9.8607	9.8681
3.9289	7.7617	8.7211	8.5865	8.4919	6.9767	9.7363	9.8326	9.8815
3.9230	7.6175	8.7122	8.5843	8.5037	6.8769	9.7111	9.8385	9.8756
3.8993	7.4789	8.7088	8.5925	8.4815	6.7553	9.6993	9.8385	9.8533
3.8741	7.3583	8.7097	8.5943	8.4815	6.5643	9.7037	9.8089	9.8607
3.8622	7.2379	8.7034	8.6025	8.4770	6.3679	9.6948	9.8163	9.8148
3.8459	7.1663	8.6856	8.5936	8.4756	6.2342	9.6933	9.8074	9.8163
3.8148	7.0420	8.6881	8.5812	8.4281	6.1100	9.7081	9.7941	9.8148
3.8044	7.0347	8.6801	8.5745	8.4489	5.9868	9.6800	9.7941	9.8105
3.7911	7.0298	8.6718	8.5793	8.4281	5.8998	9.6800	9.7837	9.7968

. The efficiencies were calculated both for 1sun and 1.2suns. It was further observed at 1000W/m^2 that as the volume flow rate increases, there is a corresponding increase in efficiency of the system. Figure 5.23 shows the increase in efficiencies from non-cooling to active cooling with water at 1sun and 1.2 suns. The highest efficiency attained with increased irradiation was 10.5659% but this is because the room air-conditioner was in operation and chilly weather condition. This could not be sustained because the temperature affected it till it dropped down to 5.0919%. The next to this was 10.53% which was sustained by cooling to 9.81%. At 1sun, the highest efficiency was 8.97% which was maintained by cooling to 8.68% during the period of the experiment.

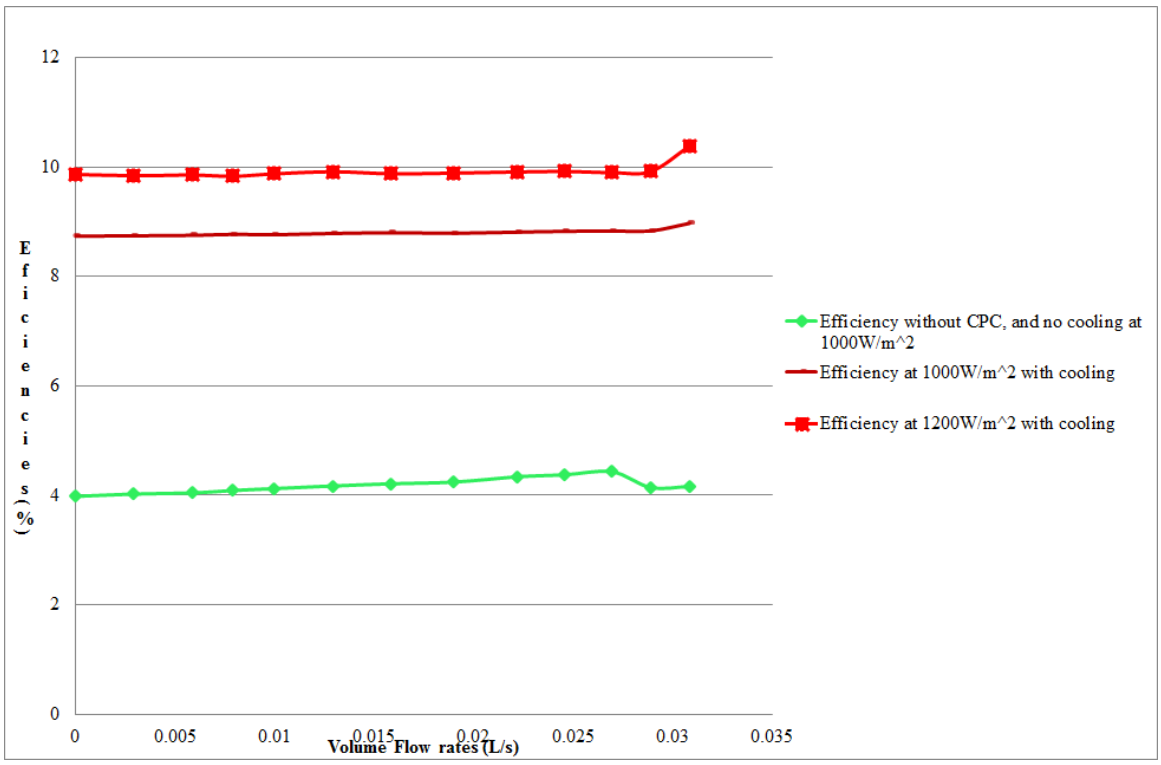

Figure 5.23: Efficiency increase, radiation increase without significant changes as volume flow rate increase.

5.10.9 ***Radiation increase effect on parameters.***

It was worth noting that as radiation increases, there are changes in all the parameters but with the same trend of effects during the cooling and without cooling. When radiation increased to 1200W/m^2 and the SRCPC was concentrating at 1200W/m^2 without cooling, the parameters declined because of the temperature rise with time. This is captured in Figure 5.24 as well as Figure 5.25 shows stability of parameters at 0.01L/s Saturation volume flow rate with cooling. The more the radiation, the more heat dissipation and more volume flow rate is required to extract the heat. The more flow rate the better the heat extraction which leads to efficiency increase.

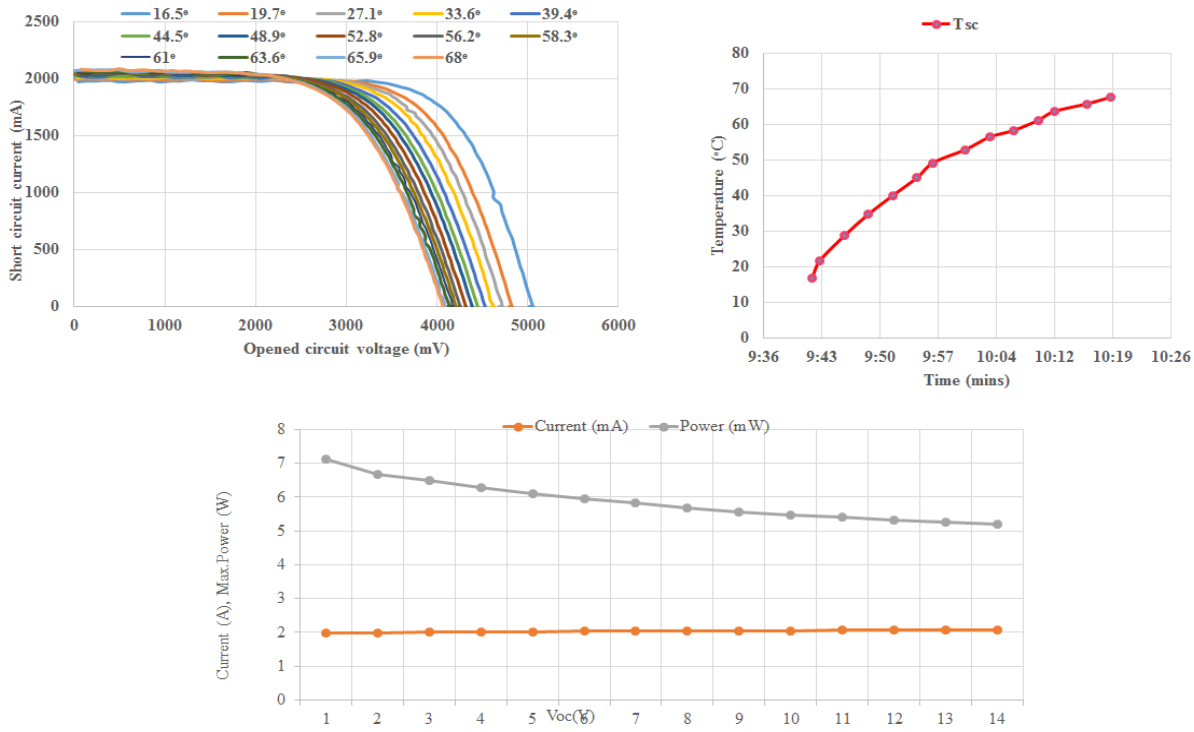

Figure 5.24: Increase radiation effect with increase parameter value but decline due to temperature rise without cooling

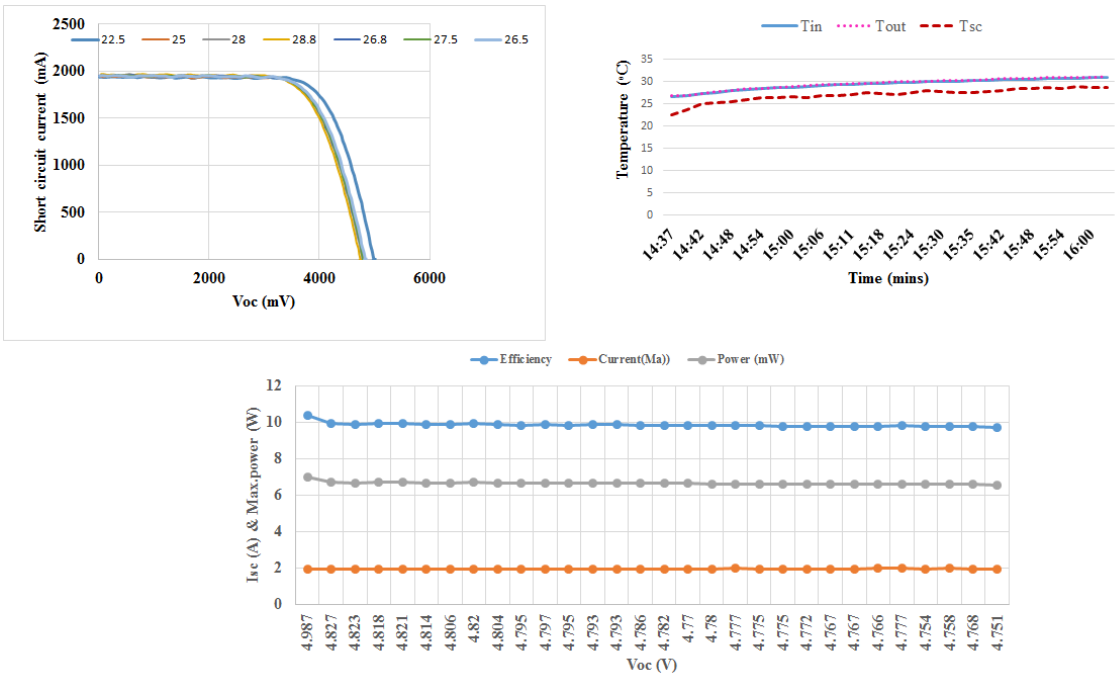

Figure 5.25: Stability of parameters at 0.01L/s volume flow rate at 1200W/m^2

5.10.10 ***SRCPC power generated***

The maximum power output of the SRCPC for different flow rates for 1 sun is shown in Figure 5.26 during the indoor experiment. The concentration and cooling has

significance increase on the power generation as shown below. At no cooling, 2.669W and 5.556W was generated without and with the SRCPC respectively. During concentration and cooling, the power generated was 5.567W, 5.903W, 5.913W, 5.931W and 5.974W as against the volume flow rate of 0.00689L/s, 0.007929L/s, 0.0158L/s, 0.00183L/s and 0.308L/s respectively.

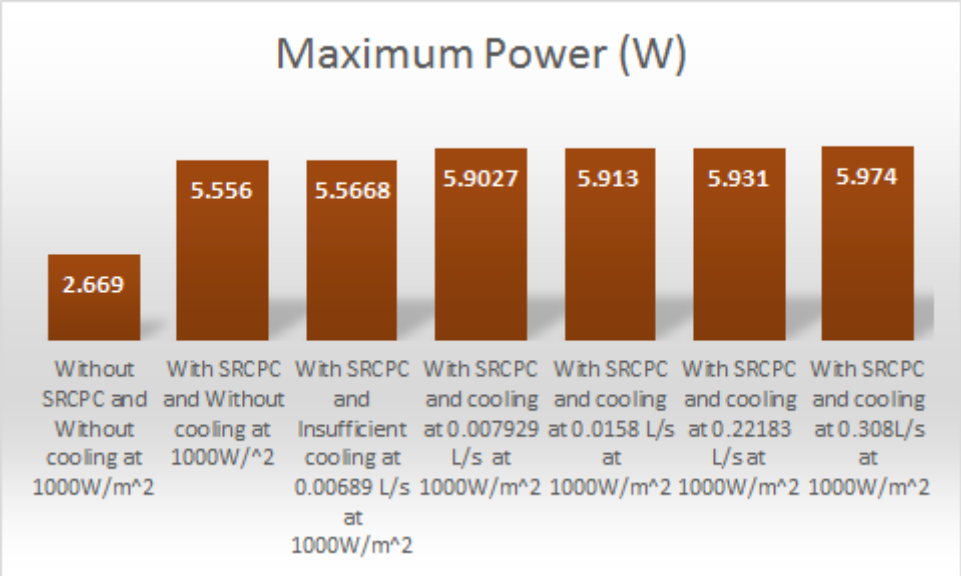

Figure 5.26: Showing maximum power output at different volume flow rates at 1sun

The maximum power generated by the SRCPC under cooling at different flow rates at 1.2 sun is shown in ***Figure 5.27***. The increase in solar radiation gave a corresponding increase in the short circuit current which led to a significance power generation. The heat extraction mode proved effective where the flow rate is a factor. At no cooling, the maximum power generated was 5.8854W before it dropped significantly. During the concentration and cooling, the maximum power generated using different flow rates are 6.68447W, 6.799W, 6.8496W, 6.974W and 6.9999W as against the volume flow rates of 0.005858L/s, 0.007029L/s, 0.01L/s, 0.022183L/s and 0.030858L/s respectively. These values were close to expectation because as the volume flow rate increases, there is a corresponding increase in the power generation no matter the quantity. Table A2 in Appendix is the characteristics summary of a parameters of the solar cell strings

The assembled SRCPC coupled with a heat exchanger medium having acceptance area of 0.0675m² was characterised electrically under indoor conditions by the used of I-V tracer and solar simulator. At a solar radiation of 1000W/m², the maximum electrical power, voltage, current and efficiency were recorded at a volume flow rate of 0.0308L/s to be 5.974W, 4.87V, 1.73A and 8.83% respectively. These values were maintained close to

expectations. At increased solar radiations to 1200W/m² at a volume flow rate of 0.0308L/s, the maximum electrical properties were 7.11W, 5.00V, 1.99A and 10.53% using the LGBC solar cells. The results from this proof of concept indicated that active cooling is imperative in CPV system operation.

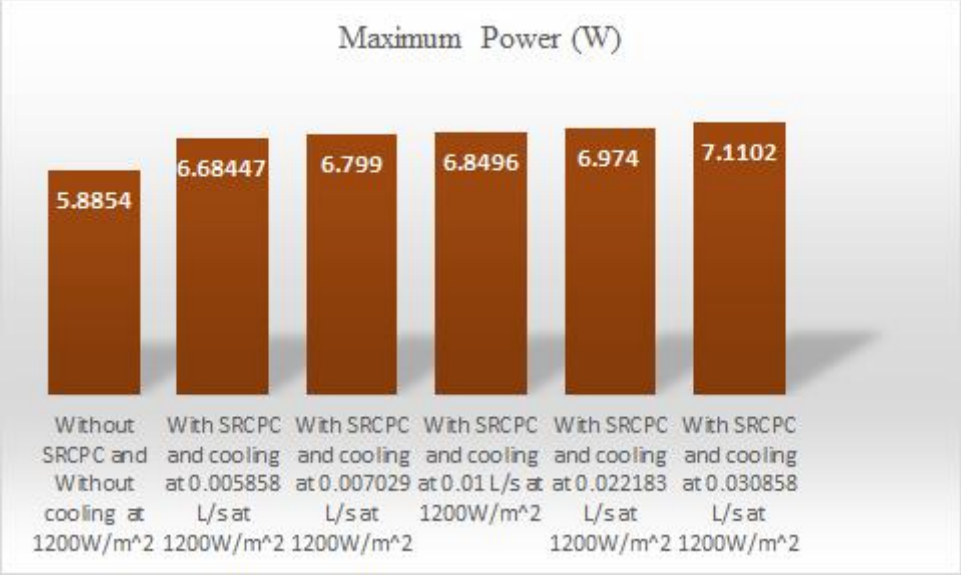

Figure 5.27: Shows maximum power output at different flow rates when the solar radiation was increased to 1.2 suns

The thermal management system was integrated and its effect is shown. The flow rate that stabilised the power generation if 0.0308L/s. More water can still be pumped but the difference may not be much. From the foregoing, it is necessary for effective operation of CPV that active cooling be integrated as part of the system to extract the heat and hence, increase the efficiency and stability of parameters.

.

5.11 Conclusion

The construction of the SRCPC is described in this chapter and followed by the indoor characterization. The optical modelling was first described in chapter 2. The material selection was the next in the process after considering their engineering properties. The construction was then followed and the assembling process using table vices, clamps, spirit level, measuring tape, veneer calliper, and araldite rapid to hold tight to position and dimensions. The thin film reflectivity was measured and then pested on the inward sides of

the parabola. The SRCPC was constructed by Pent land Precision Engineering Limited in Scotland and assembled at Exeter University. The SRCPC was coupled with the electrical connection of the solar cells employing high level distinct techniques and precision devices.

The trends of the experiment agrees with the modelled trends and also shows that the efficiency increases with volume flow rate of the cooling medium but careful observations must be taken to stop at the saturating volume flow rate to avoid unnecessary cost and waste of resources.

The good agreement of the optical and experimental trends coupled with the heat exchanger validate the SRCPC constructed thereby allowing its general use to design further geometries of optical devices especially concentrator devices. Therefore, the next chapter will focus on the outdoor characterisation for the validation of the optical model.

Chapter 6 **SRCPC OUTDOOR EXPERIMENTAL CHARACTERIZATION**

In this chapter, a detailed outdoor experimental characterisation of the developed SRCPC system is presented. The twin SRCPC developed model coupled with a heat exchanger was constructed assembled and mounted for outdoor condition monitoring and to validate indoor result by exposing the designed systems under ideal weather conditions. This was installed lying in the east-west direction but facing the south – north direction at the sustainability institute building 2nd floor at the University of Exeter. The equipment for the outdoor experiment together with the measuring and monitoring device have been introduced and discussed. An optimal tilt angle model is developed in order to be sure that the optimal angle of inclination at which the solar radiation meets perpendicularly with the SRCPC model thereby producing maximum power conversions from the system. A peristaltic pump is also installed to ensure the volume flow rate to the heat exchanger that moderates the fluid flow for proper cooling while the temperature recorder captures the periodic changes in temperature. Towards the end of the chapter is the result of the outdoor experimental measurements to enable the characterisation of the developed SRCPC model. The obtained results are used to validate the optical, electrical and thermal properties of the designed and developed SRCPC model.

6.1 Introduction

From the indoor characterisation study, it becomes necessary that the performances of the SRCPC that is simulated be experimented in real outdoor conditions similar to where they will be installed. Here the developed SRCPC is non- imaging but static type whose performances are directly connected to their inclined positions being perpendicular to the solar rays because it is directly proportional to the electrical converted energy and the optical efficiencies. The outdoor experimental set up and methodology used are introduced in this chapter. More to this, optimised tilt angle model was developed to ensure optimum angle inclination of the SRCPC module to incline perpendicularly for maximum electrical power conversion and validation during the outdoor testing conditions. The fact that the experiment was carried out under outdoor condition necessitates the combining of both direct and diffuse solar radiations contrary to the indoor experiments that focused only on direct radiation. The outdoor experimental study presented in this chapter provided a set of results used to compare the experimental

values and modelled optical efficiencies for validation. The chapter finally concludes with the results of the outdoor test.

6.1.1 *SRCPC model outdoor composition*

A twin SRCPC model was designed, optimised, indoor tested, and made of the same size and frame as for real applications. The assembling procedures and manufacturing process used in Chapter 5 did not change. The major difference here is that the empty compartment inside the enclosure was filled with cavity and expanding foam to insulate and prevent heat escaping from any source except through the heat exchanger medium as a maximum heat control measure. Another addition to this is the aluminium adhesive tape that was used to cover the top surface of the cavity and expansion foam. This is intended to reflect all possible solar radiation that is not entering the concentrator acceptance aperture to be reflected back. Total internal reflection was achieved through this means. Furthermore, to this was added the tough low iron cover crystal clear glass surrounded from all sides by rubber gasket that prevents ingress of moisture into the SRCPC system. The heat exchange, K-type thermocouples, water pipes were connected and were not visible except the leads were connected to their equipment for recording and monitoring purposes. The SRCPC model was composed in this way to enable it withstand all the weather conditions around it. The thermocouple positions were placed underneath between the solar cell and heat exchanger to monitor the temperature of the solar cells as well as the inlet and the outlet flow of the heat-extracting medium to monitor the temperature. Figure 6.1 shows the cavity and expansion foam laid round SRCPC inside the enclosure and the K-type thermocouple position while Figure 6.2 shows the SRCPC system surrounded with thermal insulation and covered with reflective materials.

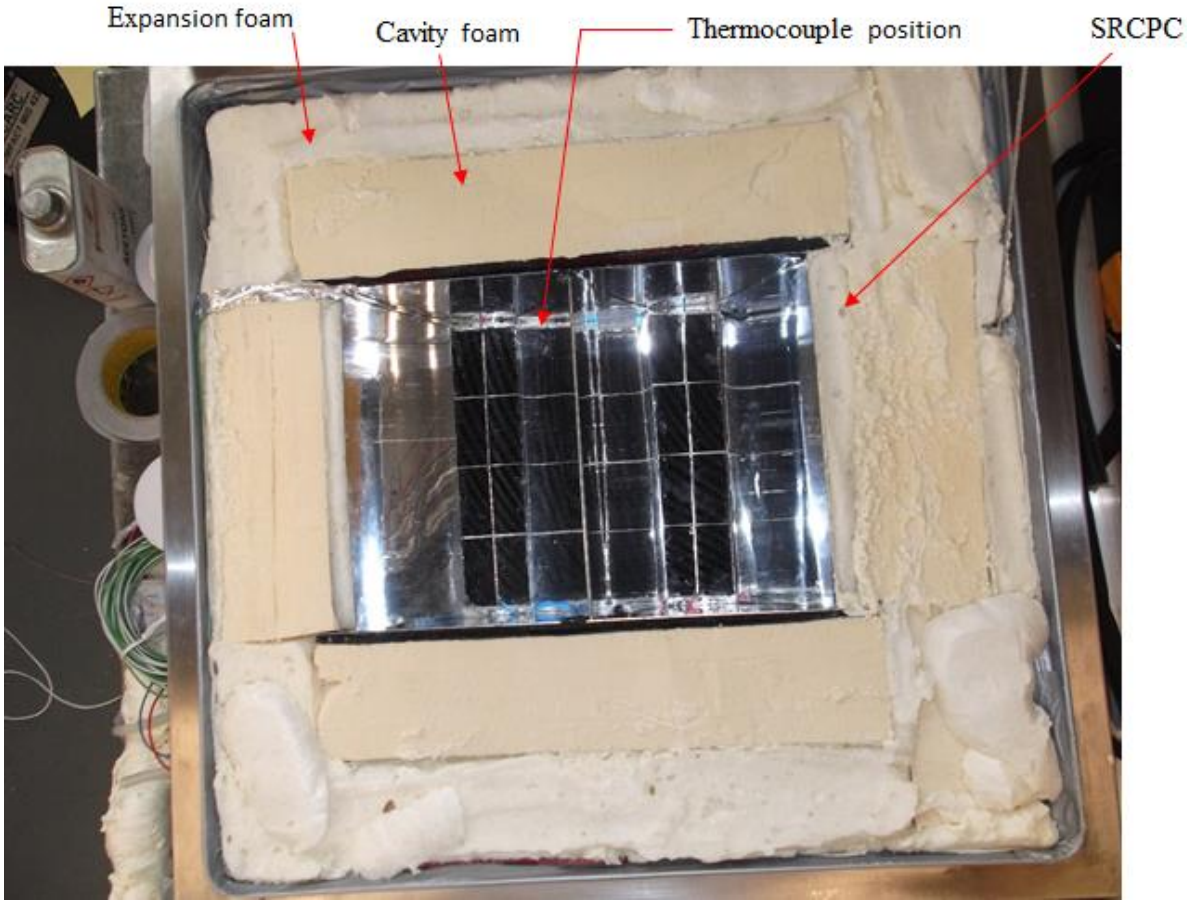

Figure 6.1: Cavity and expansion foams laid round the SRCPC and thermocouple position

The enclosure and the SRCPC model were manufactured using alloy steel due to its non-corrosive nature and temperature resistance and also, because it will be exposed to all weather conditions. Figure 6.2 shows the SRCPC system was covered with aluminium reflective materials to prevent additional thermal penetration through any source apart from the acceptance aperture of the concentrator. The double grooved weather resistant rubber holds the glass firm and prevents ingress of moisture.

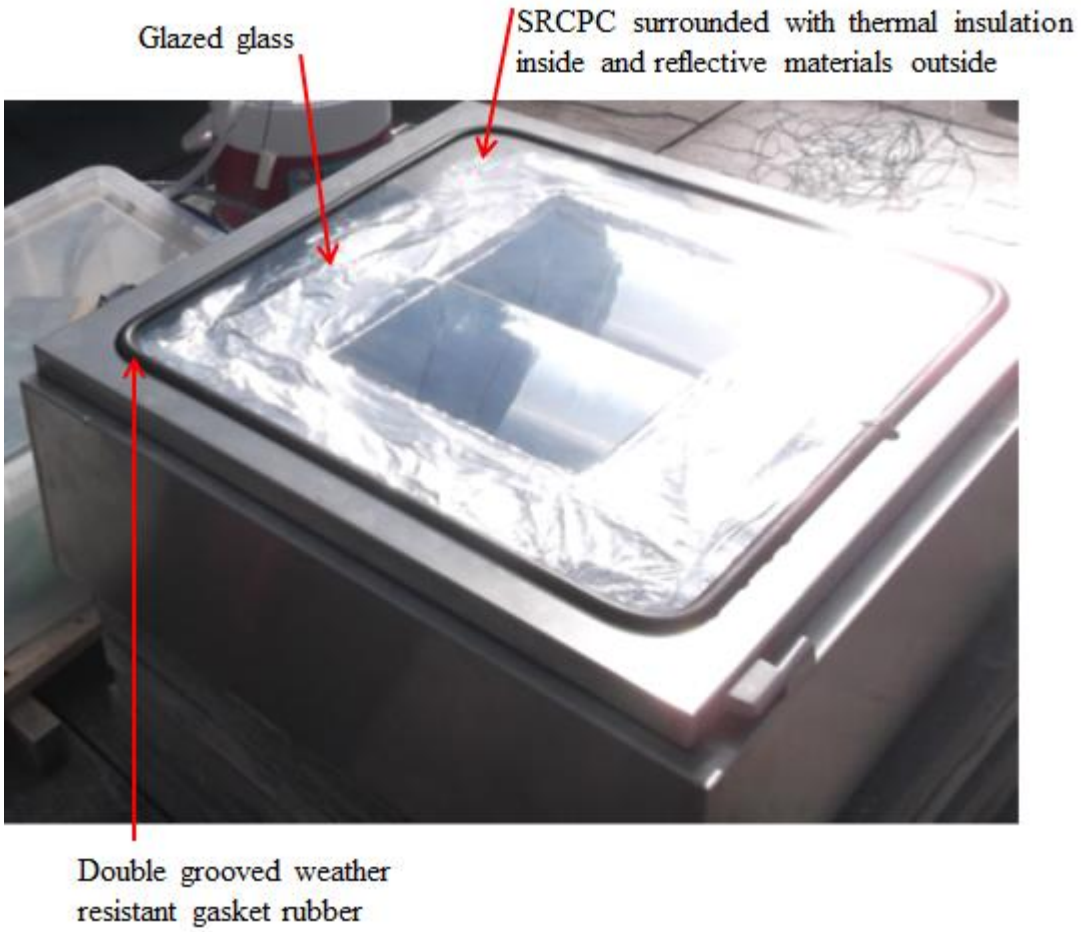

Figure 6.2: SRCPC system surrounded with thermal insulating inside, aluminium reflective materials and double groove weather resistant rubber.

6.2 Modelling optimum SRCPC incident slope (tilt) angle

The power incidence on a CPV array or panel depends not only on the power contained in the sunlight, but also between the module and the sun. When the absorbing surface and the sunlight are perpendicular to each other as shown in Figure 6.3, the power density on the surface is equal to that of the sunlight.

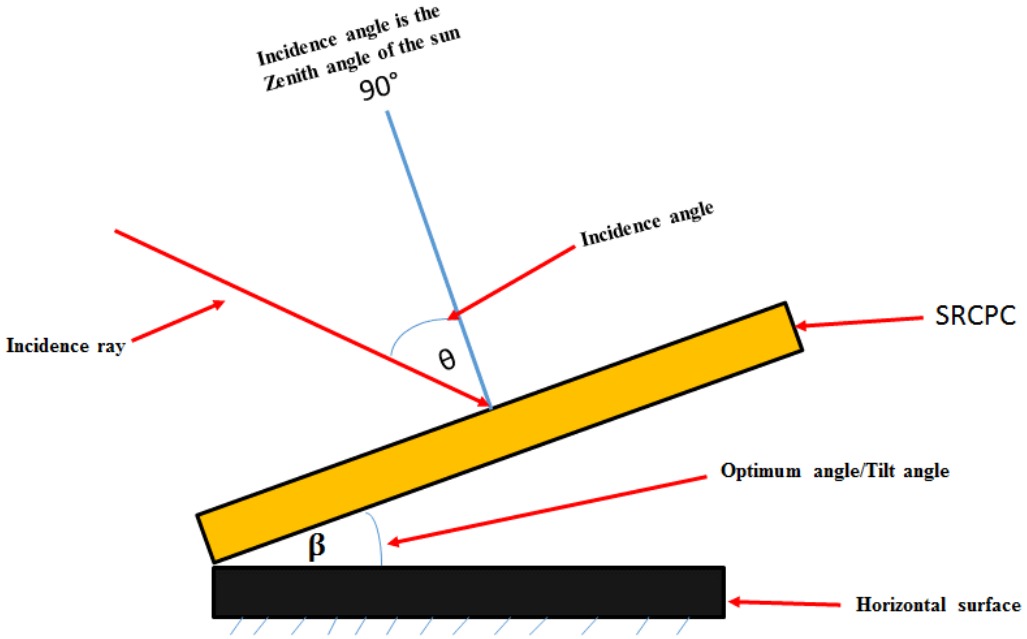

Figure 6.3: Incidence angles on a horizontal surface

This means the power density will always be at its maximum when the SRCPC is perpendicular to the sun. As the angle between the sun and a fixed SRCPC is continually changing, the power density on a fixed slope angle is less than that of the incident sunlight. To get the most optimum energy from the developed SRCPC, solar panels or CPV, one need to point them in the direction that captures the most sun. There are a number of variables in figuring out the best direction. Here the SRCPC is fixed but has an optimum or tilt angle that must be adjusted in order to get the optimum solar energy expected. At what angle from horizontal should the SRCPC be elevated or tilted?

6.2.1 ***Modeling optimum slope angle***

The main factors influencing the captured quantity of absorbed solar radiation energy is the orientation of solar collector. When the position of solar concentrator is stationery because the optimal angles depends on the geographical position of the investigation period which can be day, week or month. This is vital because the trajectory of the sun changes. Also, the solar irradiation energy, sunlight duration per day and year changes as well. The use of sunray concentrators with reflectors is another way to increase the quantity of solar radiation energy. However, the main reason of all solar concentrators is to increase the quantity of solar radiation energy through the use of cheap materials and equipment of solar concentration.

The modelling of solar position, the duration of solar radiation, the intensity of radiation energy, and the cross-section of solar rays falling into a solar collector depends on time. This part of the thesis presents a mathematical model designed to find the optimal angles for the SRCPC which has reflectors and the results of an experimental investigation. An estimation of the sun's position, sunlight duration per year, the geographical position and geographical parameters were required.

6.2.2 Mathematical modelling of optimal angles for SRCPC

The quantity of solar radiation energy [W/m^2] per time, falling into the SRCPC depends on many factors. These dependable factors can be categorized into two groups:-

These factors are selected factors and ordinary factors. The selected factors includes geographical parameters with the SRCPC, length [m], width S[m], height L[m], angles β and γ that describes the orientation of the concentrator; latitude ψ, height above sea level, the reflection coefficient of the SRCPC including the investigation period D.

Also, the group of ordinary factors includes angles X and Y. These angles describes the position of the sun in space, the intensity of solar radiation energy Q [W] and the duration of sunlight. The ordinary factors are time dependent. Mainly, they are described by known mathematical functions and sometimes are obtained from experimental data for a long period [1].

Furthermore, in this mathematical model, the selected factors which are variables are B and Y. The remaining ordinary factors depends on the geographical position and investigation period. They have numerical value in most situation.

6.2.3 Determination of Optimal orientation Angles

The incident angle of the direct solar radiation on the tilted surface, θ, has other angles joined relationship as in Equation 6.1[156].

6.2.4 The declination angle

$$\delta = 360\,\frac{284+n}{365} \qquad 6.1$$

δ = 22.9° when n = 160

The declination angle and hour angle were used for the modelling. The sun rising hour angles ω_r and sunset ω_s for a south facing, $\gamma = 0$. The angle used to model the optimum angle [206] includes $\delta = 22.9°$, $\omega_r = 10°$ (6:40hrs), $\omega_s = 49.5°$ (20.57hrs). The height of Penryn in Cornwall above sea level is 29m [207]. Also, since Cosθ can represents the solar radiation reaching the concentrator, the surface optimum tilt angle is associated with the value of β that maximizes Cosθ. By differentiating $\frac{dCos\theta}{d\beta} = 0$, we have

$$A = 2(\sin\delta \sin\phi \cos\beta - \sin\delta \cos\phi \sin\beta \cos\gamma) \times (\cos\delta \cos\phi \cos\beta + \cos\delta \sin\phi \sin\beta \cos\gamma) \quad 6.2$$

and

$$B = (\cos\delta \cos\phi \cos\beta + \cos\delta \sin\phi \sin\beta \cos\gamma)^2 + (\cos\delta \sin\beta \sin\gamma) \quad 6.3$$

The optimum angle was modelled and determined using excel by iterating for the values for which the extra-terrestrial solar radiation measured on the SRCPC surface is maximum for a particular day or specific period. In a normal case of concentrator's orientation, it is necessary to search for the maximum Watt of the function W= f (β, γ). From here, we will get the optimal orientation angles β and γ through calculation results. The selected factors numerical values are presented in Table 6.1

Table 6.1: Selected factors and their numerical values

S/N	Selected factors	Notation	Numerical value
1.	Height of SRCPC	L	0.105m
2.	Length of SRCPC	N	0.225m
3.	Width of SRCPC	S	0.15m
4.	Latitude of (Penryn in Cornwall)	ψ	50.17°N, 5.11°W
5.	Height above sea level	A	29m
6.	Reflection coefficient of SRCPC	H	0.86 – 0.82
7.	Investigation period D	160th day of the year	June 8th
8	Declination angle	δ	22.9°
9	Sunrise hour angle	ω_r	10° (6:40hrs),
10	Sunset hour angle	ω_s	49.5° (20.57hrs).

It is important to note that the normal of the surface plane of the concentrator is orientated towards the South. Any day of the year can be modelled. You only need to substitute the number of the day in the year and change the latitude in the model to get any optimum tilt angle of any location anywhere in the world. The 160th day of the year corresponds to the June 8th which was a bright day that gave good solar radiations and results among others that is used for illustration, see Table 6.2.

Table 6.2: SRCPC modelled optimum tilt (Slope) angles

Day/Month	Number of day of the year	Elevation decimal	Modelled slope angle
8th June, 2015	160	0	0^0
		0.1	5.7^0
		0.2	11.5^0
		0.3	17.2^0
		0.4	22.9^0
		0.5	28.6^0
		0.6	34.4^0
		0.7	40.1^0
		0.8	45.8^0
		0.9	51.6^0
		1	57.3^0

Figure 6.4 shows the maximum power generated by each tilt angle. The incidence angles, optical efficiencies, concentration ratio, absorber area, and solar radiations were used to model the optimum power generated by each tilt angle.

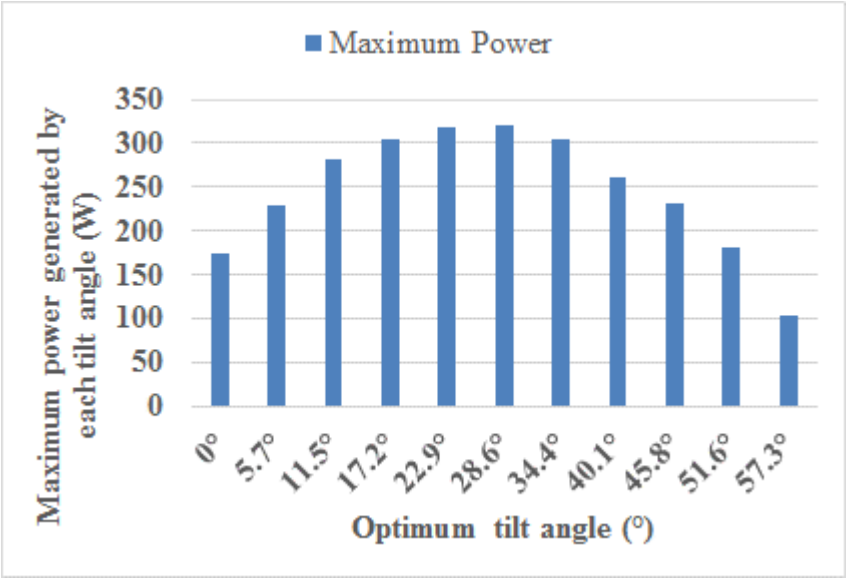

Figure 6.5: Maximum power generated by each tilt angle

From the results, the modelled optimum slope (tilt) angles were 28.6º and 22.9º .The power generated were 321.38W and 319.35W respectively. Therefore, the best optimum tilt angle for SRCPC maximum power conversion from the solar radiation is 28.6º. The modelled SRCPC slope angles result is shown in Table 6.2 above [208], while the graphs for each modelled slope angle are in Figure 6.6. The latitudes and longitudes of Penryn in Cornwall, United Kingdom were used in modelling being the location site for the outdoor experiment. From the graph, the best way to identified the optimum tilt angle apart from the maximum solar energy is its sharpness at 0º which is 12:00noon [209, 210].

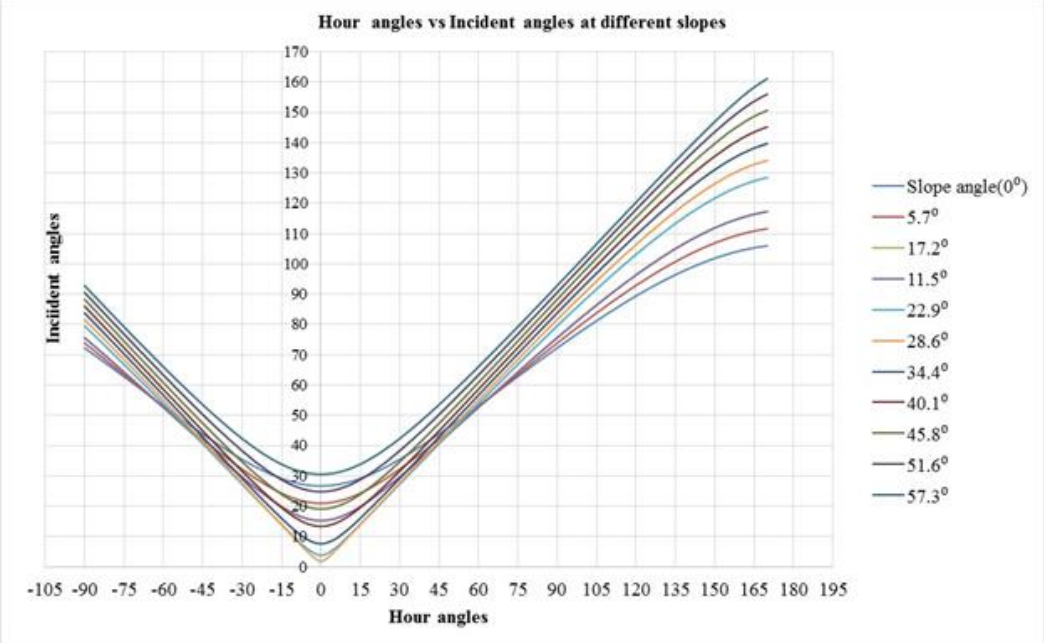

Figure 6.6: Graphs showing different SRCPC modelled slope angles results

The best slope angle for the solar radiation to be perpendicular to the constructed SRCPC model surface is 28.6^0 which correspond to the 28.5° tilt angle obtained and used by Rohit Tripathi et al [189]. The SRCPC was positioned at a slope angle of 28.6° where optimum power conversion was achieved. The SRCPC was laid in the East – West direction but facing the sun in the North – South direction as indicated in Figure 6.7. Other slope angles were tested at different direction but the best results were achieved at this optimum slope angle.

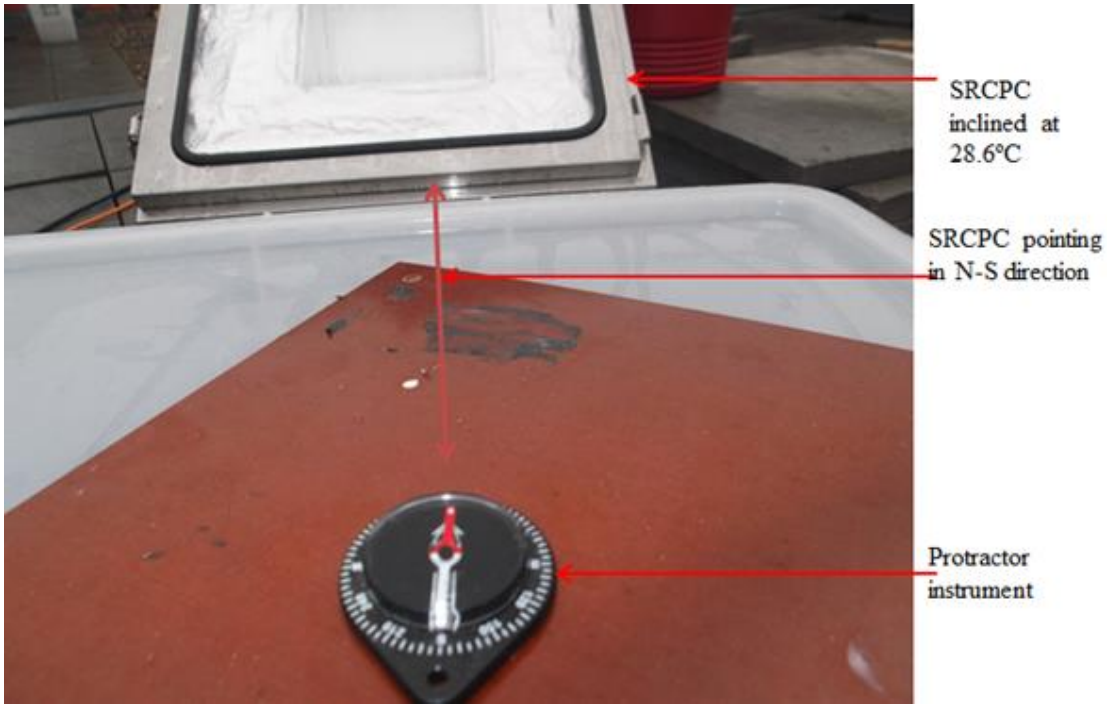

Figure 6.7: SRCPC mounted in the N-S direction

6.3 Location of the experiment

The site location where the experiment was carried out is Penryn Campus of The University of Exeter which is located in Cornwall, United Kingdom at latitude of 50.17°N and longitude of -5.11°W. The experimental site is located on top of the 2nd floor roof of the Sustainability Institute (SI) of the University with opened field without shading obstruction from buildings and trees. Figure 6.8 shows the experiment site with opened field and existing equipment.

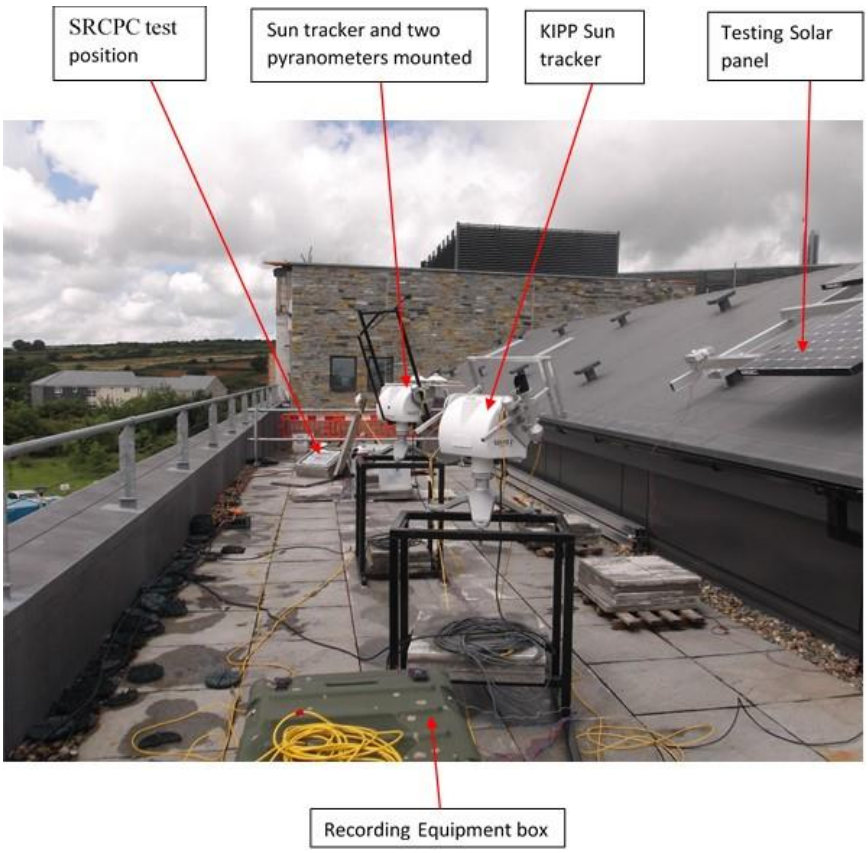

Figure 6.8: Experimental site with opened field, existing equipment and without shading at Sustainability Institute, University of Exeter, Penryn CampusUnited Kingdom.

6.4 Outdoor experimental set up and apparatus description

The outdoor experimental setup for the SRCPC is as shown in Figure 6.98. It is mounted on a slab surface on top of the 2nd floor of the Sustainability Institute building of the University of the Exeter, Penryn Campus because of the weight and strong wind purposes. The modelled optimum slope angle at which it was tilted is 28.6° which correspond with the incident angle of the sun rays at noon in Penryn – Cormwall the site of the outdoor experiment. The variation of the incident angle of solar radiation has to be kept at the minimum possible for static concentrators as already indicated by Sellami and Mallick [211]. However, this cannot be achieved except the SRCPC model is facing the North – South direction in order to achieve this low variation of incident angle. This is why the present choice orientation and slope of the experimental set up.

The Kipp and Zonen sun tracker in Figure 6.8 is used in this study for accurate measurements of direct, global and diffuse radiation. In order to characteriase the SRCPC model, the measurement of different solar radiation at different times during the day was required. It was only possible by the use of the three pyranometers which were connected

to the data logger and I – V tracer in the solar station to measure: 1) The global radiation on the horizontal plane. 2) The solar radiation on the slope plane of the SRCPC model connected to the I – V tracer.

On the sun tracker, a pyrheliometer is connected to data logger to measure the direct radiation.The SOLYS 2 sun tracker is the type used where the pyrheliometer are mounted to track sun and measure the direct radiation [212].

One of the Pyranometers measures the global radiation while the other pyranometer measures the diffuse radiation with the aid of the shading assembly to block the direct radiation created by the second pyranometer. The shading assembly covers the solar radiation so that only diffused radiation can be measured. Also, directly connected to the SRCPC is another pyranometre that measures the global radiation captured by the SRCPC system as shown in Figure 6.9.

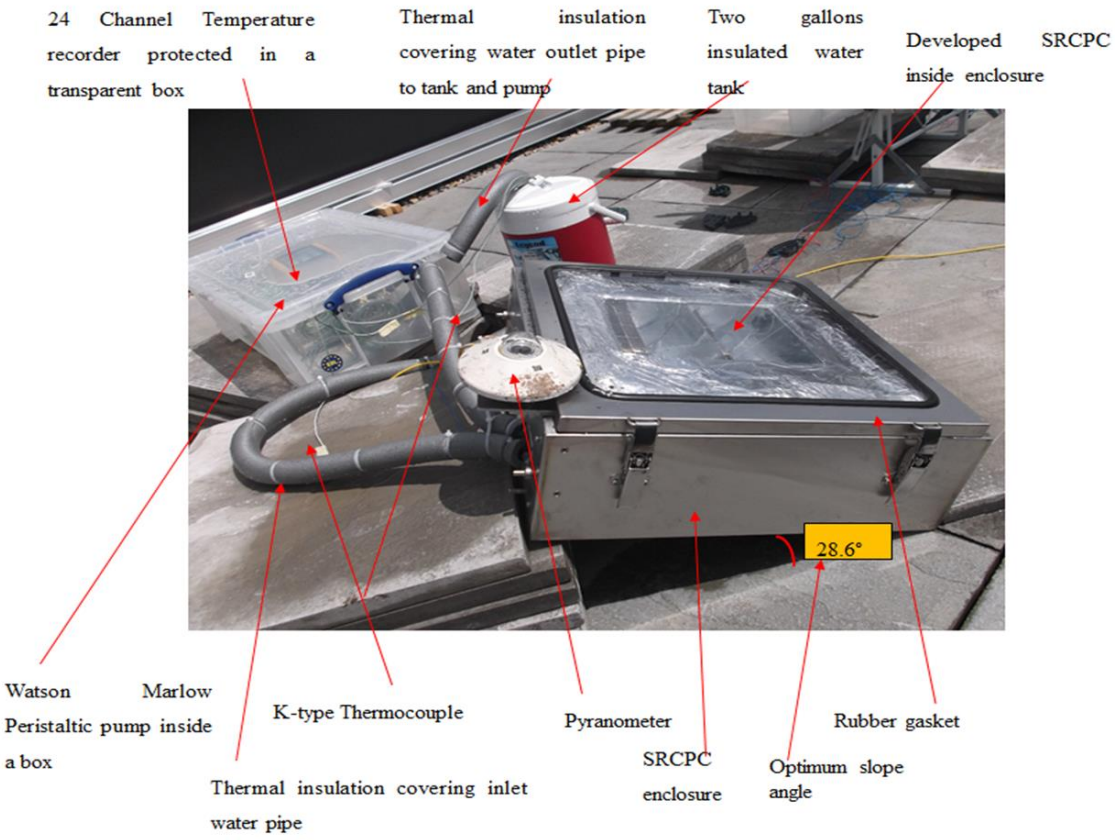

Figure 6.9: SRCPC experimental set up at The Sustainability Institute of University of Exeter, Penryn Campus, UK at a slope (inclined) angle of 28.6° with a pyranometer to measure the Direct radiation.

For the second pyranometer to measure the diffuse radiation, a shadow is created with precision adjustment of a ball shape that changes position corresponding to the sun's

position. The SOLYS 2 sun tracker tracks the sun's position by employing two possible options depending on the condition of the weather. First it employs the use of a sun sensor when the sky is clear and there are no clouds hiding the direct radiation of the sun [for instance when the solar radiation is more than 300W/m^2] . The exact position of the sun is deteremined by the use of the sun's sensors position accuracy which is about 0.02°. the secondary option of tracking the sun's position is that an integrated GPS reciever is used when the sun is cloudy and no direct sun radiation can be detected and hence, automatic configuration of the time, location and solar position with an accuracy within 0.1°.The CMP – 11 pyranometers used in this technology are KIPP and ZONEN. The CMP – 11 pyranometers uses temperature compensated detectors technology to generate voltage that can be converted to solar irradiation by the use of sensitivity factor. These pyranometers has a spectral range from 285nm to 2800nm that are capable of measuring maximum solar radiation up to 400W/m^2 .

CHP -1 pyreheliometer products are used with the sun tracker from KIPP and ZONEN [213]. The spectral range of the CHP – 1 pyreheliometers is from 200nm to 4000nm which is capable of measuring up to 4000W/m^2 with a response time of less than five seconds. It is worth noting that the direct solar radiation measured by the pyreheliometers is used to confirm the reading from the other pyranometers and to confirm the accuracy of the solar tracker working correctly

For proper characterisation of the SRCPC sytems , the modules was connected to a channel in the IV tracker which was also connected to the control panel in the lab for the data recording. The pyranometers were connected to the data acquisition system as follows : Channel 1 was connected to collect direct radiation having a sensitivity of $7.92x10^{-6}$ V/$Wm^{2\cdot}$. Channel 2 was connected to collect direct radiation from the SRCPC model having a sensitivity of $9.44x10^{-6}$ V/Wm^2, Channel 3 was connected to collect diffuse radiation having a sensitivity of $8.72x10^{-6}$ V/Wm^2, Channel 4 was connected to collect global horizontal radiation having a sensitivity of $13.44x10^{-6}$ V/Wm^2. Channel 5 was connected to collect direct radiation from another project having a sensitivity of 9.22V/Wm^2 [214, 215].

The 12-channel thermocouple meter used was chosen because it has a temperature measuring range between -100°C to 1300°C. It has an accuracy of measurement of ±0.4% or reading and a resolution of 0.1° . The instrument has a further build-in K-type thermocouple beadded wire temperature probes. Figure 6.8 shows the thermocouple

meter. The K – type thermocouples were used for sensing the four temperatures that were recorded. The temperature of the solar cell [Tsc], the tenperature of the inlet water pipe [Tin], temperature of the outlet water pipe [Tout] and the temperature of the insulation tank [Ttank]. These four thermnocouples were logged unto a 12 channel temperature data logger (W/SD) card data logging [215]. The temperature of solar cell (Tsc) connected and recorded at channel 1. Channel 2 recorded the temperature of inlet water pipe (Tin) while Channel 3 recorded the temperature of the outlet water pipe (Tout) and the temperature of insulation tank (Ttank) was assigned to channel 4. This 12 – channel instrument accurately measures temperature independently. The data is recoreded on SD card in excel format for easy transfer to a computer system for analysis. It has a data logging capacity up to 20,000 records using a 2G SD card and a manual store with a recall of up to 99 records. This temperature recorder meter has automatic temperature compensation.

In this study a high speed data acquisition system supplied from national instrument was used to collect solar irradiation data. This National Instrument (NI) data logger has chassis for different modules insertions for different parameters such as voltage, temperature, current and power. There are different NI modules available for different parameters depending on the device that reqiures test. The data to be measured is collected through a data cable from the chassis [216]. A programmable time switch was used to turn on the peristallic pump when the sun rise and turn off the pump when the sun set. A 323 model Watson Marlow peristaltic pump [217] was used to pump water into the SRCPC system to extract the heat generated by the solar cells during the operating time, and to reduce the temperature dependent effect and maintain the sytem parameters at equilibrium thereby increasing efficiency of the solar cells. The I-V tracer, Eko scan [218], data logger and computers mentioned and used in this study were kept and maintained at room temperature in a control room located in the lab in the SI building.

Figure 6.10 shows available captured solar radiations data at the test site. These types of data were collected between May and July 2015 at the weather station during the experiment at the site.

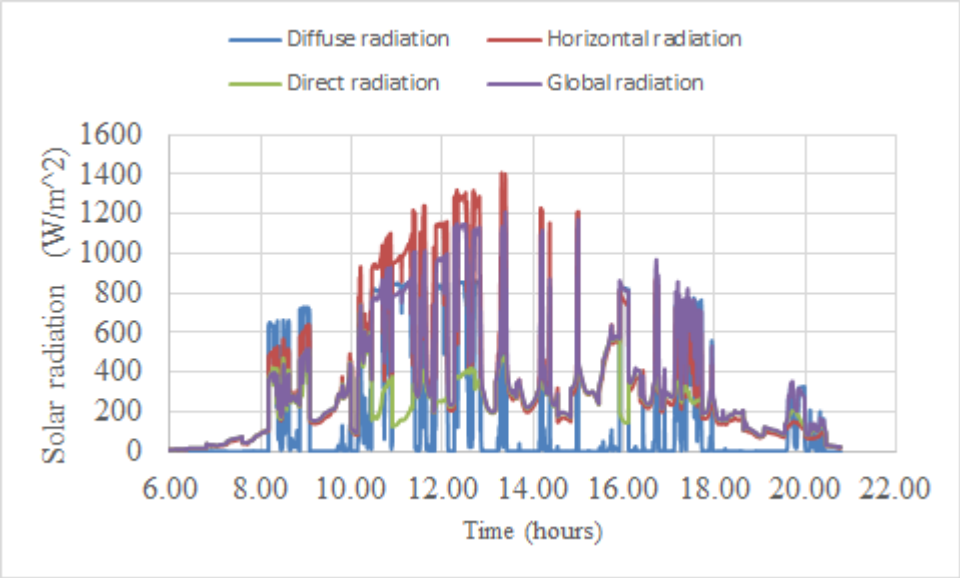

Figure 6.10: Available captured solar radiations against time on 8th June 2015.

6.5 Solar cell temperature measurement

Detail steps taken to measure and validate the temperature of the solar cells is what this section is all about. The thermocouple measuring the temperature were placed in different positions. 1) The thermocouple measuring the temperature of the solar cell was placed directly under the solar cell and the heat exchanger plate surface. 2) The one measuring the temperature of the inlet water was placed inside the inlet pipe. 3) Another thermocouple was placed at the outlet pipe to measure the outlet temperature and 4) the temperature of the tank was equally measured with another thermocouple when concentrating solar radiations on the SRCPC system. This enabled the recording of temperatures on seconds, minutes, hourly, daily and the months of the experiment. The glazing glass (internal and external) was not measured because our focus was on the heat extra method though the internal was assumed to be same with that of the solar cells while the external was also assumed to be equal to the ambient temperature. This assumption was necessary to be verified so as to be sure that the obtained results from the outdoor experiment are valid.

The solar radiation that produce the IV curves of the SRCPC model and the temperature of the solar cells were measured and recorded by the three pyranometers at the interval of 5 seconds and two seconds respectively for 24 hours daily.

6.5.1 ***Temperature of the solar cell validation***

A 3D heat transfer model was introduced using ANSYS 12.1 CFX to examine the effects of solar radiation and the concentration of the solar radiation upon the tempearture of the solar cells. Mallick et al [219] developed this model originally but was later used by Sarmah [180], and Sellami [220] to predict the temperature of similar solar cells in an integrated concentrating photovoltaic system. The developed 3-D transfer model had the energy, momentum and continuity equations solved with a converging criteria of 10^{-4}. The experimental measurements validated the results of the solar cell temperatures obtained.

The same 3D heat transfer model is employed in this present study of the indoor characterisation of the SRCPC model comprising of 8 solar cells in series coupled with the concentrator consist of $0.01125m^2$ module area. A heat exchange was prefered because active cooling using water was involved. The uniform solar radiation exposed to the SRCPC at the entry aperture was $1000W/m^2$. The optical efficiency of the SRCPC was 0.987 at 0° angle of incidence. Therefore, heat source dissipated on the solar cell is equal to $U = 0.987 \times C_g \times 1000$ (Where C_g is the concentration ratio of the system = 3×). $U = 2961W/m^2$ which is the expected heat dissipated by the solar cell. This is the value of heat which corresponds to the amount of energy that will reach the solar cells after concentration. Therefore, in the heat transfer model, a heat source of $2961W/m^2$ is considered on the top surface of each solar cell. A temperature of 19°C is considered to be the ambient temperature as used in the simulation. This happened to be the temperature of the laboratory during some series of measurement being carried out on the SRCPC when measuring the temperature of the solar cells. When the SRCPC is exposed outside, a heat transfer coefficient of $7W/m^2$ is considered between the ambient air and the different component of the SRCPC system [221].

6.6 SRCPC power output modelling

The well-known two-diode equivalent circuit model for a single solar cell is used to model the electrical characteristics of a photovoltaic module indicated in Figure 6.11 . Two main components are available in the SRCPC concentrator for the modelling of power output. They include the solar cell electrical component and the solar concentrator optical component. Two types of modelling are required for the power output being the optical and electrical modelling.

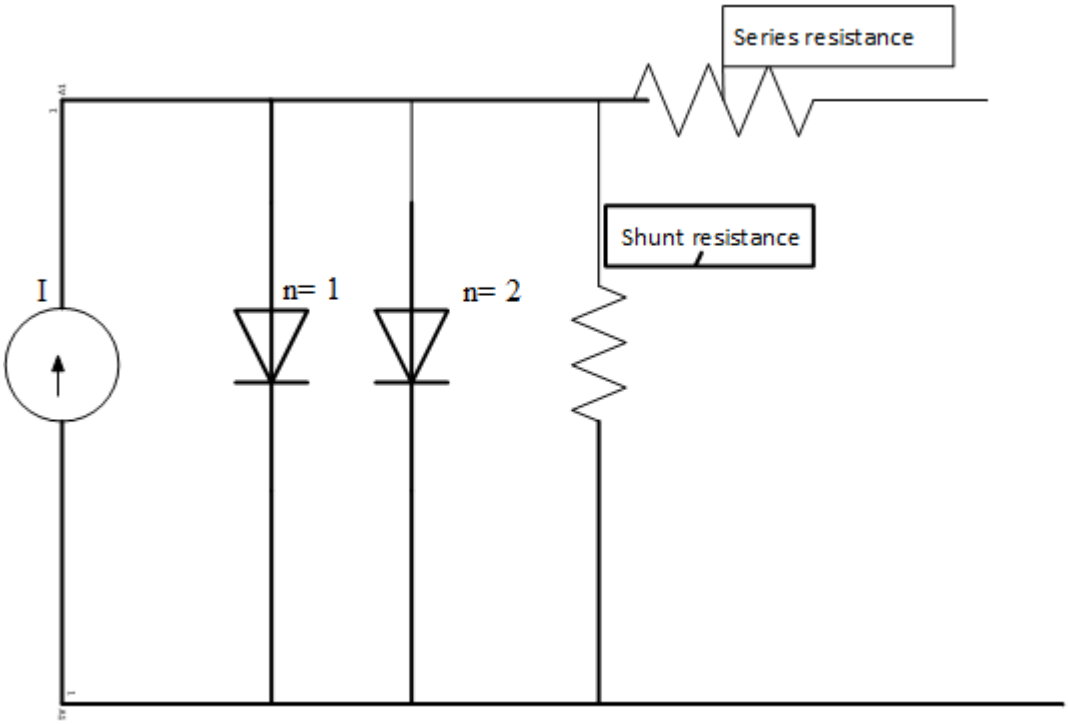

Figure 6.11: Double diode circuit model diagram with the parasitic series and shunt resistances.

These modelling requires inputs of the solar energy radiation and temperature on the solar cells to give the SRCPC output. The energy radiation acquisition on the solar cell is predicted by the use of the optical modelling. This can be done through the calculation of incidence angles together with the solar azimuth angles of the sun for the whole day. Therefore, it is crucial to know the energy of the solar radiation entering the SRCPC acceptance aperture, incidence angles of the sun rays, solar azimuth and solar radiation energy so that the energy at the exit aperture of the concentrator on the solar cell can be calculated by the use of the optical efficiencies simulation. However, for the prediction of power output for the SRCPC, both models will be used [222, 223].

6.6.1 *The two-diode model parameters required for the LGBC silicon solar cell*

The short circuit current temperature coefficient α and open circuit voltage temperature coefficient β are experimentally calculated. Also, the parallel (R_{sh}) and series (R_s) resistances are calculated to complete the two-diode model. Further to this, the power and I-V characteristics for the solar cell can be obtained for different values of solar radiation [224].

6.6.1.1 *Ideality factor*

Ideality factor n is established as a function of applied voltage V and it depends on a relation between the width of Schottky barrier and depletion layer. The parameters of semiconductors are depended on the values of V at which the I-V characteristics acquire an ohmic nature. The ideality factor usually lies between 1 and 2 but can be above 2 [225]. The ideality factor in a single diffuse diode is assumed to be a constant equal to 1 in line with p-n junction diffusion theory [226]. This is on the condition that at high voltage the surfaces and the bulk regions dominate the recombination in the device. However, the ideality factor in reality is a function of voltage across the device. Recombination in the junction dominates at lower voltages and the ideality factor approaches 2 according to recombination theory. This is accomplished by adding a second diode in parallel with the first diode.

6.7 Temperature coefficient for the PV cell used

The rate of change (derivative) with respect to temperature of different PV performance parameters is provided by temperature coefficients. This rate of change can be determined for:

1. Short circuit current (I_{sc})
2. Maximum power current (I_{mp})
3. Open circuit voltage (V_{oc})
4. Maximum power voltage (V_{mp})
5. Maximum power (P_{mp})
6. Fill Factor (FF)
7. Efficiency

However, the ASTM standard methods used for performance testing of cells and modules considers only two temperature coefficients. The first is the current and the second is the voltage. Four temperature coefficients for V_{oc},V_{mp}, I_{sc}, and I_{mp} are necessary and sufficient to accurately model electrical performance for a wide range of operating conditions for outdoor characterization of modules and arrays [227-229]. Temperatures coefficients were determined using super WACOM standard simulator at spectral distribution of 1000W/m^2 irradiance. Practically, there is a need to apply other irradiance level as well. There are practical issues regarding the measurements and applications of temperature coefficients that still need to be ironed out.

6.7.1 ***Measurement Procedures***

More research is still being required for the procedures for measuring the coefficients for modules and arrays standardization. Systematic influences are common in the test methods used to measure them. The temperature coefficient for the solar cells used were typically measured by placing the prepared soldered strings of cells on a temperature controlled text fixture which illuminated the solar cell by the 0.21m x 0.21m down shinning area of the WACOM super solar simulator that measured the cell's current – voltage (I-V) curves for a range of cell temperatures within a specified time. The temperature coefficient was then calculated for the desired parameter with temperature. The temperature coefficients for arrays and modules can be measured under outdoor operational conditions and also with a solar simulator under indoor conditions. Figure 6.11 curves were obtained using indoor test by the module being exposed using WACOM Solar Simulator that focused 1000W/m^2 irradiation on the solar cells in order to achieve a range of temperatures. Also, the module can first be shaded for outdoor test to lower its temperature to almost ambient temperature then unshaded with i-v curves measures as it is heats up to operating temperature. It is to be noted that in both cases, the average module temperature was measured using thermocouples attached to the rear surface.

Also, there are alternative temperature coefficients for modules and arrays have also been estimated using regression analysis from performance data measured for a range of operating conditions [230, 231].

6.7.2 *Limitation of temperature coefficient application*

Practically, temperature coefficient is possible to be measured for a large number of cells, average the values followed by the calculation of the coefficients for arrays and modules using the average values. It is observed however that the test results for arrays and modules sometimes does not support this argument. There are systematic influence. Occurrences during the testing or system operation which often result in apparent temperature coefficients that differs from anticipated values. This difference is typically as a result of non-uniform temperature distributions and or measured temperature that are not indicative of actual cell temperature.

6.7.2.1 *α and β calculation*

Experimentally, the silicon solar cell is used to determine the coefficients of α and β . The solar simulator exposes 1000W/m^2 radiation onto the solar cell that is placed on a temperature controller. The I-V tracer records the I-V curves generated by the solar cells for different temperatures. There is temperature variation from 26.2ºC to 70ºC. The obtained I-V curves are shown in Figure 6.12. It is evidenced in the I-V curves that the short circuit current I_{sc} increases slightly as the temperature increase. This temperature increase is characterised by the short circuit current temperature coefficient represented by α.

Mathematically,

$$\alpha = \frac{1}{I_{sc\,ref}} \times \frac{I_{sc} - I_{sc\,ref}}{T - T_{ref}} \qquad 6.4$$

Where $I_{sc\,ref}$ is light generated current at the reference temperature of a surface radiation 1000W/m^2. T_{ref} is the reference temperature of the solar cell. Contrary to what is happening with I_{sc}, the open circuit voltage V_{oc} is significantly decreasing as the temperature increases [224]. The temperature dependence which affect the V_{oc} is characterised by the open circuit voltage temperature coefficient β which is mathematically expressed as

$$\beta = \frac{1}{I_{oc\,ref}} \times \frac{V_{oc} - V_{oc\,ref}}{T - T_{ref}} \qquad 6.5$$

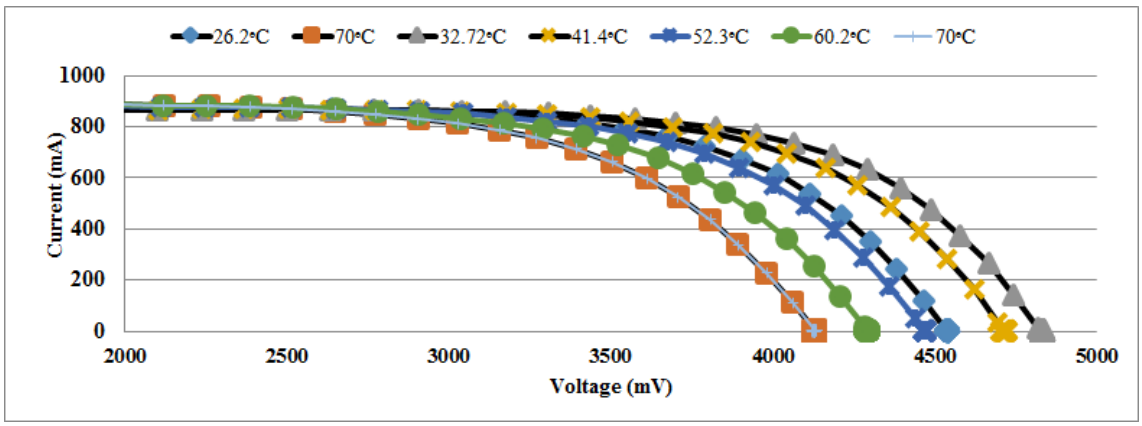

Figure 6.12 I-V curves for the strings of solar cells used in the SRCPC at different temperatures using 1 sun.

By applying equation (6.2) and (6.3) using the values in Figure 6.10, the temperature coefficients for the short circuit current and open circuit voltage is

$\alpha \approx 0.0006$ A/ ºC

$\beta \approx -0.0035$ V/ ºC

This result is verifyable as the deacrease of the maximum power generated by the solar cell is also calculated using the equation [232].

$$\mathcal{E} = \frac{1}{P_M} X \frac{dP_M}{dT} \qquad 6.6$$

Where P_M stands for the solar cell maximum power generated. The result obtained from the calculation shows that $\mathcal{E}$ = -0.4% /°C. This is the known and verified figure for the silicon solar cell [233].

6.7.3 ***Standard reference Silicon solar cells test parameters***

The reference LGBC/LFC and LGBC solar cells using Cz monocrystalline silicon with 100 μ m and 160 μ m thickness are presented in Table 6.3. These are the reference parameters used to determine α and β. The LGBC /LFC solar cell have demonstrated significantly higher open circuit voltages and higher short circuit current densities than the standard LGBC cell. These cells have also shown potentials for higher cell efficiencies [222].

Table 6.3: Reference test parameters for silicon solar cell structure and thickness for standard LGBC solar cell and LGBC/LFC solar cell.

Cell structure	Cell thickness	Efficiency (%)	V_{oc} (mV)	I_{sc} (mA)	Fill Factor (%)
LGBC/LFC	160 μ m	18.3	640	37.30	76.8
LGBC	160 μ m	17.7	610	35.43	82.0
LGBC/LFC	100 μ m	16.9	625	36.33	74.5
LGBC	100 μ m	16.7	601	34.61	80.0

6.7.3.1 *Series and shunt resistance*

The parallel and series resistances are the only parameters still missing for the completion of the two-diode model denoted as R_{sh} and R_s respectively. There is a simple method applied to approach their calculation in a single silicon solar cell from the I-V curve experimentally measured. The equation required to solve the R_{sh} and R_s by varying their values when using a MATLAB code is

$$f\,I = -I + I_{ph} - I_{01}\, e^{\frac{qV+I\,x\,R_S}{n_1\,x\,K\,x\,T}} - 1 - I_{02}\, e^{\frac{qV+I\,x\,R_S}{n_2\,x\,K\,x\,T}} - 1 - \frac{V+I\,xR_S}{R_{sh}} = 0 \qquad 6.7$$

where I_{ph} is the photon current, n_1 is the Ideality factor of diode 1, n_2 is the ideality factor of diode 2, the reverse saturation current of diode 1 and, I_{02} is the reverse saturation current of diode 2.

It is worth to note that n_1 and n_2 are the ideality factors having values close to 1 and 2 respectively. There is need now to run the simulation for each iteration for the values of I_m, V_m and P_m which should be calculated and compared to the experimental values found. The simulation ends only when the differences between the experimental and simulation values of I_m, V_m and P_m becomes minimal, then, the values corresponding to R_s and R_{sh} are recorded as summarised in Table 6.4.

Table 6.4: Simulation and experimental values of maximum Voltage, power and current.

R_s=0.01 Ω R_{sh}=405 Ω	Simulation	Experimental
V_m	0.4900	0.4909
P_m	0.014869	0.014869
I_m	0.0303	0.0302

MATLAB is used to run the simulation. The electrical model code is written and validated using the comparison between power curves and I-V curves from carried out simulation and experimental results for a single solar cell. The I-V cures of one LGBC solar cell is illustrated in Figure 6.13. The first curve measured indoors using an I-V tracer and and solar simulator while the second curve is simulated using the same conditions which are applicable in the indoor experiment set up and the R_s, R_{sh} are the resistances obtained during the iteration. It is a proof as illustrated in the curve that the MATLAB code simulated obtained from the two-diodes model is similar to the one from experiment. Since the two-diode model different parameters are obtained and equally validated, they can now be employed to predict the the I-V curves together with the maximum power of the SRCPC model at different weather conditions.

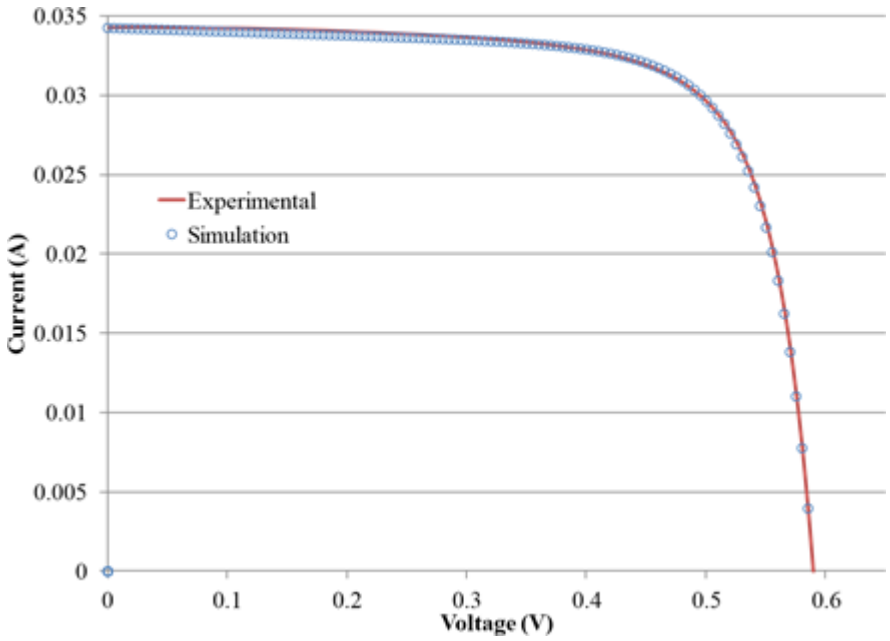

Figure 6.13: Experimental and simulated I-V curves for a single solar cell.

6.7.4 ***The electrical model MATLAB code***

The summary of the different parameters of a single cell are obtained and validated and are put together in Table 6.5. By using Newton Raphson method [234] and MATLAB code, these parameters are used to solve equation (6.5). The likes of this equation is applicable and used to solve Newton Raphson method equations.

To solve the equation, there is an initial assumption for the root that needs to be found that must be made called I^0. Then a generated sequence in the form of I^0,I^1, I^2,I^3,I^4,I^5 will converge to the exact root. A formula for each approximation in terms of the previous is required for the implementation of this method analytically and written a

$$1^{n+1} = 1^n - \frac{f\,I_n}{f\prime I_n} \qquad 6.8$$

Where I^0 is the initial guest value for example I^0= 0. This iteration is repeated several times until the difference between I^0 and I^{n+1} is close to zero. The written MATLAB code iterated parametric LGBC single cell values are summarised in Table 6.5 below. These are the electrical model parameters to be used to simulate the power output of the SRCPC.

Table 6.5: LGBC Single cell parametric values

Conditions	
Radiation = 1000W/m^2 AM1.5	
Temperature 26ºC	
Parameter	
V_{oc}	0.5909
I_{sc}	0.0342
I_m	0.0303
P_m	0.0148
V_m	0.4900
R_s	0.01 Ω
R_{sh}	405 Ω
n_1	1
n_2	2
β	-0.0035V/ °C
α	0.006 A/C
κ	1.3806503x10^{-23}J/K
q	1.60217646x10^{-19}C

6.8 Electrical model I-V simulated results

The electrical model simulated results is used to study the effects of the concentration ratios and the temperatures on the I_{sc}, V_{oc} and P_m of the LGBC of solar cell. The effect of simulation of temperature on the I-V are compared and validated at different temperature with measured I-V curves.

6.8.1 ***Solar cell temperature effect***

Earlier before now, the values of α and β were integrated into the two-diode electrical model. Simulated different I-V curves at various temperatures are equally illustrated. There is a high degree of agreement between the simulated and experimental

results of the I-V curves at various temperatures. The temperature increase of the solar cell leads to small increase of the I_{sc} and a corresponding drop in the voltage.

Figure ***6.14*** shows a linear relationship of mono-crystalline silicon cells measured temperature coefficients with uniform and non-uniform during testing.

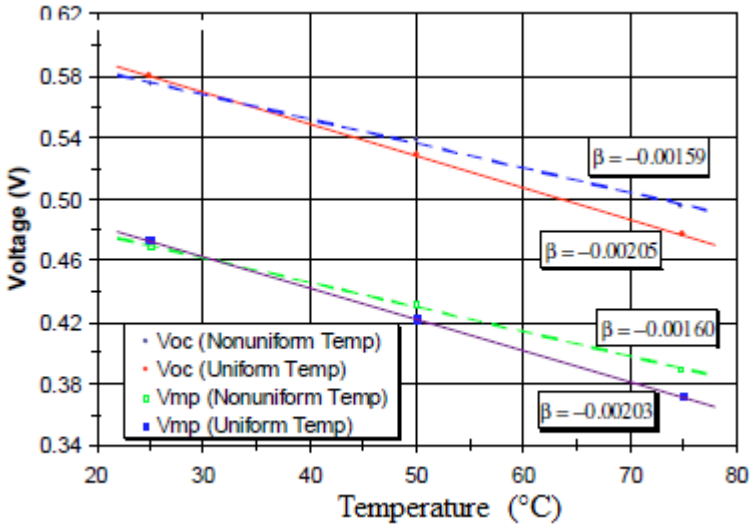

Figure 6.14:Measured temperature coefficients showing linearity relationship of monocrystalline silicon cell with uniform and non-uniform temperature during testing[230]

6.9 Incidence angles and energy modelling for the SRCPC

There was the necessity of modelling incidence angles with respect to the solar radiations that are falling perpendicularly to the surface of the SRCPC in order to model the power generated. This started with first modelling the pattern of radiation available in Exeter University, Penryn campus the test site for one year as shown in Figure 6.15

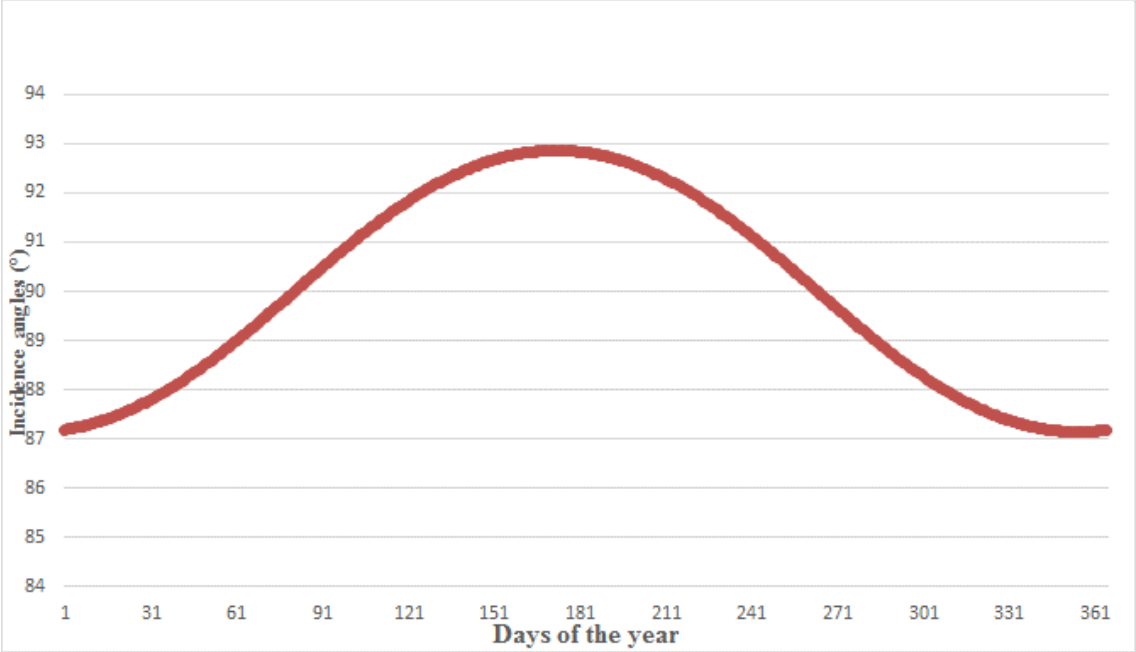

Figure 6.15: Modelling available pattern of solar radiation in Penryn caExeter University

It became expedient to model the irradiation so that we can be sure of the power generation on a monthly basis. The data for this modelling was collected from European Commission Joint Research Centre (JRC). The data collected was for average daily solar irradiance. Photovoltaic Geographical Information System (PVGIS) was used to calculate this average daily solar irradiance. It requires inputting the Latitude and Longitude of the test site to get the information. The 17th of each month was used to calculate the irradiance. The irradiance was used to modelled as shown in Figure 6.16 for University of Exeter, Penryn campus. The highest irradiation occures in the month of May, June and July.

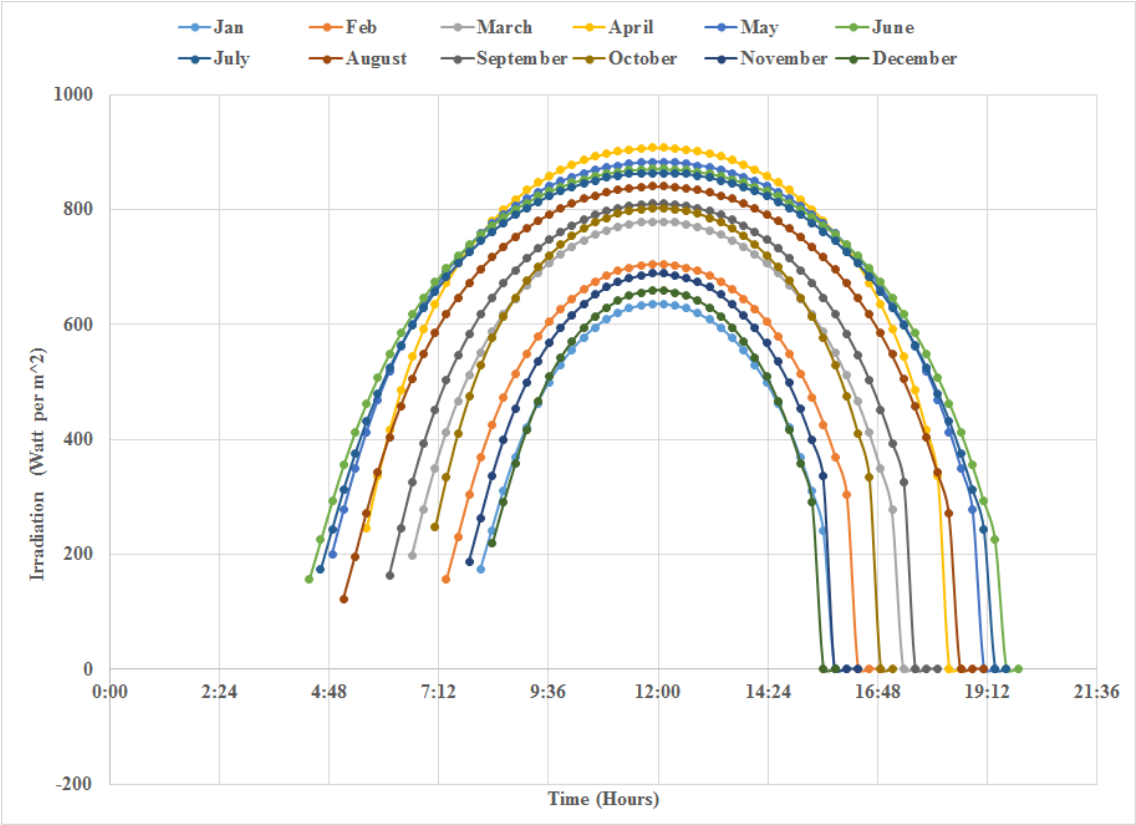

Figure 6.16: Available solar irradiation in Penryn Campus the test site on the 17th of each month.

6.9.1 Modelling of incidence angles and choice of concentrator's acceptance half angle

Due to the available solar radiation together with the knowledge of incidence angles when it can be maximumly obtained, the power for three concentrators was modelled. It was used first to confirm the best concentrator that gives the highest energy yield. Among the three concentrators, the topmost SRCPC 10º acceptance angle gave the highest power yield. The next to this is the SRCPC 15° and followed by the SRCPC 20°. The modelled total power yield by each SRCPC for the 17th day of each month typical for Penryn is as shown in Figure 6.17.

Each irradiation in Figure 6.17 was further picked to model the electrical power for the 17th day of each month of the year for the the three concentrators. Each concentrator generated a daily average energy shown in Figure 6.17.

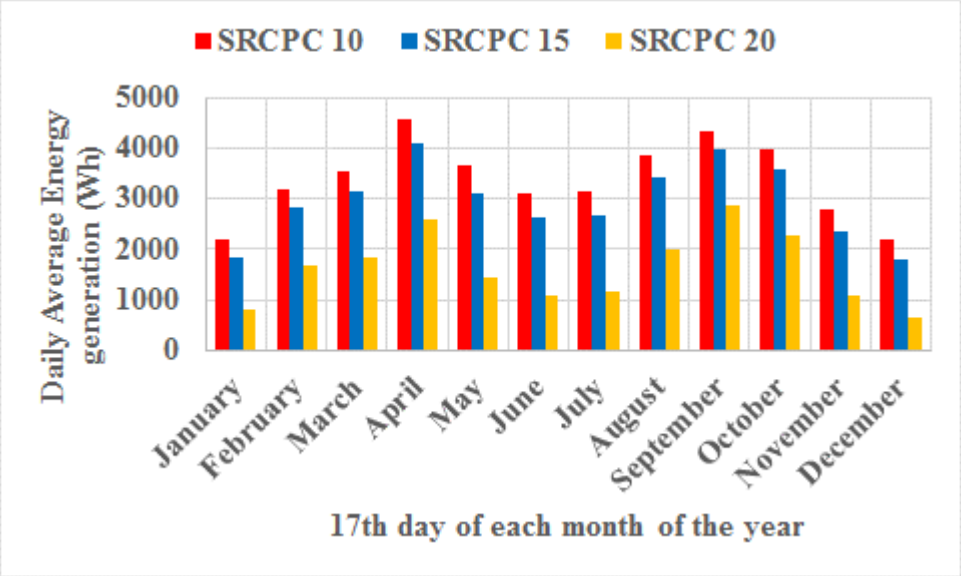

Figure 6.17: Shows energy generation for three different SRCPC concentrators with SRCPC 10º acceptance aperture as the best, followed by SRCPC 15º acceptance aperture and lastly by SRCPC 20º Acceptance aperture.

The SRCPC 10° generated energy more than the SRCPC 15° and SRCPC 20°. SRCPC 10° was picked because it generated power more than others. Therefore, it was possible to model the maximum (peak), average and minimum power from the SRCPC 10°. The modelled SRCPC 10° hourly peak power, average hourly power and minimum power is shown in Figure 6.18.

To get the incidence angles, the parameters of latitude, day of the year, hour angle, time, declination angle, zenith angle and surface azimuths angles were used in excel. The hour angle started from -90° to 90° but decreases with -0.25°. The time started from 6.07 and decreases with about 1 minute till 18.07 pm. The power generated by each CPC 10° was achieved by multiplying the solar irradiation, optical efficiency, solar cell efficiency, CPC exit area and concentration ratio. Power was generated for every 25 minutes. Each power has a specific amount of power generated. From the power generated, you could pick the minimum and maximum (peak) power generated but the average power has to be the total power generated divided by the hours it was generated.

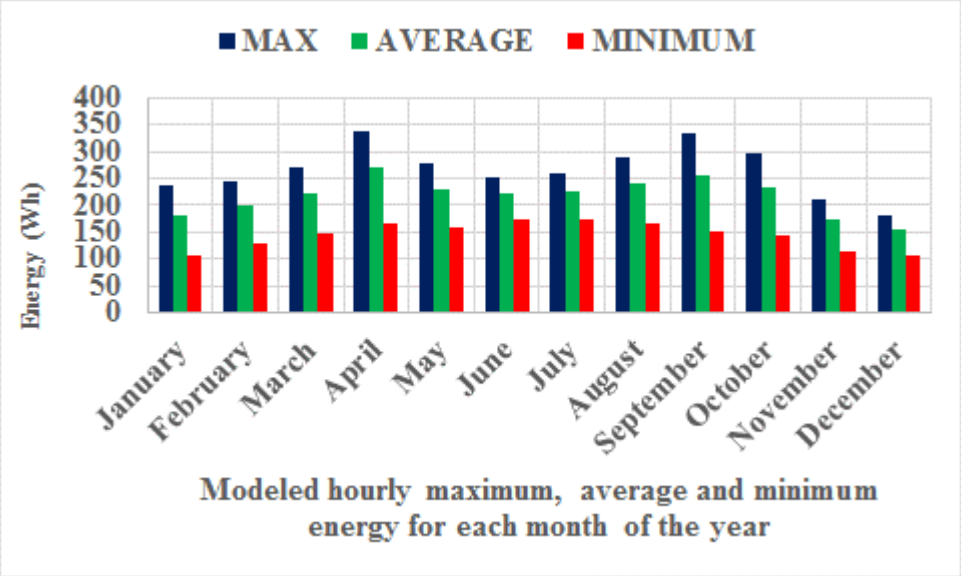

Figure 6.18: Shows modelled hourly peak, hourly average and minimum power for the chosen SRCPC for different months of the year.

6.10 SRCPC model power generation

Experimental real data measured from the north –south (NS) was used as the input to the developed model. These experimental data includes measured global and diffuse solar radiation, the temperatures of the solar cells, inlet, outlet and tank. These all form the input as used in the developed integrated model. This is a deliberate attempt that the simulated result of the power output used in the integrated model be used to compare with the power measured by the IV tracer for the purpose of validating the model. This integrated model was developed and first used by Sellami [220] and also used in this present work as shown in Figure 6.19.

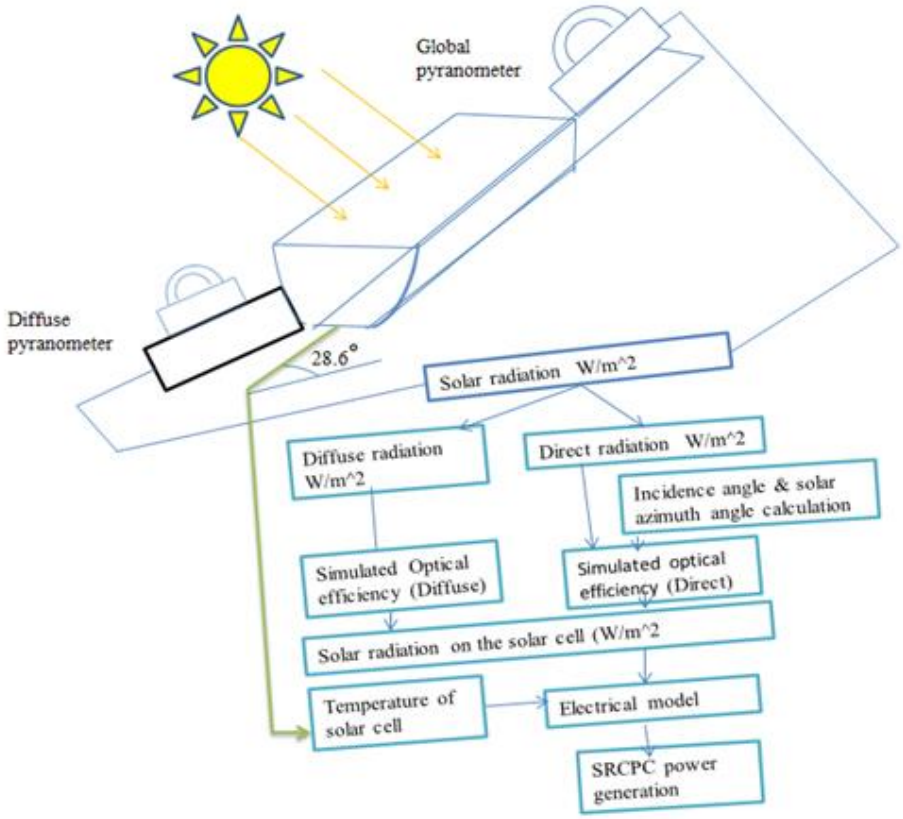

Figure 6.19: Integrated power model block diagram and flow chart.

A MATLAB code was used to experiment the integrated power model. The result is presented in the later part of this chapter. The steps involve for the execution are as follows: i) The radiation reaching the solar cell captured by the diffuse pyranometer is first calculated by multiplying the optical efficiency of the SRCPC used and geometrical concentration ratio, ii) The solar azimuth angles and incidence angles are calculated minute by minutes. This is corresponding to the same time as if the solar radiation is measured. In order to determine the optical efficiency of the SRCPC, these calculations are very necessary which in turn will then be used to calculate the direct radiation reaching the solar cells. The SRCPC optical efficiency of the direct radiation is determined by the solar azimuth angles and incidence angles calculation from the simulated values.

The recording of the direct and diffuse radiations on the entry aperture of the SRCPC is done by the outdoor experimental set up to measured on the slope of the SRCPC that is 28.6ºC. Also, for the calculation of the radiation reaching the solar cell, it is by multiplying the optical efficiency of the direct radiation by SRCPC geometrical concentration ratio. Hence, the sum of the diffuse and direct radiations is the total radiation reaching the solar cells.

The temperature of the solar cell (Tsc), inlet (Tin), Outlet (Tout) and tank (Ttank), the total radiation radiation reaching the solar cells and the total number of cells in the SRCPC model are all used as the input for the developed electrical model. These combined inputs gives the result that is used to obtain the electrical output of the SRCPC model during the hours of the day.

6.11 SRCPC outdoor experimental results and discussion

This section presents the experimental results of the outdoor experiment for the characterisation of the SRCPC model. The obtained result is used to validate the developed integrated electrical and optical model. It can be recalled that the electrical model was developed using an equivalent two diode circuit. The electrical model parameters were characterised and validated using the indoor experimental study on the LGBC solar cell. OptisWorks software was used to develop the optical model which was validated with the indoor experimental characterisation. Most importantly, the integrated electrical model was developed to predict the power output of the SRCPC model in all-weather outdoor conditions.

The SRCPC model was designed for building integration, stand-alone systems and industrial scale at large. It was installed, tested and monitored in outdoor conditions where both diffuse and direct radiations were collected at the 2nd floor of the ESI building at Penryn Campus of the University of Exeter. The outdoor experiment started on the 21st May 2015 until 11th July 2015 where the electrical power output of the SRCPC was captured, measured and monitored under various weather conditions.

6.11.1 ***SRCPC outdoor power output***

As the SRCPC model was exposed to solar radiation in the N-S direction, the model concentrator generated electrical power in various capacities during the day and the entire experiment period. However, there were fluctuations of solar irradiance on the SRCPC affecting the power generation depending on the time, weather condition of the day and seasons of the year. The monitored experimental data during the test period (summer) when the sun is available was characterised by a lot of weather conditions which were typical of South-England.

More so, the recorded experimental results from the testing of the SRCPC in outdoor conditions is represented to reflect all possible weather conditions experienced that might occur throughout the year. These include sunny days, windy days, cloudy days and rainy days. It was possible to monitor the electrical performance of the SRCPC model under these variety of weather conditions.

The experiment was carried out daily from March 21st to July 11th 2015. The measured and recorded experimental data is presented for the SRCPC electrical and thermal performance to reflect periods in May, June and July while the daily power generation during the test period are also included. This will reflect in; a) the experimental electrical power output (W), b) the global irradiance (W/m^2), c) the temperatures of the solar cell (Tsc), inlet (Tin), Outlet (Tout) and tank (Ttank) to ensure the effectiveness of the designed cooling system at different flow rates. At this time, a peristaltic pump was used for the cooling flow rate. The effectiveness of the peristaltic pump and effective saturation flow rate controlled the operating temperature.

Figure 6.20 and Figure 6.22 shows the maximum power generation and radiation availability on 22nd and 31st May with Figure 6.21 and Figure 6.23 being temperatures against time for 22nd and 31st May respectively. Figure 6.24 and Figure 6.26 shows power and radiation against time on 8th June and 10th July respectively while Figure 6.25 and Figure 6.27 are the temperature performance against time corresponding to same days accordingly.

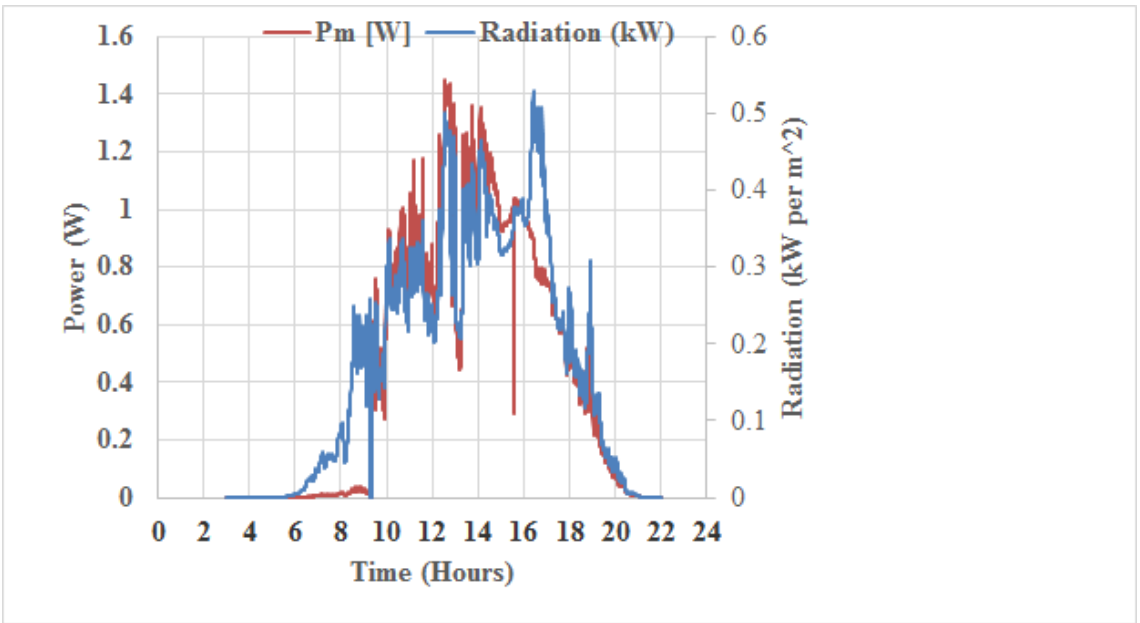

Figure 6.20: Maximum Power (W) and Radiation (kW/m^2) against Time on 22nd May 2015.

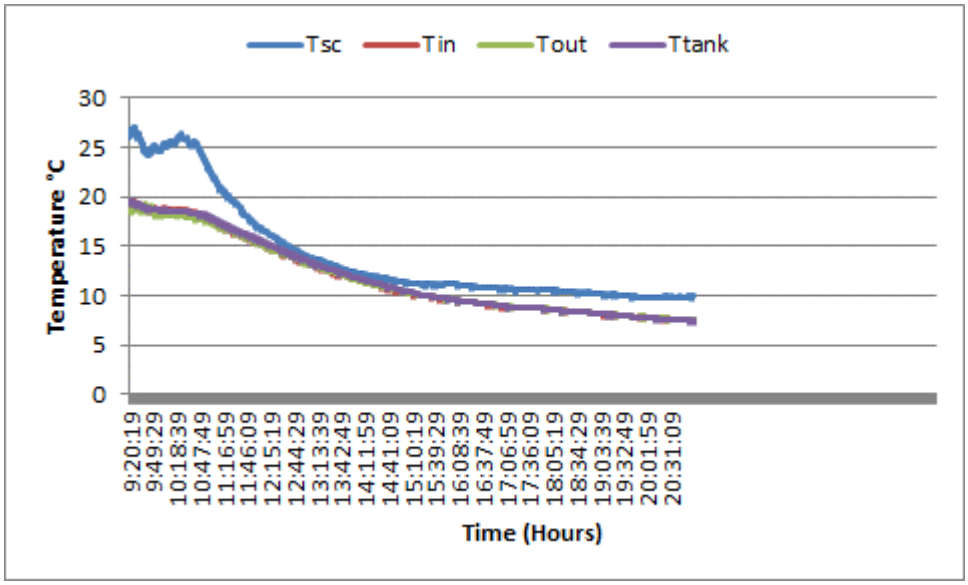

Figure 6.21: Temperature against Time on 22nd May 2015

Figure 6.21 indicates temperature against time when the outdoor experiment was conducted. The starting temperature for the solar cell was 26°C while the temperatures of the inlet, outlet and tank were 20°C. Because the solar cell is embedded inside the system, this allows the difference in the starting temperatures. The initial drop and rise in the staring temperature of the solar cell is informed by the fact that the solar cell adjusted to the temperature of the environment. Also, the initial rise in temperature was the normal temperature effect before the pump was switch-on for cooling to start. The temperature of the environment chilly that also contributed to the cooling process to bring down the solar cell temperatures and that of the inlet, outlet and tank respectively.

Figure 6.22 shows maximum power and radiations against time. It is shown clearly from the graph when solar radiations was available during the day. Most of the solar radiations were available after mid-day. The SRCPC has a maximum concentrating time to be 12:00noon but the radiations was available after this maximum time, hence the area producing little power. Also, remember that the SRCPC is a stationary type without tracking system.

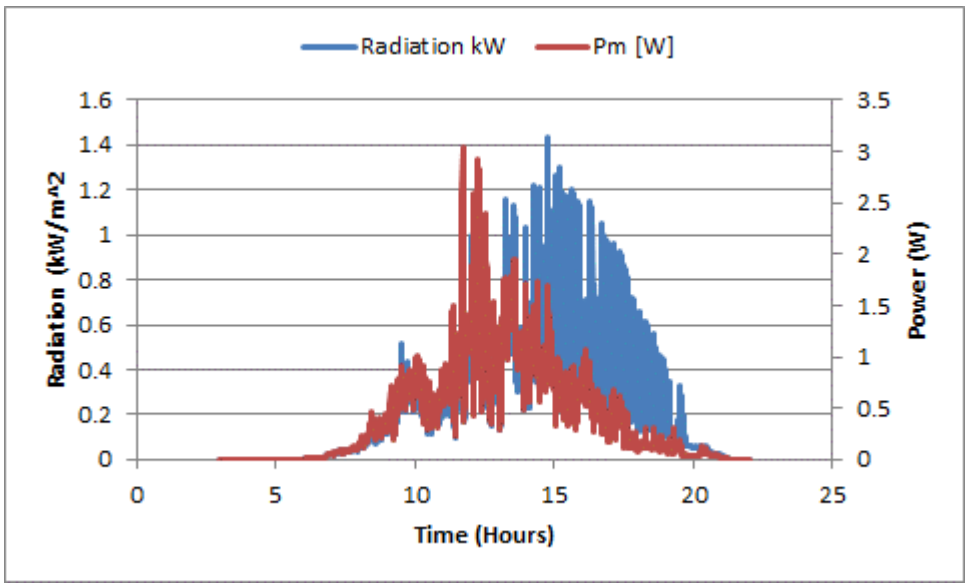

Figure 6.22:Maximum Power (W) and Radiation (KW/m2) against Time on 31st May 2015

Figure 6.23 is temperature against time. The cooling started as well as the concentration but the was less solar radiations in the morning that could cause significant effect. The cooling was maintained without any change even when the radiation increase.

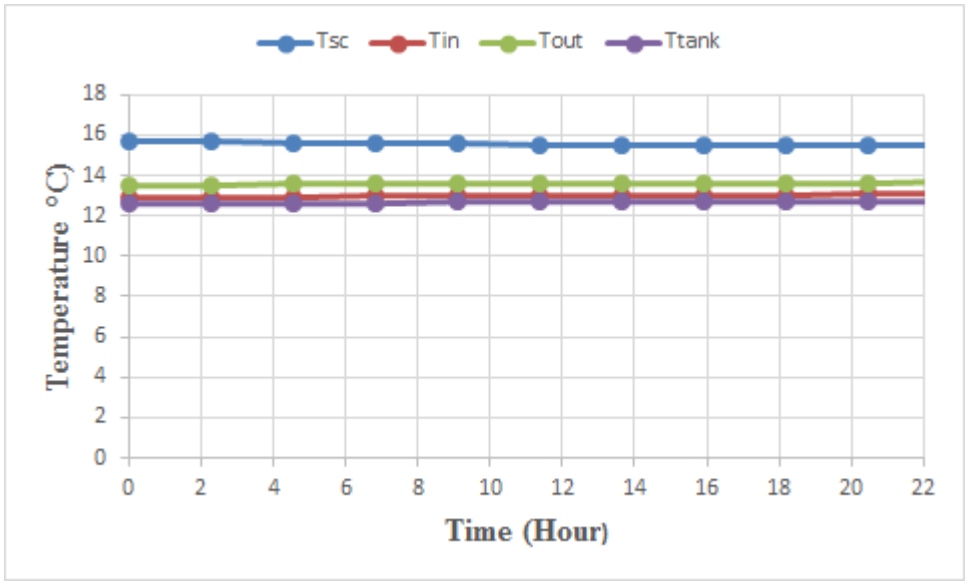

Figure 6.23: Temperatures against Time on 31st May 2015

Figure 6.24 is the SRCPC instantaneous power and global radiation on June 8th June 2015. The concentrator acceptance aperture by design has a maximum time between 9:45am – 2:15pm. Any time outside this range will be minimal power generation.

Maximum power could be achieved if one use a device to rotate the SRCPC to track the sun from morning to evening.

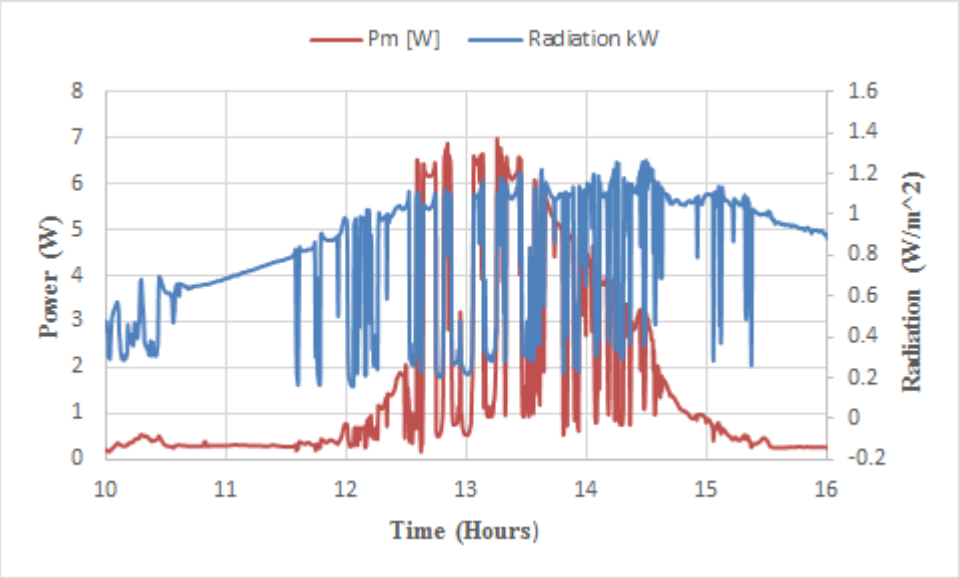

Figure 6.24: SRCPC Instantenous Power (W) and Global radiation (kW/m^2) on June 8th 2015

Figure 6.25 illustrates the temperatures of the solar cell, tank, outlet and inlet respectively. The tank temperature was close to the solar cell temperature but because the surrounding temperature affect the tank, the inlet temperature was affected. Cooling was maintained.

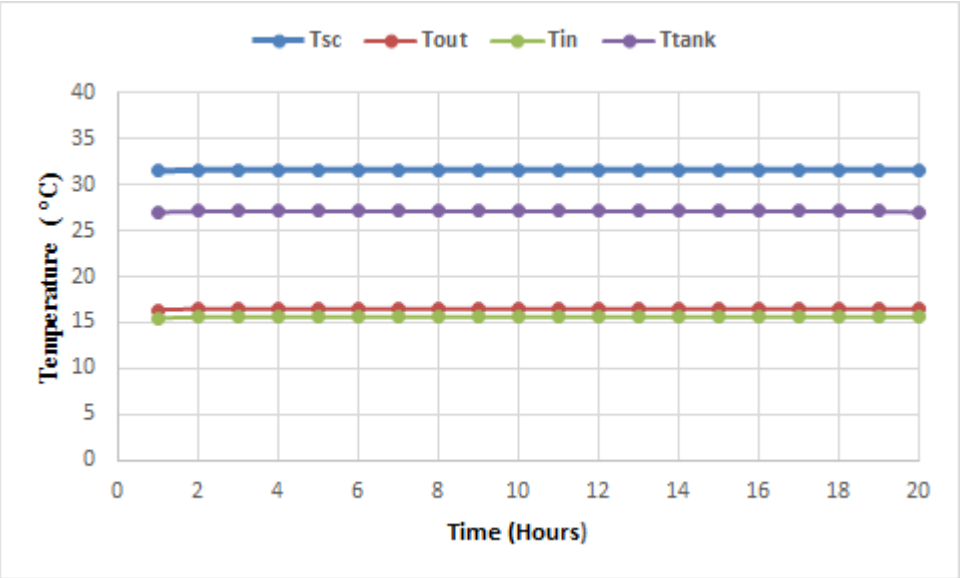

Figure 6.25: Temperatures of solar cell (Tsc), inlet (Tin), Outlet (Tout) and Tank (Ttank) during the test day of 8th June 2015.

Figure 6.26 shows maximum power and global radiations against time. Power was generated only with the solar radiation available between 9:45-2:15pm the maximum time. Solar radiations became available beyond this time. Therefore, the concentrator acceptance aperture could not receive any significance radiations to generate.

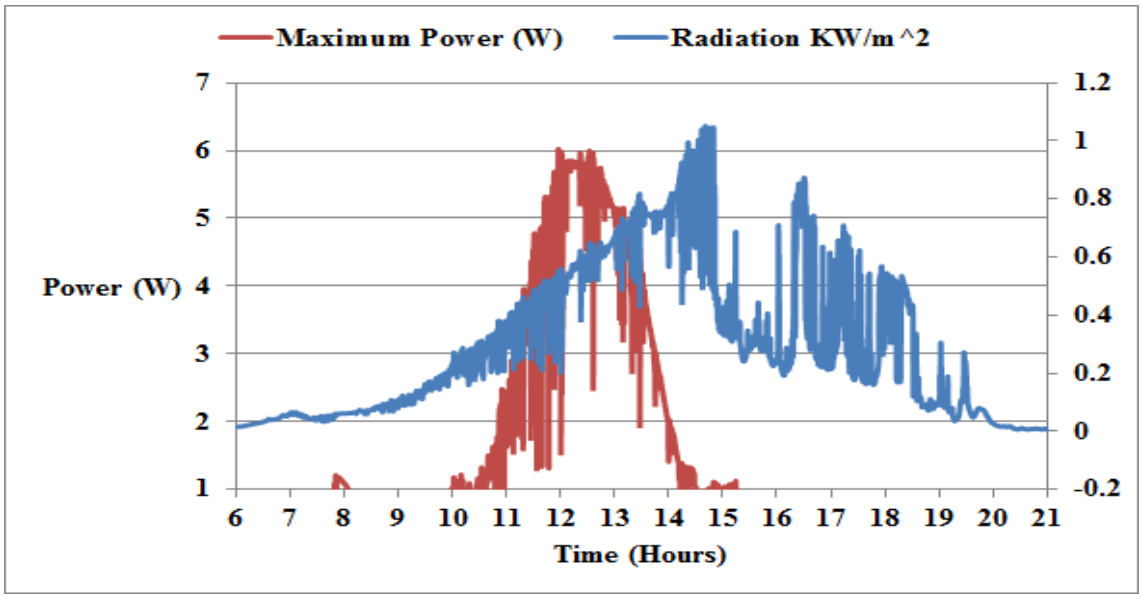

Figure 6.26: Maximum Power (W) and Global radiation against Time on 10th July 2015

Figure 6.27 shows temperatures against time on 10th July 2015. The solar cells, outlet, tank and inlet temperatures shows the cooling was effective to maintain the solar cell temperature to about 25.9°C. The outlet and tank temperatures are almost equal in value as indicated in Table A5 in Appendix.

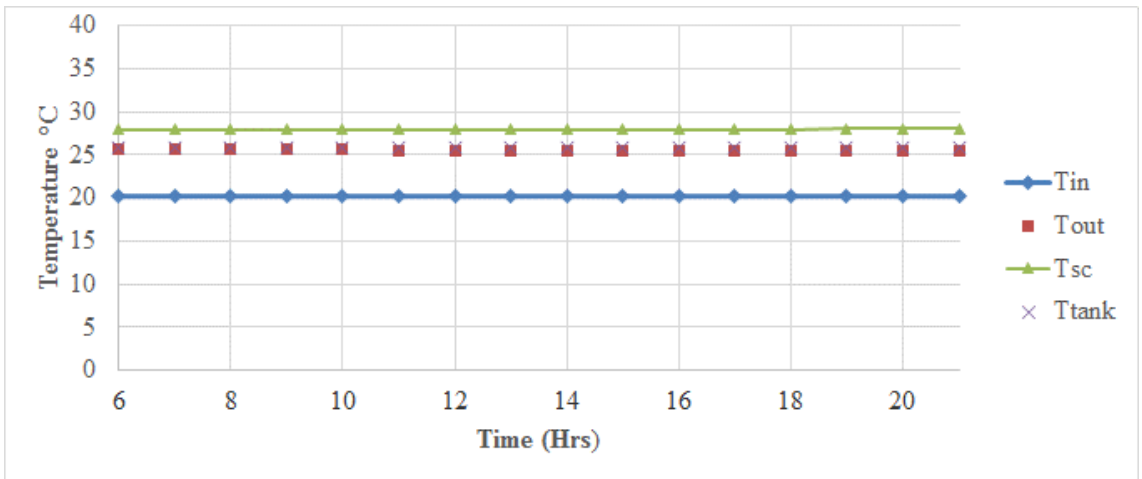

Figure 6.27: Temperature against Time on 10th July 2015

Figure 6.28 and Figure 6.29 represents the daily average power generation and daily peak instantaneous power generation by the SRCPC in part of May. Also in June, the average power generation daily and the peak instantaneous power generation is shown in Figure 6.30. Daily average power generation by the SRCPC in June and Figure 6.31 while

Figure 6.32: Daily average power generation by the SRCPC in part of July confirming the indoor characteristics. Table A2 in Appendix represents part of July daily average power generation as well as the daily peak instantaneous power generation by the SRCPC. In the starting month of May, the power generation was affected by the factors of rainy, cloudy, windy, and lack of positioning the SRCPC according to the optimum tilt angle for the concentrator. The case was different with the power generation in June and July. The SRCPC was positioned at the optimum tilt angle for maximum energy yield when the solar radiation is available. There was effective active cooling method employed with a saturating flow rate for stability of parameters and maximum power generation during radiation availability. On few occasion also the weather was affected by cloudy, rainy and windy periods. The effect of weather conditions and availability of solar radiations are shown in the amount of average power generation on daily bases. The low bars shows that the solar radiation was very low due to weather conditions while the high bars significance the presence of high solar radiations throughout the test period.

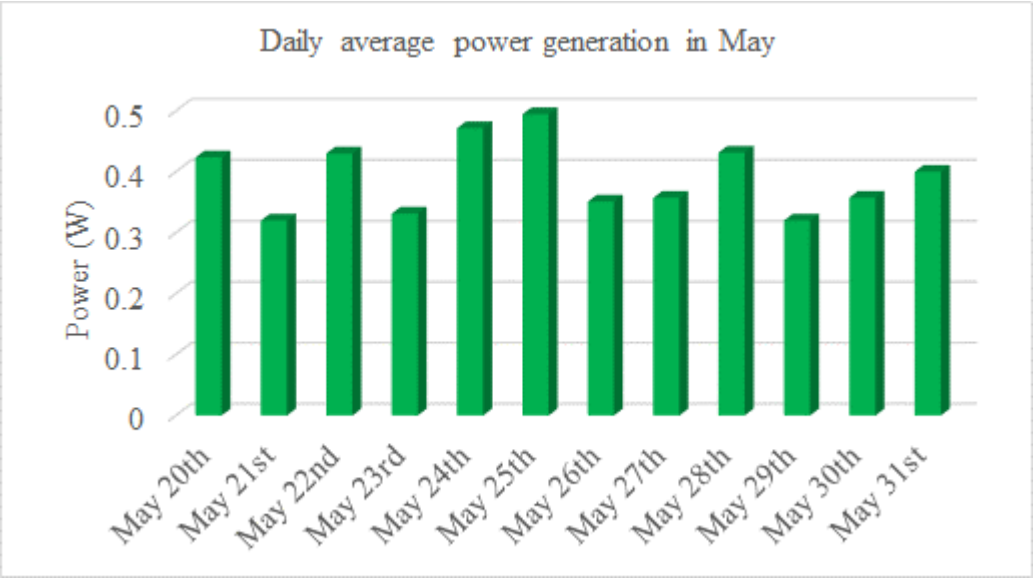

Figure 6.28: Daily average power generation (W) for 12 days in part of May 2015

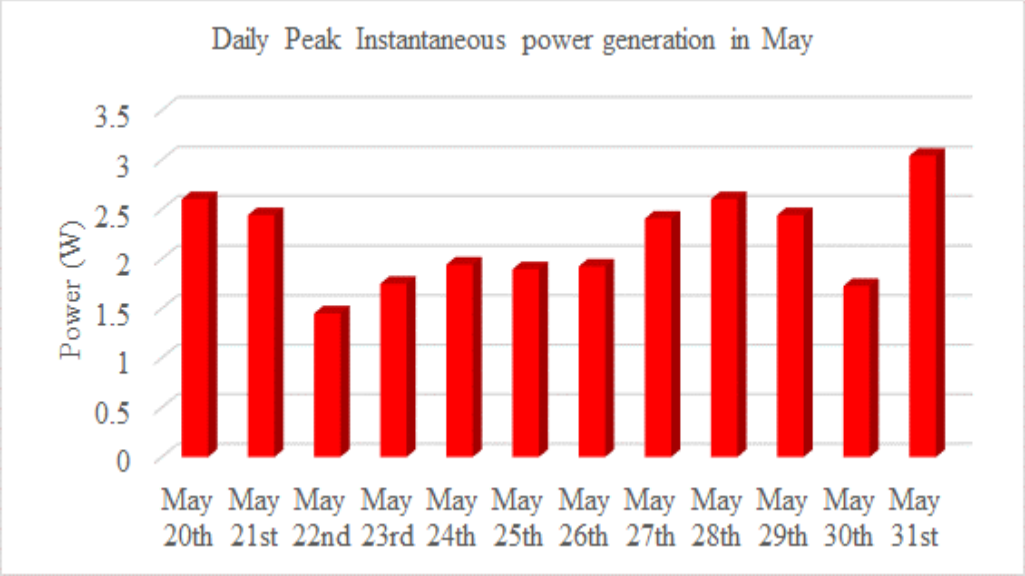

Figure 6.29: Daily peak instantaneous power generation by SRCPC in part of May

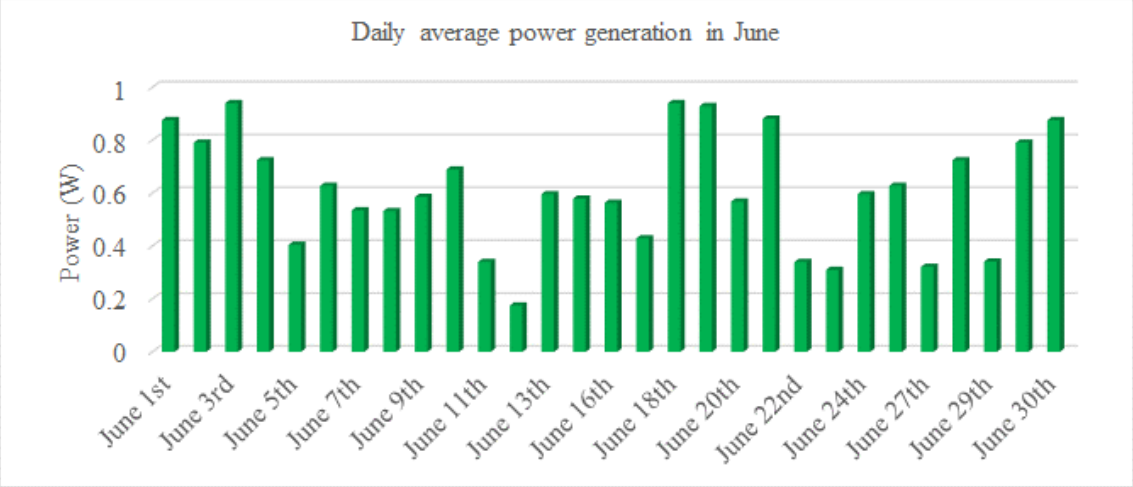

Figure 6.30: Daily average power generation by SRCPC in June

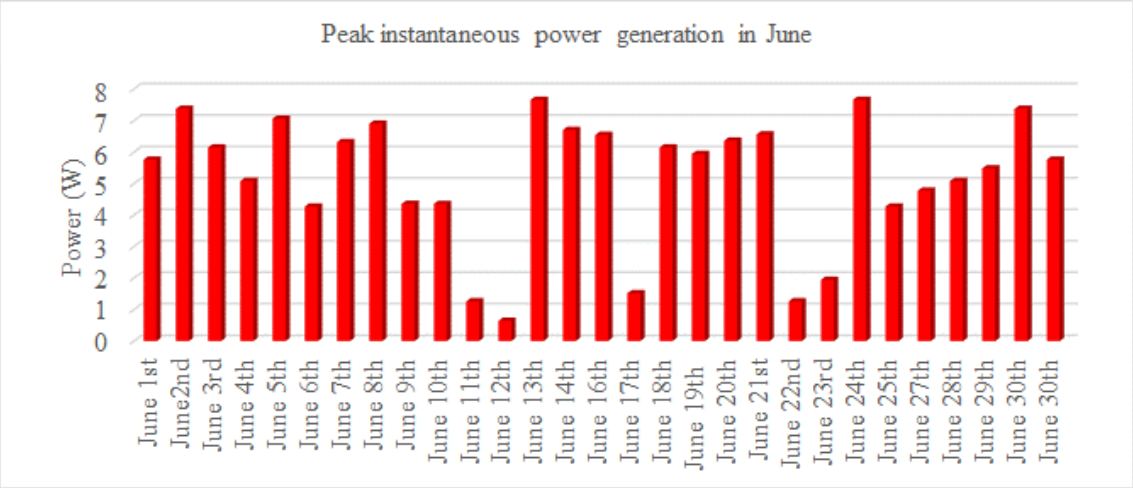

Figure 6.31: Daily peak instantaneous power generation by the SRCPC in June confirming the indoor characteristic

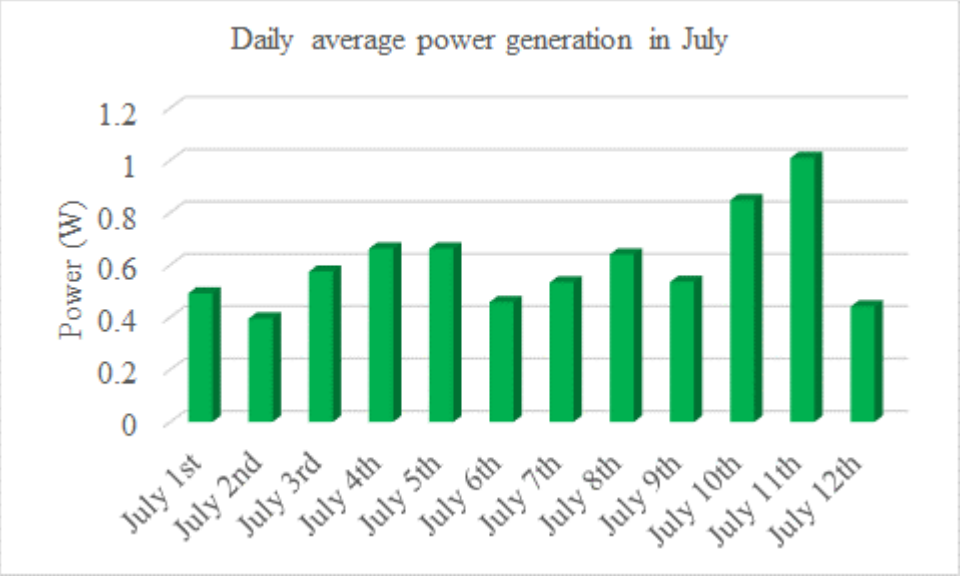

Figure 6.32: Daily average power generation by the SRCPC in part of July confirming the indoor characteristics

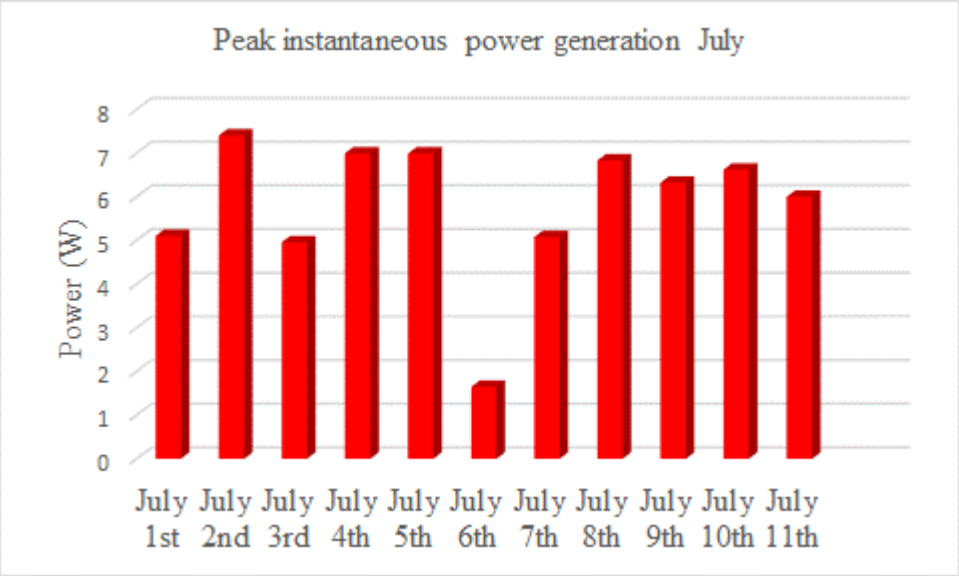

Figure 6.33: Daily peak instantaneous power generation by the SRCPC in part of July confirming the indoor characteristics

The daily peak instantaneous power is shown in Figure 6.33 for July. The peak power is 7.66W at a solar radiation of 1206W/m^2. The power generation in W in Figures 6.28-6.33 shows the potentiality of the SRCPC model as a proof of concept with only 5cm x 5cm LGBC silicon crystalline solar cell with small area as well as the power output. Figure 6.34 is a comparison between the indoor peak power and outdoor peak power output for the concentrator. There is similarity of all the bars. The difference in the month of May indicates low radiation availability. The availability of radiation in the months of

June and July clearly shows their peak power generated by the SRCPC. This confirms the integrated electrical model and expected result out come.

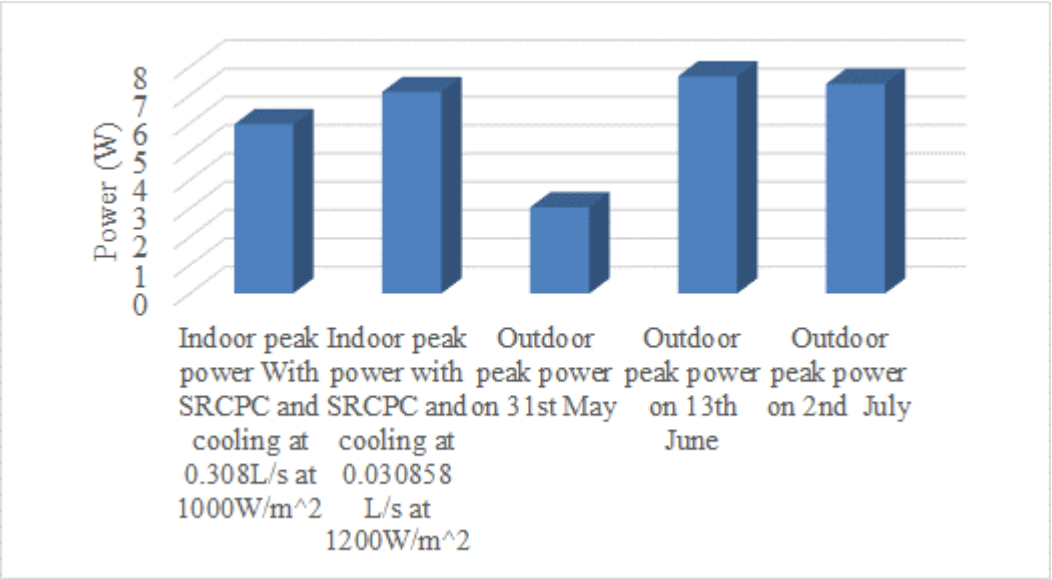

Figure 6.34: shows a comparison between indoor peak power and outdoor peak power on 31st May, 13th June and 2nd July during the experimental concentrating on the SRCPC

6.11.2 ***Comparing average power outputs of the model, indoor and outdoor***

Figure 6.35 illustrates by comparing the maximum, average and minimum power output of the model, indoor and outdoor experiment carried out for the period of the experiment. For the months of May. June and July that the experiment was carried out, the maximum, average and minimum was picked. This comparison enable us to see clearly the trend of similarities in the model, indoor and outdoor power output. The level of agreement between the model, indoor and outdoor power output confirms the success of the designed SRCPC model. This is not without the challenges of thermal management system, flow rates, weather conditions and radiation availability.

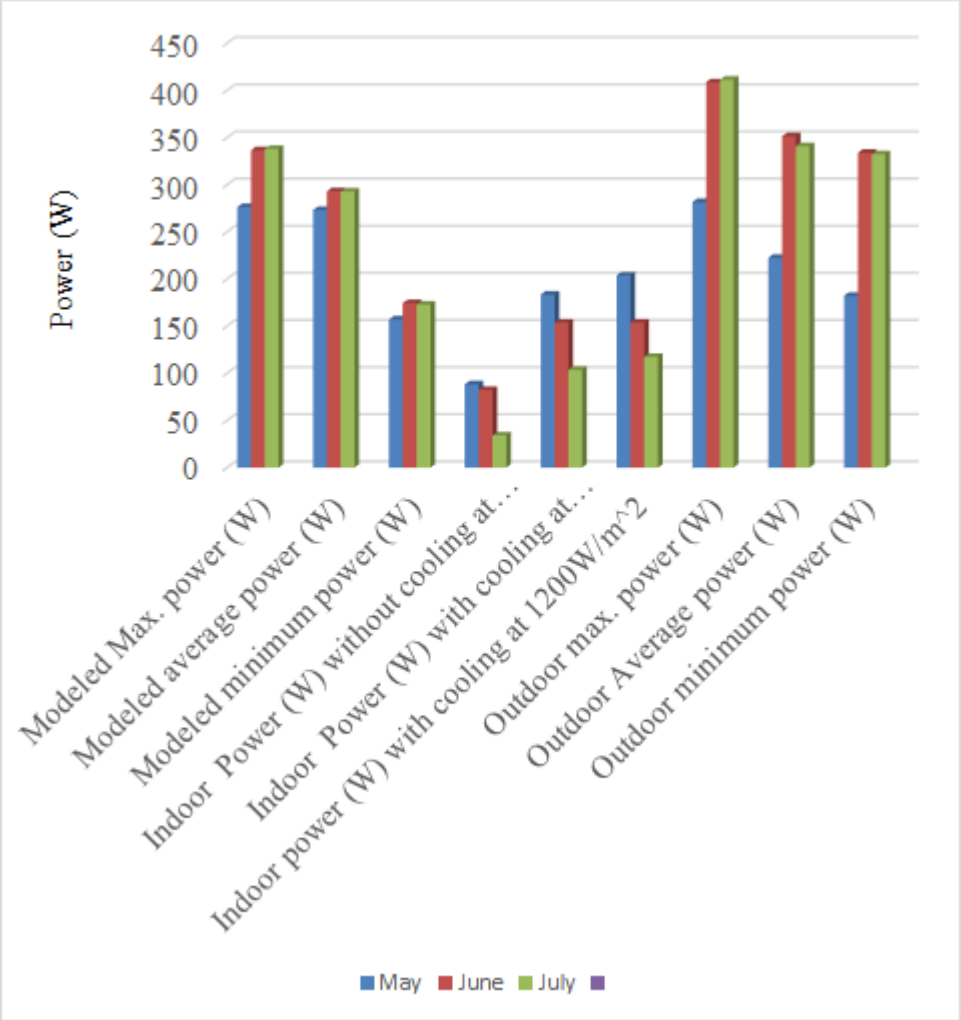

Figure 6.35: Compares the maximum, average and minimum power output of the model, indoor and outdoor experimental carried out

6.12 Discussion and analysis

The SRCPC is a low stationary concentrator having concentration ratio of 3x. The concentrator begins to accept solar radiation directly between the hours of 10:20am at a tilt angle of 0°, 10:00am at a tilt angle of 5.7°, 9:40am at a tilt angle of 11.5°. The concentrator receives full solar radiation from 9;40am at tilt angles of 11.5°, 17.2°, 22.9°, 28.6°, 34.4° and start to decline at 2:20pm.

The incident angles, optical efficiencies, concentration ratio, absorber area together with solar radiations are used to model the power for the optimum tilt angle for the SRCPC concentrator. Despite the fact that the concentrator receives full solar radiations at these tilt angles, the maximum power generated was from the tilt angles of 28.6° hence the choice of the 28.6° as the optimum tilt angle of the concentrator.

The SRCPC was installed at a tilt angle of 28.6°at a constant flow rate of 0.03L/s and monitored from 20th may 2015 to 12th July 2015. In May, the setup had initial challenges that were overcome. In addition, there was low solar radiation in general. The SRCPC generated the peak power to be 3.0W and lowest to be 1.45W but the daily hourly average power was 0.49W.

In June, the solar radiation was available in abundance. The peak power generation above 7W were 7.38W on 2nd, 7.06W on 5th, 7.66W on 13th, 7.66W on 24th and 7.38W on 30th at solar radiations of 116W/m² at 2:20pm, 1044 W/m² at 12:47pm 1205W/m² at 12:48pm, 1206W/m² at 11:45pm and 1168W/m² at 12:42pm respectively. The highest daily average power for June occurred on June 1st = 0.875W, June 3rd = 0.904W, June 18th = 0.939W, June 21st = 0.881W and June 30th = 0.875W.

In the month of July, the concentrator generated peak power on July 2nd = 7.4W, July 4th = 7.0W, July 5th = 6.99W, July 8th = 6.8W and 6.6W on July 10th and lowest = 1.65W on 6th. The corresponding available solar radiation that produced these powers are 1168W/m² at 2:22pm, 1158W/m² at 11:00am, 1162 W/m² 2:32pm, 1132 W/m² at 1:22pm and 1146 W/m² at 12:48pm accordingly. The highest daily average power in the month of July is 1.01W, which occurred on the 11th, while the lowest occurred in the July 2nd and is 0.3951W. Table A4 and Table A6 in Appendix shows the radiation data collected from the testing site and data of 2nd July 2015 that generated the maximum power respectively.

The highest peak power production was 7.66W from the highest radiation of 1206W/m² in June while the lowest power output was the presence of low available solar radiations. The results of the outdoor experiment validated the indoor experiment results even with higher values. The solar radiations that gave maximum power yields occurred at different times of the day.

6.13 Potentiality, benefits and commercialisation prospects of the SRCPC technology

The potentiality of the technology have been demonstrated and proven. It has the potential of advancing to the next level of commercialisation for implementation for building integration, stand-alone and industrial applications. The potentialities and benefits of SRCPC technology among others includes;

1. It uses both direct and diffuse solar radiations.
2. This technology saves space compared to PV.
3. At standardised size (1m x 1m), it generates more power than flat PV of the same size on scale-up.
4. It could also produce energy at full capacity from morning to evening when minimal tracking devices are employed.
5. In addition to electricity on scale-up, there is potential for the system to supply heat when heat is removed from the solar cells.
6. The SRCPC system design is unique and no one else has reported this specific design for both heat and power generation simultaneously. There are many literatures around the CPC design specifically for PV use. However, this design is primarily for CPV and thermal use.
7. The SRCPC technology has demonstrated strong benefits of increase power output when active cooling methods are used thereby increasing the conversion efficiency of the solar cell.
8. At a commercial scale-up, there are multiple benefits of the SRCPC system. The system provides both power and heat. It provides optical efficiency improvement compared to previously designed systems. It is designed to have latitude specifics.
9. The heat can be channelled into use for domestic heating, swimming pools, desalination for maximum benefits of the technology.

6.14 Conclusion

In this chapter, the SRCPC model experiment is ending. The construction of the SRCPC model was covered. The integrated developed electrical and optical models presented the result of the outdoor performance of the SRCPC model. It showed the maximum power generated to be 7.66W at a radiation of 1206W/m^2.

For the constructed SRCPC process to be validated, the designed thermal management system was integrated to control the temperature of the solar cells using active cooling process. The operating temperature of the solar cell was reduced 16°C where the maximum power was recorded. This is indication that thermal system was effective thereby validating the use of the thermal management system.

Further to this, part of the development of the integrated electrical model and the LGBC single solar cells parameters were characterised and experimentally determined.

The LGBC solar cell were found to have opened circuit voltage temperature coefficient β = -0035 (V/ ºC) and a short circuit current temperature coefficient α = 0.0006 (A/ ºC). These characterise the temperature effects on the solar cell output. The calculated parameters were used to develop the electrical model using a two diode equivalent circuit of the solar cell. A MATLAB code was written to affect this. The outdoor characterisation of the solar cell results under different temperature conditions agreed with the result obtained from the simulation of MATLAB written code thereby validating it.

Solar irradiance and temperature were the inputs in the electrical model. These in turn gave the power output of different I-V characteristics of the SRCPC for the outdoor test. To achieve the energy radiation on the solar cell, the different simulated optical efficiencies together with the developed optical model were used. The combination of the two models allowed the integrated electrical model to be expanded for the prediction of the SRCPC power output. The integrated electrical model requires the input of diffuse and direct radiations, simulated optical efficiencies of the SRCPC, solar irradiance and temperatures as inputs. The steps to implement the integrated electrical model for simulation were detailed.

Furthermore, the SRCPC measured power output for the outdoor conditions were presented and discussed. The minimum and maximum power output with the associated solar cell temperatures were also examined for various outdoor weather conditions. These conditions include the sunny, cloudy, windy and rainy days. The performance characteristic results were observe to indicate that the measured power output and simulated power output were comparable for the SRCPC model which was the case for all weather conditions. However, the experimental results agreed or validated the integrated model. From the measured power generated by the SRCPC over the test period, data recorded show that the highest power generated during the test period was in May 25th, June 18th and July 10th. The highest energy was generated in the month of June because it was a full month testing.

The thermal management system stabilised the temperature of the solar cell below 34ºC and in some other cases below 30ºC during the test period indicating the effectiveness of the cooling system at the saturated flow rate. In a general note, the designed SRCPC model has the capacity to generate power for building integration, stand-alone systems and industries at large scale. The maximum power generated by the model during indoor and outdoor experiments were 7.11W and 7.4W respectively. The

proof of concept have indicated the potentiality of the symmetric reflective compound parabolic concentrators to replace conventional energy resources thereby reducing their carbon footprint and increasing their energy efficiencies.

Chapter 7 CONCLUSIONS AND FUTURE RECOMMENDATIONS

7.1 The optical efficiency of the SRCPC model

This thesis began with the study of the geometry of non-imaging static concentrator on which the research was carried out. A review on both asymmetric and symmetric as well as reflective and refractive concentrators were carried out. Co-ordinates were used to draw the geometry of the concentrator and a commercial software was used for the optical simulations. The reflective optical performance of the SRCPC was investigated using ray-tracing techniques. The reflective compound parabolic concentrator's theoretical optical performance was simulated using a developed MATLAB code where the results was compared with experimental results and validated. The commercial optisworks software was further used to validate the same theoretical results of the optical simulation. The refractive optical performance of the CPC was also studied and compared to the performance of the reflective CPC using the optisworks software. The result indicated that the CPC made from the refractive materials had a larger acceptance angle having 10% less of the maximum optical efficiency compared to the reflective CPC but had the problem of the total internal reflection. Furthermore, to the optical study of reflective and refractive, this part of the thesis represents the main tools required for the design of the novel SRCPC for photovoltaics. It is revealed in the study that;

1. The coordinates of the parabola were obtained using excel and later transferred to Solid Works software where it was extruded to have a 2-D solid profile.

2. The advantage of 2-D SRCPC compared to 3-D circular sectional CPC is that it has a more convenient acceptance and absorbing apertures but achieves almost the same optical efficiency.

3. A maximum optical efficiency of the reflective SRCPC shown in the simulation to be greater than 90% for reflectivity of 94% of the side wall.

4. The indoor condition experiment of the reflective SRCPC gave an experimental optical efficiency greater than 80% which agrees reasonably with the simulation expectation of optical efficiencies with deviation up to 12%. This deviation is likely to be attributed to flaws from the manufacturing process.

5. The use of Solid Works with ADD- IN OptisWorks for the simulation of the optical efficiency of the reflective SRCPC saved time in the process of the simulation. The optical efficiencies simulation of the reflective SRCPC using MATLAB are similar with Optis Works software simulated optical efficiencies which validates the obtained results from these two methods thereby confirming the use of OptisWorks through to the finishing of this thesis.

6. The studied optical performance of the SRCPC refractive result using OptisWorks software shows a larger entry angle having lower maximum optical efficiency of 70% when contrasted with reflective SRCPC having maximum optical efficiency of 80% with the same built measurement.

7. A comparative analysis between the refractive and reflective shows that the refractive SRCPC showed better overall performance with larger acceptance angles combined with high optical efficiency but has a setback of totally internally reflectance.

7.2 Contribution to knowledge

The major contribution of this thesis to research includes

- It uses both direct and diffuse solar radiations
- This technology saves space compared to PV
- At standardised size (1m x 1m), it generates more power than flat PV of the same size.
- It could also produce energy at full capacity from morning to evening when minimal tracking devices are employed

- In addition to electricity on scale-up, there is potential for the system to supply heat when it is removed from the solar cells.

- The SRCPC system design is unique and no one else has reported this specific design for both heat and power generation simultaneously. There are many literatures around the CPC design specifically for PV use. However, this design is primarily for CPV and thermal use.
- The SRCPC technology has demonstrated strong benefits of increase power output when active cooling methods are used thereby increasing the conversion efficiency of the solar cell.

- At a commercial scale-up, there are multiple benefits of the SRCPC system. The system provides both power and heat. It provides optical efficiency improvement compared to previously designed systems. It is designed to have latitude specifics.
- The technology will be cost effective at scale-up level
- The heat can be channelled into use for domestic heating, swimming pools, desalination for maximum benefits of the technology.
- Design and integration of thermal management system to control temperature effect.
- Parameter stability and increase performance of the SRCPC
- Modelled optimum tilt angle for SRCPC to enhance concentration performance
- Design system cost reduction is achieved despite 89% height reduction

7.3 Design and optimisation of the SRCPC

It is important to list the main findings and achievements in the design process of the SRCPC synopsized as follows;

1. The design, development, experimental study and performance of a hybrid symmetric reflective compound parabolic concentrator to generate power.

2. It performs better with active cooling of solar cells thereby increasing efficiency and system reliability where the flow rate is a factor in this process.

3. The designed and developed thermal management system being part of the novelty allows for the achievement of this result.

4. The developed concentrator had no tracking but achieved high efficiency, reliability and parametric stability.

5. It also ensured that the design principle collects maximum solar radiation within the boundary acceptance angles to match the concentration to generate power thereby achieving the aims and objectives of the research.

6. The obtained geometry of the SRCPC followed a novel improved 2-D geometry. It is a very specific geometrical concept that has both the acceptance and exit apertures as rectangular shapes.

7. The rectangular specification of the exit aperture corresponded with the shape of the rectangular shape of the commercial solar cells available. Wastage of solar cell material is reduced and silicon materials are saved when compared with other designs where solar cells are trimmed.

8. Stainless steel was used because of its intrinsic properties. The parabolic material profile used gave a perfect entry aperture thereby achieving Total Internal Reflection where maximum solar radiation was collected for energy generation and losses were minimised.

9. The SRCPC optical efficiency profiles were investigated for different geometry profile for selecting the best-optimised profile.

10. Ray tracing technique was used to achieve this through OptisWorks software. This was based on acceptance half angle (Q_a), height truncation, optical ratio, distribution flux and geometric concentration ratio (Cgeo) of 3x.

11. The optical efficiencies simulation results investigation of the SRCPC profile for wider entry and exit apertures with high C_{geo} indicates reductions in the maximum optical efficiency.

12. For general consideration of the Q_a, the results indicates that the larger the acceptance angle the lower the optical efficiency of the concentrator. This is the general trend irrespective of the C_{geo}.

13. To probe further, the concentrators were categorise for symmetric and asymmetric, un-truncation and truncation that was further revealed to be challenging.

14. During the investigation of the effect of C_{geo} on the optical performance of the SRCPC, it shows that for all height ratios as the optical efficiency increases, there is a linear corresponding decrease of. C_{geo} As further revealed, the SRCPC with lowest C_{geo} 3x has the highest efficiency.

For an un-truncated SRCPC, the higher the concentrator height the less hours of concentration, long distance zigzag travel of solar rays, bulky with high cost implication, non-uniform flux distribution and hot spot creation. It has the advantage of high optical efficiency. However, truncation allows little compromise of C_{geo} to reduce system cost

but with pave way for uniform flux distribution, high optical efficiency and longer hours of concentration.

However, the optimisation process was challenging but in order to move further in the optimisation process, the optical concentration ratio was further investigated because it provides important information on the amount of concentration of solar rays that will reach the solar cells at the exit aperture. The investigation shows clearly that when the concentration is from 8x to 10x upward, the have lower values of optical concentration ratios and lowest optical efficiencies.

Further examination on the optical flux distribution at the rectangular exit aperture shows that the smaller the SRCPC concentrator becomes, the more uniform the optical flux distribution becomes.

7.4 Optical model validation

The optimised SRCPC was constructed and tested under indoor conditions. Theoretical predicted optical efficiencies were compared with the experimental optical efficiencies. The simulated results by means of the optical model showed the main results found to be as follow:

The thin film reflective used in the SRCPC had similar characteristics with the optical material used in the optimisation process. The SRCPC short circuit current I_{sc} generated without coupling the concentrator was compared with the solar cell I_{sc} for the purpose of determining the experimental optical efficiencies.

It showed that the SRCPC experimental optical efficiencies had a good degree of agreement compared with the simulated optical efficiencies.

In addition to this, the obtained gain values were found to be equal to the optical concentration ratios obtained from the optical simulation with small variation.

The obtained SRCPC experimental results for the various incidence angles established the results obtained from the optical simulation consequently validating the optical model developed.

Through the confirmation or validating of the optical model used, a reliable instrument for the study and reflective optical solar concentrator devices is confirmed for use in future study.

7.5 SRCPC performance in real outdoor conditions

An optical and electrical integrated model was developed. It involves the sun calculation. The purpose of the model was for the prediction of energy generation by the SRCPC in different weather conditions and different locations. When the SRCPC was exposed to solar radiation in real outdoor conditions testing necessary for the validation of the integrated model and power output generation monitoring under different weather conditions, the summary results of the main findings of the outdoor experiment includes:

The integrated model which includes the electrical model is using a two diode-equivalent circuit. Experimentally, all the different parameters of the electrical model were determined by the means of the same LGBC solar cells used in the SRCPC. The validation of the electrical model was done twice. During the first instance using the indoor experimental results on one of the LGBC solar cells. The 2nd instance is the SRCPC outdoor experiment overall results of the power out.

More optical simulations were carried out with regards to the optical model for the purpose of accounting for the diffuse radiation including the variation of the solar azimuth angle during the day. Little variation was discovered of about 10% difference amongst incidence angles measured at different solar azimuth angles.

It is clearly observed that the power output of the SRCPC followed the same variation pattern along that of the solar irradiance during the day.

The SRCPC model is able to concentrate solar beams for an average of six hours daily for the acceptance angle of 10º.

The taller the SRCPC becomes, the lower the acceptance angle becomes and less solar radiation was concentrated during the day.

The calculated power output simulated used in the integrated model has confirmed the measured power output of the SRCPC in varied weather conditions. The high degree

of agreement of the experimental and simulated results of the power output having minimal variations validates the integrated model.

The outdoor experiment was carried out during the summer period from the 20th May to 11th July 2015 with highest days of energy generation in June and July. The power generated by the SRCPC in June being a full month is higher than other months. This was achieved because of a combination of smaller acceptance angles, high optical efficiency and effective thermal management system.

7.6 Limitations

There are lots of limitations encountered during the period this study was carried out. These limitations borders on i) manufacturing equipment and procedures, ii) reflective placement, iii) heat exchanger construction, iv) solar cells soldering and v) simulator capacity.

7.6.1 ***Manufacturing:***

There were no capable equipment suitable at Heriot Watt University for the manufacturing of the concentrator. This was contracted out to a company with the specifications where it was constructed with only reasonable accuracy and precision. However, the design details were handed over to the company including soft copies and the model design was constructed to specifications.

7.6.2 ***Reflective placement:***

The thin film reflective placement on the concentrator was carried out manually. The surface was cleaned and polished with thinner before the placement. The tendency of handprints to affect the reflectivity was avoided by the use of hand gloves. There was difficulties in the thin film reflective perfectly fitting the edges of the concentrator but it was carried out with carefulness. The best option to these challenges was to use aluminium vacuum deposition, which is costly, but for large scale, production would be cost effective.

7.6.3 *Heat exchanger construction:*

The parallel flow was difficult to manufacture, as there was no drilling bit long enough to contain the desired length. It was constructed in pieces and later joined at the centre using 6mm channels, which were carefully fitted to avoid some flow obstruction.

7.6.4 *Solar cells soldering:*

The solar cells soldering was carried out manually. The cells were fragile and are susceptible to breaking. The positioning, assembling and soldering of the solar cells manually could have damage many solar cells if not carefully handled. The manual soldering could cause mis-alignment of the solar cells with the reflective solar concentrator if the soldering is not centralised between individual cells. This challenge could be overcome during large scale production as industrial soldering procedures are followed.

7.6.5 *Simulator capacity:*

The capacity of the simulator used during the indoor characterisation could not cover the SRCPC entry aperture fully. This means that part of the SRCPC was not simulated because the simulator collimator area was smaller compared to the acceptance area of the SRCPC. The indoor characterisation results might be affected minimally. This could be avoided if there are simulators having larger collimated areas or reduce the SRCPC dimension to the simulator area but this will not bring much innovation if one is restricted.

7.6.6 *Prediction of solar cell temperature:*

The prediction of yearly temperature of the solar cell poses a problem. At the moment, no accurate equation or method is available to predict the temperature of the solar cells for static solar concentrator.

7.7 Future work recommendations

This thesis presents a design novel proof of concept, which embraces the parametric equation development, geometrical design, numerical modelling involving written codes and commercial software. Apart from the manufacturing of the SRCPC model, indoor

and outdoor testing in different environmental conditions coupled with the development of integrated model for power output or energy prediction is also carried out.

Considering the power generation potentials from the obtained results of the SRCPC system as a proof of concept using a small area, a study for the procedure to advance the SRCPC to large scale production would be helpful for its development.

Temperature dependence is a major issue in concentrating photovoltaic but an effective thermal management system was designed and applied that gave stability to parameters that ensured good capacity power generation. Therefore, effective thermal management system is recommended to be part of the concentrating photovoltaic system.

It is necessary to perfect the design of the heat exchanger so that you can maximise the useful heat output. A detailed analysis of the heat production rate need to be carried out for concentrators.

For optimum power yield, an optimum tilt angle was developed to enable the SRCPC entry aperture stay perpendicularly to the solar radiation for maximum energy yield. For consistent maximum power generation of the SRCPC from morning to evening, a sun tracker device is recommended that is required to mount the SRCPC on top to track the sun from morning to evening for maximum power generation.

Optical performance can be increased with better reflectors and anti-reflectance glazing materials.

The reason for the above recommendations is for the purpose of moving the SRCPC to advance level of commercialisation and to offer more solutions that will help in the design process of solar concentrator in the future. They could also point to other researchers' subjects worth researching as well as using them for business purposes targeting the SRCPC for commercialisation.

7.8 Conclusion

The design, development, experimental study and performance of a hybrid symmetric reflective compound parabolic concentrator has been presented. It performs better with active cooling of solar cells thereby increasing efficiency and system reliability where the flow rate is a factor in this process. The designed and developed

thermal management system being part of the novelty allows for the achievement of this result. The developed concentrator had no tracking but achieved high efficiency, reliability and parametric stability. It also ensured that the design principle collects maximum solar radiation within the boundary acceptance angles to match the concentration to generate power thereby achieving the aims and objectives of the research.

In specific or summary terms, this thesis has established the optical performance of a 2-D novel nonimaging static SRCPC concentrator. It started with the geometry, the CPC structure, its development as well as the construction of the SRCPC. Many different techniques were employed for to facilitate a thorough study of the SRCPC. It is worthwhile to say that the research has not just widened our knowledge on CPC but presented a new geometry with high future potentials for building environment. Due to the fact that the SRCPC design was based on power needs, a novel design was presented having rectangular exit aperture to match the available shape of the solar cell in the market. It has a rectangular entry aperture to accept solar beam during the day from the parabolic profile at the sides of the SRCPC concentrator. It also has an elevated optical performance when put side by side with other profiles.

The widened knowledge gained from this thesis about nonimaging concentrators with special focus on symmetric reflective compound parabolic concentrator (SRCPC) which offered a potential solution for replacement of conventional energy. The developed integrated model's importance for energy prediction in any location and positioning is already emphasised. The thermal management system is to form part of the SRCPC system for stability of parameters. Also, investigating the effects of optical flux distribution on efficiency of SRCPC for developing numerical model and equations being a function of the optical flux distribution pattern for complete overview of the optical efficiency of the SRCPC. Due to the results achieved in this thesis work on the SRCPC, envisage this will pave the way for fully commercialised cost effective systems for clean, energy efficient powered houses for the built environment. This technology if commercially developed will enable countries to fulfil their renewable energy targets and Co2 reduction. This research work aims at contributing to research that guarantee a secured energy supply for the future with the goal of greenhouse gas emission reduction and ultimately slow down climate change activities.

APPENDIX

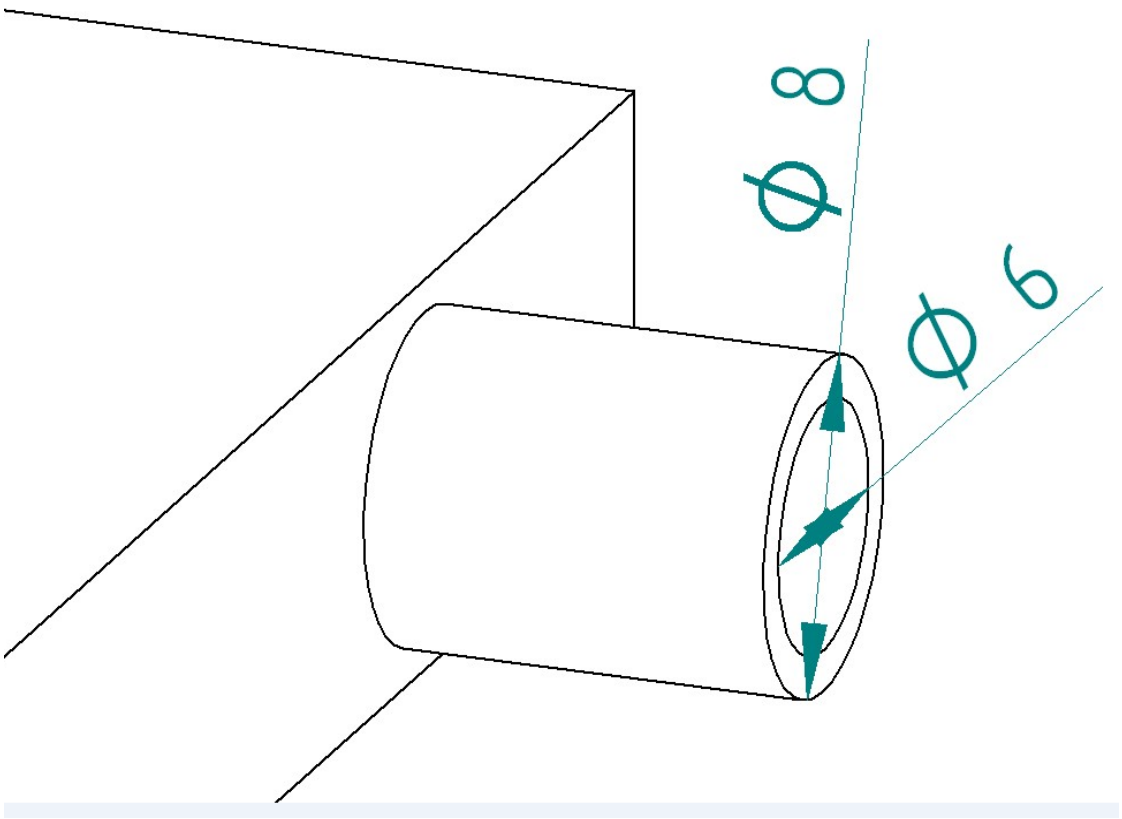

Figure A1: Shows the designed inlet and outlet pipes of the heat exchange having the inner and outer dimensions in mm.

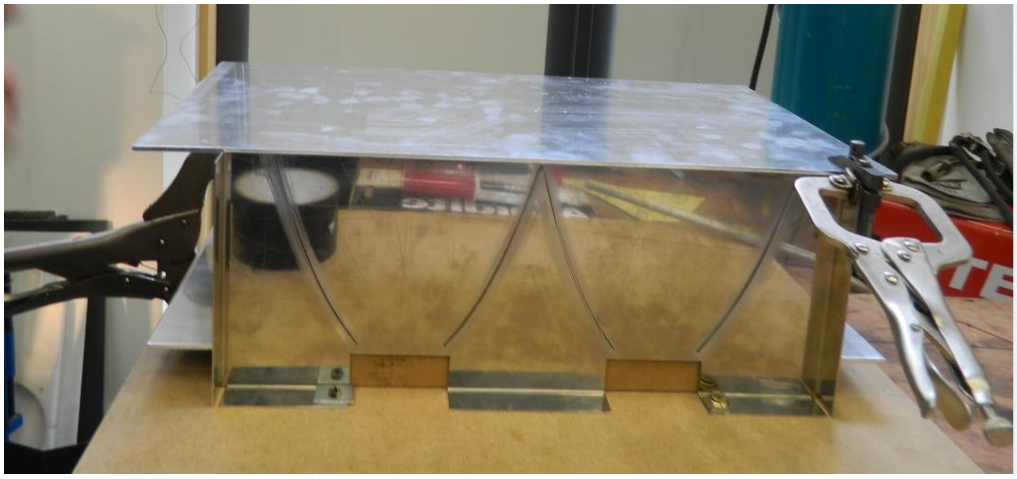

Figure A2: Showing the assembling of the twin SRCPC using clamps and vice machine

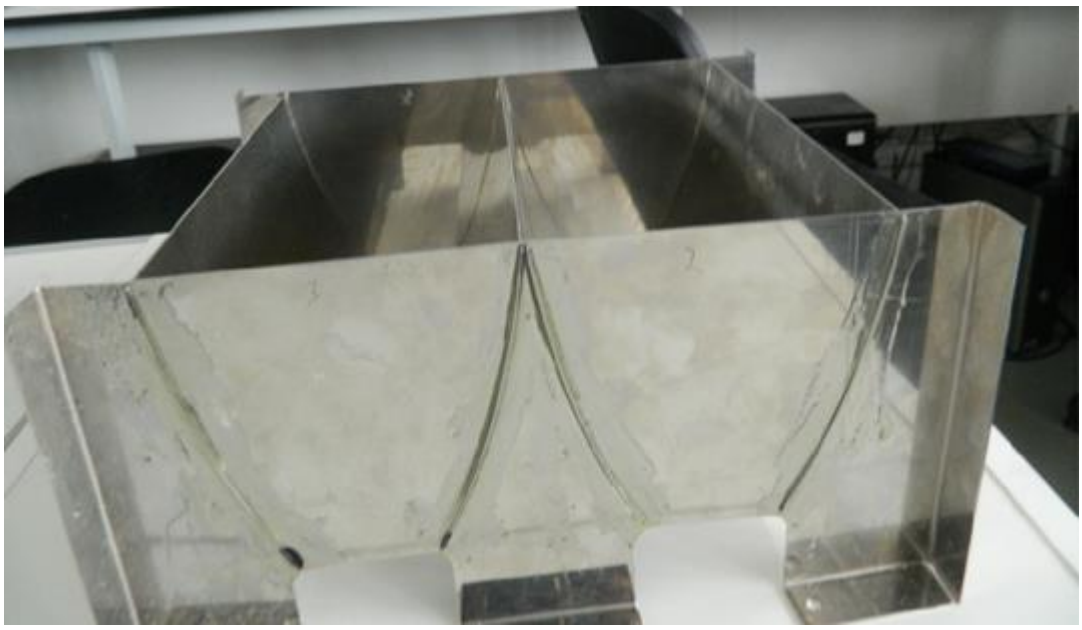

Figure A3: Showing the front view of the twin SRCPC

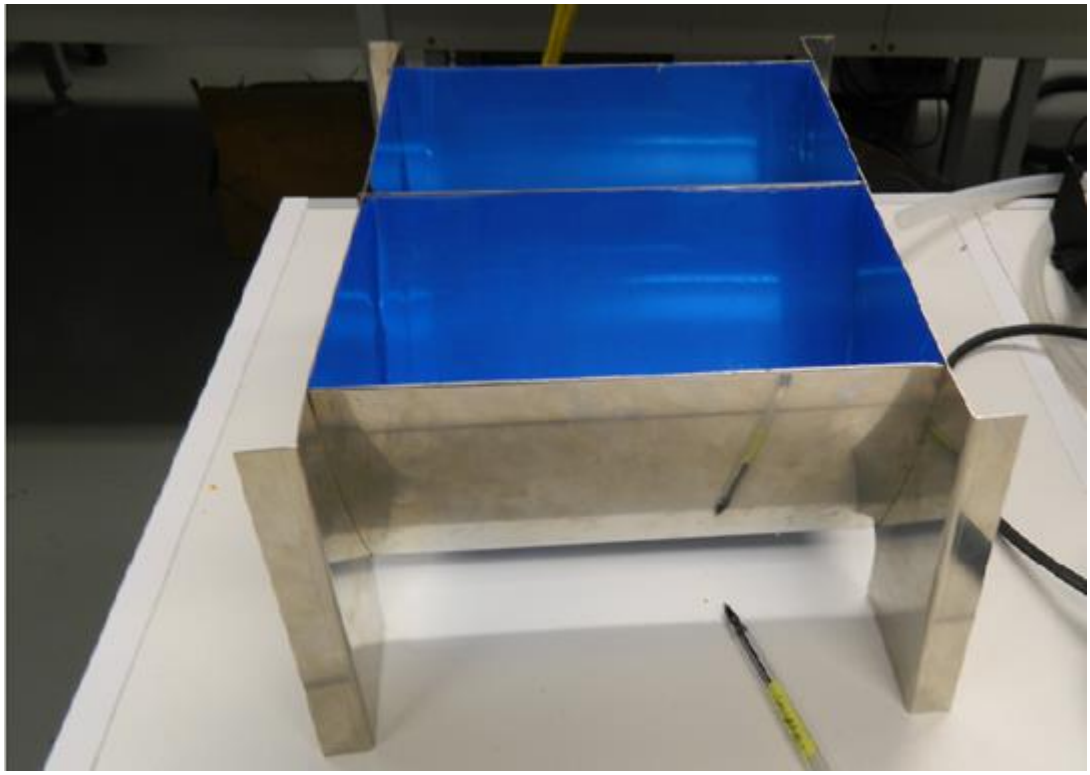

Figure A4: Showing the side view of the SRCPC

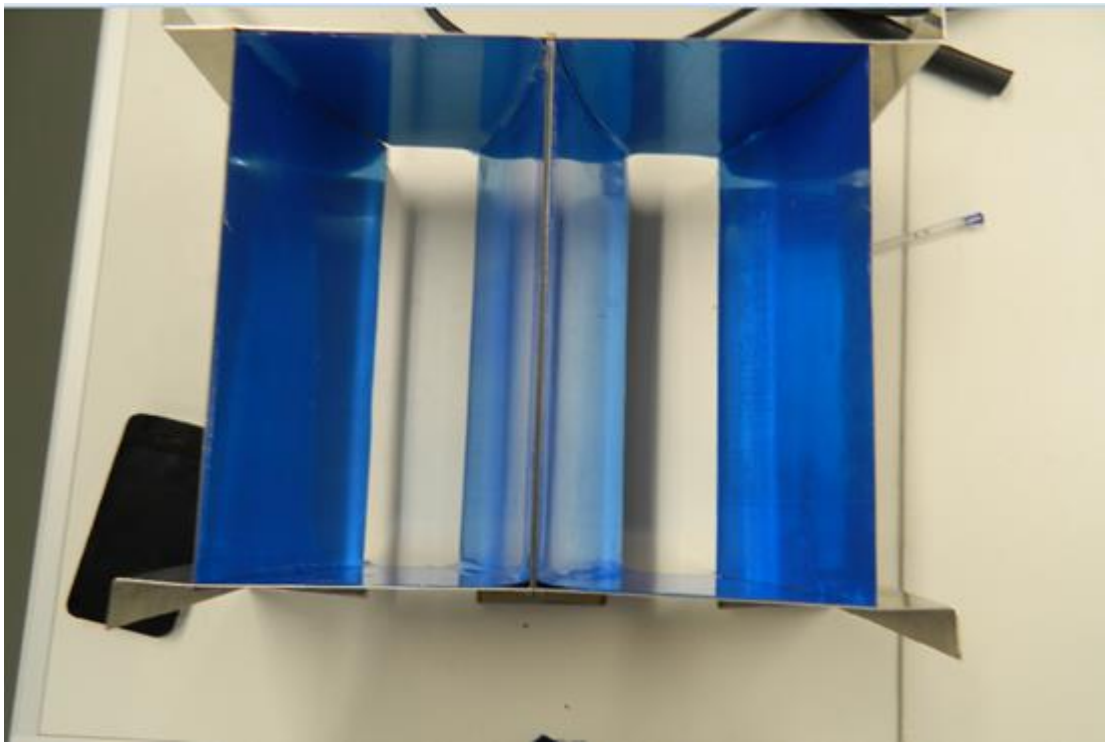

Figure A5: Showing the top view of the twin SRCPC

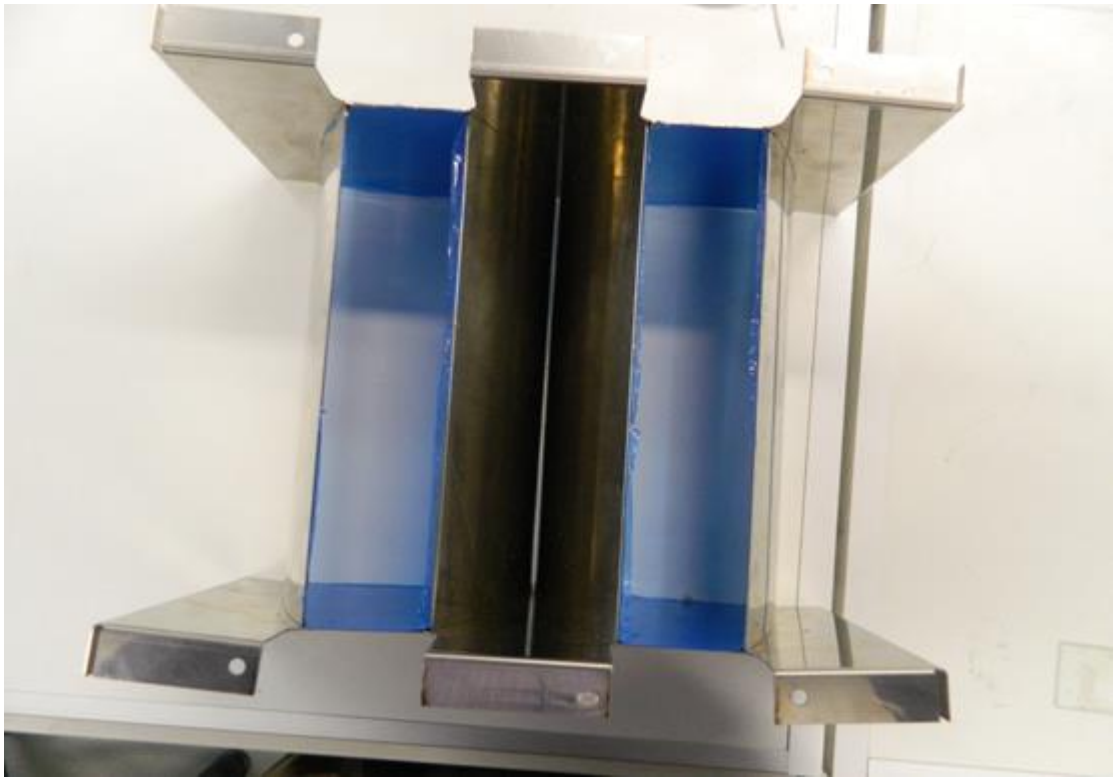

Figure A6: Showing the bottom view of the SRCPC

Table A1: Shows declaration performance data of thermally toughened soda lime silicate safety glass[193]

Low Iron

Essential Characteristic	Glass thickness (mm)			
	4	6	10	
Resistance to fire	npd	npd	npd	
Reaction to fire	A1	A1	A1	
External fire performance	npd	npd	npd	
Bullet resistance	npd	npd	npd	
Explosion resistance	npd	npd	npd	
Burglar resistance	npd	npd	npd	
Pendulum body impact resistance	1(C)2	1(C)2	1(C)2	
Resistance against sudden temperature changes and temperature differentials	200	200	200	
Wind, snow, permanent and imposed load resistance	4	6	10	
Direct airborne sound insulation	30(-2;-2)	31 (-2,-3)	33(-2;-3)	
Thermal Properties				
Normal emissivity of coated glass surface εn	npd	npd	npd	
Thermal transmittance (U-value) W/(m².K)	5.8	5.7	5.6	
Radiation Properties				
Light transmission τV	0.92	0.91	0.91	
Light reflection ρV	0.08	0.08	0.08	
Solar energy transmission τE	0.91	0.89	0.88	
Solar energy reflection ρE	0.08	0.08	0.08	

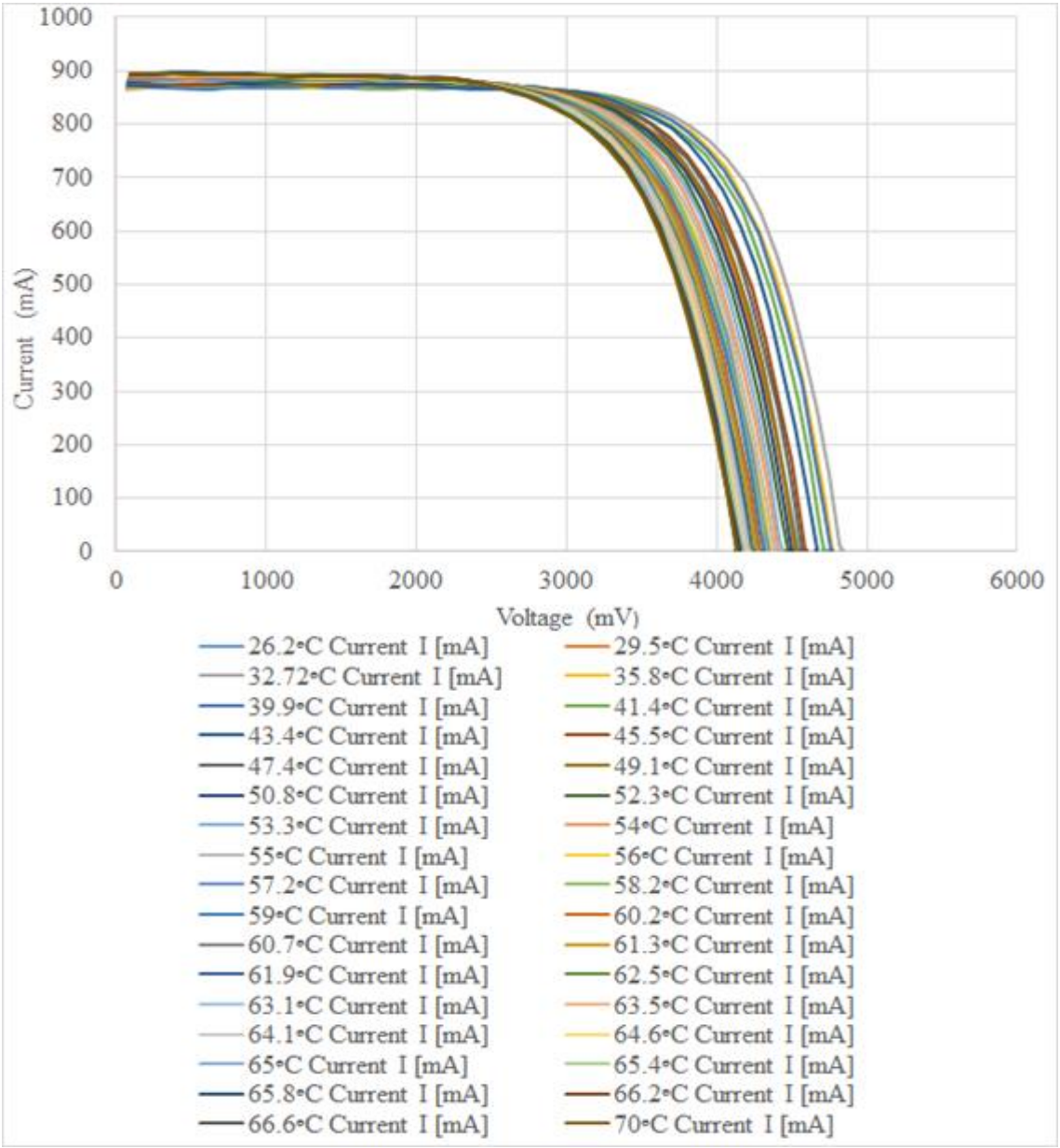

Figure A7: I-V curves showing Solar cell temperature rise from 26.2°C to 70°C without cooling where the voltage drop is significant but minimal current increase.

Table A2: The characteristics summary of parameters of the solar cell strings used in the optimised SRCPC under concentration and cooling using different volume flow rates during the indoor characterization

S/N	Parameter condition	Power (W)	Voltage (V)	Current (A)	Efficiency (%)
1	With concentration and cooling at 0.0069L/s flow rate at 1 sun	5.84	4.79	1.73	8.67
2	With concentration and cooling at 0.007929167L/s at 1 sun	5.96	4.87	1.73	8.83
3	With concentration and cooling at 0.015858L/s flow rate at 1sun	5.85	4.8	1.72	8.66
4	With concentration and cooling at 0.02218L/s flow rate at 1 sun	5.82	4.87	1.63	8.62
5	With concentration and cooling at 0.03085L/s flow rate at 1 sun	5.81	4.77	1.74	8.61
6	With concentrator but no cooling at 1.2 suns 7.13 5.05 2.005 10.57	7.13	5.05	2.005	10.57
7	With concentration and cooling at 0.01L/s at flow rate at 1.2 suns	7.01	4.99	1.95	10.39
8	With concentration and cooling at 0.02218L/s flow rate at 1.2 suns	6.88	4.91	1.96	10.2
9	With concentration and cooling at 0.005858L/s flow rate at 1.2 suns	7.11	5.002	2.003	10.53
10	With concentration and cooling at 0.030858L/s flow rate at 1.2 suns	6.79	4.85	1.96	10.05

Table A3: showing (X, Y) coordinates and incremental X', Y' from excel application

X'	Y'		X	Y		X-
4.924039	2.06588		2.5	0		-2.5
5.924039	2.990184		3.324304	1.08391		-3.3243
6.924039	4.084896		4.119017	2.33564		-4.11902
7.924039	5.350018		4.884139	3.75519		-4.88414
8.924039	6.785549		5.619669	5.342559		-5.61967
9.924039	8.391488		6.325608	7.097749		-6.32561
10.92404	10.16784		7.001957	9.020759		-7.00196
11.92404	12.11459		7.648713	11.11159		-7.64871
12.92404	14.23176		8.265879	13.37024		-8.26588
13.92404	16.51933		8.853454	15.79671		-8.85345
14.92404	18.97732		9.411437	18.391		-9.41144
15.92404	21.60571		9.939829	21.15311		-9.93983
16.92404	24.40451		10.43863	24.08303		-10.4386
17.92404	27.37372		10.90784	27.18078		-10.9078
18.92404	30.51334		11.34746	30.44635		-11.3475
19.92404	33.82337		11.75749	33.87974		-11.7575
20.92404	37.3038		12.13792	37.48095		-12.1379
21.92404	40.95465		12.48877	41.24998		-12.4888
22.92404	44.7759		12.81002	45.18683		-12.81
23.92404	48.76756		13.10168	49.2915		-13.1017
24.92404	52.92964		13.36376	53.56399		-13.3638
25.92404	57.26212		13.59624	58.00429		-13.5962
26.92404	61.76501		13.79913	62.61242		-13.7991
27.92404	66.4383		13.97242	67.38837		-13.9724
28.92404	71.28201		14.11613	72.33214		-14.1161
29.92404	76.29613		14.23025	77.44373		-14.2302
30.92404	81.48065		14.31477	82.72314		-14.3148
31.92404	86.83558		14.3697	88.17036		-14.3697
32.92404	92.36093		14.39505	93.78541		-14.395
33.92404	98.05668		14.3908	99.56828		-14.3908

Table A4: Showing radiation data collected from the testing site*Error! Not a valid link.*

Date	Time	Diffuse radiation	Horizontal radiation	Direct radiations	Global radiations
24/06/2015	11:44:57	0.5127	207.0693	235.3021	236.1721
24/06/2015	11:45:02	0.548	206.9815	235.3822	236.1804
24/06/2015	11:45:07	0.4833	206.946	235.3939	236.1887
24/06/2015	11:45:12	0.5127	206.8089	235.3929	236.2074
24/06/2015	11:45:17	0.5127	206.7447	235.4185	236.2753
24/06/2015	11:45:22	666.4907	1338.0788	636.1991	1198.3697
24/06/2015	11:45:27	663.3204	1333.7517	636.0282	1196.5424
24/06/2015	11:45:32	659.0601	1328.1499	635.6779	1193.887
24/06/2015	11:45:37	652.5867	1320.4793	635.2891	1190.38
24/06/2015	11:45:42	639.6717	1302.5978	634.8192	1183.7062
24/06/2015	11:45:47	618.9027	1282.5694	634.2916	1174.1324
24/06/2015	11:45:52	607.1377	1277.3317	633.7277	1166.5114
24/06/2015	11:45:57	609.6588	1282.2428	633.2011	1162.967
24/06/2015	11:46:02	615.5408	1285.6297	632.5293	1161.1875
24/06/2015	11:46:07	618.1983	1279.5742	631.8437	1158.8141
24/06/2015	11:46:12	616.9072	1272.7806	631.1163	1156.1317
24/06/2015	11:46:17	621.4333	1274.517	630.342	1155.3147
24/06/2015	11:46:22	628.718	1282.6039	629.7172	1155.9335
24/06/2015	11:46:27	631.8612	1288.5954	629.0497	1156.3029
24/06/2015	11:46:32	622.7985	1280.836	628.5125	1153.6232
24/06/2015	11:46:37	597.1471	1255.0816	627.9464	1144.8983
24/06/2015	11:46:42	565.2223	1222.575	627.1924	1131.6069
24/06/2015	11:46:47	541.9051	1198.8164	626.3102	1118.1083
24/06/2015	11:46:52	533.3903	1189.2467	625.4056	1107.8748
24/06/2015	11:46:57	530.3718	1180.2689	624.5544	1099.1721
24/06/2015	11:47:02	515.948	1155.6698	623.6625	1087.1154
24/06/2015	11:47:07	484.5888	1119.7053	622.869	1069.4723
24/06/2015	11:47:12	452.0478	1091.3888	622.2186	1050.6532
24/06/2015	11:47:17	428.8976	1068.9986	621.8608	1032.8673
24/06/2015	11:47:22	411.3647	1053.7629	621.7006	1016.8387
24/06/2015	11:47:27	399.9878	1044.653	621.9153	1003.2832
24/06/2015	11:47:32	393.358	1042.8613	622.4557	992.7047
24/06/2015	11:47:37	397.1362	1054.4161	623.2257	987.2477
24/06/2015	11:47:42	413.8788	1084.8557	624.1442	989.082
24/06/2015	11:47:47	451.2352	1139.9083	624.9153	1001.6112
24/06/2015	11:47:52	511.9299	1210.5408	625.4793	1025.6225
24/06/2015	11:47:57	577.5717	1272.6652	625.3874	1055.6611

24/06/2015	11:48:02	623.9791	1306.7384	624.7616	1083.1954
24/06/2015	11:48:07	632.9548	1298.463	623.5493	1099.4569
24/06/2015	11:48:12	602.8115	1254.5725	622.2453	1100.56
24/06/2015	11:48:17	544.1029	1181.3995	620.9903	1085.979
24/06/2015	11:48:22	472.2135	1104.3138	619.855	1060.193
24/06/2015	11:48:27	411.0214	1047.3581	618.8073	1031.1349
24/06/2015	11:48:32	372.8195	1013.8621	617.9219	1005.0704
24/06/2015	11:48:37	359.2412	1000.6785	617.1967	985.6144
24/06/2015	11:48:42	361.78	999.7156	616.5495	971.9204
24/06/2015	11:48:47	362.776	998.9974	615.992	961.0605
24/06/2015	11:48:52	366.9435	1000.2346	615.5637	954.3562
24/06/2015	11:48:57	378.2957	998.1973	615.004	951.3793
24/06/2015	11:49:02	390.3018	990.6905	614.4401	949.6227
24/06/2015	11:49:07	388.3674	979.3686	613.6743	945.025
24/06/2015	11:49:12	379.6927	976.1159	612.8701	940.0309
24/06/2015	11:49:17	380.3771	979.1762	611.8074	937.3312
24/06/2015	11:49:22	387.1492	982.3017	610.7746	936.605
24/06/2015	11:49:27	396.199	985.6718	609.5154	936.3624
24/06/2015	11:49:32	400.4593	993.148	607.9956	935.2905
24/06/2015	11:49:37	399.7973	1005.3006	606.0411	933.8824
24/06/2015	11:49:42	392.9664	1010.633	603.7534	931.1778
24/06/2015	11:49:47	376.7271	1000.3678	601.1869	924.0501
24/06/2015	11:49:52	345.73	970.1027	598.8266	910.0089
24/06/2015	11:49:57	305.0681	930.3696	596.5912	890.8829
24/06/2015	11:50:02	266.0549	893.8142	594.4295	869.7271
24/06/2015	11:50:07	234.6674	864.7045	592.3169	849.0745
24/06/2015	11:50:12	209.6875	840.8363	590.2983	829.7239
24/06/2015	11:50:17	191.776	821.7097	588.3545	812.1896
24/06/2015	11:50:22	178.4682	806.4593	586.5293	795.9538
24/06/2015	11:50:27	167.3758	794.5297	584.83	780.8101
24/06/2015	11:50:32	155.5814	784.5772	583.3027	766.2907
24/06/2015	11:50:37	144.6619	775.7375	581.9666	753.2203
24/06/2015	11:50:42	135.5368	763.9993	580.9178	741.856
24/06/2015	11:50:47	128.2074	750.1153	580.2247	731.8755
24/06/2015	11:50:52	123.2838	735.6847	579.9107	722.8512
24/06/2015	11:50:57	122.0938	726.1446	580.0057	715.5205
24/06/2015	11:51:02	127.7523	726.4001	580.2663	711.2069
24/06/2015	11:51:07	143.0462	736.9041	580.5088	711.2145
24/06/2015	11:51:12	167.2488	752.3321	580.4511	716.0139
24/06/2015	11:51:17	189.9157	764.6356	580.3026	723.0168
24/06/2015	11:51:22	197.7814	767.034	579.915	728.1121
24/06/2015	11:51:27	186.1481	757.5136	579.7686	728.2181
24/06/2015	11:51:32	165.7731	746.094	579.7665	724.9931

24/06/2015	11:51:37	151.367	737.7091	579.9961	721.0509
24/06/2015	11:51:42	146.8327	737.3273	580.1723	718.1177
24/06/2015	11:51:47	153.2331	750.3323	580.0762	718.2167
24/06/2015	11:51:52	165.7578	771.7596	579.7708	721.6461
24/06/2015	11:51:57	176.6397	790.7028	579.3756	726.3443
24/06/2015	11:52:02	181.6867	801.6162	579.1086	730.852
24/06/2015	11:52:07	186.0564	806.0805	578.9804	735.3873
24/06/2015	11:52:12	193.5681	808.613	578.9516	739.9518
24/06/2015	11:52:17	203.4434	809.6943	578.8587	744.4899
24/06/2015	11:52:22	211.4902	808.8093	578.8063	748.2949
24/06/2015	11:52:27	214.9333	806.6181	578.8341	750.637
24/06/2015	11:52:32	212.6508	803.3121	578.9772	751.3452
24/06/2015	11:52:37	207.0182	800.0683	579.0915	750.7015
24/06/2015	11:52:42	199.4783	796.787	579.2261	749.0335
24/06/2015	11:52:47	194.5159	795.5182	579.3275	747.7405
24/06/2015	11:52:52	193.7045	793.8766	579.3286	747.0905
24/06/2015	11:52:57	195.2932	790.6485	579.3927	746.5272
24/06/2015	11:53:02	195.3038	783.6389	579.3083	744.8073
24/06/2015	11:53:07	191.0199	776.6175	579.3329	741.7708
24/06/2015	11:53:12	186.2034	773.5147	579.2741	738.6601
24/06/2015	11:53:17	182.8814	776.5297	579.35	736.7497
24/06/2015	11:53:22	184.6959	785.2806	579.4728	737.1072
24/06/2015	11:53:27	192.1406	800.2656	579.6373	740.371
24/06/2015	11:53:32	209.2183	823.9561	579.7654	747.8978
24/06/2015	11:53:37	236.2608	851.3769	579.6832	759.8546
24/06/2015	11:53:42	262.546	871.9814	579.5091	773.0879
24/06/2015	11:53:47	277.8481	879.724	579.194	783.839
24/06/2015	11:53:52	276.5887	870.8537	578.8341	789.0603
24/06/2015	11:53:57	259.2358	849.0801	578.408	787.7202
24/06/2015	11:54:02	234.8391	824.2856	577.9498	781.6201
24/06/2015	11:54:07	210.9728	802.3216	577.4638	772.8717
24/06/2015	11:54:12	191.3021	785.1435	577.0975	763.2632
24/06/2015	11:54:17	176.4221	772.8784	576.8871	753.9791
24/06/2015	11:54:22	167.8756	767.8883	576.854	746.417
24/06/2015	11:54:27	167.0466	771.0286	577.059	741.7749
24/06/2015	11:54:32	171.9584	777.6948	577.4126	739.9532
24/06/2015	11:54:37	176.9489	781.8552	577.9711	739.2533
24/06/2015	11:54:42	178.5788	783.5945	578.6985	738.631
24/06/2015	11:54:47	178.8257	785.8706	579.6042	738.3746
24/06/2015	11:54:52	181.5526	794.0137	580.717	739.6178
24/06/2015	11:54:57	193.1613	813.904	582.1001	744.7892
24/06/2015	11:55:02	217.0499	846.6226	583.4768	755.5514
24/06/2015	11:55:07	254.4945	895.8692	584.5737	773.6637

24/06/2015	11:55:12	312.0601	966.1328	584.8386	801.7836
24/06/2015	11:55:17	382.6184	1040.5616	584.0685	837.6811
24/06/2015	11:55:22	445.1416	1090.3933	582.3266	873.916
24/06/2015	11:55:27	470.372	1087.4494	579.9331	898.7312
24/06/2015	11:55:32	450.1322	1038.7089	577.2374	906.2746
24/06/2015	11:55:37	396.239	962.443	574.6944	896.4826
24/06/2015	11:55:42	328.4323	886.6754	572.2497	875.0393
24/06/2015	11:55:47	267.8693	823.2626	570.1777	848.2471
24/06/2015	11:55:52	213.601	769.0258	568.3311	818.3291
24/06/2015	11:55:57	165.0875	724.9844	566.9864	787.4562
24/06/2015	11:56:02	125.9508	692.7758	565.9537	758.0155
24/06/2015	11:56:07	98.6826	673.0848	565.1687	732.1776
24/06/2015	11:56:12	82.8289	662.9409	564.5834	710.9436
24/06/2015	11:56:17	75.4465	659.3024	564.0173	694.2227
24/06/2015	11:56:22	73.7356	659.2225	563.7546	681.5522
24/06/2015	11:56:27	74.3024	659.6931	563.4416	671.853
24/06/2015	11:56:32	74.5869	658.9443	563.3733	664.0414
24/06/2015	11:56:37	73.912	658.3741	563.4299	657.6725
24/06/2015	11:56:42	74.6916	661.4384	563.5858	653.2771
24/06/2015	11:56:47	80.0667	670.6539	563.9767	651.772
24/06/2015	11:56:52	92.0975	686.2151	564.2865	653.864
24/06/2015	11:56:57	108.5402	704.8573	564.5823	659.0958
24/06/2015	11:57:02	126.5246	722.1637	564.8312	666.3156
24/06/2015	11:57:07	140.6356	733.1571	564.6592	673.5708
24/06/2015	11:57:12	147.7099	734.6932	564.5428	679.034
24/06/2015	11:57:17	143.4566	724.1004	564.232	680.4414
24/06/2015	11:57:22	130.4287	708.8174	564.1337	678.0826
24/06/2015	11:57:27	118.0569	699.7222	564.2683	674.3455
24/06/2015	11:57:32	111.3166	698.4476	564.5407	671.2924

Table A5: Temperatures of solar cell, outlet, tank and inlet where the difference in outlet corresponds to tank temperature or negligible

Time	Tin	Tout	Tsc	Ttank
06:00:00	20.1	25.6	27.9	25.9
06:00:02	20.2	25.6	27.9	25.9
06:00:04	20.2	25.6	27.9	25.9
06:00:06	20.2	25.6	27.9	25.9
06:00:08	20.2	25.6	27.9	25.9
06:00:10	20.2	25.6	27.9	25.9
06:00:12	20.2	25.6	27.9	25.9
06:00:14	20.2	25.6	27.9	25.9
06:00:16	20.2	25.6	27.9	25.9
06:00:18	20.2	25.5	27.9	25.9
06:00:20	20.2	25.5	27.9	25.9
06:00:22	20.2	25.5	27.9	25.9
06:00:24	20.2	25.5	27.9	25.9
06:00:26	20.2	25.5	27.9	25.9
06:00:28	20.2	25.5	27.9	25.9
06:00:30	20.2	25.5	27.9	25.9
06:00:32	20.2	25.5	27.9	25.9
06:00:34	20.2	25.5	28	25.9
06:00:36	20.2	25.5	28	25.9
06:00:38	20.2	25.5	28	25.9
06:00:40	20.3	25.5	28	25.8
06:00:42	20.3	25.5	28	25.8
06:00:44	20.3	25.5	27.9	25.8
06:00:46	20.3	25.5	27.9	25.8
06:00:48	20.3	25.5	27.9	25.8
06:00:50	20.3	25.5	27.9	25.7
06:00:52	20.3	25.5	27.9	25.7
06:00:54	20.3	25.5	27.9	25.7
06:00:56	20.3	25.5	27.9	25.7
06:00:58	20.3	25.5	27.9	25.7
06:01:00	20.3	25.5	28	25.7
06:01:02	20.3	25.5	28	25.7
06:01:04	20.3	25.5	28	25.7
06:01:06	20.3	25.5	28	25.7
06:01:08	20.3	25.5	28	25.7
06:01:10	20.3	25.5	28	25.7
06:01:12	20.3	25.5	28	25.7
06:01:14	20.3	25.5	28	25.7
06:01:16	20.3	25.6	28	25.7
06:01:18	20.3	25.6	28	25.7
06:01:20	20.3	25.6	28	25.7
06:01:22	20.3	25.6	28	25.7

Table A6: Showing data of 2nd July 2015 that produced the maximum power

Voc	Isc	Jsc	Pm	Vpm	Ipm	Eta	FF	Time	Temp	Radiation
[V]	[A]	[mA/cm^2	[W]	[V]	[A]	[%]			C	kW
4.990941	1.934984	0	6.625311	3.726834	1.777732	0	0.686035	12.66444	16.6	0.785256
4.990386	1.967153	0	6.706963	3.727219	1.799455	0	0.683209	12.67	16.6	0.789744
4.991763	2.015242	0	6.817039	3.703945	1.840481	0	0.677664	12.67556	16.7	0.797222
4.973069	1.741967	0	6.137602	3.766595	1.629483	0	0.708491	12.68111	16.7	0.759936
4.819817	0.882465	0	2.941308	3.855881	0.762811	0	0.691532	12.68667	16.8	0.568803
4.828863	0.642573	0	2.327815	3.889983	0.598413	0	0.750207	12.69222	16.8	0.39594
5.011964	1.454976	0	5.323342	3.888037	1.369159	0	0.729996	12.69778	16.9	0.587073
5.052257	2.134243	0	7.402767	3.746797	1.975759	0	0.686538	12.70333	16.9	0.789637
4.998086	1.751355	0	6.245372	3.781248	1.651669	0	0.713478	12.70889	17	0.692735
4.7689	0.632754	0	2.182363	3.845927	0.567448	0	0.723226	12.71444	17	0.519872
4.800842	0.523404	0	1.934704	3.912959	0.494435	0	0.769945	12.72	17.1	0.372436
5.00651	1.5632	0	5.574239	3.864241	1.442519	0	0.712256	12.72556	17.1	0.571688
4.889193	0.878964	0	3.184963	3.923543	0.811757	0	0.741133	12.73111	17.2	0.500962
5.040082	2.1146	0	7.273993	3.741115	1.944338	0	0.682507	12.73667	17.2	0.754487
4.997674	2.04157	0	6.946265	3.715718	1.869427	0	0.680799	12.7425	17.3	0.82703
4.987687	2.044979	0	6.922967	3.706778	1.867651	0	0.678741	12.74806	17.4	0.826389
4.983279	2.055355	0	6.919197	3.689102	1.875578	0	0.675544	12.75361	17.4	0.823718
4.98149	2.050267	0	6.895695	3.690706	1.868394	0	0.675163	12.75917	17.5	0.823611
4.97705	2.035512	0	6.857041	3.679217	1.863723	0	0.676848	12.76472	17.5	0.822756
4.974919	2.005594	0	6.789789	3.68057	1.844766	0	0.680499	12.77028	17.6	0.823077
4.972024	1.973812	0	6.728327	3.701374	1.817792	0	0.685596	12.77583	17.6	0.824252
4.972378	1.947375	0	6.674447	3.709414	1.799327	0	0.68929	12.78139	17.7	0.819979
4.969864	1.9323	0	6.639888	3.725116	1.782465	0	0.69142	12.78694	17.7	0.814957
4.970144	1.9247	0	6.623257	3.70612	1.787113	0	0.692372	12.7925	17.8	0.806731
4.969828	1.926104	0	6.629042	3.715977	1.78393	0	0.692516	12.79806	17.8	0.802992
4.969462	1.9469	0	6.677828	3.706581	1.801614	0	0.690212	12.80361	17.9	0.804594
4.968511	1.9552	0	6.699967	3.692187	1.814634	0	0.689692	12.80917	17.9	0.803312
4.968773	1.9707	0	6.73214	3.691968	1.823456	0	0.687517	12.81472	18	0.80203
4.969473	1.9827	0	6.759646	3.695585	1.829114	0	0.686051	12.82028	18.1	0.799145
4.966387	1.980279	0	6.739625	3.693725	1.824615	0	0.685281	12.82583	18.2	0.795833
4.967006	1.95968	0	6.690531	3.693073	1.811643	0	0.687354	12.83139	18.3	0.788782
4.965548	1.950929	0	6.689697	3.702983	1.80657	0	0.690554	12.83694	18.3	0.787286
4.967242	1.945245	0	6.705104	3.705703	1.809402	0	0.69393	12.84278	18.4	0.771902
4.959213	1.972017	0	6.761444	3.71483	1.820122	0	0.691379	12.84806	18.4	0.81891
4.962525	1.359357	0	5.165556	3.863596	1.336982	0	0.765739	12.85361	18.5	0.554274
4.989262	1.893331	0	6.649913	3.761869	1.767715	0	0.703968	12.85917	18.5	0.799893
4.982805	1.774436	0	6.452861	3.763978	1.714373	0	0.729824	12.86472	18.7	0.713248
4.968978	1.851731	0	6.549458	3.725609	1.757956	0	0.711804	12.87028	18.8	0.777778
4.964686	1.872136	0	6.607453	3.739716	1.766832	0	0.710894	12.87583	18.8	0.809722
4.961213	1.858888	0	6.576159	3.74771	1.754714	0	0.713069	12.88139	18.9	0.801282
4.964146	1.925168	0	6.784569	3.722817	1.822429	0	0.709919	12.88694	19	0.818483
4.964994	1.9603	0	6.90043	3.72232	1.853798	0	0.708981	12.8925	19	0.837607
4.955395	2.015061	0	6.981165	3.704254	1.884635	0	0.699136	12.89806	19.1	0.852244
4.932742	1.3258	0	4.752658	3.885772	1.223092	0	0.726725	12.90361	19.1	0.542094
4.981319	2.041864	0	7.124975	3.701115	1.925089	0	0.700506	12.90917	19.1	0.842735
4.789	0.870069	0	2.987319	3.82274	0.78146	0	0.71694	12.91472	19.2	0.653739

REFERENCES

1. Duffie, J.A. and W.A. Beckman, *Solar Engineering of Thermal Processes*. 3rd ed. 2006, Hoboken, New Jersey, USA: John Wiley & Sons Inc. 908.

2. Enerdata, *Global Energy Statistical Yearbook 2014.* Total Energy consumption, 2014.

3. Mekhilef, S. and S. Rahman, *A review on solar energy use in industries.* Renewable and Sustainable Energy Reviews, May 2011. **15**(4): p. 1777-1790.

4. O'Gallagher, J.J., *Nonimaging Optics in Solar Energy*, ed. P.E. Frank Kreith, University of Colorado. 2008. 119.

5. Gielen, D., *Renewable Energy Technologies:Cost Analysis series.* International Renewable Energy Agency, 2012. **1**(2/5): p. 1-41.

6. Jauregui, E. and E. Luyando, *Global radiation attenuation by air pollution and its effects on thermal Climate in Mexico City.* International Journal of Climatology, May 1999. **19**(6): p. 683-694.

7. Green, M.A., et al., *Solae cell: Operating Principles, technology and system applications.* 1982.

8. John A. Duffie, W.A.B., *Solar Engineering of Thermal Processes.* 2006: p. 3-12.

9. Muneer, T., *Solar Radiation and Daylight Models.* 2004: p. 46-50, 237, 266-268.

10. Tiwari, G.N., *Solar Energy: Fundamentals, Design, Modelling and Apllications.* 2002.

11. Kalogirou, S., *Solae Energy Engineering:Process and Systems.* Elsevier Academic Press, 2009.

12. Kreider, J.F. and F. Kreith, *Solar Energy Handbook.* McGraw-Hill. 1981.

13. Goswami, D.Y. and J.F. Kreider, *Principles of Solar Engineering.* 2000.

14. Miles R.W, Hynes K.M, and F. I., *Photovoltaic solar cells: An overview of the-state of the art cell development and environmental issues.* . Progress in crystal growth and characterization of materials, 2005. **51**: p. 1-42.

15. Conibeer, G., *Third generation photovoltaics Review.* ARC Photovoltaics Centre for Excellence, School of Photovoltaic and Renewable Energy Engineering; University of New South Wales, Sydney, Australia, 2007. **10**(11): p. 42-50.

16. Mankins, J., *The case for Space Solar Power Kindle Edition*. January 5, 2014: Virginia Edition Publishing: First Edition 709.

17. Society, N.S., *Space Solar Power: Limitless clean energy from space.* National Space Society, October 2007.

18. Green, M.A., et al., *Solar cell efficiency tables (Version 48).* Progress in Photovoltaics, 2016. **24**(7): p. 905-913.

19. Bony, L., et al., *Achieving Low-Cost Solar PV: Industry Workshop Recommendations for Near-Term Balance of System Cost Reduction*. September, 2010, Rocky Mountain Institute. p. 1-43.

20. Philipps, S., *Solar cells efficiency tables version 1-47: Progress in Photovoltaics - Research applications.* Fraunhofer Institute for Solar Energy Systems (ISE) and National Renewable Energy Laboratory (NREL), 2016. **1993-2015**.

21. Pentsch, J., *Current efficiencies of sellected commercial PV modules.* Fraunhofer Institute for Solar Energy Systems (ISE) and National Renewable Energy Laboratory (NREL), November 2015. Company product data sheets.

22. Hermann, A.M., *Polycrystalline thin film solar cells -a review*. Solar Energy Materials and Solar Cells, 1998. **55**: p. 75-81.

23. Green, M.A., et al., *Solar cell efficiency table (Version 45).* Progress in Photovoltaics, January 2015. **23**(1): p. 1-9.

24. Coutts T.J, Yamaguchi M, and Meakin J.D, *Current Topics in Photovoltaic.* Academic Press, 1989. **3, London**: p. 79-234.

25. Ward J.S, et al., *Proceeding 22nd IEEE PV specialist conference.* 1991: p. 365.

26. Solar, F. *First Solar PV Modules: The Industry benchmark for Utility-scale power plants*. Technology advantage brochure II 19th August 2015; 1-9]. Available from:http://firstsolar.com/-/media/Images/OurAdvantage/TechnologyAdvantage_BR_19AUG15.ashx?la=en.

27. Gratzel, M., *Dye-sensitized solar cells.* Journal of Photochemistry and Photobiology C: Photochemistry Reviews, 2003. **4**(2): p. 145–153.

28. CleanTechnica, *Which Solar Panel Are Most Efficient/.* March 21, 2015.

29. Winston, R. and H. Hinterberger, *Principles of cylindrical concentrator for solar energy.* Solar Energy, 1975. **17**: p. 255-258.

30. John A. Duffie, W.A.B., *Solar Engineering of Thermal Processes.* 2006: p. 347-372.

31. Philipps, S., et al., *Present status in the development of III - V multi-junction Solar cells.* Next Generation of Photovoltaic New cocept, Spring, 2012: p. 1-21.

32. Sarmah, N., B.S. Richards, and T.K. Mallick, *Design, development and indoor performance analysis of a low concentrating dielectric photovoltaic module.* Solar Energy, 2014. **103**: p. 390-401.

33. Sellami, N., *Design and Characterisation of a novel translucent solar concentrator.* Heriot Watt University, Edinburgh, June, 2013. Doctoral Thesis.

34. Welford, W.T. and R. Winston, *The optics of nonimaging concentrators.* Light and Solar Energy:Academic press, New York, 1978.

35. Luque, A. and S. Hegedus, *Handbook of photovoltaic Science and Engineering.* 2003.

36. Winston, R., J.C. Minano, and P. Benitez, *Nonimaging Optics.* Elsevier, 2005.

37. Davies, P.A., *Edge- Ray Principleof nonimaging optics.* Journal of optics society, America, 1994. **11**: p. 1256-1259.

38. Rabl, A., *Comparison solar concentrators.* Solar Energy, 1976. **18**: p. 93-111.

39. Winston, R. and W.T. Welford, *Designs of nonimaging concentrators as second stages in tandem with image forming first stage concentrators.* Applied Optics, 1980. **19**: p. 347-351.

40. Baig, H. and T. Mallick, *Challenges and opportunities in concentrating photovoltaic research.* Mod Energy Rev, 2011. **3**(2): p. 20-26.

41. Nishioka K, T.T., Agui T, Kaneiwa M, Uraoka Y, Fuyuk T, *Annual output estimation of concentrator photovoltaic systems using high -efficiency InGap/InGaAs/Ge tripple junction solar cellsbased on experimental solar cell's characteristics and field test meteorological data.* Solar Energy Materials solar cells, 2006. **50**: p. 57-67.

42. Fei-Lu S, Kok Keong C, and C.-W. W, *A comprehensive study of densely array concentrator photovoltaic system using non-imaging planar concentrator.* Renewable Energy, 2013. **62**: p. 542-555.

43. Basore P A, *Optimum grid-line patterns for concentrator solar cells under non-uniform illumination.* Solar cells, 2010. **14**: p. 249-60.

44. Royne, A., C.J. Dey, and D.R. Mills, *Cooling of photovoltaic cells under concentrated illumination: a critical review.* Solar Energy Materials and solar cells, 2004. **86**: p. 451-483.

45. Sala, G., *CHP and Cooling of Solar cells, in:Cells and optics for photovoltaic concentration.* Adam Hilger, Bristol, 1989: p. 239-267.

46. Dalal, V.L. and A.R. Moore, *Design considerations for high intensity solar cells.* Applied Physics, 1977. **48**(3): p. 1244-1251.

47. Mbewe, D.J., H.C. Card, and D.C. Card, *Amodel of Silicon solar cells for concentrator photovoltaic and photovoltaic thermal system design.* Solar Energy, 1905. **35**(3): p. 247-258.

48. SunPower, *Application notes for HED312 Silicon Concentrator Solar cell.* 2002.

49. Horne, W.F., *Solar Energy system.* Patent US5269851, USA, 1993.

50. Luque, A., S. G, and Arboiro J.C, *Electric and thermal model for non-uniformly illuminated concentration cells.* Solar Energy Materials and Solar Cells, 27 February 1998. **51**(3-4): p. 269-290.

51. Edenburn, M.W. and J.R. Burns, *Shading Analysis of a photovoltaic cell string illumination by a parabolic trough concentrator.* Conference record, 15th IEEE PVSC, 1981: p. 63-68.

52. Karatepe, E. and M. Boztepe, *Developing of a suitable model for characterizing photovoltaic arrays with shaded solar cells.* Solar Energy, 2007. **81**: p. 977-92.

53. Faiman, D., *Large area concentrators.* Conference record , second workshop on the path to Ultra high efficiency Photovoltaics, 2002. JRC Ispra Italy.

54. Xu, D.X. and M. Qu, *Compound Parabolic Concentrators in solar thermal applications: A Review.* Proceedings of the ASME 2013 International Conference on Energy sustainability, July 14-19, 2013.

55. Zhang, X.X., et al., *Review of R&D progress and practical application of the solar photovoltaic/thermal (PV/T) technologies.* Renewable & Sustainable Energy Reviews, 2012. **16**(1): p. 599-617.

56. Skoplaki, E. and J.A. Palyvos, *Operating temperature of photovoltaic modules: A survey of pertinent correlations.* Renewable Energy, 2009. **34**(1): p. 23-29.

57. Skoplaki, E., *On the Temperature dependance of Photovoltaic module electrical performance: A review of of efficiencies/power correlations.* Solar Energy, 2009. **83**: p. 614-24.

58. D.Swapnil, N.S.Jatin, and S.Bharath, *Temperature Dependent Photovoltaic (PV) Efficiency and Its Effect on PV production in the world-A Review.* Energy Procedia (PV Asia Pacific Conference 2012), 2013. **33**: p. 311-321.

59. P.A. Salvado, et al., *A statistical analysis of the temperature coefficients of industrial silicon solar cells.* Energy Procedia (4th International Conference on silicon Photovoltaics, Silicon PV 2014), 2014. **55**: p. 578-588.

60. A.Tiwari and M.S.Sodha, *Performamance evaluation of a solar PV/T systems: A parametric study.* Renewable energy, 2006. **31**: p. 2460-2474.

61. F, T., et al., *Low temperature coefficient for solar cells processed from solar grade silicon purified by metallurgical rout.* Progress Photovolt, April 2011. **19**: p. 996-972.

62. M.Miller, et al., *Influence of the wafer sensitivity on the temperature coefficient of industrial silicon solar cells and on the expected performance behavior*. 25th European Photovoltaic Solar Energy Conference and Exhibition, Valentia, Spain, 2010: p. 2600-2603.

63. I. Zhao, et al., *Reduced temperature coefficients for recent high performance silicon solar cells.* Progress Photovolt, April, 1994. **2**: p. 221-225.

64. T.Mishima and et.al, *Development status of high efficient HITsolar cells.* Solar Energy Materials and Solar Cells, 2011. **95**(1): p. 18-21.

65. M.A.Green, *General temperature dependence of solar cells performance and implications for devide modeling.* Progress Photovolt, 2003. **11**: p. 333-340.

66. M.Tayyib, I.O.Odiden, and T.O.Saetce, *Effect of temperature and sun intensity on multicrystalline silicon solar cells.* 28th European Photovoltaic Solar Energy Conference and Exhibition, Paris, France, 2013: p. 1595-1598.

67. D. Macdonald and A. Cuevas, *Recombination in compensatedcrystalline silicon for solar cells.* Appliied Physics, 2011. **109**: p. 43704.

68. Bhosale, J., et al., *Temperature dependence of band gabs in semiconductors: electron-photons interactions.* American Physics Society, 2012. **86**: p. 195208.

69. Fraser, D.A., *The Physics of Semiconductor Devices*. Fourth ed. 1986, Unites States of America: Oxford University Press. 196.

70. Riffat, S.B. and E. Cuce, *A review on hybridphotovoltaic/thermal collectors and systems.* International journal of low-carbon Technologies, 2011. **6**: p. 212-241.

71. Chow, T.T., *A review on photovoltaic/thermal hybrid solar technology.* Applied Energy, 2010. **87**(2): p. 365-379.

72. Luque, A., G. Sala, and J.C. Arboiro, *Electric and thermal model for non-uniformly illuminated concentration cells.* Solar Energy Materials and Solar Cells, 1998. **51**(3-4): p. 269-290.

73. Luque A, et al., *Some results of the EUCLIDES photovoltaic concentratorprotoytpe.* Program Photovoltaic Res. Application, 1997. **5**: p. 195-212.

74. Akbarzadeh A and W. T, *Heat pipe base cooling system for photovoltaic cells under concentrated solar radiation.* . Applied thermal Engineering, January 1996. **16**(1): p. 81-87.

75. Moshfeg, B., *Flow and heat transfer in the air gap behind photovoltaic panels.* Renewable & Sustainable Energy Review, 1998. **2**: p. 287-301.

76. Brinkworth, B.J., et al., *Thermal Regulation of photovoltaic Cladding.* Solar Energy, 1997. **61**: p. 169-178.

77. Akbarzadeh A, W.T., *Heat pipe base cooling system for photovoltaic cells under concentrated solar radiation.* Applied Therm Eng, 1996. **16 (1)**: p. 81-7.

78. Abdelhamid, M., et al., *Novel double-stage high-concentrated solar hybrid photovoltaic/thermal (PV/T) collector with nonimaging optics and GaAs solar cells reflector.* Applied Energy, 15th November, 2016. **182**: p. 68-79.

79. *International Journal of Low Carbon Technologies.* Energy & Environmental Science, 2011. **6**: p. 212-241.

80. Zhao, Y., *Photovoltaic cell radiating and combined heat and power system.* Patent CN 200820123998 u, 2008.

81. Quan, Z., et al., *The experiment researchfor solar PV/T system based on flat-plate heat-pipes.* In proceedings of the 17th Chinese national. HVAC&R academic conference, 2010.

82. Tang , X., Y. Zhao, and Z. Quan, *The experimental research of using novel flate-plate heat-pipe for solar cells cooling.* In proceeding of the Chinese thermal Engineering physics of heat and mass transfer conference, 2009: p. 239-41.

83. Zhang, X., et al., *Review of R&D progress and practical application of the solar photovoltaic/thermal (PV/T) technologies.* Renewable & Sustainable Energy Reviews, 1st January, 2012. **16**: p. 599-617.

84. Hegazy, A.A., *Comparative study of the performances of four Photovoltaic /Thermal S olar air collectors.* Energy Conversion Manage, 2000. **41**: p. 861-81.

85. Zondag, H.A., et al., *The yield of different combined PV-thermal collector designs.* Solar Energy, 2003. **74**(3): p. 253-269.

86. Aste N, Chiesa G, and Verri F, *Design, development and performance monitoring of a photovoltaic-thermal (PV/T) air collector.* Renewable Energy, 2008. **33**: p. 914-27.

87. Bakker, M., et al., *Performance and costs of a roof-sized PV/thermal array combined with a ground coupled heat pump.* Solar Energy, 2005. **78**(2): p. 331-339.

88. Bazilian, M.D., *Photovoltaic co-generation in the built environment.* Fuel and Energy Abstract, 2002. **43**: p. 269-73.

89. Talavera D.L, N.G., Aguilera J, et al, *Tables for the estimation of the internal rate of return of photovoltaic grid-connected systems.* Renewable & Sustainable Energy Review, 2007. **11**: p. 447-66.

90. Alfegi MEA, S.K., Othman MYH, Yatim BB, *Transient mathematical model of both side single pass photovoltaic/thermal air collector.* ARPN Journal of Engineering and applied science, 2007. **5**: p. 22-6.

91. Ibrahim A, et al., *Hybrid photovoltaic thermal (PV/T) air and water based solar collectors suitatable for building integrated applications.* American Journal of Environmental Science, 2009. **5**: p. 618-24.

92. Duffie, J.A. and W.A. Beckman, *Solar Engineering of Thermal Processes*. 2006. p. 324 - 372.

93. Segal A, E.M., Yogev A,, *Hybrid concentrated photovoltaic and power thermal conversion at different spectral bands.* Solar Energy 2004. **76**: p. 591-601.

94. Royne A, D.C.J., Mills D.R,, *Cooling of Photovoltaic cell under concentrated illumination: A critical review.* Solar energy mater Sol. cell, 2005. **86**: p. 451-83.

95. Rosell Ji, V.X., Lechon M.A, Ibanez M, , *Design and simulation of a low concentrating Phovoltaic/Thermal system.* Energy conversion management, 2005. **46**: p. 3034-46.

96. Coventry, J.S., *Performance of a concentrating phovoltaic /thermal collector.* Solar Energy, 2005. **78**: p. 211-22.

97. Kribus A, K.D., Mittelman G., Hirshfeld A, Flitsanov Y, Dayan A.A,, *Miniature concentrating photovoltaic and thermal system.* Energy Conversion, 2006. **47**: p. 3582-90.

98. Verobiev, Y., et al., *Thermal-photo hybrid system for efficient solar energy conversion.* Solar Energy, 2006. **80**(2): p. 170=6.

99. Vorobiev , Y.V., J. Gonzalez-Hernandez, and A. Kribus *Analysiss of potential conversion efficiency of a solar hybrid system with high temperature stage.* Solar Energy Eng. Trans ASME .2006. **128**: p. 258-60.

100. Tripanagnostopoulos, Y., et al., *Design and Performance of a Hybrid PV/T Solar Water Heater.* 7th International Conference of the Balkan Physical Union Vols 1 and 2, 2009. **1203**: p. 1019-1024.

101. Tyagi, V.V., S.C. Kaushik, and S.K. Tyagi, *Advancement in solar photovoltaic/thermal (PV/T) HYBRID COLLECTOR TECHNOLOGY.* Renewable & Sustainable Energy Reviews, 2012. **16**: p. 1383-1398.

102. Brett T. Gage, R.B., *Technological niches: Concentrated Solar Thermal VS Photovoltaic Solar.* White Paper, 2012.

103. Hoffmann, W., *PV Solar electricity Industry:Market Growth and Perspective.* Solar Energy matters solar cells, 2006. **90**: p. 3285-311.

104. Ibrahim, A., M.Y. Othman, and M.H. Ruslan, *Recent Advances in Flat plate photovoltaic / Thermal (PV/T) sOLAR COLLECTORS.* Renewable & Sustainable Energy Review, 2011. **15**: p. 352-65.

105. S.Coventry, J., *Performance of a concentrating Photovoltaic/Thermal solar collector.* Solar Energy, 2004. **78**(2005): p. 211-222.

106. Chow T.T, *Areview on photovoltaic/thermal hybrid solar technology.* Applied Energy, 2010. **87**: p. 365-79.

107. Arif Hassan M, S.K., *Photovoltaic thermal module concepts and their performance analysis: a review.* Renewable & Sustainable Energy Review, 2010. **14**: p. 1845-59.

108. Hjothman, M., et al., *Performance analysis of a double pass photovoltaic/thermal (PV/T) solar collector with CPC and fins.* Renewable Energy, 2005. **30**: p. 2005-17.

109. Mallick, T.K., Eames Philips C, and B. Norton, *Non concentrating and asymmetric compound parabolic concentrating building facade integrated photovoltaics:An experimental comparison.* Solar Energy 2005. **80**: p. 834-849.

110. Mallick, T.K., et al., *The design and experimental characterisation of an asymmetric compound parabolic photovoltaic concentrator for building facade integration in the UK.* Solae Energy, 2004. **77**: p. 319-327.

111. Mallick, T.K., et al., *The design and experimental characterisation of an asymmetric compound parabolic photovoltaic concentrator for building facadeintegration in the UK.* Solar Energy, 2004. **77**: p. 319-327.

112. Mallick, T.K., et al., *The design and experimental characterisation of an assymmetric compound parabolic photovoltaic concentrator for building facades integration in the UK.* Solae Energy, 2004. **77**: p. 319-327.

113. Kribus A, K.D., Mittelman G et al, *A miniature concentrating photovoltaic and thermal system.* Energy Conversion Manage, 2006. **47**: p. 3582-90.

114. Kribus, A., et al., *A Miniature Concentrating Photovoltaic and Thermal System.* Energy Conversion and Management, December, 2006. **47**(20): p. 3582-3590.

115. Mallick, T.K. and P.C. Eames, *Design anc fabrication of low concentrating second generationPRIDE concentrator.* Solar Energy Materials and Solar Cells, 2007. **91**: p. 597-608.

116. Mallick, T.K. and P.C. Eames, *Design and fabrication of low concentrating second generation PRIDE concentrator.* Solar Energy Materials and Solar Cells, 2007. **91**(7): p. 597-608.

117. Sellami, N., T.K. Mallick, and D.A. McNeil, *Optical characterisation of 3-D static solar concentrator.* Energy Conversion and Management, 2012. **64**(0): p. 579-586.

118. Sellami, N. and T.K. Mallick, *Design Of Nonimaging Static Solar Concentrator For Window Integrated Photovoltaic.* 8th International Conference on Concentrating Photovoltaic Systems (Cpv-8), 2012. **1477**: p. 106-109.

119. Bahaidarah, H.M., et al., *Experimental and numerical study on non-concentrating and symmetric unglazed compound parabolic photovoltaic concentration systems.* Applied Energy,, 31st Dec 2014. **136**: p. 527-536.

120. Kostic L. T, P.T.M., Pavlovic Z.T,, *Optimal design of orientation of PV/T collector with reflectors.* Applied Energy, 2010. **87**: p. 3023-9.

121. Coventry, J.S., *Performance of a concentrating photovoltaic/thermal solar collector.* Solar energy, 2005. **78**: p. 211-22.

122. Kurtz S, G.J., *Multijunction solar cells for conversion of concentrated sunlight to electricity.* Optics Express, 2010. **18**: p. A73-8.

123. Baig, H., K.C. Heasman, and T.K. Mallick, *Non-uniform illumination in concentrating solar cells.* Renewable & Sustainable Energy Review, 2012. **16**: p. 5890-5909.

124. Kruger D, P.Y., Hennecke K, Schmitz M, , *Parabolic Trough collector testing in the frame of the REACt project.* Desalination and Water Treatment, 2008. **220**: p. 612-8.

125. Toa T, Z.H., Su Y, RIFFAT S.B., *Anovel combined solar concentration /wind augmentation system: Construction and preliminary testing of a prototype* Applied Thermal Engineering, 2011. **31**: p. 3664-8.

126. Mittelman, G., Kribus A, Mouchtar O, Dayan A, *Awater dissalination with concentrating photovoltaic/thermal (CPVT0 systems.* Solar Energy, 2009. **83**: p. 1322-34.

127. Chemisana, D., M. Ibanex, and J. Barau, *Comparison of Fresnel concentrators for building integration photovoltaics.* Energy Conversion and Management, 2009. **50**: p. 1079-84.

128. Xie, W.T., et al., *Concentrated solar energy application using Fresnel Lenses: a review*. Renewable & Sustainable Energy Review, 2011. **15**: p. 2588-606.

129. Mallick, T.K. and P.C. Eames, *Desing and fabrication of low concentrating second generation PRIDE concentrator.* Solar Energy Materials and Solar Cells, 2007. **91**: p. 597-608.

130. Mallick, T.K., P.C. Eames, and B. Norton, *Power losses in an asymmetric compound parabolic photovoltaic concentrator.* Solar Energy Materials and Solar Cells, 2007. **91**: p. 1137-46.

131. Uematsu T, Y.Y., Joge T, Kokunai S, *Fabrication and characterization of a flat - plate static concentrator photovoltaic module with prism array.* Solar Energy Materials and Solar Cells, 2001. **67**: p. 415-23.

132. Weber KJ, E.V., Deenapanray P N K, Franklin E, Blakers Aw, *Modeling of static concentrator modules incorporating Lambertian or V-groove rear reflectors.* Solar Energy Materials and Solar Cells, 2006. **90**: p. 1741-9.

133. Yamada N, K.K., Hayashi K, Tokimitsu T, , *Performance of see-through prismCPV module for window integrated photovoltaics.* Optics Express, 2011. **19**: p. A649-56.

134. Alonso J, D.V., Hernandez M, Bercero F, Canizo C, Pou I, et al, *A new static concentrator PV module with bifacial cells for integration in facades: the PV VENETIAN store. Photovoltaic Specialists Conference, .* Conference Record of the Twenty-Ninth IEEE, 2002. **2002**: p. 1584-7.

135. Van Sark W G, B.K.W., Slooff L H, Chatten A J, Buchtemann A, Meyer A et al, *Luminescent Solar Concentrator?* A review recent results Optic Express, 2008. **16**: p. 21773-92.

136. Slooff, L.H., et al., *The Luminescent concentrator: A bright idea for spectrum conversion.* 20th European Photovoltaic solar Energy conference and exhibition , Barcelona:Spain, 2005. **1**: p. 6-10.

137. Philipps, S.P., et al., *Current status of concentrator Photovoltaic (CPV) Technology.* Fraunhofer Institute for Solar Energy Systems (ISE) and National Renewable Energy Laboratory (NREL), 2015. TP-6A20-63916: p. 1-24.

138. Platform, E.P.T., *A Strategic Research Agenda for Photovoltaic Solar Energy Technology.* 2011.

139. Concas, G., et al., *A revamped Technology Platform to accelerate the energy transformation.* European Technology and Innovation Platform, Brussel-March 2016. Press release.

140. Dang, A., *Concentrators: A review.* Energy Conversion and Management, 1986. **26**(1): p. 11-26.

141. Wiston, R., *Principles of solar concentrators of a novel design* solar Energy, 1974. **16**: p. 89-95.

142. Rabl, A., *Optical and thermal properties of Compound Paraboli Concentrators.* Solar Energy, 1976. **18**: p. 497-511.

143. Winston, R. and W.T. Welford, *Geometrical vector flux and some new non-imaging concentrators* Journal of the optical society of America, 1979. **69**(4): p. 532-536.

144. Welford, W.T. and R. Winston, *High Collection Non-Imaging Optics.* Academic Press, New York and London, 1989.

145. Winston, R. and W. Zhang, *Pushing concentration of stationary solar concentrators to the limit.* Optics Express A64, 2010. **18**.

146. Scharlack, R.S., *All dielectric compound parabolic concentrator.* Applied Optics, 1977. **16**(10): p. 2601- 2602.

147. Fraidenraich, N., et al., *Analitic solutions for the geometric and optical properties of stationary compound parabolic concentrators with fully illuminated inverted V receiver.* Solar Energy, 2008. **82**(2): p. 132-143.

148. Welford, W.T., *High collection non-imaging optics.* Academic Press, New York, 1989.

149. Qu, D.X.a.M., *Compound Parabolic concentrators in solar thermal applications: A Review.* Proceedings of the ASME 2013 7th International Conference on Energy sustainability, 2013.

150. Scharlack, R.S., *All dielectric Compound Parabolic Concentrator.* Applied Optics, 1977. **16**(10): p. 2601-2602.

151. OptisWorks, *Optis Illumination the Design Process.* The integrated software solution for the physics based simulation of light and human vision, 2012.

152. Sellami, N., T.K. Mallick, and D.A. McNeil, *Optical Characterisation of 3D solar concentrator*. Energy Conversion and Management, 2012.

153. Wirz, M., M. Roesle, and A. Steinfeld, *Three dimentional optical and Thermal numerical model of solar tabular receiverin parabilic trough concentrators.* ASME, Journal of solar Energy Engineering, 2012. **134**: p. 041012-1/9.

154. Sellami, N., T.K. Mallick, and D.A. McNeil, *Optical characteracterisation of a 3-Dstatic solar concentrator*. Energy Conversion and Management, 2012. **54**: p. 579-586.

155. Nasmi Sellami, T.K.M., *Opticall efficiency study of PV Cross Compound Paraboli Concentrator*. A review recent results Optic Express, 2013. Applied Energy(102): p. 868-876.

156. Duffie, J.A. and W.A. Beckman, *Solar engineering of thermal processes*. 3rd ed. 2006: Willey Interscience Publishers.

157. Cooper, P.I., *The absorption of radiation in solar stills.* Solar Enrergy, 1969. **12**: p. 333-346.

158. Honsberg, C. and S. Bowden, *Properties of sunlight.* PVEDUCATION.ORG, 2016. Declination angle.

159. NREL, *Reference Solar Spectral Irradiance: AM 1.5.* American Society for Testing and Materials (ASTM) Terrestial Reference Spectral for Photovoltaic Performance Evaluation.

160. Toledo, F.J. and J.M. Blanes, *Analytical and quasi-explicit four arbitrary point method for extration of solar cell single-diode model parameters.* Renewable Energy, 19th February, 2016. **92**: p. 346-356.

161. Instrument, N., *Photovoltaic cell I-V Characterization Theory and LabVIEW Analysis Code.* National Instrument : LabVIEW VI Toolkit for Researchers and Engineers, May 2012. Part two: p. 1-6.

162. Sharma, D.K. and G. Purohit, *Fill Factor based Maximum Power Point Tracking for standalone solar PV system.* IVth International conference on advance in energy research December 2013. **332**: p. 1-8.

163. Instrument, N., *Part II - Photovoltaic Cell I-V characterization Theory and LabVIEW Analysis Code.* National Instrument : LabVIEW VI Toolkit for Researchers and Engineers, 10th May 2012: p. 1-6.

164. Sharma, D.K. and G. Purohit, *Fill Factor based maximum power point tracking (MPPT) for standalone solar PV systems.* IVth International conference on advances in energy research: India Institute of technology Bombay, Mumbai, December 2013. **332**: p. 1-8.

165. KEITHLEY, *Measuring photovoltaic cell I-V charcteristics with the Model 2420 SouceMeter Instrument* Application Note series. **1953**.

166. Baig, H., K.C. Heasman, and T.K. Mallick, *Non-uniform illumination in concentrating solar cells.* Renewable & Sustainable Energy Reviews, 2012. **16**: p. 5890-5909.

167. K, M.T. and E.P. C., *Non-concentrating and asymmetric compound parabolic concentrating for building facade integrated photovoltaics: An experimental comparison.* Solar Energy, July 2006. **80**(7): p. 834-849.

168. Schaap, A.B. and W.B. Veltkamp, *Solar Engineering of thermal process.* Solar Energy, Dec 1993. **51**(6): p. 521.

169. O'Gallagher, J.J., *Nonimaging Optics in Solar Energy.* 2008.

170. Maehlum, M.A. *Which solar panel type is best?: Mono-crystalline or Poly-crystalline*. 18, May 201.

171. Sellami, N. and T.K. Mallick, *Optical charcterisation and optimisation of a static window integrated concentrating photovoltaic system.* Solar Energy, May 2013. **91**: p. 273-282.

172. Carvalho, M.J., et al., *Truncation of CPC solar collectors and its effect on Energy collector.* Solar Energy, Jan 1985. **35**(5): p. 393-399.

173. Zhi-Yong, L., S.V. Petar, and J.Y. Jin, *Recent developments in applied thermal engineering: Process integration, heat exchangers, enhanced heat transfer, solar thermal energy, combustion and high temperature processes and thermal process modelling.* Applied thermal Engineering, 25th July, 2016. **105**: p. 755-762.

174. Winston, R., J.C. Minano, and P. Benitez, *NONIMAGING OPTICS*. 2005, USA: Elsevier Acadamic Press. 493.

175. Winston, R., J.C. Minano, and Benitez, *"Some designs of image-forming concentrators" in Non-imaging Optics.* Academic Press, 2005: p. 25-41.

176. Bhattacharjee, P.R., *Addressing some issues of Ray Optics on the basis of the newly discovered generalised vectorial laws of reflection and refrsction.* Optik-International Journal for Light and Electron Optics, Dec 2013. **124**(23): p. 6250-6254.

177. OptisWorks, *Illuminating the design process " Compound parabolic concentrator (CPC)" : Modelling using OpticsWorks.* OPTIS, Aug 2010.

178. Andreev, V.P., et al., *Effects of nonuniform light intensity distribution on temperature coefficients of concentrator solar cells.* In proceedings of 3rd World conference on photovoltaic Energy conversion, 2003. **1**: p. 881-884.

179. Lu, Z.H., et al., *The Effect of Non-Uniform Illumination on the Performance of Conventional Polycrystalline Silicon Solar Cell.* Proceedings of ISES World congress 2007, 2007. **1-v**: p. 1445-1448.

180. Sarmah, N., *Design and Performance Evaluation of a low concentrating line-axis Dielectric Photovoltaic systems.* Heriot Watt Theses Repository, 2012.

181. Franklin, E. and J. Conventry, *Effects of highly non-uniform illumination distribution on electrical performance of solar cells.* 2002.

182. Corning, D., *Sylgard 184 Silicon Elastomer.* Product Information (Electronics), 2nd April, 2014.

183. Mammo, E.D., N. Sellami, and T.K. Mallick, *Performance analysis of reflective 3-D cross compound parabolic concentrating photovotaic system for building facade integration: Performance analysis of a reflective 3-D CPCPV system.* Progress in Photovoltaics Research and Apllications, April 2012.

184. Gerber, J.D., et al., *Thermal modelling of low concentrator Photovoltaic systems.* Journal of Energy in Southern Africa, 2013. **24**(1): p. 51-55.

185. Teo, H.G., P.S. Lee, and M.N.A. Hawlader, *An active cooling system for photovoltaic modules.* Applied Energy, 2012. **90**: p. 309-315.

186. Rai, G.D., *SOLAR ENERGY UTILIZATION.* Book, 2004. Fifth Edition: p. 17-38, 384-403, 404-411.

187. Toolbox, T.E., *Resources, Tools and Basic Information for Engineering and Design of Technical Application.*

188. Sleigh, P.A., *An Introduction to Fluid Mechanics (CIVE 1400): Continuity and Conservation of Matter.* Civil Engineering, University of Leeds.

189. Tripathi, R., G.N. Tiwari, and I.M. AL-Helal, *Thermal modelling of N partially covered photovoltaic thermal (PVT) - Compound parabolic cooncentrator (CPC) collectors connected in series.* Solar Energy, 2015. **123**: p. 174-184.

190. Helmers, H., et al., *Modeling of concentrating photovoltaic and thermal systems.* Preogress in Photovoltaic: Research and Applications, 2014. **22**: p. 427-439.

191. Atheaya, D., et al., *Analytical characteristic equation for partially covered photovoltaic thermal (PVT) Compound parabolic concentrator (CPC).* Solar Energy, 2014. **111**: p. 176-185.

192. Rapid, A., *Araldite Professional Adhesive.* Company instruction manual, 2011. **2 x 15ml**.

193. Glass, D.B., *Declaration performance of thermally toughened soda lime silicate safety glass.* Declaration of conformity: BS EN12150-2 ANNEX ZA, 2013. British Standard Institute.

194. *www.pilkington.com/en-gb/uk/products*.

195. Woollam, J.A. and P.G. Snyder, *"VASE- Variable angle Spectroscopic Ellipsometry", C R Brundle, C A Evans, and WILSON.* Encyclopedia of material characterisation, 1992. **Eds**: p. 401-411.

196. Amiotti, M. and G. Landgren, *Ellipsometric determination of thickness and refractive index at 1.3, 1.55 and 1.7 micro meter foe IN(1-X) GaxAsyP (1-Y) Films on InP.* Journal Applied Physics, March 1993. **73**(6): p. 2965-2971.

197. Ho, J.H., C.L. Lee, and T.F. Lei, *Refractive index profile measurement of compound thin films by ellipsometry.* Electron Lett, Aug 1989. **25**(16): p. 1084-1086.

198. Fernandes, V.R., et al., *Refractive index characterisation of waveguide channels using spectroscopic ellipsometry.* in 2011 IEEE EUROCON- International conference of computer as a tool (EUROCON), 2011: p. 1-4.

199. Corning.com, D., *Sealants and Tools (Adhesives).*

200. A, D. and O. C, *Measurement of the complex refractive index of liquid in the tetrahertz using Elippsometry.* 2010.

201. *Electornic Product Design.* Customs Software/Electronics design End Product development. Components.com.

202. Fraser, D.A., *The Physics of semiconductors devices*. Fourth ed, ed. Fourth. 1986, Oxford: Clarendon Press. 193.

203. Peter, Y.Y. and M. Cardona, *Fundamentals of semiconductors physics and materials properties*. Third ed. 2001, New york: Springer -Verlag Berlin Heidelberg New york. 639.

204. Balkanski, M. and R.F.Wallis, *Semiconductors Pyhsics and Application*. First ed. 2000, New Yor, United States: Oxford University Press. 487.

205. Bunea, G., et al., *Low Light performance of monocrystalline Silicon solar cell.* In Proceedings of 4th World conference on Photovoltaic Energy conference, 2006, Waikoloa: p. 1312-1314.

206. Handoyo, E.A., D. Ichsani, and Prabowo, *The optimal tilt angle of a solar collector*. Energy Procedia: International Conference on Sustainable Energy Engineering and Application, 2013. **32**: p. 166 - 175.

207. Citipedia. *Sunrise, Sunset, Down, Dusk Charts for the year*. Available from: http://www.citipedia.info/city/sunriseandsunset/United+Kingdom_Cornwall_Penryn_id_2640413.

208. Muneer, T., *Solar radiation and daylight models.* ELSEVIER, 2004: p. 52-57.

209. Gunerhan, H. and A. Hepbasli, *Determination of the optimum tilt angle of solar collectors for building applications.* Building and Environment, 2005. **42**: p. 779-783.

210. Grigoniene, J. and M. Karnauskas, *Mathmatical modelling of optimum tilt angles of solar collector and sunray reflector.* ENERGETIKA, 2009. **55**: p. 41-46.

211. Sellami, N. and T.K. Mallick, *Optical Efficiency study of crossed Compound Parabolic Concentrator.* Applied Energy, Feb 2013. **192**: p. 868-876.

212. Anon, D.s., *CMP-11 Pyranometer.* D. Kipp & Zonen, 2010. education, Delft: p. The Netherlands.

213. Anon, D.s., *SOLYS 2, in.* D.Kipp & Zonen, 2010. Educatiion: p. The Netherlands.

214. Anon, D.s., *CHP1 Pyrheliometer, in.* D.Kipp & Zonen, 2010. Education(Delft): p. The Netherland.

215. RDXL12SD, *12 ChannelTemperature Recorder with Excel - formatted Data Logger SD Card.* User Manual. For immediate Technical application assistance.

216. Instrument, N., *Multi-Channel Data Loggers.* User Manual.

217. Pump, W.-M.P., *Single Channel and accurate dispensing.* User Manual. Fluid Liquid Group.

218. Instrument, E., *I-V Tracer series.* Photovoltaic Evaluation systems. Environmental Measurement and Analysis.

219. Sendhil Kumar, N., et al., *Experimental Validation of a heat transfer model for concentrating Photovoltaic systems.* Applied Thermal Engineering, 2012. **175182**: p. 33-34.

220. Sellami, N., *Design and Characterisation of a novel translucent Solar concentrator*. Heriot Watt University Doctoral Theses Repository, June 2013. Institute of Mechanical, Process and Energy Engineering.

221. Singh, H. and P.C. Eames, *A review of natural convective heat transfer correlations in rectangular cross-section cavities and their potential applications to compound parabolic concentrating (CPC) solar collector cavities.* Applied Thermal Engineering, 2011. **31**: p. 2186-2196.

222. Morrison, D.J., et al., *Development of rear passivated Laser Groove Buried Contact (LGBC) Laser Fired Contact (LFC) Silicon solar cells using thin wafer.* 27th EUPVSEC 2012, 2nd February, 2012. **27th** (Munich, Frankfurt, Germany): p. 1512-1515.

223. Tamrakar, V., S.C. Gupta, and Y. Sawle, *Single-Diode and two-Diode PV cell modeling using MATLAB for studying characteristics of solar cell under varying*

conditions. Electrical & Computer Engineering: An International Journal (ECIJ) Volume 4, Number 2, June 2015 June 2015. **4**(2): p. 67-77.

224. David L. King, J.A.K., William E. Boyson, *Temperature coefficients for PV modules and array: Measurement, Methods, Difficulties and Results.* Photovoltaic Specialist Conference, 29th Sept - 03rd Oct. 1997(26th IEE): p. 1183-1136.

225. Klyukanov, A.A., P.A.Gashin, and R.Scurtu, *Ideality factor in transport theory of Schottky barrier diodes.* Semiconductor Physics Lab, Faculty of Physic: Moldova State University, 60A Mateevici Str. Chisinau MD, Republic of Moldova, 2009.

226. Lab, R.A., *Characterisation and reliability testing of the Schottky diode.* School of Physics and Astronomy:Physics and Space Research, The University of Birmingham., 2006/7: p. Millimeter Wave Technology.

227. ASTM, *Electrical performance of non-concentrator terrestial photovoltaic module and arrays using reference cells.* **948**.

228. ASTM, *Electrical performance of non-concentrator terrestrial photovoltaic modules and arrays using reference cells.* E. **1036**.

229. King, D.L., *Photovoltaic Module and Array performance characterization Method for All System Operating Conditions.* NREL/SNL, 1996. Program Review(AIP Press): p. 347-368.

230. King, D.L., J.A. Kratochvil, and W.E. Boyson, *Temperature Coefficients for PV Modules and Arrays: Measurement Methods, Difficulties and Results* IEEE Photovoltaic Specialists Conference September 29th -October 3, 1997,. **26th**

231. Whitaker, C.M., et al., *Effects of irradiance and other factors on PV temperature coeffients.* Pacific Gas and Electric Co., San Ramon, CA, USA, 1991.

232. Osterwald, C.R., T. Glatfelter, and J. Burdick, *Comparison of the temperature coefficients of the basic I-V parameters for various types of solar cells.* IEEE 1987. **Ed**(IEEE PV Specialist Conference): p. 188-193.

233. Platz, R., et al., *Hybrid collectors using hybrid collectors using thin-film technology*. Photovoltaic Specialist Conference, 1997. **12**(Conference Record of the 26th IEEE): p. 1293-1296.

234. Kaw, A., *Newton Raghson Method of solving non-Linear Equations.* University of South Florida: Holistic Numerical Method Institute: p. 1-15.